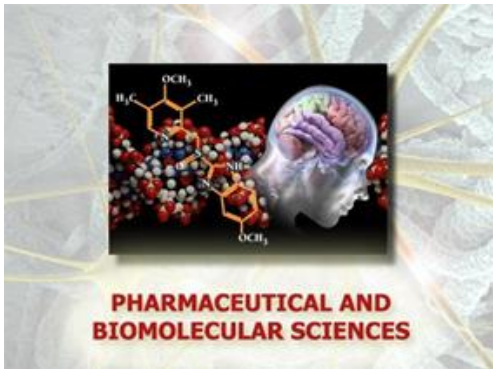

Università di Torino

Doctoral Program in Pharmaceutical and Biomolecular Sciences

Department of Drug Science and Technology

XXXVIIth Cycle

Development of nanosystems to overcome resistance in pancreatic cancer cells

Supervisor:
Prof. Silvia Arpicco

Ph.D. candidate:
Valeria Bincoletto

Coordinator:
Prof. Roberta Cavalli

Academic Years: 2021/2022-2022/2023-2023/2024

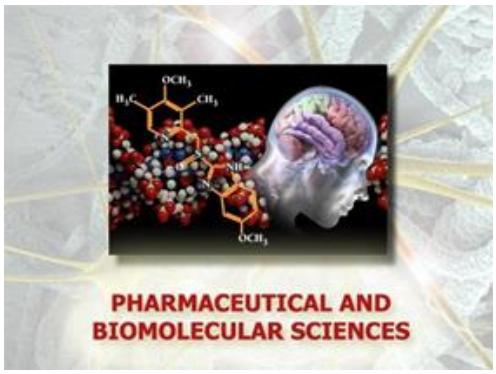

Università di Torino

Doctoral Program in Pharmaceutical and Biomolecular Sciences

Department of Drug Science and Technology

Cicle: XXXVII

Title of the Thesis: Development of nanosystems to overcome resistance in pancreatic cancer cells

Candidate: Valeria Bincoletto

Supervisor: *Prof.* Silvia Arpicco

Coordinator: *Prof.* Roberta Cavalli

Academic Years: 2021/2022-2022/2023-2023/2024

Scientific sector: 03/CHEM-08

Revisors: *Ch.ma Prof.ssa* Genta Ida, *Ch.mo Prof.* Caviglioli Gabriele

Evaluators: *Ch.ma Prof.ssa* Genta Ida, *Ch.mo Prof.* Caviglioli Gabriele

To my Grandparents

“Strength is measured by how often
we rise, not how rarely we fall”.

Table of Contents

Abstract

Nanomedicine represents a promising strategy to enhance the therapeutic potential of conventional drugs through the design of advanced drug delivery systems. Pancreatic cancer remains one of the most aggressive cancers, with a poor prognosis due to late diagnosis and resistance to chemotherapy. The aim of this work was the development of nanocarriers for the targeted and efficient delivery of gemcitabine (GEM) and its prodrugs (GEM-C12 and GEM-C18), with the goal of overcoming drug resistance and enhancing GEM therapeutic efficacy in pancreatic cancer.

In the first part of the project, carbon nano-onions (CNOs) were covalently functionalized with hyaluronic acid (HA) to selectively target CD44-overexpressing pancreatic cancer cells. These nanocarriers exhibited excellent biocompatibility and selective uptake in $CD44^+$ pancreatic cancer cell lines. CNOs were successfully loaded with GEM-C12 and GEM-C18, which showed strong cytotoxic activity even in GEM-resistant pancreatic cancer cells, with enhanced efficacy when delivered *via* the nanocarrier.

In the second part, mixed micelles based on PEG-DSPE and HA-phospholipid conjugate (HA-DPPE) were developed to encapsulate GEM-C18. Mixed micelles demonstrated suitable physico-chemical characteristics, high encapsulation efficiency, and specific uptake by $CD44^+$ cells. The presence of HA enabled active targeting without compromising micelle structure.

The third part of the work included a literature review of current and emerging therapeutic strategies in pancreatic cancer, highlighting the limitations of standard chemotherapy regimens and exploring the potential of drug repurposing. In this context, the combination of GEM with disulfiram (DSF), a repurposed ALDH inhibitor, emerged as a promising approach to enhance cytotoxicity and overcome resistance mechanisms.

Finally, two different liposomal formulations were developed to encapsulate either GEM or its prodrug GEM-C18. Both systems were characterized for their physico-chemical properties and *in vitro* release profiles. While the free drugs in combination with DSF demonstrated a significant increase in cytotoxicity in resistant pancreatic cancer cells, further studies are needed to confirm whether the liposomal formulations can replicate or enhance this synergistic effect. Nevertheless, their physico-chemical properties and controlled release profiles support their potential for combination therapy.

Overall, this work presents complementary nanomedicine approaches to improve drug delivery and therapeutic outcomes in pancreatic cancer, offering promising strategies to overcome the limitations of conventional treatments.

Introduction

1. Pancreatic cancer

Pancreatic cancer, particularly the form known as pancreatic ductal adenocarcinoma (PDAC), is characterized by its aggressiveness and high mortality rate. In fact, the five-year survival rate is less than 10% [1]. The disease progresses silently in many cases and often goes undetected until it has spread to other organs. This, coupled with the fact that symptoms often do not manifest until the disease is already in a late stage, poses significant challenges to early detection and effective treatment. A distinguishing feature of pancreatic cancer is its tendency to metastasize rapidly to distant organs, often before the onset of symptoms, which further complicates early intervention [2]. The deep anatomical location of the pancreas represents a significant challenge in the context of routine screening, underscoring the need for effective biomarkers to facilitate early detection [3].

In the contemporary clinical context, surgical intervention, in conjunction with chemotherapy and radiation therapy, constitutes the primary therapeutic modality for pancreatic cancer [4]. Amongst the chemotherapeutic agents employed in clinical praxis, gemcitabine (GEM) has emerged as the prevailing standard. GEM is a nucleoside analog which enters cells *via* nucleoside transporters and needs to be phosphorylated to its active forms to fulfil its function. Concurrently, combination therapies comprising other chemotherapeutic agents, such as 5-fluorouracil, irinotecan, leucovorin, and oxaliplatin (FOLFIRINOX) and nanoparticle albumin-bound paclitaxel (nab-paclitaxel), have been introduced with the aim of enhancing clinical outcomes [5, 6]. Nab-paclitaxel is a formulation of the chemotherapy drug paclitaxel bound to albumin nanoparticles (of around 130 nm in size). This improves drug solubility, enhances delivery to the tumor *via* the albumin transport mechanism, and reduces the need for toxic solvents. Nab-paclitaxel helps to break down stromal barriers (such as desmoplastic tissue), making it easier for GEM to penetrate and accumulate in the tumor. It may also inhibit cytidine deaminase, the enzyme that breaks down GEM, thereby increasing its intracellular concentration [7]. Since its approval, the nab-paclitaxel + gemcitabine regimen has become the standard first-line treatment for patients with advanced or metastatic pancreatic cancer, particularly in those who are ineligible for more aggressive regimens such as FOLFIRINOX. On the other hand, FOLFIRINOX is significantly more effective than GEM monotherapy in terms of survival and response rate. It attacks cancer cells through multiple mechanisms: i) 5-FU disrupts DNA and RNA synthesis; ii) irinotecan inhibits topoisomerase I, preventing DNA replication; iii) oxaliplatin forms DNA cross-links, damaging the DNA structure; iv) leucovorin enhances the effect of 5-FU. Nevertheless, FOLFIRINOX is associated with a

higher degree of toxicity in comparison to alternative treatment options and is not universally appropriate for all patients. Common adverse effects include neutropenia, febrile neutropenia, diarrhea, nausea, vomiting, peripheral neuropathy (from oxaliplatin), fatigue, mucositis, and weight loss. To enhance the tolerability of the treatment, modified FOLFIRINOX (mFOLFIRINOX) with reduced doses is frequently employed in clinical practice [8].

Furthermore, targeted therapies, which are directed towards specific molecular pathways driving tumor progression, have been developed. However, these have demonstrated only limited success [9]. Moreover, immunotherapy, a field which has undergone rapid development in the treatment of other cancers, is still in its initial stages for pancreatic cancer and has met with disappointing results in clinical trials [10]. Despite these advancements, the overall prognosis for pancreatic cancer patients remains poor, underscoring the urgent need for novel therapeutic strategies.

A significant challenge in the management of pancreatic cancer is the inherent and acquired resistance to chemotherapy, which is attributable to the dense stromal microenvironment of PDAC tumors. This microenvironment is characterized by extracellular matrix components and cancer-associated fibroblasts, which contributes to poor drug delivery and limits the effectiveness of chemotherapies [11]. The complexity of the genetic profile of pancreatic tumors, in which various resistance mechanisms are frequently activated, further complicates treatment strategies. These include the upregulation of drug efflux pumps (e.g., P-glycoprotein) [12], mutations in key tumor suppressor genes (e.g., TP53) [13], and dysregulation of DNA repair pathways [14]. Consequently, these factors contribute to frequent relapses and the inability to achieve long-term survival, even with aggressive treatment regimens [15].

To address the challenges currently being faced in the management of pancreatic cancer, several new treatments are currently in clinical trials. Immunotherapy approaches, such as immune checkpoint inhibitors (e.g. pembrolizumab and nivolumab), are being tested in combination with traditional therapies to enhance the immune response against pancreatic tumor cells [16]. Notably, studies on tumor-infiltrating lymphocytes and CAR-T cell therapies are in their early phases, but have shown promising results in preclinical studies, suggesting that these could enhance immune-mediated tumor destruction [17]. Additionally, vaccines targeting specific tumor antigens, such as the GVAX vaccine, are under investigation for their potential to stimulate a more effective immune response. GVAX is an investigational therapeutic cancer vaccine, rather than a preventative one. Its objective is to

stimulate the patient's immune system to recognize and attack pancreatic cancer cells. Its composition for pancreatic cancer consists of irradiated allogeneic pancreatic tumor cells that have undergone genetic modification to secrete granulocyte-macrophage colony-stimulating factor. This cytokine helps recruit and activate antigen-presenting cells (such as dendritic cells), which are essential for initiating an immune response [18]. Within the domain of research, there is a promising avenue that has emerged. This pertains to the utilization of PARP inhibitors, including olaparib, in tumors exhibiting defects in DNA repair mechanisms, particularly those that harbor BRCA1/2 mutations. Clinical trials are underway to assess the efficacy of these agents in combination with chemotherapy or other targeted therapies [19, 20]. Moreover, there has been rigorous testing on targeted therapies that inhibit key molecular pathways, including the KRAS signaling pathway. This pathway is frequently mutated in PDAC. For instance, agents that target KRAS G12C mutations (e.g., adagrasib and sotorasib) have shown early promise in preclinical models and are currently entering clinical trials for patients with PDAC [21]. Moreover, nanomedicine approaches are being explored with a view to improving drug delivery and overcoming the dense tumor stroma. Nanoparticle-based delivery systems have been developed for the more effective targeting of PDAC cells, ensuring higher drug concentrations in the tumor while minimizing off-target effects. The use of nanoparticles to deliver chemotherapeutic agents or targeted therapies, including small RNA molecules or gene editing tools, has been demonstrated to hold significant potential in overcoming drug resistance and improving therapeutic outcomes [22-24].

Metabolic reprogramming represents a dynamic domain of research that holds considerable promise for the development of new therapeutic interventions targeting the metabolic vulnerabilities of PDAC cells. These interventions involve the inhibition of specific enzymes implicated in glycolysis or the pentose phosphate pathway, a process that has been the focus of recent research [25]. Furthermore, investigations are currently underway into the capacity of cell-based therapeutic interventions delivered by means of extracellular vesicles to target the tumor microenvironment and disrupt the communication between malignant cells and surrounding stromal components [26].

These innovative therapeutic interventions, which are currently undergoing clinical evaluation, have generated a renewed optimism for enhancing the efficacy of PDAC treatment. They exemplify novel approaches to addressing the resistance mechanisms that limit the effectiveness of existing therapeutic modalities, thereby offering a more personalized and effective strategy for combating this deadly disease.

2. Nanomedicine

The advent of nanotechnology has deeply transformed several disciplines of science, facilitating advancements in different fields. The domain of nanoscience encompasses a wide array of research, including the study of structures, devices and systems that exhibit distinctive characteristics and functionalities. These properties are a consequence of the nanoscale arrangement of atoms, with a diameter ranging from 1 to 100 nm. The emergence of nanoscience has been met with a heightened level of public awareness, accompanied by a surge in controversies in the early 2000s. Concurrently, this period also witnessed the inception of commercialized applications of nanotechnology. The field of nanotechnologies has had a profound impact on different scientific disciplines, including physics, materials science, chemistry, biology, computer science, and engineering. A notable development in recent years has been the application of nanotechnologies in the field of human health, with particularly encouraging results in cancer treatment [27, 28]. The field of nanomedicine has undergone a paradigm shift with the advent of these novel entities, which have been shown to possess advantageous properties such as small size, large surface area, and the capacity for customization of surfaces. In comparison with conventional methodologies, these innovations have been demonstrated to enhance the pharmacokinetics and distribution of therapeutic agents [29]. A variety of nanosystems have been developed for the targeted delivery of therapeutic nucleic acids, chemotherapeutic agents, and immunotherapeutic agents. These include lipid-based, polymeric, and inorganic nanoparticles. The evaluation of these nanosystems has been conducted in preclinical studies [30, 31]. Furthermore, some of these nanomedicines have progressed to clinical trials and are currently being utilized in clinical treatments. Since the early 1990s, nano-formulations have been marketed for medical use against cancer. Examples include the polymer-protein conjugate zinostatin stimalamer [32], which was approved in Japan for the treatment of hepatocellular carcinoma. In the intervening period, a plethora of additional nano-formulations have been developed and authorized for medical use by numerous global agencies. Among the nanosystems approved for clinical use, liposomes are the most widely used. These drug delivery systems are biocompatible, biodegradable and have been extensively studied for their bioavailability and biodegradability due to their composition, which makes them similar to the cell membrane. Numerous studies have demonstrated the efficacy of liposomes in the treatment of solid tumors. The use of liposomes has been shown to protect the incorporated molecule from being inactivated following intravenous administration. This, in turn, results in a reduction in accumulation of the anticancer drug in healthy tissues before it reaches the

desired site of action [33]. There are several approved liposomal systems for the delivery of doxorubicin, used in Kaposi's sarcoma, ovarian and breast cancer. The first of these to be approved is Doxil®, which has been on the market in the United States since 1995. It is a pegylated liposomal formulation that exploits the Enhanced Permeability and Retention (EPR) effect to accumulate in tumor tissue, which was marketed as an anti-ovarian cancer drug formulation [34]. Another interesting commercialized liposomal formulation is Vyxeos®, the first formulation specifically approved by FDA for the treatment of acute myeloid leukemia (2017-EMA, 2019-FDA). Vyxeos® is based on the co-encapsulation of two drugs, daunorubicin and cytarabine; daunorubicin works by intercalating into DNA and inhibiting topoisomerase II, while cytarabine inhibits DNA synthesis [35]. For pancreatic cancer treatment, Onvyde® a liposomal formulation of the topoisomerase I inhibitor irinotecan has reached the clinic in 2015. The encapsulation of irinotecan leads to increased drug accumulation at the tumor site via the EPR effect. Onivyde® has been approved for use in combination with fluorouracil and leucovorin for the treatment of metastatic pancreatic cancer following progression on GEM-based therapy. Clinical studies have demonstrated that this formulation improves overall survival and progression-free survival in comparison to conventional irinotecan. Furthermore, it has been shown to mitigate some of the gastrointestinal toxicity that is commonly associated with the free drug [36].

In clinical treatments, antibody-drug conjugates (ADCs) represent a transformative class of targeted cancer therapies that combine the specificity of monoclonal antibodies (Mab) with the cytotoxic potency of chemotherapy. Two HER2-targeted ADCs, Kadcyla® (ado-trastuzumab emtansine) and Enhertu® (trastuzumab deruxtecan), have been approved for clinical use and have demonstrated significant advancements in the treatment of HER2-positive breast cancer [37]. The pharmaceutical compound known as Kadcyla® functions by linking trastuzumab, an antibody directed against the HER2 receptor, to the microtubule inhibitor DM1. This linkage is facilitated by a non-cleavable linker, a synthetic molecule that serves to connect the two drugs. The result of this linkage is that Kadcyla® delivers cytotoxic activity directly to tumor cells that express HER2, while retaining the antibody's anti-HER2 properties [38]. In contrast, Enhertu® utilizes a cleavable linker and a topoisomerase I inhibitor payload (deruxtecan), which facilitates a potent bystander effect and broader antitumor activity, including efficacy in HER2-low tumors. These agents underscore the capacity of ADCs to circumvent resistance mechanisms and broaden the therapeutic scope in the field of oncology [39]. Another ADC is Mylotarg® (gemtuzumab ozogamicin), which comprises a humanized anti-CD33 Mab linked to the cytotoxic agent

N-acetyl gamma calicheamicin. Mylotarg® has been engineered to target CD33, a cell surface antigen expressed on myeloid cells, with the objective of delivering direct cytotoxic effects to malignant cells. It was approved by FDA in 2000 but withdrawn from the US market in 2010 due to safety concerns and lack of survival benefit in clinical trials. It was associated with higher mortality and serious side effects, including veno-occlusive disease. However, it was reintroduced in 2017 with a revised dosing regimen and updated clinical data demonstrating improved safety. Clinical studies have demonstrated its efficacy, with remission rates ranging from 26% to 30% in relapsed AML patients. However, its use is associated with significant adverse effects, necessitating careful patient selection and monitoring [40]. Numerous others are presently in clinics, some examples are summarized in Table 1 [41, 42].

Although nanomedicine holds great promise for the treatment of pancreatic cancer, only a few formulations have been approved for clinical use. One of the most notable examples is Abraxane, a nanoparticle albumin-bound formulation of paclitaxel approved for advanced pancreatic cancer in combination with GEM [43]. This formulation increases the bioavailability of paclitaxel and reduces some of the side effects associated with conventional therapy. Despite progress in nanomedicine research, most nanoparticle-based therapies for pancreatic cancer remain in preclinical or early clinical stages, highlighting the need for further investigation to establish their efficacy and safety in this challenging malignancy.

Table 1 Example of approved nanomedicine drugs in the market for cancer treatment [41, 42].

Material	Drug	Product name	Cancer type	Characteristics (pros and *cons*)	Approval year
Liposome	Doxorubicin hydrochloride	Doxil (Caelyx)	Ovarian cancer and AIDS-related Kaposi's sarcoma	Prolonged drug circulation time and tumor targeting *Long-term administration could predispose female patients to oral squamous cell carcinoma*	1995 (FDA)
	Daunorubicin	DaunoXome	HIV-related Kaposi sarcoma	Slow release into circulation *Cardiotoxicity*	1996 (FDA)
	Doxorubicin	Lipo-Dox	Kaposi's sarcoma, breast and ovarian cancer	Longer half-life and better tolerance *Mild myelosuppression and other nonhematological toxicities*	1998 (Taiwan)
	Doxorubicin	Myocet	Breast cancer	Less cardiotoxicity *Relative instability*	2000 (EMA)
	Muramyl tripeptide phosphatidyl ethanolamine	Mepact	Non-metastatic osteosarcoma	Longer half-life and less toxicity *Chills, fever, headache, myalgias*	2009 (EMA)
	Paclitaxel	Lipusu	Breast cancer, non-small-cell lung cancer	Less toxicity *Nausea, vomiting, dyspnea, peripheral neuritis*	2013 (EMA)

	Cytarabine	Depocyt	Lymphomatous malignant meningitis	Improve delivery and reduce toxicity *Arachnoiditis and neurotoxicity*	1999 (FDA)
	Vincristine	Marqibo	Leukemia	Slow release into circulation *Drug toxicity and adverse side effect*	2012 (FDA)
	Irinotecan	Onivyde	Pancreatic cancer	Enhanced delivery and reduced systemic toxicity *Diarrhea, nausea, vomiting, neutropenia, and febrile neutropenia*	2015 (FDA)
	Daunorubicin and cytarabine	Vyxeos	Acute myeloid leukemia (AML)	Improved overall survival *Febrile neutropenia, fatigue, pneumonia, hypoxia, hypertension, bacteremia, and sepsis*	2017 (EMA)
Lipid nanoparticles	Paclitaxel	DPH107	Advanced gastric cancer	Absorption without the need for P-glycoprotein inhibitors or Cremophor EL *Neutropenia and leukopenia*	2016 (Korea)
Polymeric micelle	Paclitaxel	Genexol-PM	Non-small cell lung cancer	Controlled and targeted drug delivery *Neuropathy, myalgia, and neutropenia*	2006 (South Korea)
	Paclitaxel	Apealea	Ovarian, peritoneal and fallopian tube cancer	Improve progression-free survival in combination with carboplatin *Neutropenia, diarrhea, nausea, vomiting, and peripheral neuropathy*	2018 (EMA)

	Docetaxel	Nanoxel	Breast and ovarian cancers, NSCLC, and AIDS-related Kaposi's sarcoma	Good efficacy and pharmacokinetic properties *Myalgia, nausea, anemia, paresthesia, alopecia, diarrhea, and vomiting*	2006 (India)
Polymeric nanoparticles	Leuprolide acetate	Eligard	Advanced prostate cancer	Controlled release and longer circulation time *Hot flushes followed by malaise/fatigue testicular atrophy, dizziness, gynaecomastia and nausea*	2002 (FDA)
Paclitaxel formulated as albumin bound nanoparticles	Paclitaxel	Pazenir	Metastatic breast cancer, metastatic adenocarcinoma of the pancreas, non-small cell lung cancer	Higher solubility and less toxicity *Affects non-cancer cells such as blood and nerve cells*	2019 (EMA)
	Paclitaxel	Abraxane	Various cancers including metastatic and pancreatic cancers	Higher solubility *Non-specific binding of paclitaxel to albumin*	2005 (FDA)
Hafnium oxide nanoparticles	Hafnium oxide nanoparticles stimulated with external radiation to enhance tumor cell death via electron production	NBTXR3 (Hensify)	Locally advanced squamous cell carcinoma	Radiotherapy enhancer *Injection site pain, hypotension, and radiation skin injury*	2019 (CE Mark)

Nanoparticles of superparamagnetic iron oxide coated with amino silane	Fe_2O_3	NanoTherm	Glioblastoma	High blood circulation time, tumor uptake and theranostic properties *Moderate adverse effect*	2013 (EMA)
Drug-antibody conjugates	Brentuximab vedotin and Auristatin Derivative MMAE	Adcetris (SGN-35)	CD30 Anaplastic Large Cell Lymphoma	Shown to improve progression-free survival in frontline and post-transplant settings *Peripheral neuropathy*	2011 (FDA)
	Gemtuzumab ozogamicin and Calicheamicin (DNA targeting)	Mylotarg	CD33 Acute Myelogenous Leukemia	Improves event-free survival in combination, can be used in adults and children *myelosuppression*	2017 (FDA)
	Trastuzumab, covalently linked to DM1 via the stable thioether linker MCC	Kadcyla	HER2+ breast cancer	High blood circulation time, selectivity and less toxicity *Nausea, fatigue, thrombocytopenia, headache, constipation, diarrhea, elevated liver enzymes, anorexia, and epistaxis*	2013 (FDA, EMA)
	Inotuzumab ozogamicin and *N*-acetyl-γ Calicheamicin	Besponsa	CD22 Acute Lymphoblastic Leukemia [6]Non-Hodgkin's Lymphoma	Can be used to reduce tumor burden before allogeneic stem cell transplantation (allo-HSCT) *Risk of veno-occlusive disease, neutropenia, thrombocytopenia, and anemia*	2017 (FDA)
	Trastuzumab deruxtecan and deruxtecan/Camptothecin	Enhertu	HER2+ breast cancer	High overall response rates, even in HER2-low breast cancer *Interstitial lung disease, nausea, and fatigue*	2019 (FDA)

PEGylated conjugate	l-Asparaginase	Oncaspar	Acute lymphoblastic leukemia	Improved stability of drug loading *Venous thromboembolism, pancreatitis, and hyperglycemia*	2006 (FDA)
Gel containing 5-aminolevulinic acid, E211, SoyPC, and PG	5-Aminolevulinic acid	Ameluz	Superficial and/or nodular basal cell carcinoma	Sustained release and low toxicity *Transient pain and erythema*	2011 (EMA)
Recombinant DNA derived cytotoxic protein	Denileukin diftitox	Ontak	Cutaneous T cell lymphoma	Targeted delivery *Acute hypersensitivity-type reactions, asthenia, nausea/vomiting*	1999 (FDA)
Polymer protein conjugate	Styrene maleic anhydride neocarzinostatin (SMANCS)	Zinostatin stimalamer	Primary unresectable hepatocellular carcinoma	Enhanced accumulation *Slightly toxic (liver dysfunction)*	1994 (Japan)

3. Active targeting strategies in nanomedicine

Nanomedicine, a multidisciplinary field, utilizes nanoscale materials and systems to enhance the diagnosis, treatment, and monitoring of diseases. A significant potential lies in the development of nanocarriers capable of delivering therapeutic agents with greater precision and efficiency to diseased tissues, particularly tumors [44]. Conventional chemotherapeutic agents frequently exhibit systemic toxicity and inadequate selectivity, resulting in substantial side effects and suboptimal therapeutic outcomes. The utilization of nanocarriers provides a promising avenue for enhancing drug solubility, extending circulation time, and modulating drug release. However, to achieve efficient and site-specific drug accumulation, targeting strategies are interesting [45]. Nanocarriers can reach tumor tissues through two main mechanisms.

1. Passive targeting utilizes the EPR effect, a phenomenon characterized by the accumulation of nanoparticles in tumor tissues due to compromised vasculature and inefficient lymphatic drainage. While this phenomenon enables the initial localization of tumors, it exhibits a lack of specificity at the cellular level and can demonstrate substantial inter-tumor and patient variability [46].
2. Active targeting is a process that involves the functionalization of nanocarriers with ligands that have the ability to specifically bind to receptors that are overexpressed on target cells. This receptor-mediated endocytosis results in the subsequent intracellular delivery of the therapeutic agent. The employment of this strategy has been demonstrated to enhance the specificity of the delivery system, thereby increasing therapeutic efficacy while simultaneously reducing systemic side effects [47].

3.1 Principles of active targeting

Active targeting relies on the specific interaction between a ligand—either covalently or non-covalently anchored to the nanocarrier surface—and a receptor that is overexpressed or uniquely present on diseased cells. This binding event triggers receptor-mediated endocytosis, enabling the internalization of the nanocarrier and the subsequent intracellular delivery of its therapeutic payload [48]. Key requirements for effective active targeting include: i) overexpression of the receptor in the target tissue and low expression in healthy tissues; ii) high affinity and specificity of the ligand-receptor interaction; iii**)** surface accessibility of the ligand on the nanocarrier; iv) preservation of nanoparticle stability and functional properties after ligand conjugation [49].

A wide range of targeting ligands has been employed in nanomedicine, each with distinct advantages and challenges.

Mab are among the most widely used ligands for active targeting, thanks to their high affinity and specificity for a wide range of cellular receptors. Their clinical use is well established, and they have been successfully applied in both diagnostics and therapeutics. However, Mab relatively large molecular size can limit its diffusion within tissues, thereby negatively affecting its pharmacokinetics. This, in turn, may result in a reduction in tumor penetration. Furthermore, the administration of Mab has been observed to elicit immune responses in some cases, and the production costs associated with their development are often substantial [50]. To overcome these limitations, several engineered antibody derivatives -such as fragment antigen-binding region (Fab), single-chain variable fragments (scFv), and nanobodies (VHH domains)- have been introduced [51, 52]. These smaller formats preserve the high specificity of full-length antibodies, while improving tissue penetration, lowering immunogenicity, and offering increased flexibility for chemical conjugation to nanocarrier surfaces [53, 54].

Peptides, which are composed of short amino acid sequences, can be rationally designed to selectively bind to specific cellular receptors. Examples of such receptors include integrins—particularly αvβ3, which is commonly targeted using the RGD motif—and vascular endothelial growth factor (VEGF) receptors. Their small molecular size has been demonstrated to enable deep tumor penetration and efficient diffusion within tissues. Furthermore, peptides generally exhibit low immunogenicity and offer distinct advantages in terms of ease of synthesis and chemical modification [55]. However, these molecules generally exhibit reduced binding affinity in comparison to antibodies and are susceptible to enzymatic degradation within biological environments. These limitations can be mitigated through structural modifications, such as the incorporation of D-amino acids or peptide cyclization, which enhance stability and biological half-life [56, 57].

Aptamers are defined as single-stranded DNA or RNA oligonucleotides that fold into specific three-dimensional structures, capable of binding molecular targets with high affinity and specificity. These structures are synthetically produced, cost-effective, and exhibit low immunogenicity, making them suitable for biomedical applications. Their diminutive proportions facilitate effective penetration of the tissue, and their malleability allows for straightforward modification. However, aptamers are susceptible to degradation by nucleases *in vivo*, necessitating structural optimization to ensure stability and functionality

[58]. A notable example is the AS1411 aptamer, which targets nucleolin, a protein overexpressed in several cancer types [59].

The use of small ligands such as folic acid, galactose, and mannose has emerged as a prevalent approach in targeted receptor modulation, particularly in the context of overexpressed receptors on specific cell types. Folic acid has been observed to bind folate receptors in various types of cancer, while galactose has been shown to target ASGPRs in hepatocytes. These ligands are characterized by their stability, cost-effectiveness, and lack of immunogenicity. However, they generally exhibit reduced binding affinity and may be internalized by non-target cells that express basal receptor levels [60, 61].

Natural polymers such as hyaluronic acid (HA) and dextran are frequently utilized as targeting ligands due to their high affinity for specific receptors. It has been demonstrated that HA binds to CD44 receptor, which is frequently overexpressed in tumors and cancer stem cells. In contrast, dextran has been shown to target scavenger receptors found on both macrophages and liver cells. These ligands possess both biocompatible and biodegradable properties, thereby enabling their utilization in both structural and targeting roles [62].

The selection of a targeting ligand is of pivotal significance in the design of actively targeted nanocarriers. A specific ligand typology offers a certain combination of advantages and limitations. These should be methodically evaluated based on the biological target, the context of the disease, and the physicochemical properties of the delivery system. As targeting strategies continue to evolve, the integration of multiple ligands, stimuli-responsive mechanisms, and personalized receptor profiles will presumably drive the next generation of precision nanomedicines [63]. Within the field of nanomedicine, active targeting represents a rational and highly promising approach to enhance both the selectivity and therapeutic efficacy of drug delivery systems. By exploiting specific receptor–ligand interactions, this strategy enables the overcoming of key limitations associated with conventional chemotherapy, allowing for controlled, cell-specific delivery of therapeutic agents. The functionalization of nanocarriers with targeting moieties—such as HA, which binds selectively to CD44 receptors—has facilitated the development of multifunctional platforms with enhanced precision. In oncological applications, such targeted systems offer the dual advantage of increased drug accumulation at the tumor site and reduced systemic toxicity, thereby improving the overall therapeutic index [49].

3.2 Hyaluronic acid

HA, or hyaluronan, is a naturally occurring linear polysaccharide composed of repeating

disaccharide units of D-glucuronic acid and N-acetyl-D-glucosamine. These monomers are connected via alternating β-1,4 and β-1,3 glycosidic linkages, resulting in a high-molecular-weight polymer that can reach several million Da. Unlike other glycosaminoglycans (GAGs), HA is non-sulfated and is synthesized at the plasma membrane by hyaluronan synthases (HAS1, HAS2, and HAS3), bypassing the Golgi apparatus [64]. The unique physico-chemical characteristics of HA-specifically its pronounced hydrophilicity, viscoelasticity, and capacity for hydrogen bonding-stem from its linear structure and abundance of hydroxyl and carboxyl functional groups. These features enable strong interactions with water and biological macromolecules, endowing HA with exceptional water retention and space-filling properties that are critical for its physiological roles in tissue hydration, lubrication, and structural integrity [65].

HA is abundantly distributed throughout the human body and constitutes a fundamental component of the extracellular matrix (ECM), particularly within connective tissues, synovial fluid, the vitreous humor, and the dermis. It plays crucial roles in a variety of physiological processes, including: i) tissue hydration and lubrication, owing to its remarkable water-binding capacity; ii) regulation of cell migration and proliferation, particularly during wound healing and tissue remodeling; iii) angiogenesis and morphogenesis, mediated by interactions with cell surface receptors and other ECM components; iv) modulation of inflammatory responses, where HA fragments of varying molecular weights can exert either pro- or anti-inflammatory effects [66]. *In vivo*, HA is continuously synthesized and degraded, with its turnover tightly regulated by the coordinated activity of hyaluronan synthases and hyaluronidases. Importantly, the biological activity of HA is strongly influenced by its molecular weight: high-molecular-weight HA is generally associated with anti-inflammatory and immunosuppressive properties, whereas low-molecular-weight HA and its oligomeric forms are known to promote inflammation, stimulate angiogenesis, and enhance cell proliferation [67].

One of the most relevant features of HA in the context of targeted drug delivery is its ability to bind selectively to specific cell surface receptors. Of these, CD44 is the most extensively studied. This transmembrane glycoprotein is critical for interactions between cells and the surrounding extracellular matrix, as well as for cell adhesion and migration. CD44 exists in multiple isoforms resulting from alternative splicing and is notably overexpressed in a variety of malignancies, including breast, ovarian, colorectal, and pancreatic cancer [68, 69]. In addition to CD44, several other HA-binding receptors have been identified:

1. receptor for HA-mediated motility (RHAMM): critical component of the regulatory network that governs cell migration and intracellular signaling pathways
2. lymphatic vessel endothelial HA receptor (LYVE-1): mainly expressed in the lymphatic endothelium and is implicated in lymphatic trafficking
3. HA Receptor for endocytosis (HARE): involved in systemic HA clearance and is involved in HA turnover in the liver and lymphoid tissues [70].

Among these, CD44 remains the most widely exploited target in nanomedicine, primarily due to its high expression levels in tumor cells and cancer stem cell populations. Its selective interaction with HA has been strategically employed to engineer receptor-mediated drug delivery systems, with the objective of enhancing the specificity and efficacy of anticancer therapies [71].

3.2.1 Hyaluronic acid as targeting ligand in nanomedicine

The high binding affinity of HA for CD44 has established it as a widely utilized ligand for the surface functionalization of nanocarriers aimed at the active targeting of cancer cells [72]. Functionalization of nanosystems—such as liposomes, polymeric micelles, dendrimers, or nanoparticles—with HA has been shown to enhance selective accumulation at tumor sites and to promote receptor-mediated endocytosis in CD44-overexpressing cells. The HA-mediated targeting mechanism relies on two fundamental steps: i) specific recognition and binding of HA to CD44 receptors expressed on the tumor cell surface; ii) receptor-mediated internalization of the HA-decorated nanocarrier, facilitating intracellular drug delivery [73].

This strategy offers several advantages, including enhanced cellular uptake by target cells, reduced off-target toxicity owing to the lower CD44 expression in normal tissues, prolonged systemic circulation due to HA's hydrophilic and stealth-like properties, and favorable safety characteristics such as biodegradability and low immunogenicity [74]. Notably, the molecular weight of HA plays a critical role in modulating targeting efficiency. High-molecular-weight HA generally exhibits stronger and more stable interactions with CD44. However, it can also influence key physicochemical properties of the nanocarrier, including but not limited to particle size, colloidal stability, and drug release kinetics. Therefore, careful tuning of HA's molecular weight is essential during the design and optimization of HA-functionalized delivery systems to achieve the desired balance between targeting performance and formulation stability [62].

The chemical structure of hyaluronic acid (HA) provides multiple functional groups-carboxyl, hydroxyl, and N-acetyl moieties-that can be exploited for chemical modification without substantially altering its intrinsic biological activity. These functional handles have been widely utilized to introduce a variety of chemical entities, enabling:

- covalent conjugation of therapeutic agents, typically via esterification or amidation reactions
- binding to hydrophobic moieties such as lipids or polymers, facilitating the incorporation of HA into amphiphilic systems including micelles and liposomes
- crosslinking for the formation of HA-based hydrogels or injectable depots for sustained drug release [75].

A significant focus has been placed on the synthesis of HA–lipid conjugates, which facilitate the stable incorporation of HA into the lipid bilayer of nanocarriers. This configuration ensures the surface presentation of the HA chains, thereby enhancing the likelihood of receptor-mediated interactions with CD44 and improving the targeting specificity of the delivery system [76].

4. Inorganic nanosystems

In recent years, a considerable number of nanosystems have been developed for the treatment of cancer. Among all the drug delivery systems that have been the subject of study, inorganic nanosystems have seen a notable increase in interest, particularly in terms of their application in various fields of medicine. They include carbon [77], gold [78], iron oxide [79] and silica nanoparticles [80]. One of the salient properties of these nanosystems pertains to the surface plasmon resonance phenomenon. This phenomenon enables the conversion of light into heat by inorganic particles, with the subsequent scattering of this heat leading to the destruction of cancer cells through the irradiation of nanoparticles. Furthermore, the surface functionalization of inorganic nanoparticles engenders enhanced biocompatibility and versatility, rendering these systems highly promising for utilization in biomedical applications [81]. In the preceding decade, a substantial volume of research has been conducted on carbon-based nanoparticles, which represent one of the most widely utilized categories of nanomaterials. These carbon-based nanoparticles have the potential to substitute conventional therapeutic modalities, to counteract drug resistance, and to facilitate novel approaches for concurrent treatment and diagnosis [82, 83].

4.1 Carbon-based nanosystems

Carbon nanosystems represent a class of materials that have garnered significant attention in the fields of diagnosis and treatment. The unique properties of these particles, which include their high surface-to-volume ratio, ease of surface modification, and capacity for loading diverse therapeutic and imaging agents, have led to their consideration as promising candidates for a range of applications. These particles include graphene, fullerenes, and carbon nanotubes, which have demonstrated remarkable properties that make them ideal for various biomedical applications [84]. Nevertheless, it is important to note that many challenges remain that require further and extensive studies. These challenges encompass reduced toxicity, optimal dimensions, and enhanced biodegradability. A significant disparity persists between laboratory research and clinical translation, underscoring the necessity for further research and development in this field. Notably, the biodegradability and metabolism of carbon nanomaterials represent substantial challenges in this field [85-87].

4.1.1 Classification of carbon-based nanosystems

Given the considerable heterogeneity of carbon nanomaterials regarding size, shape, composition, etc., there are numerous possible classifications [88]. In general, researchers

are commonly used to classify carbon nanomaterials into 0-dimensional, 1-dimensional and 2-dimensional carbon nanomaterials according to their spatial dimension characteristics (Figure 1). It has been determined that carbon nanotubes are categorized within the family of one-dimensional nanomaterial. Conversely, carbon nanodiamonds and carbon nano-onions are classified as zero-dimensional nanomaterials [89].

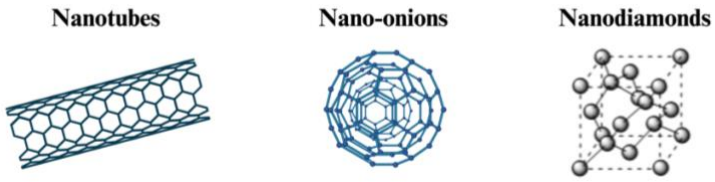

Figure 1. Carbon-based nano drug delivery systems (created with Biorender).

Carbon nanotubes (CNTs) are a distinctive type of one-dimensional carbon nanomaterial that possess an exceptional hollow tubular morphology, with a hemispherical fullerene structure serving as a cap. The generation of nanotubes is predominantly accomplished by the bottom-up method [90]. CNTs can be composed of single-layer or multilayer carbon atomic structures, according to which they can be divided into single-walled CNTs (SWCNTs) and multiwalled CNTs (MWCNTs) [91]. Since the first discovery and subsequent reporting on the subject, carbon nanotubes have been the focus of intensive research in the domain of carbon nanomaterials. The exploration of their physical and chemical properties is ongoing, and the development of their industrial macro-scale preparation and related application fields is a current focus [92-94].

Nanodiamonds (NDs) with a diameter smaller than 100 nm are regarded as zero-dimensional carbon nanomaterials [95]. In NDs, carbon atoms are primarily sp3-hybridised and arranged in a cubic crystal structure known as a diamond lattice [96]. Imperfections and defects in this structure may take the form of interstitial impurities or vacancies, which can give NDs properties that are very different from those of other carbon nanosystems [97-99]. Among the various defects, numerous negatively charge nitrogen-vacancy (N-V) defects have the function of acting as fluorescent emission centers. It is due to these centers that application as fluorescent sensors for quantum information processing, specific sensing and bioimaging is possible for NDs [100-102].

Carbon nano-onions (CNOs), a recent and widely studied class of carbon nanostructure, were discovered in 1980 by Iijima *et al.* [103] and subsequently defined in 1992 by Ugarte *et al.* [104]. CNOs consist of concentric, multilayered, closed nanographene shells that

enrobe one another around a fullerene inner core, forming a structure that bears a resemblance to an onion. Morphologically, CNOs are positioned between fullerenes and multiwall nanotubes, and they have a low density and high surface-area-to-volume ratio [105]. The diameter of CNOs typically ranges from 2 to 100 nm [106]. The distinctive onion-like structural arrangement of CNOs is known to result in the presence of small graphitic sp2-hybridised carbon atoms and a notable degree of localization of π-electrons [107]. Recent investigations have highlighted the potential of CNOs as nanocarriers in drug delivery systems. This growing interest can be attributed to unique properties that CNOs offer over traditional drug delivery systems. Notably, their biocompatibility has been validated through extensive *in vitro*, *in vivo*, and *ex vivo* studies [108-110]. CNOs production is known to require a rigorous process, resulting in a product of high purity and narrow polydispersity, obviating the necessity for any subsequent removal of catalysts, as is often the case in the synthesis of nanotubes. Moreover, their high stability further reduces the requirement for specialized storage conditions. Another advantage of CNOs is their ease of functionalization. The large sp^2 hybridized carbon surface allows for functionalization with various moieties, enabling CNOs to be tailored for a wide range of applications. However, a significant challenge regarding CNOs pertains to their limited dispersibility, but this can be mitigated through the employment of specific solvents and surfactants [111-113].

Several studies have explored the use of CNOs for targeted drug delivery. It has been observed that most research conducted thus far on CNOs in the field of drug delivery is of recent origin, signifying a rapidly escalating degree of interest in this domain. The versatility and promising applications of CNOs underscore their viability as a leading candidate for future nanocarrier technologies [114-116].

4.1.2 Functionalization of carbon-based nanosystems surface

The surface functionalization of carbon-based nanomaterials is a critical step in enhancing their solubility, stability, biocompatibility, and targeting capabilities in biomedical applications. Pristine carbon nanostructures, including CNTs, graphene derivatives, and CNOs, possess an intrinsic hydrophobic nature and are susceptible to aggregation in aqueous environments. This necessitates surface modifications to enhance their dispersion and biological performance [117].

Functionalization strategies are broadly categorized into two approaches: covalent and non-covalent. Each of these categories offers distinct advantages and limitations [118].

Covalent functionalization is defined as the process of forming stable chemical bonds between functional groups and the carbon surface. This is typically achieved through oxidative treatments (e.g., with nitric or sulfuric acid) that introduce carboxyl and hydroxyl groups onto the surface. These moieties can then undergo further modification via amide or ester formation, carbodiimide coupling, or click chemistry, allowing the covalent attachment of drugs, polymers, or targeting ligands [119]. For instance, carboxylated CNTs have been conjugated with PEG to enhance biocompatibility and circulation time in drug delivery systems [92, 120]. In a similar manner, graphene oxide has been modified with amine-terminated molecules to enable the attachment of anticancer drugs [121]. Covalent strategies have been demonstrated to provide enhanced stability and control over surface chemistry. However, these strategies have also been observed to disrupt the sp^2-hybridized π-conjugated network, which may potentially affect the electronic and optical properties of the nanomaterial [122].

Conversely, non-covalent functionalization maintains the structural integrity and electronic properties of the carbon core. The observed phenomenon is attributable to weaker interactions, including π–π stacking, van der Waals forces, hydrophobic interactions, and electrostatic adsorption. Non-covalent agents that are frequently utilized include surfactants (e.g., SDS, Pluronic), biopolymers (e.g., chitosan, dextran), and aromatic molecules (e.g., pyrene derivatives), which adsorb onto the surface without altering the carbon framework [123]. For instance, SWCNTs have been non-covalently functionalized with DNA strands for biosensing applications [124]. Furthermore, graphene oxide has been coated with PEG through π–π interactions to enhance its solubility and facilitate the loading of hydrophobic drugs. This method enables reversible modification and facile substitution of surface functionalities; however, it may exhibit reduced stability under physiological conditions in comparison to covalent approaches [125].

The choice between covalent and non-covalent functionalization depends on the intended biomedical application. Covalent strategies are preferred for stable, long-term modification and controlled ligand attachment, particularly for drug delivery and active targeting. In scenarios where preserving the inherent electronic or optical properties of a specimen is paramount, such as in imaging or sensing applications, non-covalent methodologies emerge as advantageous. In this context, a hybrid approach integrating both methods has emerged as a strategy to optimize the balance between stability and functional performance [126].

5. Lipid nanosystems

The employment of lipid-based nanoparticles as carriers has emerged as a promising approach due to their favorable physicochemical properties, with specific applications and strengths that are particularly useful in the delivery of chemotherapeutic agents [28]. The typical lipid-based drug delivery nanosystems consist of liposomes, lipid nanoparticles (LNPs), solid lipid nanoparticles (SLNs), nanostructured lipid carriers (NLCs), nanoemulsions, and hybrid lipid nanoparticles [127, 128]. Lipid-based drug delivery systems offer several advantages over alternative delivery mechanisms, including enhanced solubility, bioavailability, and cellular uptake. This property allows for the loading of both hydrophilic and hydrophobic drugs, thereby ensuring the versatility and effectiveness of these delivery systems as carriers for therapeutic agents. In addition to these properties, lipid-based delivery systems can offer protection to drugs from degradation, controlled release, and potential targeting to specific tissues or cells, thus increasing therapeutic efficacy [129-131].

5.1 Classification of lipid-based nanosystems

The classification of lipidic nanosystems can be undertaken based on their internal structure (Figure 2).

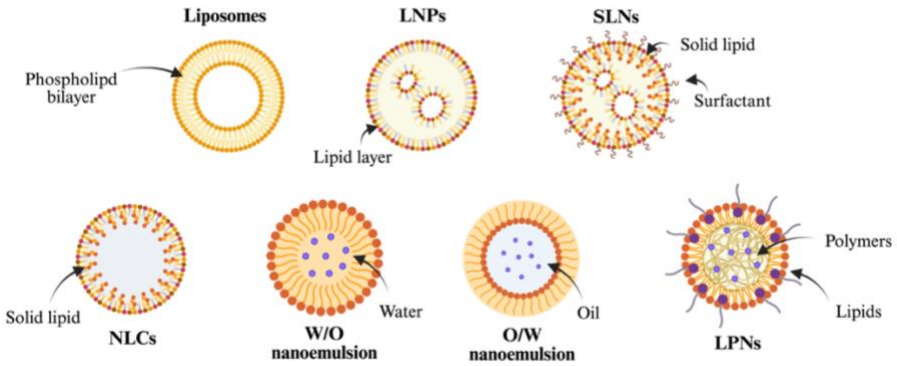

Figure 2. Lipid-based nano drug delivery systems (created with Biorender).

In recent years, liposomes have emerged as the most prevalent and extensively researched drug delivery system [132]. Liposomes can be defined as bilayer vesicle structures consisting of an aqueous-phase core encapsulated by a bilayer of lipids that display special biocompatibility, high encapsulation rate, and good biodegradability. These structures provide both hydrophilic and lipophilic compounds with a convenient means of encapsulation, thereby facilitating co-administration of drugs [133]. In the field of drug delivery, liposomes exhibit enhanced transport and uptake capabilities, thereby prolonging

the circulation time of drugs *in vivo*, extending the half-life, and mitigating adverse effects in comparison to free drugs [134-137].

Another class of lipid-based nanosystem is constituted of lipid-based nanoparticles (LNPs), which represent a highly adaptable class of nanocarriers. LNPs have seen considerable usage in medical research and pharmacology [138]. Their ability to encapsulate a diverse array of therapeutic agents, encompassing small molecules, nucleic acids, and monoclonal antibodies, renders them highly versatile for a variety of applications. LNPs are typically composed of cationic or ionizable lipids, which facilitate interactions with negatively charged nucleic acids, thereby enhancing the capacity for drug loading [139, 140].

Furthermore, solid lipid nanocarriers are a category of lipid-based nanosystems characterized by the exploiting of lipids that possess high biocompatibility and biodegradability, with a melting point that is above 40 °C [141, 142]. This ensures that these nanosystems maintain a solid form at both ambient and body temperatures. These primarily comprise solid lipid nanoparticles (SLN) and nanostructured lipid carriers (NLC). The internal matrix of SLN is characterized by a well-organized 'brick wall' structure, in contrast to the more unstructured configuration observed in NLCs [143, 144].

Another class owing to lipid nanocarriers are nanoemulsions, colloidal systems of reduced size and dimensions that are kinetically stable and serve as carriers for drug molecules. They feature negatively charged, amorphous, and lipophilic surfaces. The classification of nanoemulsions can be categorized into different types: water-in-oil nanoemulsions (W/O) and oil-in-water nanoemulsions (O/W) [145]. The composition of nanoemulsions comprises an oil phase, an aqueous phase, and an emulsifier, with the presence of these components contributing to the stability of the drug-carrying system [146, 147].

Finally, the emergence of lipid-polymer hybrid nanoparticles (LPNs) as a novel nanoplatform for drug delivery has garnered significant attention in the field of nanotechnology. These particles are composed of lipids and polymers, which serve as the fundamental building blocks. LPNs offer several advantages when compared to free drug solutions, including alterations to pharmacokinetics, biodistribution, and toxicity profile of the drug payload. This enhanced physical stability, and biocompatibility can be attributed to the integration of the advantageous properties of biomimetic lipid-based nanoparticles (e.g. SLNs and NLCs) and biocompatible polymeric nanoparticles [148]. The incorporation of lipids has been demonstrated to enhance the capacity for drug loading and permeability across biological membranes, whilst the polymeric composition serves to regulate the release rate of encapsulated drugs [149].

6. Polymer nanosystems

The utilization of polymer-based nanocarriers for targeted drug delivery has witnessed a marked increase in popularity in recent years, owing to the numerous advantages they offer. These include their physicochemical properties, such as non-toxicity, water solubility, and biodegradability. The extensive range of polymers employed in their composition identifies polymer NPs as optimal candidates for the delivery of molecules of a wide type. Furthermore, polymer-based nanosystems can be administered via a variety of routes, including intravenous injection, due to their size [150].

These nanocarriers possess a prolonged circulation time in the bloodstream, thereby reducing the risk of biological clearance. Moreover, these nanocarriers possess the ability to accumulate and remain in tumor locations, and when decorated with receptor-mediated ligands, they can selectively target cancer cells, thereby enhancing their efficacy as anti-cancer agents [151].

6.1 Classification of polymer-based nanosystems

The field of nanotechnology has seen a proliferation of research and development over recent decades, with a particular emphasis on polymer-based nanosystems. The classification of these systems is primarily based on structural, compositional, and functional criteria. The structural classification is centered on the different shapes and forms that polymeric nanosystems can assume (Figure 3).

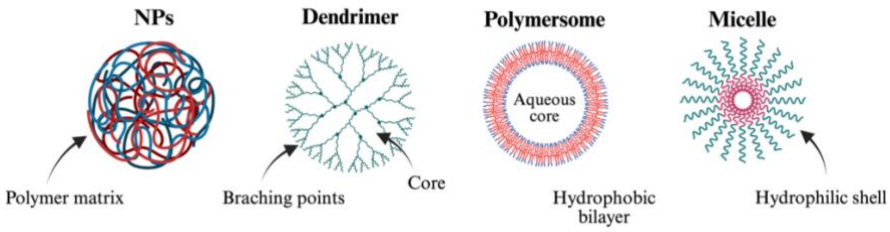

Figure 3. Polymer-based nano drug delivery systems (created with Biorender).

It is noteworthy that each structural category offers distinct advantages, including enhanced stability, controlled release of drugs or other substances, and targeted delivery [152].

Polymeric nanoparticles (NPs) can be defined as solid, nanosized particles which are produced with synthetic or natural polymers, and have the capacity to encapsulate drugs, genes, or other therapeutic agents [153]. Of the polymers utilized in the synthesis of NPs, those that are biodegradable and biocompatible are given preferential selection to minimize

the toxicity of the nanocarrier. These particles can assume a spherical, rod-like or irregular shape [154, 155].

Polymeric dendrimers are defined by their highly branched, tree-like polymer structures, which bear multiple functional groups at their surfaces. They possess a structure comprising layers of repeating monomer units, resulting in a compact and symmetrical nanosystem. The precise encapsulation of drugs or bioactive agents is enabled by their highly controlled structure [156, 157].

Polymersomes have been the focus of significant research due to their potential applications in the field of drug delivery. These vesicular macromolecular assemblies consist of a hydrophobic and a hydrophilic block, with the membrane composed of a bilayer structure. The properties of the polymersomes, including membrane rigidity, fluidity, stability, and responsiveness to external stimuli, are dictated by the chemical composition and length of these blocks [158]. The therapeutic potential of polymersomes has garnered attention in the realm of drug delivery for various conditions, such as cancer, inflammation, and metabolic diseases [159, 160].

Polymeric micelles are composed of amphiphilic block copolymers, which self-assemble in aqueous environments to form micelles. These micelles are endowed with a hydrophobic core, an essential feature for the encapsulation of drugs, in conjunction with a hydrophilic shell, which contributes to their stability in water. Typically, they manifest as spherical in shape, with the hydrophobic drugs and other lipophilic substances being encapsulated within the core [161]. A notable example of this class of polymer-based nanosystem is mixed micelles. These are self-assembled nanostructures formed by combining different surfactants or amphiphilic molecules (*e.g.* lipids and polymers). These systems offer several advantages, including enhanced solubilization and stability, as well as the capacity for targeted delivery at the cellular level [162]. Mixed micelles have found application in the fields of drug delivery [163], gene therapy [164] and cosmetic formulations [165]. It is important to note that these micellar systems offer distinct advantages, including reduced toxicity and enhanced treatment effectiveness. Nevertheless, challenges concerning formulation and large-scale production must not be overlooked [166, 167].

References

[1] R. L. Siegel, K. D. Miller, and A. Jemal, "Cancer statistics, 2020," *CA Cancer J Clin,* vol. 70, no. 1, pp. 7-30, 2020, doi: 10.3322/caac.21590.

[2] X. Y. He and Y. Z. Yuan, "Advances in pancreatic cancer research: moving towards early detection," *World J Gastroenterol,* vol. 20, no. 32, pp. 11241-8, 2014, doi: 10.3748/wjg.v20.i32.11241.

[3] C. Blanco Abad *et al.*, "Hereditary Pancreatic Cancer: Advances in Genetic Testing, Early Detection Strategies, and Personalized Management," *J Clin Med,* vol. 14, no. 2, 2025, doi: 10.3390/jcm14020367.

[4] T. Conroy *et al.*, "FOLFIRINOX versus gemcitabine for metastatic pancreatic cancer," *N Engl J Med,* vol. 364, no. 19, pp. 1817-25, 2011, doi: 10.1056/NEJMoa1011923.

[5] B. Zhang *et al.*, "The role of FOLFIRINOX in metastatic pancreatic cancer: a meta-analysis," *World J Surg Oncol,* vol. 19, no. 1, p. 182, 2021, doi: 10.1186/s12957-021-02291-6.

[6] D. D. Von Hoff *et al.*, "Increased survival in pancreatic cancer with nab-paclitaxel plus gemcitabine," *N Engl J Med,* vol. 369, no. 18, pp. 1691-703, 2013, doi: 10.1056/NEJMoa1304369.

[7] L. Mastrantoni *et al.*, "Comparison of first-line chemotherapy regimens in unresectable locally advanced or metastatic pancreatic cancer: a systematic review and Bayesian network meta-analysis," *Lancet Oncol,* vol. 25, no. 12, pp. 1655-1665, 2024, doi: 10.1016/s1470-2045(24)00511-4.

[8] R. Eid *et al.*, "Predictive factors of FOLFIRINOX chemotherapy toxicity in pancreatic adenocarcinoma patients," *Future Oncol,* vol. 21, no. 6, pp. 691-697, 2025, doi: 10.1080/14796694.2025.2461442.

[9] A. Boileve *et al.*, "Role of molecular biology in the management of pancreatic cancer," *World J Gastrointest Oncol,* vol. 16, no. 7, pp. 2902-2914, 2024, doi: 10.4251/wjgo.v16.i7.2902.

[10] B. Yu, S. Shao, and W. Ma, "Frontiers in pancreatic cancer on biomarkers, microenvironment, and immunotherapy," *Cancer Lett,* vol. 610, p. 217350, 2025, doi: 10.1016/j.canlet.2024.217350.

[11] P. P. Provenzano and S. R. Hingorani, "Hyaluronan, fluid pressure, and stromal resistance in pancreas cancer," *Br J Cancer,* vol. 108, no. 1, pp. 1-8, 2013, doi: 10.1038/bjc.2012.569.

[12] Y. Tian, Y. Lei, Y. Wang, J. Lai, J. Wang, and F. Xia, "Mechanism of multidrug resistance to chemotherapy mediated by P-glycoprotein (Review)," *Int J Oncol,* vol. 63, no. 5, 2023, doi: 10.3892/ijo.2023.5567.

[13] Z. Y. Hu, D. Ding, Y. Song, Y. F. Deng, C. M. Zhang, and T. Yu, "Molecular mechanism of pancreatic ductal adenocarcinoma: The heterogeneity of cancer-associated fibroblasts and key signaling pathways," *World J Clin Oncol,* vol. 16, no. 2, p. 97007, 2025, doi: 10.5306/wjco.v16.i2.97007.

[14] J. Calheiros, V. Corbo, and L. Saraiva, "Overcoming therapeutic resistance in pancreatic cancer: Emerging opportunities by targeting BRCAs and p53," *Biochim Biophys Acta Rev Cancer,* vol. 1878, no. 4, p. 188914, 2023, doi: 10.1016/j.bbcan.2023.188914.

[15] Y. Gu *et al.*, "Molecular mechanisms and therapeutic strategies in overcoming chemotherapy resistance in cancer," *Mol Biomed,* vol. 6, no. 1, p. 2, 2025, doi: 10.1186/s43556-024-00239-2.

[16] T. Demir, C. Moloney, and D. Mahalingam, "Threading the Needle: Navigating Novel Immunotherapeutics in Pancreatic Ductal Adenocarcinoma," *Cancers (Basel),* vol. 17, no. 5, 2025, doi: 10.3390/cancers17050715.

[17] C. K. Looi, F. F. Chung, C. O. Leong, S. F. Wong, R. Rosli, and C. W. Mai, "Therapeutic challenges and current immunomodulatory strategies in targeting the immunosuppressive pancreatic tumor microenvironment," *J Exp Clin Cancer Res,* vol. 38, no. 1, p. 162, 2019, doi: 10.1186/s13046-019-1153-8.

[18] T. Heumann *et al.*, "A platform trial of neoadjuvant and adjuvant antitumor vaccination alone or in combination with PD-1 antagonist and CD137 agonist antibodies in patients with resectable pancreatic adenocarcinoma," *Nat Commun,* vol. 14, no. 1, p. 3650, 2023, doi: 10.1038/s41467-023-39196-9.

[19] F. Quiñonero *et al.*, "PARP1 inhibition by Olaparib reduces the lethality of pancreatic cancer cells and increases their sensitivity to Gemcitabine," *Biomed Pharmacother,* vol. 155, p. 113669, 2022, doi: 10.1016/j.biopha.2022.113669.

[20] T. Golan *et al.*, "Maintenance Olaparib for Germline BRCA-Mutated Metastatic Pancreatic Cancer," *N Engl J Med,* vol. 381, no. 4, pp. 317-327, 2019, doi: 10.1056/NEJMoa1903387.

[21] U. N. Wasko *et al.*, "Tumour-selective activity of RAS-GTP inhibition in pancreatic cancer," *Nature,* vol. 629, no. 8013, pp. 927-936, 2024, doi: 10.1038/s41586-024-07379-z.

[22] M. Agbaria, D. Jbara-Agbaria, E. Grad, M. Ben-David-Naim, G. Aizik, and G. Golomb, "Nanoparticles of VAV1 siRNA combined with LL37 peptide for the treatment of pancreatic cancer," *J Control Release,* vol. 355, pp. 312-326, 2023, doi: 10.1016/j.jconrel.2023.01.084.

[23] A. Thakkar *et al.*, "Novel nano-drug combination therapeutic regimen demonstrates significant efficacy in the transgenic mouse model of pancreatic ductal adenocarcinoma," *Am J Cancer Res,* vol. 8, no. 10, pp. 2005-2019, 2018.

[24] G. A. McCarthy *et al.*, "A Novel 3DNA® Nanocarrier effectively delivers payloads to pancreatic tumors," *Transl Oncol,* vol. 32, p. 101662, 2023, doi: 10.1016/j.tranon.2023.101662.

[25] X. Zhao, G. Wu, X. Tao, D. Dong, and J. Liu, "Targeted mitochondrial therapy for pancreatic cancer," *Transl Oncol,* vol. 54, p. 102340, 2025, doi: 10.1016/j.tranon.2025.102340.

[26] F. Y. Chew, C. H. Tsai, K. H. Chang, Y. K. Chang, R. H. Chou, and Y. J. Liu, "Exosomes as promising frontier approaches in future cancer therapy," *World J Gastrointest Oncol,* vol. 17, no. 1, p. 100713, 2025, doi: 10.4251/wjgo.v17.i1.100713.

[27] S. Bayda, M. Adeel, T. Tuccinardi, M. Cordani, and F. Rizzolio, "The History of Nanoscience and Nanotechnology: From Chemical-Physical Applications to Nanomedicine," *Molecules,* vol. 25, no. 1, 2019, doi: 10.3390/molecules25010112.

[28] S. S. Godase, N. S. Kulkarni, and S. N. Dhole, "A Comprehensive Review on Novel Lipid-Based Nano Drug Delivery," *Adv Pharm Bull,* vol. 14, no. 1, pp. 34-47, 2024, doi: 10.34172/apb.2024.012.

[29] S. Mosleh-Shirazi *et al.*, "Nanotechnology Advances in the Detection and Treatment of Cancer: An Overview," *Nanotheranostics,* vol. 6, no. 4, pp. 400-423, 2022, doi: 10.7150/ntno.74613.

[30] K. Xu, Y. Liu, and C. Chen, "Future prospects in clinical translation of inorganic nanoparticles," *Acta Pharm Sin B,* vol. 14, no. 11, pp. 5082-5084, 2024, doi: 10.1016/j.apsb.2024.08.001.

[31] Q. Liu, J. Zou, Z. Chen, W. He, and W. Wu, "Current research trends of nanomedicines," *Acta Pharm Sin B,* vol. 13, no. 11, pp. 4391-4416, 2023, doi: 10.1016/j.apsb.2023.05.018.

[32] U. Bulbake, S. Doppalapudi, N. Kommineni, and W. Khan, "Liposomal Formulations in Clinical Use: An Updated Review," *Pharmaceutics,* vol. 9, no. 2, 2017, doi: 10.3390/pharmaceutics9020012.

[33] N. Kaur, P. Gautam, D. Nanda, A. S. Meena, A. Shanavas, and R. Prasad, "Lipid Nanoparticles for Brain Tumor Theranostics: Challenges and Status," *Bioconjug Chem,* vol. 35, no. 9, pp. 1283-1299, 2024, doi: 10.1021/acs.bioconjchem.4c00293.

[34] A. L.-C. E. Beltrán-Gracia, I. Higuera-Ciapara, J. B Velázquez-Fernández, A. A. Vallejo-Cardona, "Nanomedicine review: clinical developments in liposomal applications," *Cancer Nanotechnology,* vol. 10, 2019, doi: 10.1186/s12645-019-0055-y.

[35] A. C. Krauss *et al.*, "FDA Approval Summary: (Daunorubicin and Cytarabine) Liposome for Injection for the Treatment of Adults with High-Risk Acute Myeloid Leukemia," *Clin Cancer Res,* vol. 25, no. 9, pp. 2685-2690, 2019, doi: 10.1158/1078-0432.Ccr-18-2990.

[36] G. Milano, F. Innocenti, and H. Minami, "Liposomal irinotecan (Onivyde): Exemplifying the benefits of nanotherapeutic drugs," *Cancer Sci,* vol. 113, no. 7, pp. 2224-2231, 2022, doi: 10.1111/cas.15377.

[37] T. Xiao, S. Ali, D. Mata, A. E. Lohmann, and P. S. Blanchette, "Antibody-Drug Conjugates in Breast Cancer: Ascent to Destiny and Beyond-A 2023 Review," *Curr Oncol,* vol. 30, no. 7, pp. 6447-6461, 2023, doi: 10.3390/curroncol30070474.

[38] G. von Minckwitz *et al.*, "Trastuzumab Emtansine for Residual Invasive HER2-Positive Breast Cancer," *N Engl J Med,* vol. 380, no. 7, pp. 617-628, 2019, doi: 10.1056/NEJMoa1814017.

[39] S. Modi *et al.*, "Trastuzumab Deruxtecan in Previously Treated HER2-Low Advanced Breast Cancer," *N Engl J Med,* vol. 387, no. 1, pp. 9-20, 2022, doi: 10.1056/NEJMoa2203690.

[40] E. L. Sievers *et al.*, "Efficacy and Safety of Gemtuzumab Ozogamicin in Patients With CD33-Positive Acute Myeloid Leukemia in First Relapse," *Journal of Clinical Oncology,* vol. 19, no. 13, pp. 3244-3254, 2001, doi: 10.1200/jco.2001.19.13.3244.

[41] M. J. Nirmala, U. Kizhuveetil, A. Johnson, B. G, R. Nagarajan, and V. Muthuvijayan, "Cancer nanomedicine: a review of nano-therapeutics and challenges ahead," *RSC Adv,* vol. 13, no. 13, pp. 8606-8629, 2023, doi: 10.1039/d2ra07863e.

[42] F. Akram, A. M. Ali, M. T. Akhtar, T. Fatima, I. Shabbir, and I. ul Haq, "The journey of antibody-drug conjugates for revolutionizing cancer therapy: A review,"

Bioorganic & Medicinal Chemistry, vol. 117, p. 118010, 2025, doi: 10.1016/j.bmc.2024.118010.

[43] T. Macarulla *et al.*, "Phase I/II Trial to Evaluate the Efficacy and Safety of Nanoparticle Albumin-Bound Paclitaxel in Combination With Gemcitabine in Patients With Pancreatic Cancer and an ECOG Performance Status of 2," *Journal of Clinical Oncology,* vol. 37, no. 3, pp. 230-238, 2019, doi: 10.1200/jco.18.00089.

[44] A. Manzur, A. Oluwasanmi, D. Moss, A. Curtis, and C. Hoskins, "Nanotechnologies in Pancreatic Cancer Therapy," *Pharmaceutics,* vol. 9, no. 4, 2017, doi: 10.3390/pharmaceutics9040039.

[45] N. Pramanik, A. Gupta, Y. Ghanwatkar, and R. I. Mahato, "Recent advances in drug delivery and targeting for the treatment of pancreatic cancer," *J Control Release,* vol. 366, pp. 231-260, 2024, doi: 10.1016/j.jconrel.2023.12.053.

[46] A. K. Alshememry, N. B. Alsaleh, N. Alkhudair, R. Alzhrani, and A. Alshamsan, "Recent nanotechnology advancements to treat multidrug-resistance pancreatic cancer: Pre-clinical and clinical overview," *Front Pharmacol,* vol. 13, p. 933457, 2022, doi: 10.3389/fphar.2022.933457.

[47] A. K. Pearce and R. K. O'Reilly, "Insights into Active Targeting of Nanoparticles in Drug Delivery: Advances in Clinical Studies and Design Considerations for Cancer Nanomedicine," *Bioconjugate Chemistry,* vol. 30, no. 9, pp. 2300-2311, 2019, doi: 10.1021/acs.bioconjchem.9b00456.

[48] J. Shi, P. W. Kantoff, R. Wooster, and O. C. Farokhzad, "Cancer nanomedicine: progress, challenges and opportunities," *Nature Reviews Cancer,* vol. 17, no. 1, pp. 20-37, 2017, doi: 10.1038/nrc.2016.108.

[49] D. Rosenblum, N. Joshi, W. Tao, J. M. Karp, and D. Peer, "Progress and challenges towards targeted delivery of cancer therapeutics," *Nature Communications,* vol. 9, no. 1, p. 1410, 2018, doi: 10.1038/s41467-018-03705-y.

[50] P. C. Balar, V. Apostolopoulos, and V. P. Chavda, "A new era of immune therapeutics for pancreatic cancer: Monoclonal antibodies paving the way," *Eur J Pharmacol,* vol. 969, p. 176451, 2024, doi: 10.1016/j.ejphar.2024.176451.

[51] R. Tsumura *et al.*, "Feasibility study of the Fab fragment of a monoclonal antibody against tissue factor as a diagnostic tool," *Int J Oncol,* vol. 47, no. 6, pp. 2107-14, 2015, doi: 10.3892/ijo.2015.3210.

[52] L. Maksymova, Y. A. Pilger, L. Nuhn, and J. A. Van Ginderachter, "Nanobodies targeting the tumor microenvironment and their formulation as nanomedicines," *Molecular Cancer,* vol. 24, no. 1, p. 65, 2025, doi: 10.1186/s12943-025-02270-5.

[53] W. Yang, Q. Hu, Y. Xu, H. Liu, and L. Zhong, "Antibody fragment-conjugated gemcitabine and paclitaxel-based liposome for effective therapeutic efficacy in pancreatic cancer," *Mater Sci Eng C Mater Biol Appl,* vol. 89, pp. 328-335, 2018, doi: 10.1016/j.msec.2018.04.011.

[54] M. K. Greene *et al.*, "Refined construction of antibody-targeted nanoparticles leads to superior antigen binding and enhanced delivery of an entrapped payload to pancreatic cancer cells," *Nanoscale,* vol. 12, no. 21, pp. 11647-11658, 2020, doi: 10.1039/d0nr02387f.

[55] E. Ruoslahti, "Peptides as targeting elements and tissue penetration devices for nanoparticles," *Adv Mater,* vol. 24, no. 28, pp. 3747-56, 2012, doi: 10.1002/adma.201200454.

[56] K. Kim and M.-H. Park, "Role of Functionalized Peptides in Nanomedicine for Effective Cancer Therapy," *Biomedicines,* vol. 12, no. 1, p. 202, 2024, doi: 10.3390/biomedicines12010202.

[57] F. Zahedipour, S. A. Hosseini, M. Astaneh, P. Kesharwani, M. R. Jaafari, and A. Sahebkar, "Application of VEGF/VEGFR peptide vaccines in cancer: A systematic review of clinical trials," *Critical Reviews in Oncology/Hematology,* vol. 187, p. 104032, 2023, doi: 10.1016/j.critrevonc.2023.104032.

[58] K. Ghasemii *et al.*, "Advances in aptamer-based drug delivery vehicles for cancer therapy," *Biomater Adv,* vol. 140, p. 213077, 2022, doi: 10.1016/j.bioadv.2022.213077.

[59] A. Van den Avont and N. Sharma-Walia, "Anti-nucleolin aptamer AS1411: an advancing therapeutic," *Front Mol Biosci,* vol. 10, p. 1217769, 2023, doi: 10.3389/fmolb.2023.1217769.

[60] Y. Lu, E. Sega, C. P. Leamon, and P. S. Low, "Folate receptor-targeted immunotherapy of cancer: mechanism and therapeutic potential," *Adv Drug Deliv Rev,* vol. 56, no. 8, pp. 1161-76, 2004, doi: 10.1016/j.addr.2004.01.009.

[61] A. A. D'Souza and P. V. Devarajan, "Asialoglycoprotein receptor mediated hepatocyte targeting — Strategies and applications," *Journal of Controlled Release,* vol. 203, pp. 126-139, 2015, doi: 10.1016/j.jconrel.2015.02.022.

[62] P. Kesharwani, R. Chadar, A. Sheikh, W. Y. Rizg, and A. Y. Safhi, "CD44-Targeted Nanocarrier for Cancer Therapy," *Front Pharmacol,* vol. 12, p. 800481, 2021, doi: 10.3389/fphar.2021.800481.

[63] X. Liu *et al.*, "Extensive Review of Nanomedicine Strategies Targeting the Tumor Microenvironment in PDAC," *Int J Nanomedicine,* vol. 20, pp. 3379-3406, 2025, doi: 10.2147/ijn.S504503.

[64] N. V. Rao *et al.*, "Recent developments in hyaluronic acid-based nanomedicine for targeted cancer treatment," *Expert Opinion on Drug Delivery,* vol. 13, no. 2, pp. 239-252, 2016, doi: 10.1517/17425247.2016.1112374.

[65] E. J. Oh *et al.*, "Target specific and long-acting delivery of protein, peptide, and nucleotide therapeutics using hyaluronic acid derivatives," *J Control Release,* vol. 141, no. 1, pp. 2-12, 2010, doi: 10.1016/j.jconrel.2009.09.010.

[66] J. R. Fraser, T. C. Laurent, and U. B. Laurent, "Hyaluronan: its nature, distribution, functions and turnover," *J Intern Med,* vol. 242, no. 1, pp. 27-33, 1997, doi: 10.1046/j.1365-2796.1997.00170.x.

[67] X. Wang *et al.*, "Effects of molecular weights on the bioactivity of hyaluronic acid: A review," *Carbohydr Res,* vol. 552, p. 109472, 2025, doi: 10.1016/j.carres.2025.109472.

[68] S. Misra *et al.*, "Hyaluronan-CD44 interactions as potential targets for cancer therapy," *Febs j,* vol. 278, no. 9, pp. 1429-43, 2011, doi: 10.1111/j.1742-4658.2011.08071.x.

[69] G. Zhang *et al.*, "Hyaluronic acid-conjugated lipid nanocarriers in advancing cancer therapy: A review," *International Journal of Biological Macromolecules,* vol. 299, p. 140146, 2025, doi: 10.1016/j.ijbiomac.2025.140146.

[70] A. Huffer, M. Mao, K. Ballard, and T. Ozdemir, "Biomimetic Hyaluronan Binding Biomaterials to Capture the Complex Regulation of Hyaluronan in Tissue Development and Function," *Biomimetics,* vol. 9, no. 8, p. 499, 2024, doi: 10.3390/biomimetics9080499.

[71] M. Bhattacharyya, H. Jariyal, and A. Srivastava, "Hyaluronic acid: More than a carrier, having an overpowering extracellular and intracellular impact on cancer," *Carbohydrate Polymers,* vol. 317, p. 121081, 2023, doi: 10.1016/j.carbpol.2023.121081.

[72] M. C. Su, S. K. Nethi, P. K. Dhanyamraju, and S. Prabha, "Nanomedicine Strategies for Targeting Tumor Stroma," *Cancers (Basel),* vol. 15, no. 16, 2023, doi: 10.3390/cancers15164145.

[73] Q. Ouyang, Y. Zhao, K. Xu, Y. He, and M. Qin, "Hyaluronic Acid Receptor-Mediated Nanomedicines and Targeted Therapy," *Small Methods,* vol. 8, no. 10, p. e2400513, 2024, doi: 10.1002/smtd.202400513.

[74] J. A. Burdick and G. D. Prestwich, "Hyaluronic acid hydrogels for biomedical applications," *Adv Mater,* vol. 23, no. 12, pp. H41-56, 2011, doi: 10.1002/adma.201003963.

[75] K. Kim, H. Choi, E. S. Choi, M. H. Park, and J. H. Ryu, "Hyaluronic Acid-Coated Nanomedicine for Targeted Cancer Therapy," *Pharmaceutics,* vol. 11, no. 7, 2019, doi: 10.3390/pharmaceutics11070301.

[76] A. Yadav, D. S. Waghmare, A. Ahir, and A. Srivastava, "Comprehensive Exploration on Chemical Functionalization and Crosslinked Injectable Hyaluronic Acid Hydrogels for Tissue Engineering Applications," *Regenerative Engineering and Translational Medicine,* 2025, doi: 10.1007/s40883-024-00368-8.

[77] Y. Li *et al.*, "Application of Carbon Nanomaterials to Enhancing Tumor Immunotherapy: Current Advances and Prospects," *Int J Nanomedicine,* vol. 19, pp. 10899-10915, 2024, doi: 10.2147/ijn.S480799.

[78] T. Yin, J. Han, Y. Cui, D. Shang, and H. Xiang, "Prospect of Gold Nanoparticles in Pancreatic Cancer," *Pharmaceutics,* vol. 16, no. 6, 2024, doi: 10.3390/pharmaceutics16060806.

[79] P. Martinkova, M. Brtnicky, J. Kynicky, and M. Pohanka, "Iron Oxide Nanoparticles: Innovative Tool in Cancer Diagnosis and Therapy," *Adv Healthc Mater,* vol. 7, no. 5, 2018, doi: 10.1002/adhm.201700932.

[80] H. Agarwal *et al.*, "Theranostic nanoparticles for detection and treatment of pancreatic cancer," *Wiley Interdiscip Rev Nanomed Nanobiotechnol,* vol. 16, no. 4, p. e1983, 2024, doi: 10.1002/wnan.1983.

[81] O. Długosz *et al.*, "Inorganic Nanomaterials Used in Anti-Cancer Therapies:Further Developments," *Nanomaterials (Basel),* vol. 13, no. 6, 2023, doi: 10.3390/nano13061130.

[82] C. Liu, H. Yu, L. Zhang, and W. Zhang, "Semiquantitative analysis of carbon quantum dot-labeled exosomes based on carrier ampholyte-free paper-based

isoelectric focusing," *Talanta,* vol. 296, p. 128412, 2025, doi: 10.1016/j.talanta.2025.128412.

[83] C. Araújo, R. O. Rodrigues, M. Bañobre-López, A. M. T. Silva, and R. S. Ribeiro, "Carbon Dots as a Fluorescent Nanosystem for Crossing the Blood-Brain Barrier with Plausible Application in Neurological Diseases," *Pharmaceutics,* vol. 17, no. 4, 2025, doi: 10.3390/pharmaceutics17040477.

[84] S. M. Hosseini, J. Mohammadnejad, R. Najafi-Taher, Z. B. Zadeh, M. Tanhaei, and S. Ramakrishna, "Multifunctional Carbon-Based Nanoparticles: Theranostic Applications in Cancer Therapy and Diagnosis," *ACS Appl Bio Mater,* vol. 6, no. 4, pp. 1323-1338, 2023, doi: 10.1021/acsabm.2c01000.

[85] X. Yuan, X. Zhang, L. Sun, Y. Wei, and X. Wei, "Cellular Toxicity and Immunological Effects of Carbon-based Nanomaterials," *Part Fibre Toxicol,* vol. 16, no. 1, p. 18, 2019, doi: 10.1186/s12989-019-0299-z.

[86] S. K. Sohaebuddin, P. T. Thevenot, D. Baker, J. W. Eaton, and L. Tang, "Nanomaterial cytotoxicity is composition, size, and cell type dependent," *Part Fibre Toxicol,* vol. 7, p. 22, 2010, doi: 10.1186/1743-8977-7-22.

[87] Y. Li *et al.*, "The triggering of apoptosis in macrophages by pristine graphene through the MAPK and TGF-beta signaling pathways," *Biomaterials,* vol. 33, no. 2, pp. 402-11, 2012, doi: 10.1016/j.biomaterials.2011.09.091.

[88] A. Barhoum *et al.*, "Review on Natural, Incidental, Bioinspired, and Engineered Nanomaterials: History, Definitions, Classifications, Synthesis, Properties, Market, Toxicities, Risks, and Regulations," *Nanomaterials (Basel),* vol. 12, no. 2, 2022, doi: 10.3390/nano12020177.

[89] C. Zhao, J. Kang, Y. Li, Y. Wang, X. Tang, and Z. Jiang, "Carbon-Based Stimuli-Responsive Nanomaterials: Classification and Application," *Cyborg Bionic Syst,* vol. 4, p. 0022, 2023, doi: 10.34133/cbsystems.0022.

[90] M. D. Angione *et al.*, "Carbon based materials for electronic bio-sensing," *Materials Today,* vol. 14, no. 9, pp. 424-433, 2011, doi: 10.1016/S1369-7021(11)70187-0.

[91] P. M. Ajayan, L. S. Schadler, C. Giannaris, and A. Rubio, "Single-Walled Carbon Nanotube–Polymer Composites: Strength and Weakness," *Advanced Materials,* vol. 12, no. 10, pp. 750-753, 2000, doi: 10.1002/(SICI)1521-4095(200005)12:10.

[92] A. Razzazan, F. Atyabi, B. Kazemi, and R. Dinarvand, "In vivo drug delivery of gemcitabine with PEGylated single-walled carbon nanotubes," *Mater Sci Eng C Mater Biol Appl,* vol. 62, pp. 614-25, 2016, doi: 10.1016/j.msec.2016.01.076.

[93] E. Ahmadian, D. Janas, A. Eftekhari, and N. Zare, "Application of carbon nanotubes in sensing/monitoring of pancreas and liver cancer," *Chemosphere,* vol. 302, p. 134826, 2022, doi: 10.1016/j.chemosphere.2022.134826.

[94] A. Thapa *et al.*, "Carbon Nanotube Matrix for Highly Sensitive Biosensors To Detect Pancreatic Cancer Biomarker CA19-9," *ACS Appl Mater Interfaces,* vol. 9, no. 31, pp. 25878-25886, 2017, doi: 10.1021/acsami.7b07384.

[95] S. Hu, F. Tian, P. Bai, S. Cao, J. Sun, and J. Yang, "Synthesis and luminescence of nanodiamonds from carbon black," *Materials Science and Engineering: B,* vol. 157, no. 1, pp. 11-14, 2009, doi: 10.1016/j.mseb.2008.12.001.

[96] V. I. Korepanov *et al.*, "Carbon structure in nanodiamonds elucidated from Raman spectroscopy," *Carbon,* vol. 121, pp. 322-329, 2017, doi: 10.1016/j.carbon.2017.06.012.

[97] S. Chauhan, N. Jain, and U. Nagaich, "Nanodiamonds with powerful ability for drug delivery and biomedical applications: Recent updates on in vivo study and patents," *Journal of Pharmaceutical Analysis,* vol. 10, no. 1, pp. 1-12, doi: 10.1016/j.jpha.2019.09.003.

[98] R. Rai *et al.*, "Biodistribution of nanodiamonds is determined by surface functionalization," *Diamond and Related Materials,* vol. 137, p. 110071, 2023, doi: 10.1016/j.diamond.2023.110071.

[99] S. Sturari *et al.*, "A comprehensive study of the effect of thermally induced surface terminations on nanodiamonds electrical properties," *Surfaces and Interfaces,* vol. 38, 2023, doi: 10.1016/j.surfin.2023.102831.

[100] F. Pan *et al.*, "Recent advances in the structure and biomedical applications of nanodiamonds and their future perspectives," *Materials & Design,* vol. 233, p. 112179, 2023, doi: 10.1016/j.matdes.2023.112179.

[101] M. Ghasemlou *et al.*, "Fluorescent Nanocarbons: From Synthesis and Structure to Cancer Imaging and Therapy," *Advanced materials (Deerfield Beach, Fla.),* vol. 36, no. 19, p. e2312474, 2024, doi: 10.1002/adma.202312474.

[102] S. Sturari *et al.*, "Designing functionalized nanodiamonds with hyaluronic acid-phospholipid conjugates for enhanced cancer cell targeting and fluorescence imaging capabilities," *Nanoscale,* vol. 16, no. 24, pp. 11610-11622, 2024, doi: 10.1039/d4nr00932k.

[103] S. Iijima, "Direct observation of the tetrahedral bonding in graphitized carbon black by high resolution electron microscopy," *Journal of Crystal Growth,* vol. 50, no. 3, pp. 675-683, doi: 10.1016/0022-0248(80)90013-5.

[104] D. Ugarte, "Curling and closure of graphitic networks under electron-beam irradiation," *Nature,* vol. 359, no. 6397, pp. 707-9, 1992.

[105] Y. Bian, L. Liu, D. Liu, Z. Zhu, Y. Shao, and M. Li, "Electrochemical synthesis of carbon nano onions," *Inorganic Chemistry Frontiers,* vol. 7, no. 22, pp. 4404-4411, 2020, doi: 10.1039/d0qi00950d.

[106] M. D'Amora *et al.*, "Biocompatibility and biodistribution of functionalized carbon nano-onions (f-CNOs) in a vertebrate model," *Scientific Reports*, vol. 6, doi: 10.1038/srep33923.

[107] J. Bartelmess, S. Giordani, and C. Ewels, "Carbon nano-onions (multi-layer fullerenes): chemistry and applications," *Beilstein Journal of Nanotechnology,* vol. 5, pp. 1980-1998, 2014, doi: 10.3762/bjnano.5.207.

[108] M. d'Amora, A. Camisasca, A. Boarino, S. Arpicco, and S. Giordani, "Supramolecular functionalization of carbon nano-onions with hyaluronic acid-phospholipid conjugates for selective targeting of cancer cells," *Colloids and Surfaces B: Biointerfaces,* vol. 188, p. 110779, 2020, doi: 10.1016/j.colsurfb.2020.110779.

[109] B. Pakhira, M. Ghosh, A. Allam, and S. Sarkar, "Carbon nano onions cross the blood brain barrier," *RSC Advances,* 10.1039/C5RA23534K vol. 6, no. 35, pp. 29779-29782, 2016, doi: 10.1039/C5RA23534K.

[110] V. Cappello *et al.*, "Ultrastructural Characterization of the Lower Motor System in a Mouse Model of Krabbe Disease," *Scientific Reports,* vol. 6, no. 1, p. 1, 2016, doi: 10.1038/s41598-016-0001-8.

[111] M. Bartkowski and S. Giordani, "Carbon nano-onions as potential nanocarriers for drug delivery," *Dalton Transactions,* 10.1039/D0DT04093B vol. 50, no. 7, pp. 2300-2309, 2021, doi: 10.1039/D0DT04093B.

[112] Z. Yang *et al.*, "Zero-Dimensional Carbon Nanomaterials for Fluorescent Sensing and Imaging," *Chem Rev,* vol. 123, no. 18, pp. 11047-11136, 2023, doi: 10.1021/acs.chemrev.3c00186.

[113] J. C. Zuaznabar-Gardona and A. Fragoso, "Determination of the Hansen solubility parameters of carbon nano-onions and prediction of their dispersibility in organic

solvents," *Journal of Molecular Liquids,* vol. 294, p. 111646, 2019, doi: 10.1016/j.molliq.2019.111646.

[114] R. Majumder, S. Karmakar, S. Mishra, A. B. Mallick, and C. Das Mukhopadhyay, "Functionalized Carbon Nano-Onions as a Smart Drug Delivery System for the Poorly Soluble Drug Carmustine for the Management of Glioblastoma," *ACS Appl Bio Mater,* vol. 7, no. 1, pp. 154-167, 2024, doi: 10.1021/acsabm.3c00688.

[115] N. Mamidi, R. M. V. Delgadillo, and A. González-Ortiz, "Engineering of carbon nano-onion bioconjugates for biomedical applications," *Mater Sci Eng C Mater Biol Appl,* vol. 120, p. 111698, 2021, doi: 10.1016/j.msec.2020.111698.

[116] M. d'Amora, A. Camisasca, A. Boarino, S. Arpicco, and S. Giordani, "Supramolecular functionalization of carbon nano-onions with hyaluronic acid-phospholipid conjugates for selective targeting of cancer cells," *Colloids Surf B Biointerfaces,* vol. 188, p. 110779, 2020, doi: 10.1016/j.colsurfb.2020.110779.

[117] N. Jayaprakash, K. Elumalai, S. Manickam, G. Bakthavatchalam, and P. Tamilselvan, "Carbon nanomaterials: Revolutionizing biomedical applications with promising potential," *Nano Materials Science,* 2024, doi: 10.1016/j.nanoms.2024.11.004.

[118] N. M. Bardhan, "30 years of advances in functionalization of carbon nanomaterials for biomedical applications: a practical review," *Journal of Materials Research,* vol. 32, no. 1, pp. 107-127, 2017, doi: 10.1557/jmr.2016.449.

[119] Y. Zou, Y. Nishina, and A. Bianco, "The use of covalent reactions to improve the biomedical applications of carbon nanomaterials," *Carbon Reports,* vol. 2, no. 4, pp. 185-198, 2023, doi: 10.7209/carbon.020405.

[120] L. R. M. de Andrade *et al.*, "Biomedical applications of carbon nanotubes: A systematic review of data and clinical trials," *Journal of Drug Delivery Science and Technology,* vol. 99, p. 105932, 2024, doi: 10.1016/j.jddst.2024.105932.

[121] A. R. Sarikhani, M. Abedi, S. S. Abolmaali, S. Borandeh, and A. M. Tamaddon, "Magnetic graphene oxide nanosheets with amidoamine dendronized crosslinks for dual pH and redox-sensitive doxorubicin delivery," *BMC Chemistry,* vol. 18, no. 1, p. 189, 2024, doi: 10.1186/s13065-024-01301-4.

[122] A. S. Gadtya, K. Deshmukh, and S. Moharana, "Functionalized Carbon Nanostructures for Targeted Drug Delivery," in *Handbook of Functionalized Carbon Nanostructures: From Synthesis Methods to Applications*, A. Barhoum and K. Deshmukh Eds. Cham: Springer International Publishing, 2024, pp. 2355-2395, doi: 10.1007/978-3-031-32150-4_80.

[123] M. Matiyani, M. Pathak, B. S. Bohra, and N. G. Sahoo, "Noncovalent Functionalization of Carbon Nanotubes," in *Handbook of Carbon Nanotubes*, J. Abraham, S. Thomas, and N. Kalarikkal Eds. Cham: Springer International Publishing, 2020, pp. 1-28, 10.1007/978-3-030-91346-5_66.

[124] H. M. Dewey, A. Lamb, and J. Budhathoki-Uprety, "Recent advances on applications of single-walled carbon nanotubes as cutting-edge optical nanosensors for biosensing technologies," *Nanoscale,* vol. 16, no. 35, pp. 16344-16375, 2024, doi: 10.1039/d4nr01892c.

[125] A. D. Sontakke, S. Tiwari, and M. K. Purkait, "A comprehensive review on graphene oxide-based nanocarriers: Synthesis, functionalization and biomedical applications," *FlatChem,* vol. 38, p. 100484, 2023, doi: 10.1016/j.flatc.2023.100484.

[126] W. Liu and G. Speranza, "Functionalization of Carbon Nanomaterials for Biomedical Applications," *C,* vol. 5, no. 4, p. 72, 2019, doi: 10.3390/c5040072.

[127] M. A. Subhan, N. Filipczak, and V. P. Torchilin, "Advances with Lipid-Based Nanosystems for siRNA Delivery to Breast Cancers," *Pharmaceuticals (Basel),* vol. 16, no. 7, 2023, doi: 10.3390/ph16070970.

[128] Z. Cheng *et al.*, "Lipid-based nanosystems: the next generation of cancer immune therapy," *J Hematol Oncol,* vol. 17, no. 1, p. 53, 2024, doi: 10.1186/s13045-024-01574-1.

[129] G. Wang *et al.*, "Tailored Borneol-Modified Lipid Nanoparticles Nasal Spray for Enhanced Nose-to-Brain Delivery to Central Nervous System Diseases," *ACS Nano,* vol. 18, no. 34, pp. 23684-23701, 2024, doi: 10.1021/acsnano.4c08279.

[130] B. Leonardini *et al.*, "Physical determinants of nanoparticle-mediated lipid membrane fusion," *Nanoscale,* 2025, doi: 10.1039/d4nr04851b.

[131] B. Aguiar *et al.*, "Exploring Nano-Delivery Systems to Enhance the Edaravone Performance in Amyotrophic Lateral Sclerosis Treatment," *Int J Mol Sci,* vol. 26, no. 5, 2025, doi: 10.3390/ijms26052146.

[132] T. M. Allen and P. R. Cullis, "Liposomal drug delivery systems: from concept to clinical applications," *Adv Drug Deliv Rev,* vol. 65, no. 1, pp. 36-48, 2013, doi: 10.1016/j.addr.2012.09.037.

[133] S. A. Salunkhe, D. Chitkara, R. I. Mahato, and A. Mittal, "Lipid based nanocarriers for effective drug delivery and treatment of diabetes associated liver fibrosis," *Adv Drug Deliv Rev,* vol. 173, pp. 394-415, 2021, doi: 10.1016/j.addr.2021.04.003.

[134] K. Mahmoud, S. Swidan, M. El-Nabarawi, and M. Teaima, "Lipid based nanoparticles as a novel treatment modality for hepatocellular carcinoma: a comprehensive review on targeting and recent advances," *J Nanobiotechnology,* vol. 20, no. 1, p. 109, 2022, doi: 10.1186/s12951-022-01309-9.

[135] Y. Huang, X. Y. Wang, J. Y. Huang, and Z. W. Huang, "Incorporation of human β-defensin-1 into immunoliposomes to facilitate targeted autophagy therapy of colon carcinoma," *World J Clin Oncol,* vol. 16, no. 3, p. 101098, 2025, doi: 10.5306/wjco.v16.i3.101098.

[136] Y. Liu *et al.*, "A protease-cleavable liposome for co-delivery of anti-PD-L1 and doxorubicin for colon cancer therapy in mice," *Nat Commun,* vol. 16, no. 1, p. 2854, 2025, doi: 10.1038/s41467-025-57965-6.

[137] G. Sun *et al.*, "Quercetin liposomes conjugated with hyaluronidase: An efficient drug delivery system to block pancreatic cancer," *J Control Release,* p. 113642, 2025, doi: 10.1016/j.jconrel.2025.113642.

[138] R. Tenchov, R. Bird, A. E. Curtze, and Q. Zhou, "Lipid Nanoparticles─From Liposomes to mRNA Vaccine Delivery, a Landscape of Research Diversity and Advancement," *ACS Nano,* vol. 15, no. 11, pp. 16982-17015, 2021, doi: 10.1021/acsnano.1c04996.

[139] M. Gomi *et al.*, "Tolerogenic Lipid Nanoparticles for Delivering Self-Antigen mRNA for the Treatment of Experimental Autoimmune Encephalomyelitis," *Pharmaceuticals (Basel),* vol. 16, no. 9, 2023, doi: 10.3390/ph16091270.

[140] J. Khirallah *et al.*, "In vivo base editing of Angptl3 via lipid nanoparticles to treat cardiovascular disease," *Mol Ther Nucleic Acids,* vol. 36, no. 2, p. 102486, 2025, doi: 10.1016/j.omtn.2025.102486.

[141] C. Carbone, A. Campisi, T. Musumeci, G. Raciti, R. Bonfanti, and G. Puglisi, "FA-loaded lipid drug delivery systems: preparation, characterization and biological studies," *Eur J Pharm Sci,* vol. 52, pp. 12-20, 2014, doi: 10.1016/j.ejps.2013.10.003.

[142] M. C. Teixeira, C. Carbone, and E. B. Souto, "Beyond liposomes: Recent advances on lipid based nanostructures for poorly soluble/poorly permeable drug delivery," *Progress in Lipid Research,* vol. 68, pp. 1-11, 2017, doi: 10.1016/j.plipres.2017.07.001.

[143] S. Nalawade *et al.*, "Surface-modified nintedanib-loaded solid lipid nanoparticles for effective targeting of non-small cell lung cancer," *Colloids Surf B Biointerfaces,* vol. 251, p. 114622, 2025, doi: 10.1016/j.colsurfb.2025.114622.

[144] C. Prathumwon *et al.*, "Curcumin and EGCG combined formulation in nanostructured lipid carriers for anti-aging applications," *Int J Pharm X,* vol. 9, p. 100323, 2025, doi: 10.1016/j.ijpx.2025.100323.

[145] A. Naseema, L. Kovooru, A. K. Behera, K. P. P. Kumar, and P. Srivastava, "A critical review of synthesis procedures, applications and future potential of nanoemulsions," *Adv Colloid Interface Sci,* vol. 287, p. 102318, 2021, doi: 10.1016/j.cis.2020.102318.

[146] M. A. Elbaset *et al.*, "Curcumin nanoemulsion counteracts hepatic and cardiac complications associated with high-fat/high-fructose diet in rats," *J Food Biochem,* vol. 46, no. 12, p. e14442, 2022, doi: 10.1111/jfbc.14442.

[147] K. Halpin-Veszeleiova *et al.*, "Oxygen-carrying nanoemulsions and respiratory hyperoxia eliminate tumor hypoxia-induced immunosuppression," *JCI Insight,* vol. 10, no. 6, 2025, doi: 10.1172/jci.insight.174675.

[148] S. S. Hallan, P. Kaur, V. Kaur, N. Mishra, and B. Vaidya, "Lipid polymer hybrid as emerging tool in nanocarriers for oral drug delivery," *Artif Cells Nanomed Biotechnol,* vol. 44, no. 1, pp. 334-49, 2016, doi: 10.3109/21691401.2014.951721.

[149] M. Packer, D. Gyawali, R. Yerabolu, J. Schariter, and P. White, "A novel mechanism for the loss of mRNA activity in lipid nanoparticle delivery systems," *Nat Commun,* vol. 12, no. 1, p. 6777, 2021, doi: 10.1038/s41467-021-26926-0.

[150] A. G. Niculescu and A. M. Grumezescu, "Polymer-Based Nanosystems-A Versatile Delivery Approach," *Materials (Basel),* vol. 14, no. 22, 2021, doi: 10.3390/ma14226812.

[151] W. Nafo, "Polymer-based nanosystems and their applications in bone anticancer therapy," *Front Chem,* vol. 11, p. 1218511, 2023, doi: 10.3389/fchem.2023.1218511.

[152] D. S. Idris *et al.*, "Polymer-based nanocarriers for biomedical and environmental applications," *e-Polymers,* vol. 23, no. 1, 2023, doi: doi:10.1515/epoly-2023-0049.

[153] A. Zielińska *et al.*, "Polymeric Nanoparticles: Production, Characterization, Toxicology and Ecotoxicology," *Molecules,* vol. 25, no. 16, 2020, doi: 10.3390/molecules25163731.

[154] S. Sonzini *et al.*, "HER2-targeted star polymer conjugates for improved tumor distribution and efficacy," *J Control Release,* p. 113654, 2025, doi: 10.1016/j.jconrel.2025.113654.

[155] L. Q. C. Silva *et al.*, "PLGA/TPGS nanoparticles for docetaxel delivery: the pegylation effect on nanoparticle physicochemical properties and uptake and

cytotoxicity in prostate cancer cells," *J Pharm Sci,* p. 103766, 2025, doi: 10.1016/j.xphs.2025.103766.

[156] R. Castro, P. L. Granja, J. Rodrigues, A. P. Pêgo, and H. Tomás, "Bioinspired hybrid DNA/dendrimer-based films with supramolecular chirality," *J Mater Chem B,* 2025, doi: 10.1039/d4tb02761b.

[157] M. M. Zorab, A. M. Qadir, and A. M. A. Ahmed, "Dendrimers as drug delivery vehicles: a comprehensive review," *Cell Mol Biol (Noisy-le-grand),* vol. 71, no. 1, pp. 1-12, 2025, doi: 10.14715/cmb/2025.70.1.1.

[158] S. Matoori, "Hallmarks of Polymersome Characterization," *ACS Mater Au,* vol. 5, no. 2, pp. 223-230, 2025, doi: 10.1021/acsmaterialsau.4c00107.

[159] Y. H. Huang *et al.*, "Combination of mannoside and phenylboronic acid polycaprolactone polymers for doxorubicin-encapsulated polymersome nanomedicine targeting MDA-MB-231 cancer cells," *Drug Deliv Transl Res,* 2025, doi: 10.1007/s13346-025-01836-6.

[160] J. Shao *et al.*, "Designing polymersomes with surface-integrated nanoparticles through hierarchical phase separation," *Nat Commun,* vol. 16, no. 1, p. 2445, 2025, doi: 10.1038/s41467-025-57711-y.

[161] H.-X. Wei, M.-H. Liu, T.-Y. Wang, M.-H. Shih, J. Yu, and Y.-C. Yeh, "Fabrication of pH- and Ultrasound-Responsive Polymeric Micelles: The Effect of Amphiphilic Block Copolymers with Different Hydrophilic/Hydrophobic Block Ratios for Self-Assembly and Controlled Drug Release," *Biomacromolecules,* 2025, doi: 10.1021/acs.biomac.4c01202.

[162] A. S. Manjappa, P. S. Kumbhar, J. I. Disouza, and V. B. Patravale, "Polymeric Mixed Micelles: Improving the Anticancer Efficacy of Single-Copolymer Micelles," *Crit Rev Ther Drug Carrier Syst,* vol. 36, no. 1, pp. 1-58, 2019, doi: 10.1615/CritRevTherDrugCarrierSyst.2018020481.

[163] B. Zurletti *et al.*, "Tailoring the Composition of HA/PEG Mixed Nano-Assemblies for Anticancer Drug Delivery," *Molecules,* vol. 30, no. 6, 2025, doi: 10.3390/molecules30061349.

[164] M. Hazekawa, T. Nishinakagawa, T. Mori, M. Yoshida, T. Uchida, and D. Ishibashi, "Preparation of siRNA-PLGA/Fab'-PLGA mixed micellar system with target cell-specific recognition," *Sci Rep,* vol. 11, no. 1, p. 16789, 2021, doi: 10.1038/s41598-021-96245-3.

[165] M. R. Rao, P. Gaikwad, P. Misal, and S. V. Gandhi, "Phyto-cosmeceutical gel containing curcumin and quercetin loaded mixed micelles for improved anti-oxidant and photoprotective activity," *Colloids Surf B Biointerfaces,* vol. 237, p. 113837, 2024, doi: 10.1016/j.colsurfb.2024.113837.

[166] M. Ansari, C. Gupta, Y. A. Kulkarni, and K. Singh, "Functionalization of polymeric nanomicelles and mixed nanomicelles for targeted retinal delivery in the management of retinoblastoma," *Int J Pharm,* vol. 671, p. 125235, 2025, doi: 10.1016/j.ijpharm.2025.125235.

[167] B. Wang, L. Liao, H. Liang, J. Chen, and Y. Qiu, "Preparation and In Vitro/In Vivo Characterization of Mixed-Micelles-Loaded Dissolving Microneedles for Sustained Release of Indomethacin," *Pharmaceutics,* vol. 16, no. 12, 2024, doi: 10.3390/pharmaceutics16121505.

Review

Breaking through the limits: nanomedicine at the service of new drug combinations to tackle pancreatic cancer

Valeria Bincoletto, Ilaria Andreana, Barbara Stella, Nazanine Modjtahedi, Silvia Arpicco, Giorgia Urbinati

---

Submitted to *WIREs Nanomedicine and Nanobiotechnology*

Pancreatic ductal adenocarcinoma is a highly lethal malignancy, primarily due to late-stage diagnosis, aggressive progression, and high resistance to conventional chemotherapies. While GEM has long been the mainstay of treatment, its efficacy is significantly hampered by intrinsic and acquired resistance mechanisms. Despite the advances made, therapeutic outcomes remain unsatisfactory and there is an urgent need for more effective and better tolerated options. In this context, nanomedicine, drug combination and repurposing are emerging as promising strategies to overcome the limitations of current pancreatic cancer therapies.

Main Aim of the Work

This review aims to explore the potential of nanomedicine, drugs combination and drug repurposing, which are emerging as promising approaches to overcome the limitations of current pancreatic cancer therapies. Among all the strategies, the combination of GEM and DSF has been examined.

Specific Objectives

- To analyze the biological basis and molecular mechanisms behind GEM resistance in pancreatic cancer.
- To present current standard and emerging drug combinations used in clinical and preclinical settings.
- To describe the anti-cancer potential and mechanism of action of DSF, especially in combination with GEM.
- To review the design and performance of lipid-based nanosystems developed for the delivery of drugs and their combination or co-delivery in pancreatic cancer models.
- To highlight criteria for designing optimal nanocarriers coencapsulating GEM and DSF, capable of overcoming the solubility, stability, and resistance issues associated with these drugs.

Highlights

- Complex resistance mechanisms limit GEM efficacy in pancreatic cancer treatment.
- Nanomedicine and multi-drug therapies show potential to overcome pancreatic cancer treatment resistance.
- DSF, when repurposed and combined with GEM, demonstrates synergistic anti-tumor activity.

- Lipid-based nanosystems enhance the efficacy of combination therapies by improving drug targeting, release control, and reducing side effects.

Breaking through the limits: nanomedicine at the service of new drug combinations to tackle pancreatic cancer

Valeria Bincoletto[a], Ilaria Andreana[a], Barbara Stella[a], Nazanine Modjtahedi[b], Silvia Arpicco[a], Giorgia Urbinati[c,*]

[a] *Department of Drug Science and Technology, University of Turin, Via P. Giuria 9, Turin, Italy*

[b] *Unité Physiopathologie et Génétique du Neurone et du Muscle, UMR CNRS 5261, Inserm U1315, Université Claude Bernard Lyon 1, Lyon, France*

[c] *Université Paris Cité, CNRS, INSERM, UTCBS (https://utcbs.u-paris.fr/), 4 avenue de l'Observatoire, F-75006, Paris*

[*] *Corresponding author e-mail address: giorgia.urbinati@u-paris.fr; phone: +33 6 99 60 54 17*

Highlights

- Complex resistance mechanisms limit GEM efficacy in PDAC treatment
- Nanomedicine and multi-drug therapies could overcome resistance to PDAC treatments
- Combining GEM with repurposed Disulfiram for an improved anti-cancer therapy
- Lipid-based nanosystems boost the efficacy of combination therapies in pancreatic cancer

Abstract

Pancreatic ductal adenocarcinoma (PDAC) is among the most aggressive cancers, with a poor prognosis due to late diagnosis and resistance to chemotherapy. Gemcitabine (GEM) monotherapy was the gold standard treatment for PDAC until the early 2010s, when two combinatorial therapies, FOLFIRINOX and GEM combined with Nab-paclitaxel, showed the benefits of the multi-drug approach and became the reference treatments for PDAC. Despite their undisputed efficacy, the overall survival of treated PDAC patients is very low, reaching approximately 12% at 5 years, and the side effects of these therapeutic protocols remain severe and not tolerated by all patients. Recent advances in understanding PDAC biology have led to new therapeutic strategies, including new drug combinations and nanomedicine. This review summarizes background information about past and present PDAC therapeutic regimens with their benefits and the drawbacks including the appearance of treatment resistance and focuses on two potential strategies to counteract the limitations of the actual therapies. First, we highlight the interest of combining disulfiram, a repurposed anti-alcoholism drug, with GEM, based on evidence of synergism between the two molecules. We then emphasize on the use of drug delivery nanosystems for their ability to improve drug stability, targeting and to potentially overcome resistance and reduce side effects. Finally, we discuss the combination of multi-drug therapies and nanomedicine through the design of apposite drug delivery nanocarriers capable of encapsulating more than one drug and ensuring sustained release. This all-in-one approach should be promising for more effective therapies of this challenging disease.

Keywords

Combination therapy; Pancreatic cancer; lipid-based nanosystems; gemcitabine; resistance

1) Introduction

Pancreatic ductal adenocarcinoma (PDAC) is a highly aggressive cancer that remains a significant clinical challenge due to its late diagnosis and resistance to chemotherapy. Approximately 90% of PDAC cases are diagnosed at an advanced stage, with unresectable disease and after metastases have occurred. This late detection has a significant impact on the efficacy of the anticancer therapies and therefore on the survival rate of the patients, which is nearly 12% at 5 years [1]. The median survival time for patients drops to less than one year when the disease is diagnosed at stage IV, regardless of the best available chemotherapy protocols [2]. Consequently, PDAC exhibits one of the poorest survival rates among all types of cancer [3] and unfortunately old molecules such as gemcitabine (GEM), a drug approved in 1996, are still the standard of care for this disease, particularly for patients with fragile overall health, who cannot support more effective but less tolerated therapeutic options [4].

Nevertheless, over the past decade, new avenues for potential therapies have been discovered because of the better understanding of the biological mechanisms underlying PDAC. However, when it comes to patients diagnosed at later stages, there is still an urgent need for more effective treatments for the metastatic and chemotherapy-resistant diseases [5]. In addition, pre-existing or acquired resistance can limit the clinical benefit of even the most advanced therapies.

Overcoming resistance and providing new treatment options can be achieved applying strategies such as the combination of cancer drugs and the nanovectorization of chemotherapeutics, namely nanomedicine. Combinations of targeted anticancer agents have the potential to improve response to existing drugs and expand treatment options. For example, FOLFIRINOX combination therapy [oxaliplatin, irinotecan, leucovorin calcium, 5-fluorouracil (5-FU)] has shown promising results in treating patients with PDAC at stage IV, extending the overall survival from 6.6 months when GEM was administered as monotherapy to 11.3 months when the FOLFIRINOX protocol was introduced [6, 7]. When looking for new drug combinations, repurposed therapeutics may also attract much attention in particular if their molecular mechanism of action is well known. In this context, disulfiram (DSF), a drug approved for the treatment of alcohol dependency, has recently been repositioned to exploit its anti-cancer properties [8].

Another fruitful strategy to overcome resistance is the loading of therapeutics into nanodelivery systems, which act as carriers and modify the solubility, distribution, mechanisms of cellular uptake and, ultimately, the efficacy of the active principles. This leads to improved treatments and, if the nanodelivery system is properly modified to recognize specific cell types, the result is a more selective drug delivery and a reduction in side effects. The two approaches - combining drugs and using nanomedicine - can be successfully merged, as in the case of the formulation of paclitaxel-loaded albumin (Nab-paclitaxel), which was combined with GEM in a randomized phase III trial. This treatment increased the overall survival compared to the treatments alone [9]. This review will explore how combination of multi-drug therapies and nanomedicine could help overcome resistance to traditional PDAC treatments.

2) GEM treatment of PDAC and occurrence of resistance

Since 1996 and until a few years ago, GEM monotherapy was the first-line treatment for patients with advanced PDAC, as clinical and survival benefits were observed compared to patients treated with 5-FU [10, 11]. For patients with compromised health, this molecule remains the standard of care.

a) GEM and its mechanism of action

GEM is a synthetic nucleoside analog widely used as an antimetabolite antineoplastic drug. The molecular targets of GEM are intracellular and therefore crossing the plasma membrane is necessary to obtain its pharmacological activity. GEM uses complex transport systems to penetrate the cell (**Figure 1**). These systems consist of several nucleoside transporter proteins (NTs). There are two major classes: the human equilibrative nucleoside transporters (hENTs) and the human concentrative nucleoside transporters (hCNTs) [12]. The hENTs' family is composed of four members, the first three differ in nucleoside specificity while hENT4 has poor affinity for nucleosides and is mainly a monoamine transporter (e.g., dopamine, serotonin). The hCNTs' family is composed of three members, which are responsible of the unidirectional co-transport of nucleosides and sodium (Na^+) or protons (H^+) into cells. The hENT1 is likely the main transporter of GEM [13]. After internalization, GEM is subsequently phosphorylated by deoxycytidine kinase (dCK) and nucleoside mono- and di-phosphate kinases to become the active form of GEM: GEM triphosphate (20,20-difluoro-20-deoxycytidine triphosphate, GEM-TP) [14].

GEM-TP acts mainly by competing with deoxycytidine triphosphate to interfere with DNA synthesis. GEM-TP is incorporated into a single DNA strand by the DNA polymerase during replication. Once incorporated into DNA, GEM-TP leads to premature chain termination after the insertion of another nucleotide triphosphate (dNTP). This GEM-TP position, known as "masked chain termination", inhibits the removal of GEM-TP by DNA repair enzymes, ultimately leading to single-strand breakage [15] (**Figure 1**). Among all the other mechanisms of action of GEM, the active molecule could also be incorporated into RNA to limit RNA synthesis, inhibit topoisomerase I cleavage complexes by enhancing their stability, and be used to improve the efficacy of immunotherapies against cancers that are traditionally unresponsive. In addition, metabolites of GEM may also inhibit other metabolic enzymes to increase the relative cytotoxicity of GEM, indirectly [12, 16].

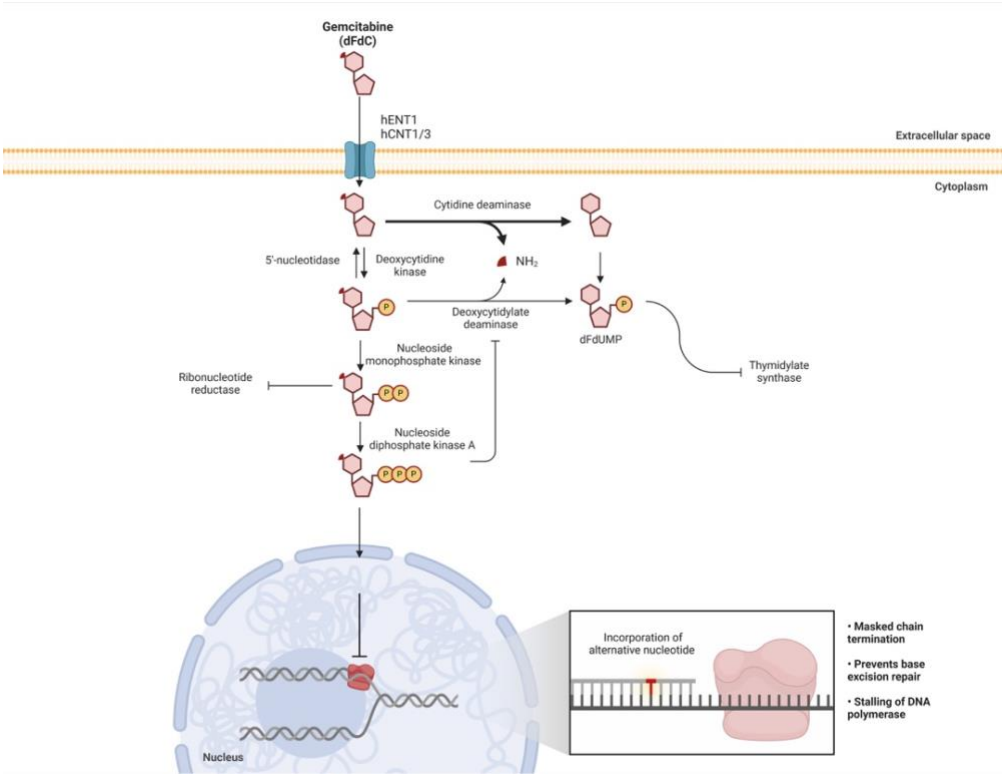

Figure 1. Mechanisms of GEM action (created with Biorender).

b) GEM and its mechanisms of resistance

Cancer therapy resistance can be classified as primary, when treatment is ineffective from the outset, or acquired, when resistance develops after an initial response. Resistance may arise from changes within cancer cells (cell-intrinsic mechanisms) or the tumor microenvironment (non-cell autonomous resistance). Both types pose significant challenges in treating PDAC. Cancer cells can evade treatment by reducing GEM uptake, enhancing detoxification, or undergoing epigenetic changes that alter their state, making them less responsive to therapy [5].

GEM resistance in PDAC is driven by several mechanisms. The role of nucleoside transporters like hENT1 is debated, with some studies linking low hENT1 expression to poor survival, while others find no survival impact [12, 17]. Resistance can also result from the downregulation of dCK, which activates GEM, with high dCK expression associated with better survival [18, 19]. GEM must outcompete endogenous deoxycytidine, but increased ribonucleotide reductase (RR) activity, especially RRM1, can reduce its incorporation into DNA, contributing to resistance [20]. Elevated glucose uptake and flux into the pentose phosphate pathway (PPP) also support resistance by enhancing nucleotide synthesis [21]. Cytidine deaminase (CDA) mediated GEM detoxification, influenced by genetic polymorphisms, further reduces treatment efficacy, with high CDA activity linked to poor outcomes and low activity associated with toxicity [22].

New mechanisms of resistance include p53 gene mutations, which is one of the most commonly mutated genes encountered in tumors (mutation rate of p53 in PDAC can be as high as 80%) [23]. GEM treatment induces a cellular DNA damage response signaling cascade that involves the activation of several factors, including p53. Once activated, p53 induces cell cycle arrest, allowing and facilitating DNA repair. However, once mutated, p53 loses its cell growth inhibitory action, and its "Gardian of genome" function, therefore, cancer cells can survive and carry even more mutations, increasing their aggressiveness. It is proposed that mutation of p53 increases resistance to GEM [24].

These findings underscore the variety of resistance mechanisms that limit the efficacy of GEM in PDAC and the need of alternative treatment options.

3) Current combinatorial treatments in clinic

In 2011 and 2013, two large phase III clinical trials proved the clear benefit of two multi-agent regimens: the FOLFIRINOX and GEM combined with Nab-paclitaxel *compared with* GEM monotherapy in terms of overall survival, which was significantly improved in both cases [6, 9].

These two combinatorial therapies are now the two main first-line options for patients with advanced PDAC, however, both treatments are associated with severe adverse effects and cannot be administered to all patients. Nevertheless, the major breakthrough of drug combination to treat PDAC and the necessity to find less toxic regimens have paved the way for the examination of new multi-drug therapeutic options. GEM remains one of the most widely used drugs in the combination therapies, as its side effects are much less than those of the above-mentioned drugs [25].

Indeed, in clinical trials, GEM is being combined with various classes of drugs, including other antimetabolites. In particular, the effects of combining GEM with S-1 and capecitabine (5-FU prodrug) have been studied [26, 27]. Another widely used drug combination option is GEM administration together with kinase or farnesyltransferase inhibitors (*e.g.* erlotinib, afatinib, AL2846). Among them, tyrosine kinase inhibitors are the most frequently used. These combinations stop the tumor from progressing and induce programmed cell death

[28-30]. Monoclonal antibodies have been combined with GEM in the treatment of pancreatic cancer to enhance its efficacy [31-34].

More recently, multi-drugs therapeutic options reconsider the combination of standard-of-care drugs with repurposed drugs whose mechanism of action and side effects are already known. The chapter below will focus on the combination of the old drug DSF with GEM and the potential interest of this combination for the treatment of PDAC.

4) Potential new combinations with the repurposed drug: disulfiram

Repurposing (or repositioning) drugs is a strategy for identifying new applications for existing drugs that offer advantages over developing entirely new drugs. The main advantages include a reduced risk of failure, a faster development time and a lower cost, as the pre-clinical testing and safety assessments have already been completed. Savings in the early stages of development can make repurposed drugs more cost-effective, although regulatory and phase III costs can remain similar to those of new drugs [35].

a. DSF and its mechanism of action

DSF is a drug candidate with significant potential for repositioning in cancer treatment; it is an anti-alcohol drug approved by the US Food and Drug Administration in 1951 [36]. It acts as a non-selective and irreversible acetaldehyde dehydrogenase (ALDH-1 and -2) inhibitor and causes acetaldehyde accumulation after alcohol consumption. This accumulation provokes several unpleasant reactions including tachycardia, nausea, flushing accompanied with headache and vomiting symptoms which should diminish the desire to consume alcohol [37]. Interestingly, the ability to reduce the expression of ALDH has also been described as an anticancer property as ALDH is a marker of cancer stem cells (CSCs) within a wide variety of tumors, and a key enzyme for the stemness of CSCs [38]. Indeed, DSF was found to possess several anticancer properties [39-41] with excellent tumor-selective toxicity [42].

b. DSF in cancer therapy

The mechanism by which DSF exerts its anti-cancer effect has been investigated for many years and in various cancers [36], revealing its multi-functional role. Li *et al.* identified the disruption of the ubiquitin-proteasome system by DSF, which results in cancer cell death [43]. Several studies suggest an anti-proliferative effect by upregulating the production of reactive oxygen species (ROS), which are involved in apoptosis-related cell death. Indeed, elevated ROS level leads to molecular damage and oxidative stress [44]. Furthermore, DSF can form disulfide bridges with the cysteines of enzymes or other proteins, inhibiting their function. One such a protein is the glycoprotein P (P-gp), an adenosine triphosphate efflux pump localized in the plasma membrane and capable of expelling a wide variety of drugs from the cell, thus conferring multidrug resistance to cancer cells. DSF, by inactivating the P-gp, contributes to reducing the development of resistance to anticancer-drugs [39].

c. DSF for PDAC treatment and synergistic effects when combined with GEM in preclinical and clinical trials

When the effects of DSF were studied on PDAC, Xu Y. *et al.* found that DSF suppressed the survival of pancreatic cancer cells after ionizing radiation exposure, both *in vitro* and *in vivo*. The results suggested that

DSF may function as a radiosensitizer for pancreatic cancer, potentially by enhancing DNA damage, cell cycle arrest, and apoptosis [8].

Furthermore, some studies have been focused on enhancing the synergistic antitumor effect of DSF by complexing it with copper (Cu) [45]. Yao Z. *et al.* observed that the DSF/Cu combination inhibited cell proliferation and induced apoptosis. In fact, DSF/Cu treatment induced autophagy by the upregulation of the transcription factor p8 and activation of the PI3K/mTOR pathway [46]. Zhang X. *et al.* investigated the role of DSF/Cu in autophagy and apoptosis in pancreatic and breast cancer cells. DSF/Cu induced autophagy-dependent apoptosis by activating the IRE1α-XBP1 pathway, a key component of the unfolded protein response (UPR). These results suggest that the use of DSF/Cu, which induces ER stress and contributes to autophagy-dependent cancer cell death, could lead to the development of new therapeutic strategies for pancreatic and breast cancer [47].

DSF has also been combined with several other anticancer drugs, among them, GEM. Dalla Pozza E. *et al.* investigated the combination of GEM and DSF, with and without zinc (Zn), on pancreatic cancer cells and tumor growth in mice. Their findings revealed that the combination therapy resulted in enhanced cell death compared with drugs used alone, showing a link between cancer cell resistance to GEM and low levels of ROS. Combining GEM and DSF increased ROS levels, which was enhanced by Zn. In human pancreatic cancer models, the combination of GEM, DSF, and Zn exhibited robust antitumor effects. Indeed, this combination led to a substantial reduction in tumor mass, nearly halting tumor growth [45].

Kim, S.K. *et al.* investigated the role of DSF in suppressing a pancreatic cancer cell subpopulation expressing high levels of ALDH and known for its high resistance to GEM. As DSF is an irreversible ALDH inhibitor, the reduction of ALDH levels induces apoptosis in cancer cells, preventing them from regaining their resistant properties. Combining DSF with low-dose GEM has shown promising results in suppressing tumor growth in experimental models while sparing hematopoietic stem cells from significant damage [48].

Although the literature on the combination of DSF and GEM in pancreatic cancer is limited, the promising results (both for the efficacy of this combination in pancreatic cancer and its effectiveness in other types of tumors [49, 50]) have allowed the development of two clinical trials.

Jatoi M. started a phase I clinical study in the USA that was conducted in patients with refractory solid tumors or metastatic pancreatic cancer to assess the optimal dose of DSF in combination with GEM and other chemotherapy. The trial was also evaluating whether DSF could reduce tumor-induced muscle wasting and increase the sensitivity of tumor cells to chemotherapy. This trial aimed to determine the maximum tolerated dose (MTD) of DSF combined with GEM in patients with inoperable solid tumors. Among the secondary aims, are the evaluation of side effects, toxicity profile, overall survival, and response rate. The study was recently closed due to a lack of fundings (https://clinicaltrials.gov/search?cond=NCT02671890).

Jameson G. set up a phase II study to evaluate DSF and copper gluconate in patients with metastatic pancreatic cancer who have increased levels of the tumor biomarker carbohydrate antigen 19-9 (CA-19-9) levels, despite treatment. Enrolled patients must have received at least 8 weeks of treatment with Nab-paclitaxel plus GEM, FOLFIRINOX, or GEM alone and have increased levels of CA-19-9 levels without radiographic progression. The study had three treatment arms of five patients, each based on prior treatment. The study measured changes in plasma CA-19-9 level (at least 30%) from baseline and overall response rate. One patient was treated, but this patient was on study for 6 weeks and ended trial participation due to progressive disease. The study was closed due to the low subject enrollment at site (https://clinicaltrials.gov/search?cond=NCT03714555).

d. Limitation of GEM and DSF in clinical use

Despite the high efficacy of DSF in various cancer cells, its clinical effectiveness as cancer treatment has been limited. This is due to its rapid metabolism and degradation by the liver and consequently its short half-life, which prevents it from reaching and accumulating in the tumor.

Similarly, GEM faces limitations due to its rapid clearance, limited stability, and significant adverse effects. In addition, the cellular uptake of GEM depends on membrane transporters and its activation requires intracellular phosphorylation. Consequently, its efficacy is closely related to the expression of the corresponding transporters and kinases, the reduction of which leads to the occurrence of resistance [15, 51].

To improve the therapeutic efficacy of DSF and GEM and to overcome their drawbacks, researchers have explored the use of advanced drug delivery systems in addition to the aforementioned drug combination strategy. These include nano-encapsulation techniques to protect the functional groups and increase drug concentration at the tumor site. Section 5 describes the latest nanodelivery systems used to encapsulate GEM or DSF and the therapeutic benefits of this encapsulation. When the use of nanodelivery systems to protect the molecules joins the strategy of combinatorial treatments, one can imagine the use of co-delivery systems to load different molecules in the same nanovector. The combination of these two strategies may further enhance the synergistic effect and help overcome drug resistance (section 5c) [52].

5) Nanomedicine

a. Benefits of using nanomedicine to treat PDAC

Surgical removal of tumors followed by systemic chemotherapy has constituted the primary treatment modality for PDAC for the past decade. However, factors such as late-stage diagnosis, metastasis, and the dense tumor microenvironments (TMEs) observed in many cases impede the efficacy of this approach. PDAC TMEs are characterized by desmoplasia. This rigid barrier hinders the infiltration of immune cells and the penetration of therapeutic agents, contributing to multidrug resistance and poor patient treatment outcomes. Despite advancements in tumor resection and combination therapy, there is an urgent need for research into the advanced stages of PDAC to develop effective therapeutic strategies [53].

Nanomedicine has gained significant attention in cancer therapy due to its ability to enhance drug absorption, permeability, site specificity, and controlled release. Nanosystems can bypass biological barriers, prevent early drug degradation, and improve cancer diagnosis and treatment. They can be passively targeted to tumors through the enhanced permeability and retention (EPR) effect or actively targeted using ligands to improve the targeting ability [54]. The following chapters will focus on the analysis of GEM- or DSF-loaded lipid-based nanosystems that are among the most biocompatible and biodegradable nanodelivery tools, and the combination of different anticancer agents within the same nanocarrier with the aim of improving efficacy against pancreatic cancer.

b. Lipid-based nanosystems for improved delivery of GEM and DSF as single agents

i. GEM encapsulating liposomes

Many research groups have focused on studying nanosystems to encapsulate GEM to increase its stability, cellular uptake and safely maximize drug efficacy and therapeutic index [55].

Higuchi T. and his group developed the liposomal GEM formulation FF-10832 with improved stability and longer circulation half-life compared to the free drug. Its safety and efficacy are currently being assessed in two ongoing clinical trials (https://clinicaltrials.gov/search?cond= NCT05318573) [56, 57].

Among the various strategies proposed to overcome GEM resistance with delivery nanocarriers, the possibility of formulating liposomes functionalized with an active targeting agent is worth of consideration. This approach consists in decorating the surface of the nanovector with ligands, aptamers or monoclonal antibodies that recognize specific receptors expressed on tumor cells. This allows the nanosystems to deliver the GEM preferentially to the target site and achieve higher *in vitro* and *in vivo* efficacy and better uptake [58-60].

The formulation of thermosensitive liposomes can enhance the efficacy of GEM in pancreatic cancer cells by prolonging the residence time of the drug and increasing its release through mild hyperthermia (mHT). GEM-loaded thermosensitive liposomes caused greater tumor regression with reduced dosage, supporting the interest of this type of drug delivery for treating pancreatic cancer [61, 62].

Moreover, numerous researchers have pursued the synthesis of lipophilic prodrugs of GEM to improve its encapsulation within the liposomes. Wang X. *et al.* bound a C13 chain to GEM, which allowed the preparation of liposomes stable for over two years at temperatures between 2 and 10 °C without any leakage of the drug [63].

Kim B. *et al.* prepared GEM-C16 lipid chain-loaded liposomes fused with human PDAC extracellular vesicles. This platform showed the potential to be an effective approach for chemotherapy in patients with PDAC [64].

Li P. *et al.* prepared GEM-C16-loaded liposomes with a surface modification consisting in the binding of a linear propanediamine derivative to the phospholipid component of liposomes [65].

Masetto F. *et al.* prepared GEM prodrugs with nitric oxide (NO)-donor moieties to enhance the metabolic stability and lipophilicity, facilitating encapsulation in liposomes. The release of NO from GEM into cells demonstrated to induce anti-tumor effects and the most effective treatment was identified when the NO-donor diethylamine NONOate was attached to GEM and encapsulated into the liposomes [66].

Bulanadi J.C. and colleagues synthesized GEM-phytanyl and formed lipid nanoparticles (GEM-LPNPs) with 1,2-dimyristoyl-sn-glycero-3-phosphocholine and cholesterol. GEM-LPNPs exhibited reduced toxicity compared to free GEM, likely attributable to the sustained release of the drug [67].

Dora C.P. *et al.* developed lipid nanoparticles incorporating a phospholipid complex of GEM (GEM-NPs). The characterization of GEM revealed that it existed in an amorphous state within the lipid matrix, which allowed a controlled release *via* diffusion, with an initial burst release followed by a sustained release. GEM-NPs demonstrated notable cytotoxicity against pancreatic adenocarcinoma cell lines [68].

Table 1 includes further information on the lipid-based nanosystems encapsulating GEM.

Table 1: Summary of lipid-based nanosystems for GEM delivery

Therapeutic system	Loaded drug	Phospholipid composition (molar ratio)	Pancreatic tumor models *in vitro/ex vivo* & ***in vivo*** *(in italic characters)*	Remarks	Ref.
Liposomes	GEM (FF-10832)	CHOL/HSPC/N-MPEG-DSPE 4/15/1	GEM metabolism and transport assessed in fractions of the liver, small intestine, tumor homogenates and isolated hepatocytes *Human Capan-1and BxPC-3 xenografted subcutaneously; SUIT-2 orthotopically administered in BALB/cAJcl-nu/nu mice*	Liposome formulation enhanced tumor drug targeting and improved therapeutic outcomes. A PBPK model revealed the pivotal roles of liposome stability, tumor accumulation, and metabolic activation in determining therapeutic success.	[56, 57]
Fucoidan-coated cationic liposomes	GEM	DPPC/DMPC/DOTAP 4/1/1	Capan-1 (human) Panc-1 (human) Human tissues from resectable pancreatic ductal adenocarcinoma	Fucoidan helped to stabilize the liposomes and then improved the drug delivery in the tumor, showing that optimized PEGylated liposomes can be a promise and effective drug delivery system.	[58, 59]
Hyaluronic acid (HA) functionalized pH-sensitive liposomes	GEM	DOPE/CHEMS/DSPC/CHOL/DSPE-mPEG2000 HA-DOPE/CHEMS/DSPC/CHOL/DSPE-mPEG2000 4/2/2/2/0.3	MiaPaCa-2 (human) Gr2000 (MIA-PaCa-2 resistant) *MiaPaca-2 and Gr2000 xenografted in NOD Scid mice*	HA pH-sensitive liposomes showed improved cellular uptake and *in vitro* cytotoxicity. *In vivo* efficacy studies also showed that decorated liposomes only partially resensitized cancer cells to GEM therapy.	[60]
Thermosensitive liposomes	GEM	DPPC/DSPC/DSPC-PEG2000 80/15/50	KPC (mouse) BXPC3 (human)	Only the KPC cell line exhibited a response to liposomal treatment that was consistent with the anticipated response of an ideal thermosensitive liposome formulation.	[61]
Thermosensitive liposomes	GEM-copper complex	DPPC/Lyso-PPC/mDSPE-PEG2000 86/10/4 DPPC/Lyso-SPC/mDSPE-PEG2000 86/10/4 DPPC/MPPC/mDSPE-PEG2000 89/7/4 DPPC/MSPC/mDSPE-PEG2000 89/7/4 DPPC/DSPC/mDSPE-PEG2000 80/15/5	KPC (mouse) *KPC xenografted in C57BL/6 mice*	The interaction between copper and GEM is imperative for achieving elevated GEM concentrations within the loading buffers. This resulted in passive loading of GEM at concentrations that are increased compared to those reported in the literature.	[62]
Liposomes	GEM-C13 diester prodrug	GEM-C13/DMPC/CHOL/mDSPE-PEG2000 1/3/0.45/0.75	AsPC-1 (human metastatic) SU.86.86 (human) *BALB/c nude mice and BALB/c mice bearing AsPC-1 subcutaneous xenografted tumors*	The uptake of liposomes by pancreatic cancer cells was observed to be more effective than the free drug. *In vivo*, liposomes demonstrated a prolonged plasma half-life, increased tumor accumulation, and superior antitumor efficacy compared to free drug.	[63]

Table 1 (continued)

Liposomes	GEM-C16 prodrug	DOPC/CHOL/mDSPE-PEG2000 70:25:5	Panc-1 (human) KPC (mouse)	The hybrid nanosystem had enhanced targeting ability, resulting in increased accumulation at the tumor site and the potential for overcoming GEM resistance.	[64]
Liposomes	GEM-C16 prodrug	LipoidE80/CHOL/mDSPE-PEG/DSPE-PEG-2N 3:1:0.8:0.2	BxPC3 (human) AR42J (rat) Panc02-luc (luciferase-tagged murine) *Female C57BL/6 mice bearing Panc02-luc*	Liposomes demonstrated superior therapeutic outcomes in an orthotopic pancreatic cancer mouse model relative to unmodified liposomes.	[65]
Liposomes	Oxide-releasing GEM prodrug	DSPC/CHOL/mPEG-DSPE 65:30:5	MiaPaCa-2 (human) Panc-1 (human)	*In vitro*, liposomal delivery of the drug led to an increase in the level of apoptosis in PDAC cells and increased the expression of pro-apoptotic proteins in comparison with standard GEM treatment.	[66]
Liposomes	GEM-phytanyl conjugate prodrug	DMPC/CHOL 73.5/8.1	CFPAC-1 (human) BxPC3 (human) MiaPaCa-2 (human) *NOD/SCID mice bearing* CFPAC-1 *xenografted tumors*	The in-situ enzymatic conversion of the prodrug to GEM was achieved with a high degree of effectiveness, depending on the enzyme concentration. *In vivo*, these liposomes exhibited superior antitumor efficacy in comparison with free GEM.	[67]
Lipid nanoparticles incorporating a phospholipid complex	Phospholipid complex of GEM (GEM-PC)	GEM-PC/TPGS (0.5-1% of surfactant)	MiaPaCa-2 (human) Panc-1 (human) *Pancreatic adenocarcinoma was induced in Sprague−Dawley rats using a chemical (DMBA) carcinogenesis approach*	*In vitro* investigations revealed that liposomes containing GEM demonstrated enhanced stability, efficacy, and safety. These systems exhibited resistance to enzymatic degradation.	[68]

Notes: Abbreviations: *Cholesterol: CHOL; hydrogenated soy phosphatidylcholine: HSPC; N-(carbonyl-methoxypolyethylene glycol 2000)-1,2-distearoyl-sn-glycero-3-phosphoethanolamine sodium salt: N-MPEG-DSPE or DSPE-mPEG2000; 1,2-dipalmitoyl-sn-glycero-3-phosphocholine: DPPC; 1,2-dioleoyl-3-triethylammonium-propane: DOTAP; 1-myristoyl-2-palmitoyl-sn-glycero-3-phosphocholine: MPPC; 1,2-dipalmitoyl-sn-glycero-3-phospoethanolamine-N-diethylenetriaminepentaacetic acid (gadolinium salt): Gd-DSPE; 1-palmitoyl-2-hydroxy-sn-glycero-3-phosphocholine: Lyso-PPC; 1-stearoyl-2-hydroxy-sn-glycero-3-phosphocholine: Lyso-SPC; 1-myristoyl-2-stearoyl-sn-glycero-3-phosphocholine: MSPC; 1, 2-dimyristoyl-sn-glycero-3-phosphocholine: DMPC; 1,2-dioleoly-sn-glycero-2-phosphocholine: DOPC; N,N-dimethyl-1,3-propanediamine conjugated to DSPE-PEG: DSPE-PEG-2N.*

ii. DSF-encapsulating liposomes

The encapsulation of DSF in liposomes has shown promising results to treat various type of cancer [69], however the number of studies concerning pancreatic cancer is limited. Marengo *et al.* focused on the development of hyaluronic acid-decorated liposomes, containing the DSF derivative diethyldithiocarbamate-copper ($Cu(DDC)_2$), to target the CD44 receptor, a marker of CSCs in PDAC. The characterization of the liposomes revealed high encapsulation efficiency, and cryo-TEM analysis confirmed the presence of Cu(DDC)2 crystals in the aqueous core. The liposomes exhibited robust antiproliferative effects on CSCs from PDAC cell lines or patient derived CSCs, predominantly through mechanisms involving ROS species [45].

c. Lipid-based nanosystems for drugs co-delivery to improve PDAC treatment outcomes

Drug-combined delivery in pancreatic cancer has many advantages, such as the potential to overcome drug resistance, reduce toxicity, and address the problem of inadequate drug accumulation in tumor tissue [70].

A considerable body of research has been conducted in recent years examining the potential of GEM in combination with other pharmaceutical agents within the same drug delivery nanosystem (**Figure 2**). This approach is meant to enhance the anticancer impact of GEM and decrease or delay the appearance of resistance to GEM [71, 72].

Yang W. *et al.* successfully developed an antibody fragment (AF) conjugated to GEM/paclitaxel-loaded liposomes (AF-GPL), with enhanced uptake in pancreatic cancer cells compared to non-targeted liposomes (GPL). Moreover, it was observed that AF-GPL cytotoxic effect was markedly increased in comparison to GPL. It is noteworthy that AF-GPL induced a substantial number of cancer cells to undergo apoptosis, with most cells exhibiting characteristics of late apoptosis [73].

Tang M. *et al.* developed a dual-drug liposomal system (pSL-GEM&ZEB) co-encapsulating GEM and zebularine. Apart from observing an improvement in GEM uptake due to the use of liposomes, its efficacy was also enhanced. Indeed, zebularine inhibited cytidine deaminase (CDA), which is the enzyme responsible for GEM inactivation. *In vivo*, liposomes reduced GEM clearance and prolonged its circulation time, increasing its bioavailability and half-life. In rats, pSL-GEM&ZEB showed better pharmacokinetics and tumor treatment than free drugs; co-delivery with zebularine also prevented cancer cell regrowth and resistance [74].

The potential of curcumin to augment the efficacy of GEM in pancreatic cancer by impeding the activity of the MRP5 transporter, a primary contributor to GEM resistance, was examined by Xu H. *et al.* The developed pH-sensitive liposomes (PSL), co-encapsulating GEM and curcumin, resulted in increased GEM accumulation and cytotoxicity within MiaPaCa-2 pancreatic cancer cells. In rats, PSL increased GEM exposure and half-life, while curcumin reduced its clearance. This dual-drug system offers enhanced drug delivery and efficacy, overcoming GEM resistance; but additional optimization is necessary for clinical use [75].

Emamzadeh M. *et al.* examined the potential of thermoresponsive liposomes (PMTL) to enhance the delivery and efficacy of GEM and cisplatin (Cis) at 40 °C. PMTL incorporation led to significant enhancement in the drugs cytotoxicity in MiaPaCa-2 and BxPC-3 pancreatic cancer cells. PMTL performed better than standard liposomes (TTL): GEM and Cis in PMTL worked synergistically at 40 °C, unlike the free drugs. PMTL formulations enhanced drug delivery and tumor cell killing through a controlled, synergistic approach to multi-drug therapies while minimizing systemic toxicity [76].

A study by Wang Y. *et al.* investigated combining GEM chemotherapy and Mcl-1 siRNA to treat pancreatic cancer. The Mcl-1 protein is overexpressed in pancreatic cancer cells and was found to enhance the effect of GEM when silenced. A liposomal formulation (LP-Gem-siMcl-1) was developed to deliver GEMs and protect

the siRNA, enhancing its uptake by tumor cells. LP-Gem-siMcl-1 was successfully internalized by PANC-1 and BxPC-3 pancreatic cancer cells, silencing Mcl-1 and increasing tumor cell death. *In vitro*, LP-Gem-siMcl-1 demonstrated markedly enhanced efficacy, with a substantially higher reduction in cell viability compared to free GEM or siMcl-1 alone. In mice, LP-Gem-siMcl-1 was more effective than free GEM or siMcl-1 at slowing tumor growth, and led to increased tumor necrosis [77].

Shrestha P. *et al.* investigated the potential of combining, within the same liposome, dordaviprone (ONC201) an inhibitor of AKT/ERK pathways and the stearoyl lipid-GEM conjugate. This liposome was further decorated with the lipidic mucin 1 (MUC1)-binding peptide for selective drug delivery to the pancreatic tumor. This combination has been observed to enhance cell cycle arrest, induce ER stress, disrupt metabolic pathways and overcome GEM resistance by inhibiting the Akt/ERK pathways. *In vivo* studies demonstrated the efficacy of lipid-GEM-ONC201 liposomes in reducing tumor growth and size, upregulating pro-apoptotic proteins, and inducing caspase-dependent apoptosis. Liposomes demonstrated prolonged drug release and enhanced tumor penetration. The targeted delivery of liposomes resulted in a more effective reduction of cell proliferation and weakening of the PDAC stroma [78].

In addition to drug combinations within the same nanosystem, the following two studies are noteworthy: each drug is encapsulated in a separate nanocarrier and both nanocarriers are then administrated together. Meng H. *et al.* combined two distinct types of nanoparticles: TGFβ inhibitor (LY364947)-loaded mesoporous silica nanoparticles (TGFβi-MSNP) and GEM-encapsulating liposomes. The TGFβi-MSNP demonstrated efficacy in targeting the tumor stroma, reducing stromal cell coverage of blood vessels, enhancing vascular permeability, and improving drug delivery. GEM was encapsulated in the liposomes using the ammonium sulfate gradient to reduce toxicity and improve tumor shrinkage. The carriers were PEGylated to prolong the circulation time, and LY364947 was efficiently loaded onto the MSNPs to interfere with TGF-β signaling. This approach demonstrated the potential to enhance drug delivery and immune responses by modifying the tumor microenvironment [79].

Kim C. *et al.* examined the potential of cromolyn, an S100P inhibitor, as a therapeutic agent for PDAC treatment. S100P overexpression is a common occurrence in pancreatic cancers, making it an ideal target for therapeutic intervention. Cromolyn was encapsulated in PEGylated liposomes (PEG-lipo-cro), resulting in an improved drug delivery system with enhanced anti-cancer effects on S100P-expressing BxPC-3 pancreatic cancer cells and, when combined with GEM (PEG-lipo-GEM), inhibited NF-κB, thereby enhancing the tumor response. *In vivo*, the PEG-lipo-cro formulation outperformed free cromolyn in inhibiting tumor growth and, when combined with PEG-lipo-GEM, showed enhanced effects without significant side effects, suggesting a promising cancer treatment strategy [80].

Figure 2 summarize some of the studies reported in this paragraph.

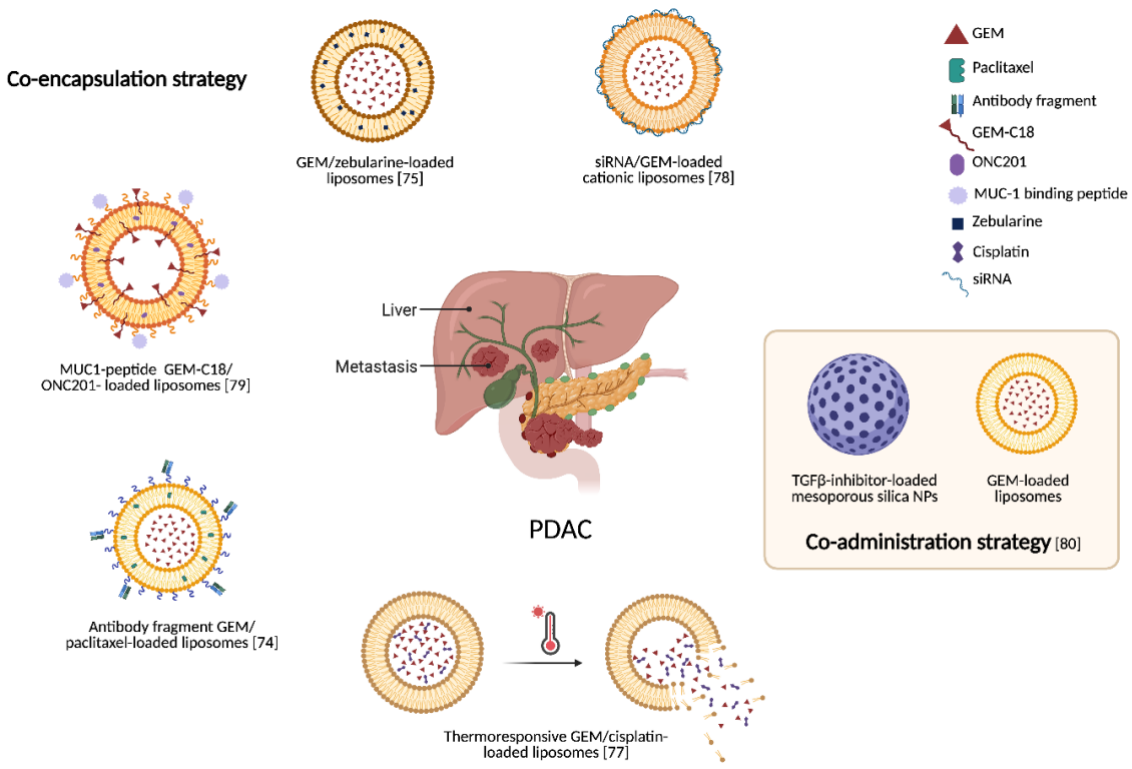

Figure 2. Examples of drug co-delivery with GEM using liposomes (created with Biorender).

d. Criteria of the ideal nanodelivery system for Gem/DSF combination

The use of nanosystems has emerged as a strategy for delivering conventional drugs. A variety of nanocarriers have been formulated for combinational therapy, including polymer nanoparticles (NPs) [81], liposomes [82], polymersomes [83], polymers/dendrimers [84], carbon nanotubes [85], magnetic NPs [86], and mesoporous silica [87]. As previously discussed, GEM is a hydrophilic drug, while DSF is a hydrophobic drug. To encapsulate both drugs in a single nanosystem, it is necessary to employ a nanocarrier composed of two distinct compartments, each exhibiting higher compatibility with one of the drugs [15]. Moreover, previous studies have shown that the increasing of ROS production by DSF could promote the effect of GEM on pancreatic cancer cells [88], so it is reasonable to propose that the administration of the two drugs should be sequential, first DSF and then GEM. Liposomes are one of the most suitable delivery systems to obtain this sequential release as DSF would be mostly encapsulated in the lipophilic bilayer of the nanocarrier and therefore released quickly while GEM would be loaded in the aqueous core of the liposomes thanks to its hydrophilicity, and it would be released with a slower kinetics.

Among other types of nanosystems that can be exploited there are the hyalurosomes, which are composed of phospholipids and hyaluronic acid. Hyalurosomes can be exploited to encapsulate two drugs: in this case lipophilic drugs are encapsulated in the phospholipid layer, and the hydrophilic therapeutic agents are entrapped in the aqueous core of the system. In a recent study, luteolin (LUT) and dexamethasone (DEX) were co-encapsulated into hyalurosomes for the transdermal treatment of rheumatoid arthritis (RA). The co-loading of these two active molecules within a single carrier enabled synergistic anti-inflammatory effects while minimizing systemic exposure. The dual encapsulation strategy resulted in enhanced drug retention, sustained release, and targeted delivery to inflamed tissues. Notably, *in vivo* results showed that the co-encapsulated

system outperformed individual formulations in reducing joint inflammation and oxidative stress, offering a promising non-invasive alternative to conventional RA injections [89].

Another study investigated the co-encapsulation of paclitaxel (PTX) and 5-fluorouracil (5-FU) into folic acid-modified, lipid-coated hollow mesoporous silica nanoparticles, which enabled the simultaneous delivery of both hydrophobic and hydrophilic drugs. In biological studies, the efficacy of this dual-loading strategy was demonstrated to be superior to single-drug-loaded or free drug treatments in MCF-7 breast cancer cells, with increased apoptosis and cell growth inhibition [90].

Polymersomes, similar in structure to liposomes but synthesized from a polymer instead of a lipid component, can encapsulate hydrophilic molecules in their aqueous interior and hydrophobic molecules in their membrane. Depending on the properties of the polymer or the encapsulated molecule, the drug release of polymersomes can be manipulated by pH, light, magnetic field and temperature [91].

6) Conclusions

Treatment options for PDAC have been stagnant for many years until the last decade, since when a better understanding of the complex biology of PDAC and the development of innovative therapeutic strategies have transformed the therapeutic landscape. Nevertheless, there are still persistent challenges ahead, particularly in terms of earlier diagnosis and overcoming chemoresistance. Recent preclinical promising results offer hope for more effective treatments. For instance, the combination of GEM with other drugs, such as DSF, has been shown to enhance antitumor effects and overcome resistance mechanisms. The synergistic potential of these combinations, particularly when paired with nanomedicine, represents a cutting-edge therapeutic approach.

In fact, nowadays, the development of multi-drug delivery systems for simultaneous delivery of multiple therapeutic agents is a key focus in nanotechnology-based pharmacology. These systems use several compartments to encapsulate drugs with different physicochemical properties, enabling release rates to be controlled and mitigating adverse effects. In fact, if the drugs work synergistically, therapeutic doses can be reduced, resulting in less toxicity for patients. Nevertheless, the inability to precisely manage the ratio of loaded drugs, the difficulty in regulating release mechanisms, and the lack of targeting are limitations to be addressed. The integration of advanced drug delivery systems such as multifunctional nanocarriers will tackle these limitations and provide better treatment outcomes in PDAC.

Over the coming years, continued research and clinical trials are essential to translate these promising strategies into concrete therapies for patients, offering new prospects in the fight against this aggressive cancer.

CRediT authorship contribution statement

Valeria Bincoletto: Conceptualization; Visualization; Writing – original draft; Writing – review and editing

Ilaria Andreana: Conceptualization; Software; Visualization; Writing – review and editing

Barbara Stella: Conceptualization; Visualization; Writing – review and editing.

Nazanine Modjtahedi: Conceptualization; Supervision; Validation; Visualization; Writing – original draft; Writing – review and editing

Silvia Arpicco: Conceptualization; Supervision; Validation; Visualization; Writing – review and editing

Giorgia Urbinati: Conceptualization; Supervision; Validation; Visualization; Writing – original draft; Writing – review and editing

Declaration of competing interest

The authors declare no conflicts of interest.

Aknowledgments

Not applicable.

List of abbreviations

5-FU: 5-fluorouracil

ALDH: acetaldehyde dehydrogenase

CA-19-9: Carbohydrate antigen 19-9 (tumor biomarker)

CD44 receptor: hyaluronic acid receptor

CDA: cytidine deaminase

CHOL: cholesterol

CSCs: cancer stem cells

$Cu(DDC)_2$: diethyldithiocarbamate-copper

dCK: deoxycytidine kinase

DEX: dexamethasone

DMPC: 1,2-dimyristoyl-sn-glycero-3-phosphocholine

dNTP: nucleotide triphosphate

DOPC: 1,2-dioleoyl-sn-glycero-2-phosphocholine

DOTAP: 1,2-dioleoyl-3-triethylammonium-propane

DPPC: 1,2-dipalmitoyl-sn-glycero-3-phosphocholine

DSF: disulfiram

DSPE-PEG-2N: N,N-dimethyl-1,3-propanediamine conjugated to DSPE-PEG-NHS

EPR: enhanced permeability and retention

FOLFIRINOX combination therapy: oxaliplatin, irinotecan, leucovorin calcium, 5-fluorouracil

Gd-DSPE: 1,2-dipalmitoyl-sn-glycero-3-phosphoethanolamine-N-diethylenetriaminepentaacetic acid (gadolinium salt)

GEM-TP: GEM triphosphate (20,20-difluoro-20-deoxycytidine triphosphate)

GEM: gemcitabine

hCNTs: human concentrative nucleoside transporters

hENTs: human equilibrative nucleoside transporters

HSPC: hydrogenated soy phosphatidylcholine

Lyso-PPC: 1-palmitoyl-2-hydroxy-sn-glycero-3-phosphocholine

Lyso-SPC: 1-stearoyl-2-hydroxy-sn-glycero-3-phosphocholine

LUT: luteolin

mHT: mild hyperthermia (mHT)

MPPC: 1-myristoyl-2-palmitoyl-sn-glycero-3-phosphocholine

MSPC: 1-myristoyl-2-stearoyl-sn-glycero-3-phosphocholine

MTD: maximum tolerated dose

MUC1: lipidic mucin-1 binding peptide

N-MPEG-DSPE or DSPE-mPEG2000: N-(carbonyl-methoxypolyethylene glycol 2000)-1,2-distearoyl-sn-glycero-3-phosphoethanolamine sodium salt

Nab-paclitaxel: paclitaxel-loaded albumin

NF-κB: nuclear factor-kappa B

NTs: nucleoside transporter proteins

ONC201: dordaviprone

P-gp: glycoprotein P

PDAC: pancreatic ductal adenocarcinoma

PPP: pentose phosphate pathway

PTX: paclitaxel

ROS: reactive oxygen species

RA: rheumatoid arthritis

RR: ribonucleotide reductase

siPlk1: small interfering RNA against Polo-like kinase-1

TMEs: tumor microenvironments

UPR: unfolded protein response

References

[1] C.J. Halbrook, C.A. Lyssiotis, M. Pasca di Magliano, A. Maitra, Pancreatic cancer: Advances and challenges, Cell, 186 (2023) 1729-1754.

[2] C. Springfeld, D. Jäger, M.W. Büchler, O. Strobel, T. Hackert, D.H. Palmer, J.P. Neoptolemos, Chemotherapy for pancreatic cancer, Presse Med, 48 (2019) e159-e174.

[3] Z.I. Hu, E.M. O'Reilly, Therapeutic developments in pancreatic cancer, Nat Rev Gastroenterol Hepatol, 21 (2024) 7-24.

[4] H.C. Kung, J. Yu, Targeted therapy for pancreatic ductal adenocarcinoma: Mechanisms and clinical study, MedComm (2020), 4 (2023) e216.

[5] L.D. Wood, M.I. Canto, E.M. Jaffee, D.M. Simeone, Pancreatic cancer: pathogenesis, screening, diagnosis, and treatment, gastroenterology, 163 (2022) 386-402.e381.

[6] T. Conroy, F. Desseigne, M. Ychou, O. Bouché, R. Guimbaud, Y. Bécouarn, A. Adenis, J.L. Raoul, S. Gourgou-Bourgade, C. de la Fouchardière, J. Bennouna, J.B. Bachet, F. Khemissa-Akouz, D. Péré-Vergé, C. Delbaldo, E. Assenat, B. Chauffert, P. Michel, C. Montoto-Grillot, M. Ducreux, FOLFIRINOX versus gemcitabine for metastatic pancreatic cancer, N Engl J Med, 364 (2011) 1817-1825.

[7] S. Gourgou-Bourgade, C. Bascoul-Mollevi, F. Desseigne, M. Ychou, O. Bouché, R. Guimbaud, Y. Bécouarn, A. Adenis, J.L. Raoul, V. Boige, J. Bérille, T. Conroy, Impact of FOLFIRINOX compared with gemcitabine on quality of life in patients with metastatic pancreatic cancer: results from the PRODIGE 4/ACCORD 11 randomized trial, J Clin Oncol, 31 (2013) 23-29.

[8] Y. Xu, L. Lu, J. Luo, L. Wang, Q. Zhang, J. Cao, Y. Jiao, Disulfiram alone functions as a radiosensitizer for pancreatic cancer both in vitro and in vivo, Front Oncol, 11 (2021) 683695.

[9] D.D. Von Hoff, T. Ervin, F.P. Arena, E.G. Chiorean, J. Infante, M. Moore, T. Seay, S.A. Tjulandin, W.W. Ma, M.N. Saleh, M. Harris, M. Reni, S. Dowden, D. Laheru, N. Bahary, R.K. Ramanathan, J. Tabernero, M.

Hidalgo, D. Goldstein, E. Van Cutsem, X. Wei, J. Iglesias, M.F. Renschler, Increased survival in pancreatic cancer with nab-paclitaxel plus gemcitabine, N Engl J Med, 369 (2013) 1691-1703.
[10] B. Pandit, M. Royzen, Recent Development of Prodrugs of Gemcitabine, Genes (Basel), 13 (2022) 466.
[11] H.A. Burris, 3rd, M.J. Moore, J. Andersen, M.R. Green, M.L. Rothenberg, M.R. Modiano, M.C. Cripps, R.K. Portenoy, A.M. Storniolo, P. Tarassoff, R. Nelson, F.A. Dorr, C.D. Stephens, D.D. Von Hoff, Improvements in survival and clinical benefit with gemcitabine as first-line therapy for patients with advanced pancreas cancer: a randomized trial, J Clin Oncol, 15 (1997) 2403-2413.
[12] C.J. Carter, A.H. Mekkawy, D.L. Morris, Role of human nucleoside transporters in pancreatic cancer and chemoresistance, World J Gastroenterol, 27 (2021) 6844-6860.
[13] D.S. Gesto, N.M. Cerqueira, P.A. Fernandes, M.J. Ramos, Gemcitabine: a critical nucleoside for cancer therapy, Curr Med Chem, 19 (2012) 1076-1087.
[14] E.J.B. Derissen, J.H. Beijnen, Intracellular Pharmacokinetics of pyrimidine analogues used in oncology and the correlation with drug action, Clin Pharmacokinet, 59 (2020) 1521-1550.
[15] A.K. Beutel, C.J. Halbrook, Barriers and opportunities for gemcitabine in pancreatic cancer therapy, Am J Physiol Cell Physiol, 324 (2023) C540-c552.
[16] A.C. Larson, K.R. Doty, J.C. Solheim, The double life of a chemotherapy drug: Immunomodulatory functions of gemcitabine in cancer, Cancer Med, 13 (2024) e7287.
[17] Y. Xi, P. Yuan, T. Li, M. Zhang, M.F. Liu, B. Li, hENT1 reverses chemoresistance by regulating glycolysis in pancreatic cancer, Cancer Lett, 479 (2020) 112-122.
[18] S. Dash, T. Ueda, A. Komuro, M. Honda, R. Sugisawa, H. Okada, Correction: Deoxycytidine kinase inactivation enhances gemcitabine resistance and sensitizes mitochondrial metabolism interference in pancreatic cancer, Cell Death Dis, 15 (2024) 384.
[19] V. Sebastiani, F. Ricci, B. Rubio-Viqueira, P. Kulesza, C.J. Yeo, M. Hidalgo, A. Klein, D. Laheru, C.A. Iacobuzio-Donahue, Immunohistochemical and genetic evaluation of deoxycytidine kinase in pancreatic cancer: relationship to molecular mechanisms of gemcitabine resistance and survival, Clin Cancer Res, 12 (2006) 2492-2497.
[20] B. Li, F. Xing, J. Wang, X. Wang, C. Zhou, G. Fan, Q. Zhuo, S. Ji, X. Yu, X. Xu, Y. Qin, Z. Li, YBX1 as a therapeutic target to suppress the LRP1-β-catenin-RRM1 axis and overcome gemcitabine resistance in pancreatic cancer, Cancer Lett, 602 (2024) 217197.
[21] A. Shimoni-Sebag, I. Abramovich, B. Agranovich, R. Massri, C. Stossel, D. Atias, M. Raites-Gurevich, K. Yizhak, T. Golan, E. Gottlieb, Y.R. Lawrence, A metabolic switch to the pentose-phosphate pathway induces radiation resistance in pancreatic cancer, Radiother Oncol, 202 (2024) 110606.
[22] A. Lumeau, N. Bery, A. Francès, M. Gayral, G. Labrousse, C. Ribeyre, C. Lopez, A. Nevot, A. El Kaoutari, N. Hanoun, E. Sarot, M. Perrier, F. Pont, J.P. Cerapio, J.J. Fournié, F. Lopez, M. Madrid-Mencia, V. Pancaldi, M.J. Pillaire, V. Bergoglio, J. Torrisani, N. Dusetti, J.S. Hoffmann, L. Buscail, M. Lutzmann, P. Cordelier, Cytidine deaminase resolves replicative stress and protects pancreatic cancer from DNA-targeting drugs, Cancer Res, 84 (2024) 1013-1028.
[23] A. Tiwari, K. Tashiro, A. Dixit, A. Soni, K. Vogel, B. Hall, I. Shafqat, J. Slaughter, N. Param, A. Le, E. Saunders, U. Paithane, G. Garcia, A.R. Campos, J. Zettervall, M. Carlson, T.K. Starr, Y. Marahrens, A.J. Deshpande, C. Commisso, P.P. Provenzano, A. Bagchi, Loss of HIF1A From pancreatic cancer cells increases

expression of PPP1R1B and degradation of p53 to promote invasion and metastasis, Gastroenterology, 159 (2020) 1882-1897.e1885.
[24] C.E. Wu, Y.R. Pan, C.N. Yeh, J. Lunec, Targeting P53 as a future strategy to overcome gemcitabine resistance in biliary tract cancers, Biomolecules, 10 (2020) 1474.
[25] S. Robatel, M. Schenk, Current limitations and novel perspectives in pancreatic cancer treatment, Cancers (Basel), 14 (2022) 985.
[26] D.H. Palmer, R. Jackson, C. Springfeld, P. Ghaneh, C. Rawcliffe, C.M. Halloran, O. Faluyi, D. Cunningham, J. Wadsley, S. Darby, T. Meyer, R. Gillmore, P. Lind, B. Glimelius, S. Falk, Y.T. Ma, G.W. Middleton, S. Cummins, P.J. Ross, H. Wasan, A. McDonald, T. Crosby, P. Hammel, D. Borg, S. Sothi, J.W. Valle, A. Mehrabi, P. Bailey, C. Tjaden, C. Michalski, T. Hackert, M.W. Büchler, J.P. Neoptolemos, Pancreatic adenocarcinoma: long-term outcomes of adjuvant therapy in the ESPAC4 phase III trial, J Clin Oncol, 43 (2025) 1240-1253.
[27] H. Eguchi, Y. Takeda, H. Takahashi, S. Nakahira, M. Kashiwazaki, J. Shimizu, D. Sakai, F. Isohashi, H. Nagano, M. Mori, Y. Doki, A Prospective, Open-Label, Multicenter Phase 2 Trial of Neoadjuvant therapy using full-dose gemcitabine and s-1 concurrent with radiation for resectable pancreatic ductal adenocarcinoma, Ann Surg Oncol, 26 (2019) 4498-4505.
[28] R. Liu, Z. Ji, X. Wang, J. Xin, L. Zhu, S. Ge, L. Zhang, M. Bai, T. Ning, Y. Yang, H. Li, T. Deng, Y. Ba, Efficacy and safety of multi-target tyrosine kinase inhibitor AL2846 combined with gemcitabine in pancreatic cancer, Invest New Drugs, 43 (2025) 81-92.
[29] D. Zhang, C. Benedikt Westphalen, M. Quante, D.T. Waldschmidt, S. Held, F. Kütting, K. Dorman, K. Heinrich, L. Weiss, M. Boukovala, M. Haas, S. Boeck, V. Heinemann, V. Probst, Gemcitabine and nab-paclitaxel combined with afatinib in metastatic pancreatic cancer - results of a phase 1b clinical trial, Eur J Cancer, 201 (2024) 113926.
[30] J.H. Jo, D.E. Jung, H.S. Lee, S.B. Park, M.J. Chung, J.Y. Park, S. Bang, S.W. Park, S. Cho, S.Y. Song, A phase I/II study of ivaltinostat combined with gemcitabine and erlotinib in patients with untreated locally advanced or metastatic pancreatic adenocarcinoma, Int J Cancer, 151 (2022) 1565-1577.
[31] Y. Li, D. Li, Q. Liu, J. Li, Combined efficacy of nimotuzumab and gemcitabine on the treatment of advanced pancreatic cancer, Pancreas, 53 (2024) e537-e542.
[32] P.E. Oberstein, A. Dias Costa, E.A. Kawaler, V. Cardot-Ruffino, O.E. Rahma, N. Beri, H. Singh, T.A. Abrams, L.H. Biller, J.M. Cleary, P. Enzinger, B.M. Huffman, N.J. McCleary, K.J. Perez, D.A. Rubinson, B.L. Schlechter, R. Surana, M.B. Yurgelun, S.J. Wang, J. Remland, L.K. Brais, N. Bollenrucher, E. Chang, L.R. Ali, P.J. Lenehan, I. Dolgalev, G. Werba, C. Lima, C.E. Keheler, K.M. Sullivan, M. Dougan, C. Hajdu, M. Dajee, M.R. Pelletier, S. Nazeer, M. Squires, D. Bar-Sagi, B.M. Wolpin, J.A. Nowak, D.M. Simeone, S.K. Dougan, Blockade of IL1β and PD1 with combination chemotherapy reduces systemic myeloid suppression in metastatic pancreatic cancer with heterogeneous effects in the tumor, Cancer Immunol Res, 12 (2024) 1221-1235.
[33] S. Qin, J. Li, Y. Bai, Z. Wang, Z. Chen, R. Xu, J. Xu, H. Zhang, J. Chen, Y. Yuan, T. Liu, L. Yang, H. Zhong, D. Chen, L. Shen, C. Hao, D. Fu, Y. Cheng, J. Yang, Q. Wang, B. Qin, H. Pan, J. Zhang, X. Bai, Q. Zheng, Nimotuzumab plus gemcitabine for k-ras wild-type locally advanced or metastatic pancreatic cancer, J Clin Oncol, 41 (2023) 5163-5173.

[34] A.L. Coveler, M.J. Reilley, M. Zalupski, T. Macarulla, C. Fountzilas, M. Ponz-Sarvisé, A. Nagrial, N.V. Uboha, S. Frentzas, M. Overman, A. Noonan, W.A. Messersmith, N. Pavlakis, N.B. Mettu, I. Bisha, Y. Wang, P. Smith, E. Murtomaki, A.A. Bielska, V. Bragulat, Z.A. Cooper, R. Kumar, D.R. Spigel, A phase Ib/II randomized clinical trial of oleclumab with or without durvalumab plus chemotherapy in patients with metastatic pancreatic ductal adenocarcinoma, Clin Cancer Res, 30 (2024) 4609-4617.
[35] S. Pushpakom, F. Iorio, P.A. Eyers, K.J. Escott, S. Hopper, A. Wells, A. Doig, T. Guilliams, J. Latimer, C. McNamee, A. Norris, P. Sanseau, D. Cavalla, M. Pirmohamed, Drug repurposing: progress, challenges and recommendations, Nat Rev Drug Discov, 18 (2019) 41-58.
[36] E. Ekinci, S. Rohondia, R. Khan, Q.P. Dou, Repurposing disulfiram as an anti-cancer agent: updated review on literature and patents, Recent Pat Anticancer Drug Discov, 14 (2019) 113-132.
[37] T. Lehner, B. Gao, B. Mackowiak, Alcohol metabolism in alcohol use disorder: a potential therapeutic target, Alcohol Alcohol, 59 (2024) agad077.
[38] Z. Yang, F. Guo, A.E. Albers, J. Sehouli, A.M. Kaufmann, Disulfiram modulates ROS accumulation and overcomes synergistically cisplatin resistance in breast cancer cell lines, Biomed Pharmacother, 113 (2019) 108727.
[39] T.W. Loo, M.C. Bartlett, D.M. Clarke, Disulfiram metabolites permanently inactivate the human multidrug resistance P-glycoprotein, Mol Pharm, 1 (2004) 426-433.
[40] W. Bu, Z. Wang, L. Meng, X. Li, X. Liu, Y. Chen, Y. Xin, B. Li, H. Sun, Disulfiram inhibits epithelial-mesenchymal transition through TGFβ-ERK-Snail pathway independently of Smad4 to decrease oral squamous cell carcinoma metastasis, Cancer Manag Res, 11 (2019) 3887-3898.
[41] J.J. Hu, X. Liu, S. Xia, Z. Zhang, Y. Zhang, J. Zhao, J. Ruan, X. Luo, X. Lou, Y. Bai, J. Wang, L.R. Hollingsworth, V.G. Magupalli, L. Zhao, H.R. Luo, J. Kim, J. Lieberman, H. Wu, FDA-approved disulfiram inhibits pyroptosis by blocking gasdermin D pore formation, Nat Immunol, 21 (2020) 736-745.
[42] K. Iljin, K. Ketola, P. Vainio, P. Halonen, P. Kohonen, V. Fey, R.C. Grafström, M. Perälä, O. Kallioniemi, High-throughput cell-based screening of 4910 known drugs and drug-like small molecules identifies disulfiram as an inhibitor of prostate cancer cell growth, Clin Cancer Res, 15 (2009) 6070-6078.
[43] Y. Li, Copper homeostasis: Emerging target for cancer treatment, IUBMB Life, 72 (2020) 1900-1908.
[44] Y. Liu, X. Guan, M. Wang, N. Wang, Y. Chen, B. Li, Z. Xu, F. Fu, Z. Zheng, C. Du, Disulfiram/Copper induces antitumor activity against gastric cancer via the ROS/MAPK and NPL4 pathways, Bioengineered, 13 (2022) 6579-6589.
[45] A. Marengo, S. Forciniti, I. Dando, E. Dalla Pozza, B. Stella, N. Tsapis, N. Yagoubi, G. Fanelli, E. Fattal, C. Heeschen, M. Palmieri, S. Arpicco, Pancreatic cancer stem cell proliferation is strongly inhibited by diethyldithiocarbamate-copper complex loaded into hyaluronic acid decorated liposomes, Biochim Biophys Acta Gen Subj, 1863 (2019) 61-72.
[46] Z. Yao, X. Li, J. Gao, Y. Wang, L. Xiao, X. Chang, F. Liu, Z. Feng, X. Zhang, Transcription factor p8 regulates autophagy in response to disulfiram via PI3K/mTOR/p70S6K signaling pathway in pancreatic cancer cells, Hum Cell, 35 (2022) 1464-1474.
[47] X. Zhang, P. Hu, S.Y. Ding, T. Sun, L. Liu, S. Han, A.B. DeLeo, A. Sadagopan, W. Guo, X. Wang, Induction of autophagy-dependent apoptosis in cancer cells through activation of ER stress: an uncovered anti-cancer mechanism by anti-alcoholism drug disulfiram, Am J Cancer Res, 9 (2019) 1266-1281.

[48] S.K. Kim, H. Kim, D.H. Lee, T.S. Kim, T. Kim, C. Chung, G.Y. Koh, H. Kim, D.S. Lim, Reversing the intractable nature of pancreatic cancer by selectively targeting ALDH-high, therapy-resistant cancer cells, PLoS One, 8 (2013) e78130.
[49] X. Guo, B. Xu, S. Pandey, E. Goessl, J. Brown, A.L. Armesilla, J.L. Darling, W. Wang, Disulfiram/copper complex inhibiting NFkappaB activity and potentiating cytotoxic effect of gemcitabine on colon and breast cancer cell lines, Cancer Lett, 290 (2010) 104-113.
[50] C. Liu, J. Qiang, Q. Deng, J. Xia, L. Deng, L. Zhou, D. Wang, X. He, Y. Liu, B. Zhao, J. Lv, Z. Yu, Q.Y. Lei, Z.M. Shao, X.Y. Zhang, L. Zhang, S. Liu, ALDH1A1 activity in tumor-initiating cells remodels myeloid-derived suppressor cells to promote breast cancer progression, Cancer Res, 81 (2021) 5919-5934.
[51] M.A. Lowery, E.M. O'Reilly, Genomics and pharmacogenomics of pancreatic adenocarcinoma, Pharmacogenomics J, 12 (2012) 1-9.
[52] Y. Lu, Q. Pan, W. Gao, Y. Pu, K. Luo, B. He, Z. Gu, Leveraging disulfiram to treat cancer: Mechanisms of action, delivery strategies, and treatment regimens, Biomaterials, 281 (2022) 121335.
[53] N. Pramanik, A. Gupta, Y. Ghanwatkar, R.I. Mahato, Recent advances in drug delivery and targeting for the treatment of pancreatic cancer, J Control Release, 366 (2024) 231-260.
[54] X. Liu, Y. Shao, Y. Li, Z. Chen, T. Shi, Q. Tong, X. Zou, L. Ju, J. Pan, R. Zhuang, X. Pan, Extensive review of nanomedicine strategies targeting the tumor microenvironment in PDAC, Int J Nanomedicine, 20 (2025) 3379-3406.
[55] S. Habib, M. Singh, Recent advances in lipid-based nanosystems for gemcitabine and gemcitabine-combination therapy, Nanomaterials (Basel), 11 (2021) 597.
[56] T. Matsumoto, T. Komori, Y. Yoshino, T. Ioroi, T. Kitahashi, H. Kitahara, K. Ono, T. Higuchi, M. Sakabe, H. Kori, M. Kano, R. Hori, Y. Kato, S. Hagiwara, A liposomal gemcitabine, FF-10832, improves plasma stability, tumor targeting, and antitumor efficacy of gemcitabine in pancreatic cancer xenograft models, Pharm Res, 38 (2021) 1093-1106.
[57] T. Matsumoto, Y. Masuo, A. Tanaka, T. Kimura, T. Ioroi, T. Yamakawa, H. Kitahara, Y. Kato, A physiologically based pharmacokinetic and pharmacodynamic model for disposition of FF-10832, Int J Pharm, 627 (2022) 122250.
[58] E.K. Silli, Z. Zheng, X. Zhou, M. Li, J. Tang, R. Guo, C. Tan, Y. Wang, Design optimization of fucoidan-coating cationic liposomes for enhance Gemcitabine delivery, Invest New Drugs, (2024) 518-530.
[59] Z. Zheng, M. Li, J. Yang, X. Zhou, Y. Chen, E.K. Silli, J. Tang, S. Gong, Y. Yuan, Y. Zong, J. Kong, P. Chen, L. Yu, S. Luo, Y. Wang, C. Tan, Growth inhibition of pancreatic cancer by targeted delivery of gemcitabine via fucoidan-coated pH-sensitive liposomes, Int J Biol Macromol, 277 (2024) 134517.
[60] M. Tang, D. Svirskis, E. Leung, M. Kanamala, H. Wang, Z. Wu, Can intracellular drug delivery using hyaluronic acid functionalised pH-sensitive liposomes overcome gemcitabine resistance in pancreatic cancer?, J Control Release, 305 (2019) 89-100.
[61] C.B. Aparicio-Lopez, S. Timmerman, G. Lorino, T. Rogers, M. Pyle, T.B. Shrestha, M.T. Basel, Thermosensitive liposomes for gemcitabine delivery to pancreatic ductal adenocarcinoma, Cancers (Basel), 16 (2024) 3048.
[62] S.T. Tucci, A. Kheirolomoom, E.S. Ingham, L.M. Mahakian, S.M. Tam, J. Foiret, N.E. Hubbard, A.D. Borowsky, M. Baikoghli, R.H. Cheng, K.W. Ferrara, Tumor-specific delivery of gemcitabine with activatable liposomes, J Control Release, 309 (2019) 277-288.

[63] X. Wang, H. Lu, F. Luo, D. Wang, A. Wang, X. Wang, W. Feng, X. Wang, J. Su, M. Liu, G. Xia, Lipid-like gemcitabine diester-loaded liposomes for improved chemotherapy of pancreatic cancer, J Control Release, 365 (2024) 112-131.
[64] B. Kim, H. Park, H. Liu, S. Kim, Y.-k. Lee, Y.-C. Kim, Hybrid nanoparticles of extracellular vesicles and gemcitabine prodrug-loaded liposomes with enhanced targeting ability for effective PDAC treatment, ACS Applied Bio Materials, 7 (2024) 6025-6033.
[65] P.W. Li, S. Luo, L.Y. Xiao, B.L. Tian, L. Wang, Z.R. Zhang, Y.C. Zeng, A novel gemcitabine derivative-loaded liposome with great pancreas-targeting ability, Acta Pharmacol Sin, 40 (2019) 1448-1456.
[66] F. Masetto, K. Chegaev, E. Gazzano, N. Mullappilly, B. Rolando, S. Arpicco, R. Fruttero, C. Riganti, M. Donadelli, MRP5 nitration by NO-releasing gemcitabine encapsulated in liposomes confers sensitivity in chemoresistant pancreatic adenocarcinoma cells, Biochim Biophys Acta Mol Cell Res, 1867 (2020) 118824.
[67] J.C. Bulanadi, A. Xue, X. Gong, P.A. Bean, S.M. Julovi, L. de Campo, R.C. Smith, M.J. Moghaddam, Biomimetic gemcitabine-lipid prodrug nanoparticles for pancreatic cancer, Chempluschem, 85 (2020) 1283-1291.
[68] C.P. Dora, V. Kushwah, V. Yadav, K. Kuche, S. Jain, Gemcitabine-phospholipid complex loaded lipid nanoparticles for improving drug loading, stability, and efficacy against pancreatic cancer, Mol Pharm, 21 (2024) 2699-2712.
[69] M.A. Farooq, M. Aquib, D.H. Khan, Z. Hussain, A. Ahsan, M. Baig, D.P. Wande, M.M. Ahmad, H.M. Ahsan, J. Jiajie, B. Wang, Recent advances in the delivery of disulfiram: a critical analysis of promising approaches to improve its pharmacokinetic profile and anticancer efficacy, Daru, 27 (2019) 853-862.
[70] H. Duan, L. Li, S. He, Advances and prospects in the treatment of pancreatic cancer, Int J Nanomedicine, 18 (2023) 3973-3988.
[71] A.L. Miller, P.L. Garcia, K.J. Yoon, Developing effective combination therapy for pancreatic cancer: An overview, Pharmacol Res, 155 (2020) 104740.
[72] A. Nishimoto, Effective combinations of anti-cancer and targeted drugs for pancreatic cancer treatment, World J Gastroenterol, 28 (2022) 3637-3643.
[73] W. Yang, Q. Hu, Y. Xu, H. Liu, L. Zhong, Antibody fragment-conjugated gemcitabine and paclitaxel-based liposome for effective therapeutic efficacy in pancreatic cancer, Mater Sci Eng C Mater Biol Appl, 89 (2018) 328-335.
[74] M. Tang, L. Lozano Hernandez, J.N. Reginald-Opara, D. Svirskis, E. Leung, H. Wang, Z. Wu, Zebularine suppressed gemcitabine-induced senescence and improved the cellular and plasma pharmacokinetics of gemcitabine, augmented by liposomal co-delivery, Int J Pharm, 602 (2021) 120659.
[75] H. Xu, Y. Li, J.W. Paxton, Z. Wu, Co-delivery using pH-Sensitive liposomes to pancreatic cancer cells: the effects of curcumin on cellular concentration and pharmacokinetics of gemcitabine, Pharm Res, 38 (2021) 1209-1219.
[76] M. Emamzadeh, M. Emamzadeh, G. Pasparakis, Dual controlled delivery of gemcitabine and cisplatin using polymer-modified thermosensitive liposomes for pancreatic cancer, ACS Appl Bio Mater, 2 (2019) 1298-1309.
[77] Y. Wang, F. Gao, X. Jiang, X. Zhao, Y. Wang, Q. Kuai, G. Nie, M. He, Y. Pan, W. Shi, S. Ren, Q. Yu, Co-delivery of gemcitabine and Mcl-1 SiRNA via cationic liposome-based system enhances the efficacy of chemotherapy in pancreatic cancer, J Biomed Nanotechnol, 15 (2019) 966-978.

[78] P. Shrestha, Y. Ghanwatkar, S. Mahto, N. Pramanik, R.I. Mahato, Gemcitabine-lipid conjugate and ONC201 combination therapy effectively treats orthotopic pancreatic tumor-bearing mice, ACS Appl Mater Interfaces, 16 (2024) 29686-29698.
[79] H. Meng, Y. Zhao, J. Dong, M. Xue, Y.S. Lin, Z. Ji, W.X. Mai, H. Zhang, C.H. Chang, C.J. Brinker, J.I. Zink, A.E. Nel, Two-wave nanotherapy to target the stroma and optimize gemcitabine delivery to a human pancreatic cancer model in mice, ACS Nano, 7 (2013) 10048-10065.
[80] C.E. Kim, S.K. Lim, J.S. Kim, In vivo antitumor effect of cromolyn in PEGylated liposomes for pancreatic cancer, J Control Release, 157 (2012) 190-195.
[81] J.L. Paris, G. Villaverde, S. Gómez-Graña, M. Vallet-Regí, Nanoparticles for multimodal antivascular therapeutics: Dual drug release, photothermal and photodynamic therapy, Acta Biomater, 101 (2020) 459-468.
[82] I.N. Reiten, F. Giraud, T.T. Augedal, J.L. Førde, P. Moreau, E.T. Gundersen, D. Chapron, F.X. Legrand, F. Anizon, L. Herfindal, Liposomes loaded with daunorubicin and an emetine prodrug for improved selective cytotoxicity towards acute myeloid leukaemia cells, Int J Pharm, 668 (2025) 124989.
[83] M. Shahriari, S.M. Taghdisi, K. Abnous, M. Ramezani, M. Alibolandi, Self-targeted polymersomal co-formulation of doxorubicin, camptothecin and FOXM1 aptamer for efficient treatment of non-small cell lung cancer, J Control Release, 335 (2021) 369-388.
[84] C. Song, Y. Xiao, Z. Ouyang, M. Shen, X. Shi, Efficient co-delivery of microRNA 21 inhibitor and doxorubicin to cancer cells using core-shell tecto dendrimers formed via supramolecular host-guest assembly, J Mater Chem B, 8 (2020) 2768-2774.
[85] G. Tian, D. Yang, C. Chen, X. Duan, D.H. Kim, H. Chen, Simultaneous presentation of dexamethasone and nerve growth factor via layered carbon nanotubes and polypyrrole to interface neural cells, ACS Biomater Sci Eng, 9 (2023) 5015-5027.
[86] H.A. Chen, Y.J. Lu, B.S. Dash, Y.K. Chao, J.P. Chen, Hyaluronic acid-modified cisplatin-encapsulated poly(lactic-co-glycolic acid) magnetic nanoparticles for dual-targeted NIR-responsive chemo-photothermal combination cancer therapy, Pharmaceutics, 15 (2023) 290.
[87] N. Nasri, S. Saharkhiz, G. Dini, S. Yousefnia, Thermo- and pH-responsive targeted lipid-coated mesoporous nano silica platform for dual delivery of paclitaxel and gemcitabine to overcome HER2-positive breast cancer, Int J Pharm, 648 (2023) 123606.
[88] E. Dalla Pozza, M. Donadelli, C. Costanzo, T. Zaniboni, I. Dando, M. Franchini, S. Arpicco, A. Scarpa, M. Palmieri, Gemcitabine response in pancreatic adenocarcinoma cells is synergistically enhanced by dithiocarbamate derivatives, Free Radic Biol Med, 50 (2011) 926-933.
[89] M. Zewail, P.M.E. Gaafar, H. Abbas, M.A. Elsheikh, Innovative rheumatoid arthritis management using injection replacement approach via dual therapeutic effects of hyalurosomes-encapsulated luteolin and dexamethasone, Colloids Surf B Biointerfaces, 249 (2025) 114497.
[90] H. Yin, Q. Yan, Y. Liu, L. Yang, Y. Liu, Y. Luo, T. Chen, N. Li, M. Wu, Co-encapsulation of paclitaxel and 5-fluorouracil in folic acid-modified, lipid-encapsulated hollow mesoporous silica nanoparticles for synergistic breast cancer treatment, RSC Adv, 12 (2022) 32534-32551.
[91] D. Zhou, Z. Fei, L. Jin, P. Zhou, C. Li, X. Liu, C. Zhao, Dual-responsive polymersomes as anticancer drug carriers for the co-delivery of doxorubicin and paclitaxel, J Mater Chem B, 9 (2021) 801-808.

Aim of the work

Pancreatic cancer is one of the most aggressive and lethal malignancies, currently ranking as the fourth leading cause of cancer-related death in developed countries. Its high mortality rate is primarily due to late-stage diagnosis (typically occurring after metastatic dissemination) and to its complex biological behavior, which includes extensive genetic heterogeneity, a dense desmoplastic stroma, and a pronounced resistance to conventional therapies.

A defining feature of pancreatic cancer is its fibrotic stromal barrier, which not only hinders drug penetration but also contributes to a tumor-protective microenvironment. Furthermore, both intrinsic and acquired chemoresistance remain major obstacles to the success of current treatment strategies.

GEM has long been a cornerstone in the chemotherapy of advanced pancreatic cancer, primarily exerting its cytotoxic effects through inhibition of DNA synthesis. However, its clinical utility is significantly limited by its short plasma half-life, rapid metabolic deactivation by cytidine deaminase, and poor tumor tissue penetration. Moreover, the emergence of resistance over the course of treatment greatly compromises its therapeutic efficacy.

DSF, an aldehyde dehydrogenase inhibitor originally used for the treatment of alcoholism, has emerged as a potential anticancer agent. DSF exhibits anticancer activity by generating reactive oxygen species (ROS), inducing oxidative stress and apoptosis in cancer cells. Additionally, DSF has been shown to inhibit efflux pumps, such as P-glycoprotein, thereby reducing drug extrusion and improving the intracellular retention of chemotherapeutic drugs in resistant cancer cells, as GEM. It has been demonstrated that DSF can also form a complex with Cu (DSF/Cu); this compound has exhibited pro-apoptotic activity, the ability to induce oxidative stress, and the suppression of cancer stem cell populations in pancreatic cancer cells. Nonetheless, clinical application of DSF remains limited due to its poor bioavailability and non-specific biodistribution, underscoring the need for delivery strategies to fully exploit its therapeutic potential. Consequently, increasing attention has been directed toward the development of innovative drug delivery systems aimed at improving GEM stability, enhancing its tumor-specific accumulation, and overcoming resistance mechanisms.

The primary objective of this doctoral thesis was to develop and characterize innovative nanocarrier-based drug delivery systems for the treatment of pancreatic cancer, with particular emphasis on the encapsulation of GEM. A comprehensive investigation into the full spectrum of drug encapsulation strategies was conducted, encompassing the exploration of lipophilic GEM prodrugs, specifically GEM-C12 and GEM-C18. This investigation

enabled the formulation of different types of nanosystems, including carbon nano-onions (CNOs), mixed micelles, and liposomes. Furthermore, the functionalization of CNOs and mixed micelles with active targeting moieties was undertaken to evaluate the potential for receptor-mediated internalization, with the objective of enhancing tumor-specific delivery. Finally, to further enhance the antitumor efficacy of GEM and GEM-C18 against chemoresistant pancreatic cancer, both free drugs were tested *in vitro* in combination with DSF. Subsequently, the liposomal formulations of GEM and GEM-C18 were also administered in combination with DSF to assess whether encapsulation could further enhance their antitumor activity.
To achieve these objectives, three distinct types of nanosystems were developed.

The initial focus of this research was on CNOs that were prepared by Prof. Silvia Giordani's research group at the Dublin City University. Specifically, CNOs were functionalized with HA *via* covalent coupling through a PEG linker. Both decorated and undecorated CNOs were evaluated for their cellular uptake and bioavailability in pancreatic cancer cell lines. Subsequently, the loading of GEM-C12 and GEM-C18 was performed, followed by physico-chemical characterization and *in vitro* release studies. These formulations were then tested by Prof. Riganti (Oncology Department of the University of Turin) for cytotoxicity in $CD44^+$ and $CD44^-$ pancreatic cancer cells to assess the targeting efficiency.
In the second part of the thesis, the investigation focused on mixed micelles, that were prepared using the commercially available 1,2-distearoyl-*sn*-glycero-3-phosphoethanolamine-N-[amino(polyethylene glycol)-2000] (ammonium salt) (PEG-DSPE) and a conjugate between HA and 1,2-dipalmitoyl-*sn*-glycero-3-phosphorylethanolamine (HA-DPPE). The HA-DPPE conjugate was synthesized in our laboratory and designed to achieve active targeting *via* the interaction of HA-CD44. Mixed micelles were loaded with GEM-C18 and characterized in terms of size, polydispersity index (PdI), and zeta potential. Structural analyses (FESEM, SAXS, and X-ray diffraction) were also conducted to better understand micellar morphology. These formulations were further evaluated *in vitro* for cytotoxicity and cellular uptake in pancreatic cancer cells, again in collaboration with Prof. Riganti's team.
The third system investigated was liposomes. Two liposomal formulations with identical phospholipid composition were developed: one encapsulating GEM in the aqueous core, and the other incorporating GEM-C18 within the lipid bilayer. Both systems were characterized for physico-chemical properties, drug loading efficiency, and *in vitro* release profile. These formulations were tested during a research stay at Gustave Roussy Institute (Villejuif,

France), in collaboration with Dr. Giorgia Urbinati and Dr. Nazanine Modjtahedi. Cytotoxicity assays were performed to compare the efficacy of the liposomal formulations to that of free drugs, and combination studies with DSF were conducted to evaluate potential synergistic effects.

Throughout the PhD project, an extensive literature review was carried out, focusing on pancreatic cancer pathophysiology, mechanisms of GEM resistance, and strategies to enhance drug delivery using lipid-based nanosystems. Particular attention was given to dual-drug delivery systems capable of co-encapsulating GEM and DSF. This research culminated in the drafting of a review article submitted to *WIREs Nanomedicine and Nanobiotechnology* (WILEY), which is included as part of this thesis.

Research articles

Enhancing pancreatic ductal adenocarcinoma (PDAC) therapy with targeted carbon nano-onion (CNO)-mediated delivery of gemcitabine (GEM)-derived prodrugs.

Michał Bartkowski, Valeria Bincoletto, Iris Chiara Salaroglio, Giacomo Ceccone, Raul Arenal, Sara Nervo, Barbara Rolando, Chiara Riganti, Silvia Arpicco, Silvia Giordani

---

Published in *Journal of Colloid and Interface Science* (659) 2024, 339-354

GEM, the standard chemotherapeutic agent for pancreatic cancer, suffers from rapid degradation and systemic toxicity, limiting its therapeutic efficacy. Nanocarriers offer a promising strategy to overcome these challenges by improving drug stability, targeting, and controlled release. Among them, CNOs are attractive due to their unique multi-layered graphitic structure, biocompatibility, and high surface functionalization capacity.

Main Aim

To develop and evaluate a smart, actively targeted drug delivery system based on functionalized CNOs for the selective and efficient delivery of GEM-derived prodrugs (GEM-C12 and GEM-C18) to pancreatic cancer cells.

Specific Objectives

- To functionalize CNOs surface with diamino-PEG and HA to achieve an active targeting towards CD44 receptor overexpressing pancreatic cancer cell lines.
- To load CNOs with GEM-derived prodrugs to increase their efficacy and obtain a controlled drug release.
- To characterize the nanocarriers in terms of structure, drug loading, release profile, and stability.
- To assess cellular uptake, cytotoxicity, and selectivity assays of the HA-targeted CNOs *in vitro* on PANC-1, CAPAN-1 and MIA PaCa-2 pancreatic cancer cell lines.

Highlights

- The synthesis and characterization of HA-functionalized CNOs were presented. CNOs were successfully loaded with GEM-C12 or GEM-C18, providing stable systems for controlled drug delivery.
- Significantly increased cellular uptake and cytotoxicity was observed in pancreatic cancer cells due to HA receptor-mediated endocytosis.
- The study confirmed the potential of HA-targeted CNOs as an effective and selective nanoplatform for PDAC therapy.

Journal of Colloid and Interface Science 659 (2024) 339–354

Contents lists available at ScienceDirect

Journal of Colloid And Interface Science

journal homepage: www.elsevier.com/locate/jcis

Enhancing pancreatic ductal adenocarcinoma (PDAC) therapy with targeted carbon nano-onion (CNO)-mediated delivery of gemcitabine (GEM)-derived prodrugs

Michał Bartkowski [a], Valeria Bincoletto [b], Iris Chiara Salaroglio [c], Giacomo Ceccone [d], Raul Arenal [e,f,g], Sara Nervo [b], Barbara Rolando [b], Chiara Riganti [c,h], Silvia Arpicco [b], Silvia Giordani [a,*]

[a] School of Chemical Sciences, Dublin City University, Glasnevin, Dublin 9, Ireland
[b] Department of Drug Science and Technology, University of Torino, Via P. Giuria 9, Torino, Italy
[c] Department of Oncology, University of Torino, Via Nizza 44, Torino, Italy
[d] European Commission, Joint Research Centre, Ispra, Italy
[e] Instituto de Nanociencia y Materiales de Aragon (INMA), CSIC-U. de Zaragoza, 50009 Zaragoza, Spain
[f] Laboratorio de Microscopias Avanzadas (LMA), Universidad de Zaragoza, 50018 Zaragoza, Spain
[g] ARAID Foundation, 50018 Zaragoza, Spain
[h] Molecular Biotechnology Center "Guido Tarone", University of Torino, Italy

HIGHLIGHTS

- Carbon Nano-onion (CNO)-based drug delivery system for targeted cancer therapy was developed.
- The nanocarrier showed versatility, adaptability, and a promising biocompatibility profile.
- Hyaluronic acid enabled targeted drug delivery to cells overexpressing the CD44 receptor.
- Gemcitabine-derived prodrugs were delivered to pancreatic adenocarcinoma (PDAC) cells.
- Results indicate potential treatments for CD44+, gemcitabine-resistant tumour types.

GRAPHICAL ABSTRACT

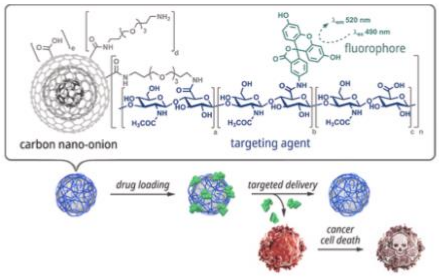

Abbreviations: ABC, ATP binding cassette; ABCC5, ABC member C5; amino-PEG-CNO, diamino-PEG-functionalised oxi-CNO; API, active pharmaceutical ingredient; ATR, attenuated total reflectance; C12GEM, 4-(N)-lauroyl-GEM; C18GEM, 4-(N)-stearoyl-GEM; C5GEM, 4-(N)-valeroyl-GEM; CD44, cluster of differentiation 44; CNO, carbon nano-onion; CNP, carbon nanoparticle; DDS, drug delivery system; dFdC, 2′,2′-difluoro-2′-deoxycytidine; diamino-PEG, 4,7,10-trioxa-1,13-tridecanediamine; DLS, dynamic light scattering; DMAP, 4-(dimethylamino)pyridine; DMF, N,*N*-dimethylformamide; DMSO, dimethyl sulfoxide; DND, detonation nanodiamond; EDCl, 1-(3-dimethylaminopropyl)-3-ethylcarbodiimide HCl; f-CNO, functionalised CNO; FDA, Federal Drug Administration; FE-SEM, field emission SEM; fluo, fluoresceinamine, isomer I; fluo-HA, fluo-tagged HA; fluo-HA-PEG-CNO, fluo-HA-functionalised amino-PEG-CNO; FTIR, Fourier-transform infrared; GEM, gemcitabine; HA, hyaluronic acid; HA-PEG-CNO, HA-functionalised amino-PEG-CNO; HPDE, human pancreatic duct epithelial; HPLC, high-performance liquid chromatography; HRTEM, high resolution transmission electron microscopy; MDR, multidrug resistance; MOF, metal-organic framework; MRP5, multidrug resistance protein 5; NHS, *N*-hydroxysuccinimide; oxi-CNO, oxidised CNO; p-CNO, pristine CNO; PBS, phosphate-buffered saline; PDAC, pancreatic ductal adenocarcinoma.

* Corresponding author.
E-mail address: silvia.giordani@dcu.ie (S. Giordani).

https://doi.org/10.1016/j.jcis.2023.12.166
Received 1 December 2023; Received in revised form 20 December 2023; Accepted 28 December 2023
Available online 30 December 2023

Consequently, as our selected anticancer drugs we investigated GEM, and GEM-derived prodrugs comprised of GEM with varying-length aliphatic side-chains; namely 4-(*N*)-valeroyl-gemcitabine (C5GEM), 4-(*N*)-lauroyl-gemcitabine (C12GEM) and 4-(*N*)-stearoyl-gemcitabine (C18GEM) (Fig. 1C). Owing to GEMs' intrinsic high aqueous solubility, these lipophilic GEM derivatives, synthesised in our laboratory, demonstrated to have a higher loading efficiency in various nanoparticle systems including liposomes, polymeric nanoparticles, and mesoporous silica nanoparticles compared to the parent drug. Moreover, they demonstrated favourable *in vitro* and *in vivo* activity [26,27,28,29].

In summary, we present an innovative approach to overcoming the challenges of GEM-resistance in PDAC by developing a CNO-based drug delivery system, utilising $HA_{200\ kDa}$ as the basis of targetability. We systematically investigate GEM-derived prodrugs in conjunction with this drug delivery system, focusing on their loading efficiency, cellular uptake, and cytotoxic activity. Our work aims to contribute to the expanding field of nanocarrier systems for targeted cancer therapy, with specific focus on the application of carbon-based nanoparticles in improving the effective treatment of GEM-resistant PDAC.

2. Materials and methods

2.1. Materials, chemicals and cell cultures

Sodium hyaluronate of 200 kDa average molecular weight (HA) was purchased from Lifecore Biomedical (MN, USA). Gemcitabine (2′,2′-difluoro-2′-deoxycytidine; dFdC; GEM) hydrochloride (GEM·HCl) was purchased from TCI EUROPE NV. *N,N*-dimethylformamide (DMF) anhydrous 99.8 %, 4,7,10-trioxa-1,13-tridecanediamine (diamino-PEG), *N*-hydroxysuccinimide 98 % (NHS), 4-(dimethylamino)pyridine ≥ 99 %

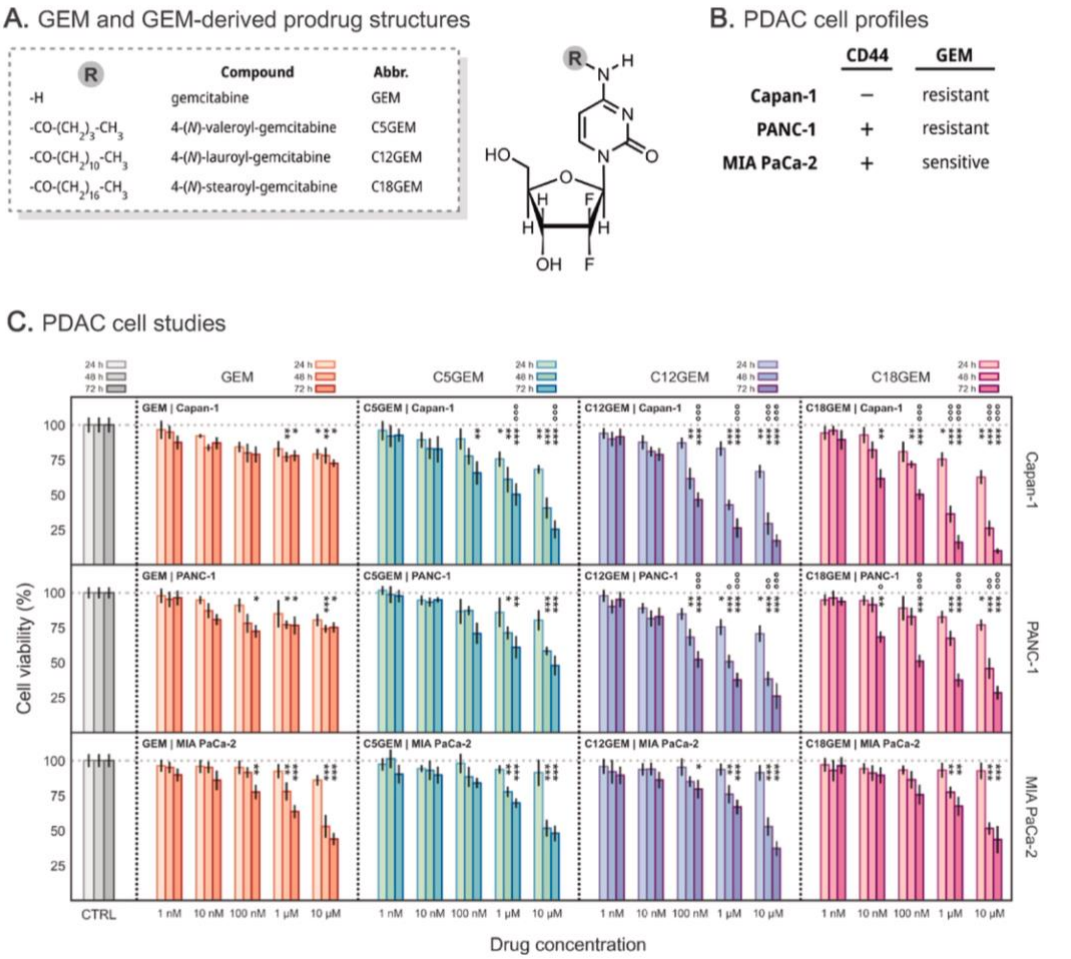

Fig. 1. GEM prodrug PDAC cell studies. A. Chemical structure of gemcitabine (GEM), and the three prodrug derivatives: 4-(*N*)-valeroyl-gemcitabine (C5GEM), 4-(*N*)-lauroyl-gemcitabine (C12GEM) and 4-(*N*)-stearoyl-gemcitabine (C18GEM); **B.** Visual reference of cellular profiles of Capan-1, PANC-1 and MIA PaCa-2 towards GEM sensitivity/resistance, and the expression of the CD44 receptor, as evaluated in this study for **C.** Cytotoxic activity of GEM, C5GEM, C12GEM and C18GEM in the PDAC cell lines: Capan–1, PANC-1 and MIA PaCa-2. Error bars represent the standard deviation of ($n = 6$) experiments for GEM, C12GEM and C18GEM; and ($n = 3$) experiments for C5GEM. Statistical significance vs. respective control (CTRL) is represented as $^{*}p < 0.05$, $^{**}p < 0.01$ and $^{***}p < 0.001$. Statistical significance vs. GEM is represented as $^{\circ}p < 0.05$, $^{\circ\circ}p < 0.01$ and $^{\circ\circ\circ}p < 0.001$.

(DMAP), and nitric acid ≥ 65 % (NHO_3) were purchased from Sigma Aldrich. 1-(3-dimethylaminopropyl)-3-ethylcarbodiimide HCl ≥ 98 % (EDCl) was purchased from Alfa Aesar. Fluoresceinamine, isomer I 99 % green-emitting, λ_{ex} 490 nm, λ_{em} 520 nm; pH dependent fluorophore tag (fluo); and dimethyl sulfoxide (DMSO) 99.9 % were purchased from Acros Organics. Deionised water (dH_2O) was purified by a MilliQ® ultra-purification system to 18.2 MΩ·cm at 25 °C. Unless otherwise specified, all other starting materials were sourced from Sigma-Aldrich.

The human non-transformed pancreatic epithelial cells (HPDE) and human pancreatic adenocarcinoma cells (PDAC): BxPC3, Capan-1, AsPC1, T3M4, CFPAC, PANC-1 and MIA PaCa-2, were purchased from ATCC (Manassas, VA). Cells were grown in DMEM medium, supplemented with 10 % v/v FCS and 1 % penicillin–streptomycin, at 37 °C, 5 % CO_2, in a humidified atmosphere.

2.2. Synthesis and functionalisation

2.2.1. Synthesis of C5GEM, C12GEM and C18GEM

Three increasingly lipophilic 4-(*N*)-acyl- derivatives of gemcitabine (Fig. 1A)—namely: 4-(*N*)-valeroylgemcitabine (C5GEM) 4-(*N*)-lauroyl-gemcitabine (C12GEM) and 4-(*N*)-stearoyl-gemcitabine (C18GEM)—were synthesised according to a previously reported procedure [30].

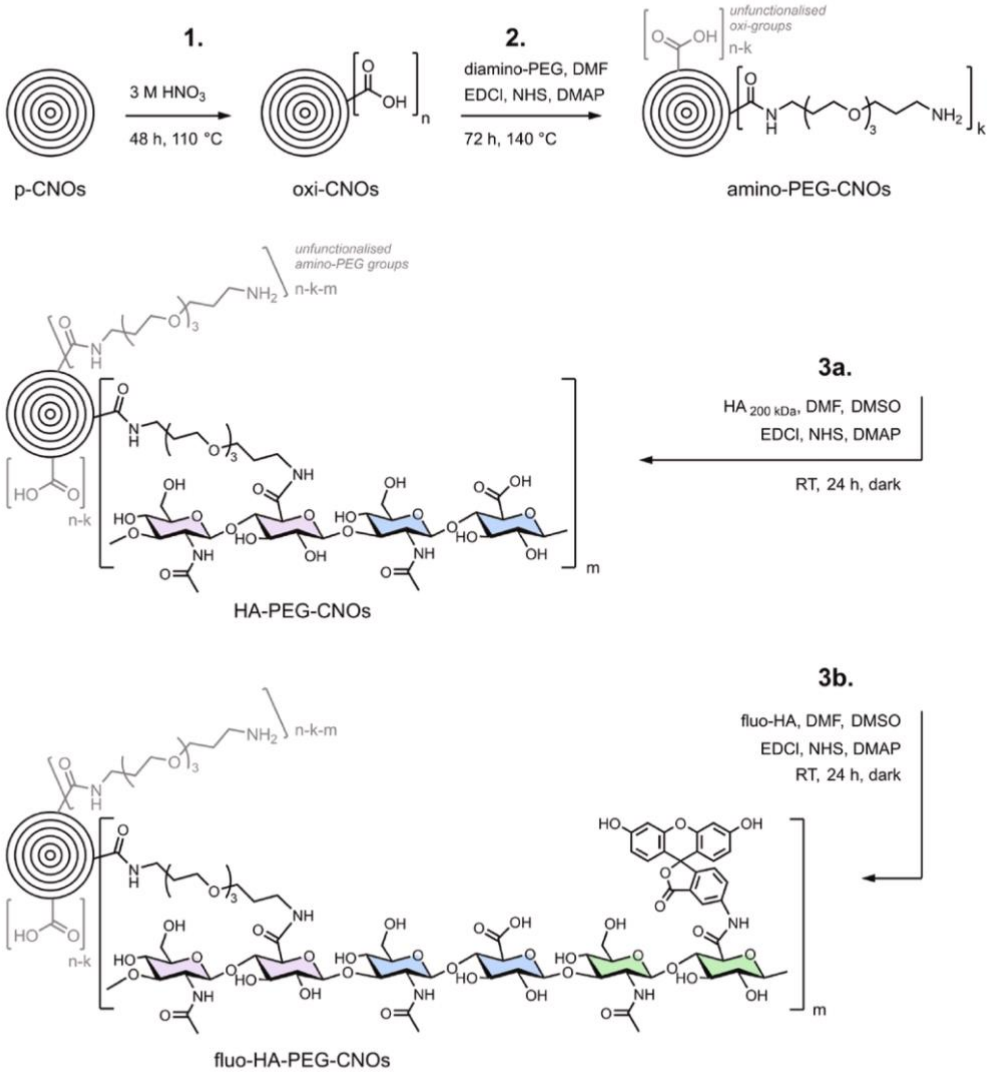

Fig. 2. CNO surface functionalisation schematics. Schematic of **1.** Nitric acid surface oxidation of p-CNOs to form oxi-CNOs; **2.** Subsequent NHS/EDC-crosslinking of oxi-CNOs with diamino-PEG to form amino-PEG-CNOs; followed by a similar amidation, covalently coupling either **3a.** HA_{200kDa} or **3b.** fluo-HA with amino-PEG-CNOs, to form HA-PEG-CNOs or fluo-HA-PEG-CNOs, respectively. For clarity, disaccharide units are colour coded to distinguish those bound to the PEG linker (*purple*); unbound (*blue*); and bound to the fluo (*green*).

2.2.2. Synthesis of fluo-HA

Labelling of HA with fluoresceinamine, isomer I (fluo), to form fluo-HA, was carried out as previously described with minor modifications [31,32]. Briefly, a solution composed of 12.5 mg of fluo in 0.25 mL of DMSO (50 mg/mL), 12.5 μL of acetaldehyde and 12.5 μL of cyclohexyl isocyanide was added to a solution of 25 mg of HA in 20 mL of dH_2O (1.25 mg/mL) and 20 mL of DMSO, and the pH was adjusted to 4.5 with 0.1 N HCl. Then, the reaction was stirred at room temperature and in darkness for 12 h. fluo-HA was precipitated with a saturated solution of NaCl and ice-cold ethanol, then collected by centrifugation and then suspended in dH_2O, extensively dialysed against dH_2O, lyophilised and stored at −20 °C in the dark before use.

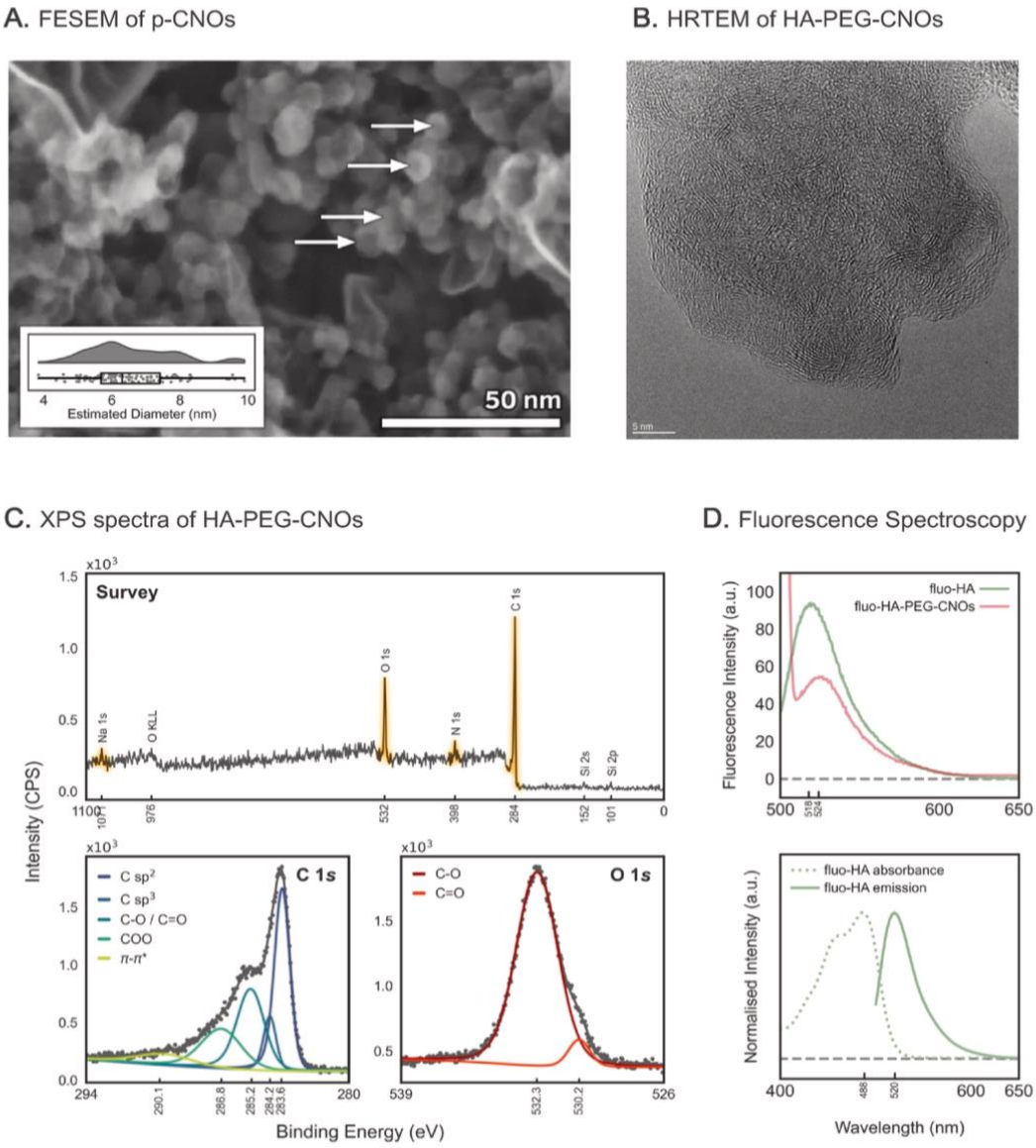

Fig. 3. Physicochemical characterisation of the CNO-DDS. A. Representative high magnification FE-SEM image (20 kV) of p-CNOs (*scale bar = 50 nm*). *Inset (bottom-left)*: raincloud plot of p-CNO size distribution with a fitted boxplot showing the median and quartiles; with the p-CNO diameter averaged at 6.5 ± 1.3 nm.; **B.** HRTEM micrographs of HA-PEG-CNOs (*scale bar = 5 nm*); **C.** XPS survey and high-resolution core level (C 1 *s*, O 1 *s*) spectra of HA-PEG-CNOs on a Si_3N_4 substrate, including fitted peak deconvolution curves. **D.** (*Top*) Fluorescence emission spectra of fluo-HA (1 μg/mL) and fluo-HA-PEG-CNOs (50 μg/mL) in dH_2O at λ_{ex} 490 nm; (*Bottom*) Stokes shift spectrum comparing the normalised absorption (100 μg/mL) and emission (20 μg/mL) of fluo-HA in dH_2O.

2.2.3. Preparation of p-CNOs

Small (6–7 nm in size; 6–8 shells) pristine carbon nano-onions (p-CNOs) were prepared through the thermal annealing of detonation nanodiamonds under a He atmosphere, as per a previously reported procedure [33].

2.2.4. Preparation of oxi-CNOs

Approx. 100.8 mg p-CNOs were dispersed in 3 M HNO_3 by sonicating at 37 kHz for 20 min. The solution was then stirred under reflux at 110 °C for 48 h. The oxidised CNOs (oxi-CNOs) produced (Fig. 2) were then isolated through centrifugation (4000 rpm for 10 min). After removing the supernatant, oxi-CNOs were redispersed in deionised water and vacuum-filtered over a 200 nm nylon filter, and washed with deionised water, DMF, methanol, and finally acetone. Finally, the material was dried at RT, yielding approx. 99.6 mg oxi-CNO.

2.2.5. Preparation of amino-PEG-CNOs

CNOs PEGylated with a diamino-PEG derivative (amino-PEG-CNOs) were prepared through the amidation of oxi-CNOs with 4,7,10-trioxa-1,13-tridecanediamine (diamino-PEG) through an EDC crosslinking amidation reaction, according to a previously reported procedure [34]. Briefly, 81.2 mg oxi-CNOs were dispersed in 24 mL dry *N,N*-dimethylformamide (DMF). To which, *N*-hydroxysuccinimide (NHS), 1-(3-dimethylaminopropyl)-3-ethylcarbodiimide HCl (EDCl) and 4-(dimethylamino)pyridine (DMAP) were added and dispersed by sonication. On stirring, 24 mL diamino-PEG was added dropwise. The solution was refluxed at 140 °C for 4 d, following which the amino-PEG-CNOs were vacuum-filtered on a GNWP 0.2 μm nylon filter, and washed with dry-DMF, then ethanol, then acetone. After drying under vacuum at RT, 95.9 mg amino-PEG-CNOs were recovered.

2.2.6. Preparation of HA-PEG-CNOs and fluo-HA-PEG-CNOs

HA-PEG-CNOs were prepared following the same type of reaction as amino-PEG-CNOs. Briefly, 20.6 mg amino-PEG-CNOs were dispersed in 15 mL dry DMF by sonication (5′). In a separate vial, $HA_{200\ kDa}$ (approx. 1:4 w/w HA to amino-PEG-CNOs) was dispersed in 10 mL dry DMF. The HA dispersion was then added to the amino-PEG-CNO dispersion, along with the coupling reagents; DMAP, NHS and EDCl. The solution was then sonicated (5′) to aid the dispersion of the coupling reagents and let stir for 24 h under ambient conditions. After 24 h, the black HA-PEG-CNO solution was vacuum-filtered on a GNWP 0.2 μm nylon filter and washed with DMF, then methanol, then acetone. Finally, after drying under vacuum at RT, 22.9 mg HA-PEG-CNOs were recovered. The fluo-HA-PEG-CNOs were prepared as above, with the exception that the HA was substituted with fluo-HA.

2.2.7. Prodrug-loading of amino-PEG-CNOs and HA-PEG-CNOs

C12GEM and C18GEM (1 mg) were mixed with 7 mg of the different CNOs (amino-PEG-CNOs and HA-PEG-CNOs) into 1 mL of isopropyl alcohol. The mixture was bath sonicated for 5 min to ensure proper mixing of CNOs and GEM prodrugs and was further allowed to stand overnight under magnetic stirring at room temperature. Then, the suspension was centrifuged at 6,000 rpm and washed with isopropyl alcohol three times. To evaluate the drug loading capacity the supernatant and the washing solutions were collected, filtered through 0.45 μm PTFE filters (Alltech) and the residual GEM prodrugs amount was measured by HPLC. The amount of drug loaded was calculated based on its initial and residual concentration.

RP-HPLC analysis were performed with an HP 1200 chromatograph system (Agilent Technologies, Palo Alto, CA, USA) equipped with an injector (Rheodyne, Cotati, CA, USA), a quaternary pump (model G1311A), a membrane degasser (model G1322A), a multiple wavelength UV detector (model G1365D), and a fluorescence detector (model G1321A) integrated into the HP1200 system. Data analysis was processed using an HP ChemStation system (Agilent Technologies, Santa Clara, CA, USA). The analytical column was AQUASIL C18 (200 × 4.6 mm, 5 μm; ThermoFisher Scientific, Waltham, MA, USA); the mobile phase consisted of CH_3CN 0.1 % HCOOH (solvent A) and water 0.1 % HCOOH (solvent B), at a flowrate of 1 mL/min with gradient conditions: 10 % A until 4 min, from 10 to 90 % A between 4 and 10 min, 90 % A between 10 and 20 min, and from 90 to 15 % A between 20 and 25 min. The injection volume was 20 μL (Rheodyne, Cotati, CA, USA). The column effluent was monitored at 250 nm referenced against 800 nm wavelength.

Quantitation of the compounds was done using calibration curves obtained using standard solutions of compounds chromatographed in the same experimental conditions (linearity determined in a concentration range of 1–150 μM; $r^2 > 0.99$).

2.3. Physicochemical characterisation

2.3.1. High-resolution transmission electron microscopy and field-emission scanning electron microscopy (FE-SEM)

High-resolution transmission electron microscopy (HRTEM) analysis was conducted using an aberration-corrected TEM instrument (Thermo Fisher Scientific Titan Cube). The operating voltage was set at 80 kV. Samples for HRTEM were prepared by depositing a drop of the nanomaterials dispersion in ethanol on a holey carbon film supported by a copper TEM grid and allowing it to dry at room temperature.

Field-emission scanning electron microscopy (FE-SEM) images were taken on a Hitachi S5500 FESTEM microscope at 20 kV in SE mode. FE-SEM micrograph contrast adjustment and statistical analysis was conducted using ImageJ software [35].

2.3.2. X-ray photoelectron spectroscopy (XPS)

X-ray photoelectron spectroscopy (XPS) was carried out on an Axis Ultra (Kratos Analytical, UK) with an Al Kα monochromatic source ($h\nu$ = 1486.6 eV). Samples were prepared through drop casting of a 150 μL DMF suspension and dried overnight. Substrates were Si_3N_4 membranes (Silson, US) (for materials containing HA and fluo-HA) and Au (for all other materials). The 'Au' substrate is a Si(100) wafer sputter-coated with a 100 nm layer of Au. Survey spectra were acquired at a 160 eV pass energy. Core level spectra were acquired at a 40 eV pass energy with a resolution of 50 meV. Spectra were calibrated with the hydrocarbon sp^2 peak at 284.50 eV. Data processed with CasaXPS v23.3 software, with peak fitting carried out using the Lorentzian function after Tougaard background subtraction. Quantification was carried out using Kratos RSF software. Data was plotted using python matplotlib.

2.3.3. Uv–vis absorption and fluorescence emission spectroscopy

UV–Vis absorption spectroscopy was carried out on a Shimadzu UV-2600 using 1 mL quartz cuvettes. The reported dilutions were prepared in deionised water, and the dispersions have been achieved through sonication for 15 min at 37 kHz. Background correction was carried out.

Fluorescence emission spectroscopy was carried out on a PerkinElmer LS-55 spectrofluorometer with FL WinLab software used for instrument control. All samples were prepared and dispersed in dH_2O, and analysed at a concentrations of 1, 2.5, 5, 10 and 20 μg/mL after 15 min of sonication. The analysis parameters optimised for fluoresceineamine, isomer I (fluo) tagged hyaluronic acid (fluo-HA) were as follows; the excitation wavelength was 490 nm (λ_{max} of fluo-HA), the emission scan range was set to 500–700 nm, the excitation and emission slit-widths were 10 nm. The fluo-HA-PEG-CNO nanoconstruct was analysed under the same parameters, with the exception of the emission slit-width, which was set to 2.5 nm to narrow down the emission bandwidth, improving spectral resolution. To generate the Stokes-shift spectrum, data were normalised to the same range using Eq. (1.1).

2.3.4. Attenuated Total Reflection Fourier-Transform Infrared Spectroscopy (ATR-FTIR)

Attenuated Total Reflection Fourier-Transform Infrared Spectroscopy (ATR-FTIR) was performed using PerkinElmer Spectrum Two and

Nicolet iS5 instruments at room temperature. The ATR crystal used was diamond, with a single reflection. Spectral resolution was optimised to achieve a data spacing of 0.482 cm^{-1}. For all CNO-based materials, 128 sample accumulations taken; 32 accumulations were conducted for all other samples. The measurements were taken over a wavenumber range of 4000 to 450 cm^{-1}, utilising a large aperture (100) and DTGS KBr detector. Norton Beer Strong apodisation and atmospheric suppression were applied. Baseline correction was applied only to the spectra of GEM, C12GEM and C18GEM for comparative purposes. Wherein indicated, normalisation was carried out as per Eq. (1.1).

$$z_i = \frac{y_i - \min(y)}{\max(y) - \min(y)} \tag{1.1}$$

Where $y_i = (y_1, \ldots, y_n)$ and z_i is the i^{th} normalised datapoint.

2.3.5. Dynamic light scattering (DLS) and zeta potential (ZP)

Dynamic light scattering (DLS) and zeta potential (ZP) analyses were performed on functionalised CNOs at concentrations of 5, 10, and 20 ppm using a ZetaSizer Ultra instrument in 173° backscatter mode. Samples were dispersed in dH_2O and sonicated for 15 min with temperature maintained at 22–26 °C, then equilibrated to 25 °C prior to analyses. A PCS1115 cell was used for DLS measurements, and a DTS1070 cell for ZP measurements. Each sample was subjected to cycles of DLS and ZP analyses at 5 min intervals. ZS XPLORER software was used to manage instrument control, data acquisition, and statistical analysis. The mean and standard deviations values presented (Tab. SI 6) are representative of the peak of highest intensity from $n \geq 3$ experiments.

2.3.6. Prodrug release profile

Studies were carried out to assess the C12GEM and C18GEM prodrug release profile from HA-PEG-CNOs (Fig. SI 15) and amino-PEG-CNOs, and to assess the corresponding loading efficiencies. Briefly, the C12GEM and C18GEM release was evaluated in pH 7.4 0.1 M phosphate buffer solutions (PBS), wherein 1 mL of PBS was added to the dried API @ HA-PEG-CNOs and API @ amino-PEG-CNOs, and each mixture was stirred at 37 °C. At predetermined time intervals of 1, 3, 6, 24, 48 and 72 h, 100 µL aliquots were taken from the suspension and centrifuged at 6,000 rpm for 15 min. The removed fluid was immediately replaced with an equal amount of fresh medium at the same temperature to maintain sink condition. The supernatants were then analysed by HPLC in the conditions described above. All release studies were carried out in triplicate.

To derive further information on prodrug loading and release, specifically further information on the mode of loading, as well as the impact of increasing lipophilicity on prodrug release, partition coefficient values of each prodrug were contrasted with the corresponding release profile and loading efficiency. To this end, we employed the partition coefficient values: C18GEM (logP 7.91) and C12GEM (logP 4.74), which we calculated as described in our previous investigation [28].

2.4. Biological studies

2.4.1. CD44-expression

The HPDE and PDAC cell lines were evaluated for their expression of the CD44 receptor by flow cytometry (Fig. SI 1), to optimise the selection of target and control cell lines for subsequent analyses. Briefly, 1×10^6 cells were rinsed and fixed with 2 % w/v paraformaldehyde (PFA) for 2 min, washed three times with PBS and stained with the anti-CD44 antibody (Abcam; 1:50 dilution) for 1 h on ice, followed by an Alexa-Fluor 488-conjugated secondary antibody (Millipore, Burlington, MA; 1:100 dilution) for 30 min. 1×10^5 cells were analysed with EasyCyte Guava™ flow cytometer (Millipore), equipped with the InCyte software (Millipore). Control experiments included incubation with non-immune isotype antibody.

2.4.2. Cell viability

Three distinct experiments were carried out evaluating cellular viabilities. For each experiment, 1×10^4 cells were seeded into a 96-well white plate and let to adhere for 6 h.

The first experimental set was carried out to evaluate cytotoxicity and optimise prodrug derivative selection for further studies. Briefly, PDAC cells were incubated for 24, 48 and 72 h with GEM and the C5GEM, C12GEM and C18GEM prodrugs at concentrations from 1 nM to 10 µM (Fig. 1C).

The second experimental set was carried out to verify the cytotoxicity of the CNO-based nanocarrier systems alone, without the therapeutic payload, in PDAC cells. Briefly, cells were incubated with HA-PEG-CNOs (Fig. 4A) or fluo-HA-PEG-CNOs (Fig. SI 2A) at 0.5, 5, 10 and 20 µg/mL for 24, 48 and 72 h. Moreover, under the same conditions, an additional experiment was carried out evaluating cellular viability of HA-PEG-CNOs in HPDE cells (Fig. SI 2B).

The third experimental set was carried out to compare the differential toxicity of the prodrugs alone and when loaded onto the HA-PEG-CNO nanocarrier. Briefly, cells were incubated for 72 h with GEM, C18GEM or C18GEM @ HA-PEG-CNOs at concentrations of GEM from 1 nM to 10 µM, to compare the differential cytotoxicity (Fig. 5). The same was carried out for C12GEM (Fig. 6). Where indicated as *CA* or *CB*, 200 µg/mL HA or a blocking anti-CD44 antibody (Abcam, Cambridge, UK; dilution: 1:10) were co-incubated as competitors, respectively. Cell viability was measured by the ATPlite Luminescence Assay System (PerkinElmer, Waltham, MA), as per manufacturer's instructions. Results were analysed by a Synergy HT Microplate Reader (Bio-Tek Instruments, Winooski, VT). The luminescence units of the untreated cells were considered 100 %; the luminescence units of the other experimental conditions were expressed as percentage versus untreated cells.

2.4.3. Cellular uptake

For cellular uptake studies (Fig. 4B), 1×10^5 cells were seeded into a 96-well white plate, let to adhere for 6 h and incubated for 1, 3, 6 and 24 h with fluo-HA-PEG-CNOs at 0.5, 5, 10 and 20 µg/mL. In competition assays, 200 µg/mL HA or a blocking anti-CD44 antibody (Abcam; diluted 1:10 in the culture medium) were co-incubated. Cells were washed twice with PBS, detached with scraper and centrifuged at 13,000 g for 5 min at 4 °C, then resuspended in 300 µL of PBS and sonicated (1×10 s, amplitude 40 %; Hielscher UP200S ultrasound sonicator, GmbH, Teltow, Germany). The protein content of cell pellets was assessed with the BCA kit from Sigma Chemicals Co. (St. Louis, MO). The amount of intracellular fluo was detected using a Synergy HT Multi-Detection Microplate Reader, with λ_{ex} at 488 nm and λ_{em} at 528 nm, respectively. A blank was prepared in the absence of cells in each set of experiments and its fluorescence was subtracted from that measured in each sample. Fluorescence was converted in nmol fluorophore per mg cell proteins using a calibration curve previously set.

3. Results and discussion

3.1. Cell line evaluation

3.1.1. Quantification of CD44-expression

Different human PDAC cell lines, including BxPC3, Capan-1, AsPC1, T3M4, CFPAC, PANC-1, MIA PaCa-2, and the non-transformed pancreatic epithelial cells HPDE, were analysed for their expression of the CD44 receptor by flow cytometry (Fig. SI 1). The different PDAC cells displayed variable levels of surface CD44, ranging from 1 % to 92 % of CD44-positive cells. However, the average expression of CD44 is higher in PDAC cells than in HPDE cells, suggesting that HA-conjugation could be an effective way of the active targeting of CNOs towards PDAC cells, with relative sparing of non-transformed epithelium. The cell lines PANC-1 and MIA PaCa-2 have shown a high expression of the CD44

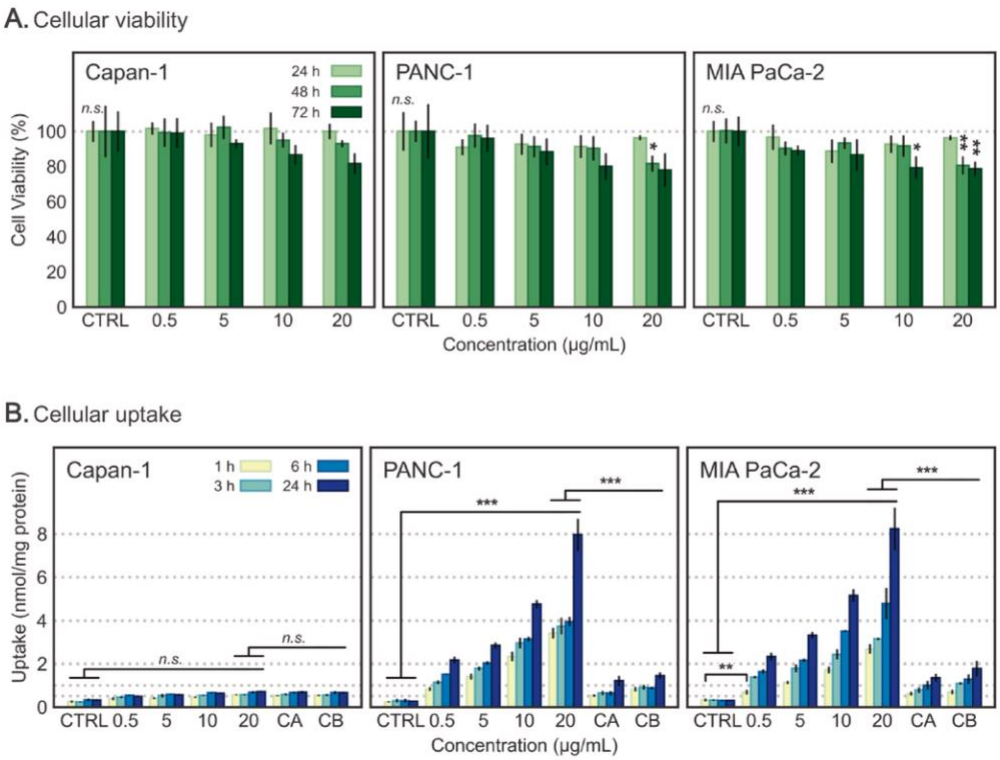

Fig. 4. Cellular viability and uptake studies. A. Cellular viability of Capan-1, PANC-1 and MIA PaCa-2 cells incubated with increasing concentrations of HA-PEG-CNOs (0.5, 5, 10 and 20 µg/mL) after 24, 48 and 72 h. **B.** Cellular uptake (intracellular fluoresceinamine isomer I; nmol/mg protein) of Capan-1 (CD44-negative control), PANC-1 (CD44+) and MIA PaCa-2 (CD44+) cells incubated with increasing concentrations of fluo-HA-PEG-CNOs (0.5, 5, 10 and 20 µg/mL). '*CA*' and '*CB*' represent competitive co-incubation of the 20 µg/mL fluo-HA-PEG-CNOs sample with a ten-fold excess of HA (*CA*; 200 µg/mL), and a CD44 blocking antibody (*CB*; 1:10 final dilution in the culture medium), respectively | Error bars represent the standard deviation of triplicate ($n = 3$) experiments. Statistical significance (vs. respective control (CTRL), unless otherwise indicated) is represented as $*p < 0.05$, $**p < 0.01$ and $***p < 0.001$; where *n.s.* = no significance.

receptor, 88 % and 92 %, respectively. Thus, they have been deemed as suitable candidates for further experiments (intracellular uptake and cell viability), while Capan-1 was selected as a CD44-negative control, as the PDAC cell line with the lowest expression (1 %) of CD44.

3.1.2. *In vitro prodrug cytotoxicity*

The cytotoxic activity of the three GEM-derived prodrugs, C5GEM, C12GEM and C18GEM (Fig. 1A), was evaluated in PDAC cells; in particular Capan-1, PANC-1 and MIA PaCa-2 cells. The cytotoxic activity of GEM itself was also evaluated and used as a point of comparison to the efficacy of the prodrugs.

In MIA PaCa-2 cells, both GEM and the prodrugs induced a dose and time-dependent decrease in cell viability, and the prodrugs did not offer any significant advantage compared to GEM (Fig. 1C). This result was expected because MIA PaCa-2 cells are intrinsically sensitive to GEM [36].

By contrast, in PANC-1 and Capan-1 cells, which are constitutively more resistant than MIA PaCa-2 cells [36], GEM has a reduced cytotoxic efficacy, significant only at 48 and 72 h and above 100 nM. The C5GEM prodrug did not differ from GEM for each concentration nor time point. C12GEM and C18GEM show a similar toxicity profile to GEM at 48 h, but they were both more cytotoxic than GEM at 48 and 72 h. Particularly, C18GEM proved the most effective prodrug, inducing a significant decrease of cell viability starting from 10 nM concentration–one order of magnitude lower than free GEM (Fig. 1C).

After thorough evaluation and analysis, we have determined that it is optimal to incorporate only C12GEM and C18GEM into the nanocarrier system for further drug delivery evaluation. This decision was influenced by the observation that C5GEM has comparatively lower cytotoxicity than C12GEM and C18GEM, although still better than that of the parental GEM (Fig. 1C). Moreover, it is also predicted that C5GEM would have inferior loading efficiency due to its low lipophilic character, which increases proportional with the length of the 4-(*N*)-acyl-sidechain [29,30]–making the more lipophilic prodrugs, C12GEM and C18GEM, ideal candidates for loading onto the CNO-based nanocarrier.

GEM has a complex mode of action, with numerous enzymes playing a role in the drug's metabolism or acting as targets for gemcitabine's various metabolites [37]. While, in principle, the intracellular efficacy of GEM can be affected by any change in enzyme activity, it is largely dependent on the balance between its deoxycytidine kinase-mediated activation of GEM (2′,2′-difluoro-2′-deoxycytidine, dFdC) into dFdCTP, a nucleoside triphosphate principally causing DNA damage [24], and its subsequent efflux facilitated by ATP Binding Cassette (ABC) transporters [36]. While we did not investigate the levels and activity of deoxycytidine kinase in the studied PDAC cell lines, we know that a critical determinant of resistance is the presence of ABC member C5/multidrug resistance protein 5 (ABCC5/MRP5). ABCC5/MRP5 is known to expedite the efflux of GEM and exhibits higher levels in PANC-1 cells but

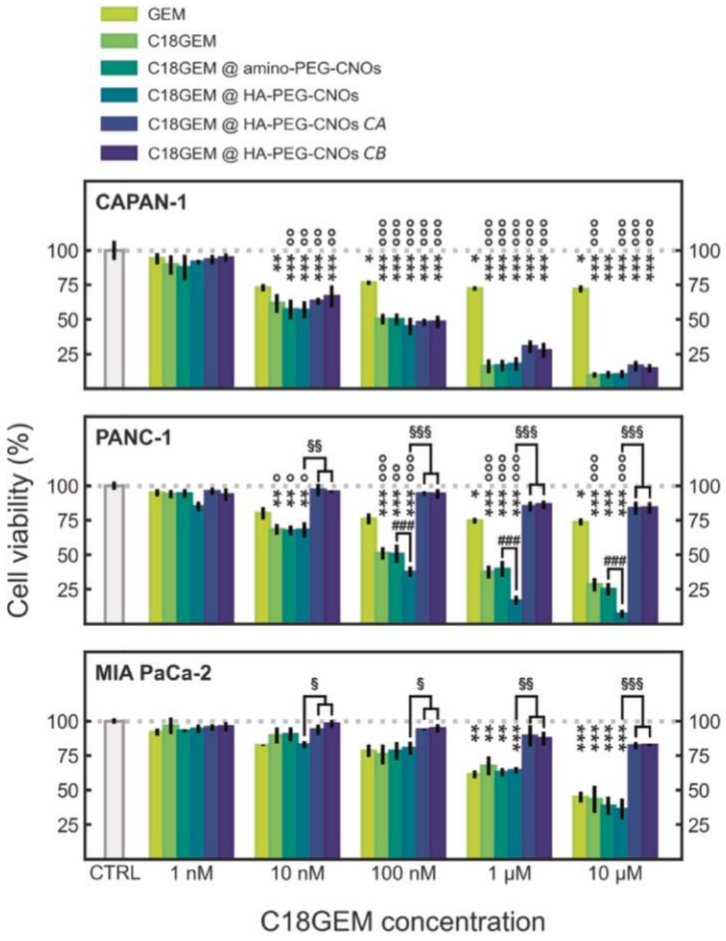

Fig. 5. C18GEM-loaded CNO-DDS cytotoxic activity. Cytotoxic activity of GEM, C18GEM, C18GEM @ amino-PEG-CNOs and C18GEM @ HA-PEG-CNOs in the PDAC cell lines MIA PaCa-2, PANC-1 and Capan-1 tested after 72 h at different prodrug concentrations (1 nM to 10 µM). Two competitive co-incubations are also presented; 10 µM C18GEM @ HA-PEG-CNOs sample with a saturating amount of HA (200 µg/mL) is denoted as '*CA*'; and a CD44 blocking antibody (final dilution in the culture medium: 1:10) is denoted as '*CB*'. Error bars represent the standard deviation of triplicate ($n = 3$) experiments. Statistical significance vs. respective control (CTRL) is represented as $^{*}p < 0.05$, $^{**}p < 0.01$ and $^{***}p < 0.001$. Statistical significance vs. GEM (at same concentration) is represented as $^{\circ}p < 0.05$, $^{\circ\circ}p < 0.01$ and $^{\circ\circ\circ}p < 0.001$. Statistical significance vs. API @ amino-PEG-CNOs is represented as $^{\#\#}p < 0.01$ and $^{\#\#\#}p < 0.001$. Statistical significance vs. API @ HA-PEG-CNOs is represented as $^{\S}p < 0.05$, $^{\S\S}p < 0.01$ and $^{\S\S\S}p < 0.001$. This figure should be presented as 'single column' in the manuscript.

lower levels in MIA PaCa-2 cells [36]. Our initial screenings of GEM and its prodrug derivatives suggests that the 4-(*N*)-acyl-GEM conjugates may have similar activation levels to GEM, while potentially being less susceptible to ABCC5-mediated efflux (Fig. 1C). Indeed, in MIA PaCa-2 cells that express ABCC5 at lower levels, the prodrugs showcased a cytotoxic potential similar to GEM, whereas in PANC-1 cells with higher ABCC5 expression, the prodrugs were significantly more cytotoxic. This finding could explain the observed differential cytotoxicity between MIA PaCa-2 and PANC-1 cells.

3.2. CNO-DDS — synthetic strategy

The overall drug delivery system (DDS) is comprised of a number of components, each engineered with specific functionality. At the foundation of the DDS are carbon nano-onions (CNOs), which serve as the nanocarrier scaffolds. The surface of the CNO scaffolds is customised with the different functional components, including the targeting agent; a spacer/linker; a fluorophore; and finally, the therapeutic payload.

Our CNO-based nanocarrier incorporates hyaluronic acid (HA) with an average molecular weight of 200 kDa ($HA_{200\ kDa}$) as the targeting agent. HA—a non-toxic and easily adaptable polymer—interacts with the CD44 receptor, making it particularly relevant for treating certain PDAC cells. $HA_{200\ kDa}$ is covalently attached to the CNO surface via a spacer/linker group, forming a bridge between the $HA_{200\ kDa}$ on one side and the CNO surface on the other. In our case, 4,7,10-trioxa-1,13-tridecanediamine (diamino-PEG) fulfils this role, ensuring the targeting agent remains at a distance from the CNO surface. Its primary amine groups allow for one-step covalent coupling, and it remains stable under

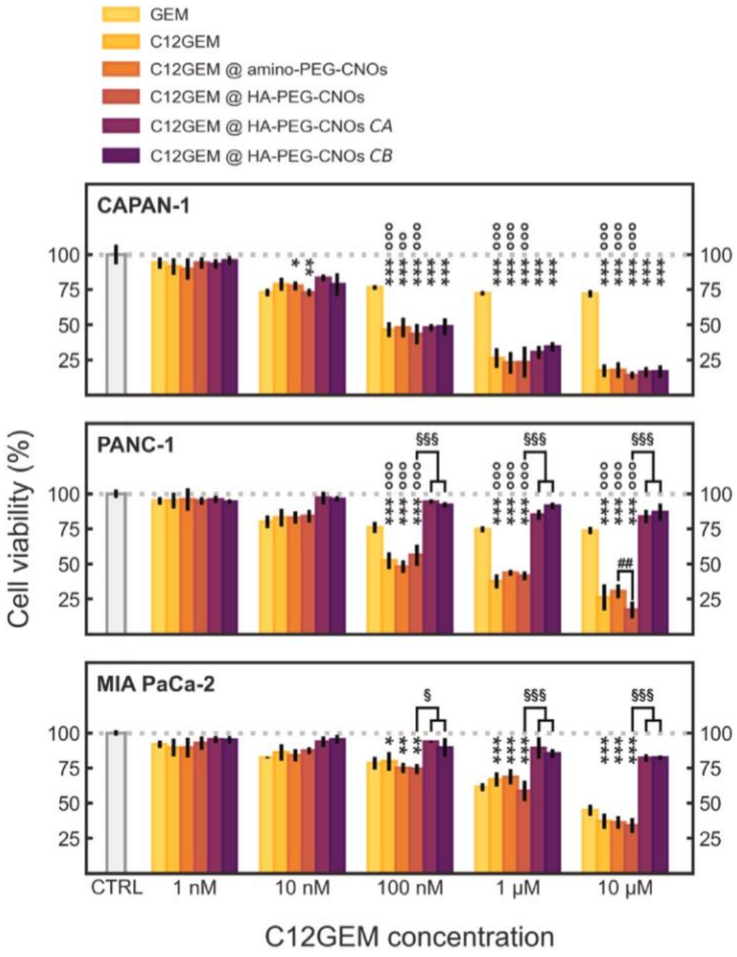

Fig. 6. C12GEM-loaded CNO-DDS cytotoxic activity. Cytotoxic activity of GEM, C12GEM, C12GEM @ amino-PEG-CNOs and C12GEM @ HA-PEG-CNOs in the PDAC cell lines MIA PaCa-2, PANC-1 and Capan-1 tested after 72 h at different prodrug concentrations (1 nM to 10 μM). Two competitive co-incubations are also presented; 10 μM C12GEM @ HA-PEG-CNOs sample with a saturating amount of HA (200 μg/mL) is denoted as '*CA*'; and a CD44 blocking antibody (final dilution in the culture medium: 1:10) is denoted as '*CB*'. Error bars represent the standard deviation of triplicate ($n = 3$) experiments. Statistical significance vs. respective control (CTRL) is represented as $^{*}p < 0.05$, $^{**}p < 0.01$ and $^{***}p < 0.001$. Statistical significance vs. GEM (at same concentration) is represented as $^{\circ}p < 0.05$, $^{\circ\circ}p < 0.01$ and $^{\circ\circ\circ}p < 0.001$. Statistical significance vs. API @ amino-PEG-CNOs is represented as $^{\#\#}p < 0.01$ and $^{\#\#\#}p < 0.001$. Statistical significance vs. API @ HA-PEG-CNOs is represented as $^{\S}p < 0.05$, $^{\S\S}p < 0.01$ and $^{\S\S\S}p < 0.001$. This figure should be presented as 'single column' in the manuscript.

physiological conditions.

The versatile nature of CNOs serves when additional functionality is required, as further components can be introduced at the surface of these nanoparticles. For instance, to facilitate emission-based analyses of the final construct, we have introduced a fluorophore tag into the system. In fact, we leveraged the green-emitting fluorophore, fluoresceinamine isomer-I (fluo), due to its integral primary amine facilitating convenient covalent attachment to the HA polymer.

The construction of our nanocarrier system, named HA-PEG-CNOs, or fluo-HA-PEG-CNOs when incorporating the fluorophore tag, is tailored for reversible loading of GEM-derived prodrugs and for ensuring dispersion in aqueous media. The synthesis of this DDS follows a systematic and sequential approach (Fig. 2).

Briefly, pristine CNOs (p-CNOs) were prepared by thermal annealing of detonation nanodiamonds (DNDs), as per a previously described procedure [13]. The first step in the preparation of the nanocarriers was the oxidation of p-CNOs, the purpose of which was to introduce carboxylic acid moieties on the CNO surface, allowing for further coupling reactions. The oxidation was carried out through the common approach utilising nitric acid [38,39]. Subsequently, to these oxidised CNOs (oxi-CNOs), diamino-PEG groups were introduced to form amino-PEG-CNOs. This was achieved through a previously reported EDC crosslinking reaction [33]. Similarly, $HA_{200\ kDa}$ was coupled to the other primary amine of the PEG-based spacer, forming HA-PEG-CNOs. In cases where green-emissive functionality was required, fluo-HA was used instead, hence forming fluo-HA-PEG-CNOs.

Finally, C12GEM and C18GEM were reversibly loaded onto HA-PEG-CNOs, forming C12GEM @ HA-PEG-CNOs and C18GEM @ HA-PEG-

CNOs. This loading was achieved through an overnight incubation process under ambient conditions, followed by thorough washing to remove any unbound prodrug. The prodrugs were bound non-covalently, leveraging the hydrophobic interaction between the lipophilic 4–(*N*)-acyl- sidechains and the CNO-surface. Also, to demonstrate the targeting ability of HA, amino-PEG-CNOs were similarly loaded as a control, conversely forming C12GEM @ amino-PEG-CNOs and C18GEM @ amino-PEG-CNOs.

3.3. CNO-DDS — physicochemical characterisation

3.3.1. High-resolution transmission electron microscopy and field-emission scanning electron microscopy (FE-SEM)

High-resolution transmission electron microscopy (HRTEM) images were obtained to investigate the p–CNOs, oxi-CNOs, amino-PEG-CNOs and HA-PEG-CNOs samples (Fig. 3B and SI 3). Well-defined nano-onions clustered together are evident in all micrographs. Importantly, the HRTEM micrographs highlight distinct structural differences between amino-PEG-CNOs (Fig. SI 3C) and HA-PEG-CNOs (Fig. 3B). Namely, the presence of HA moieties is visibly detectable; and the overall aspect and visual impression of the HA-PEG-CNO sample diverges from that of the amino-PEG-CNOs. Thus, the HRTEM micrographs provide an additional, visual evidence the successful covalent functionalisation of amino-PEG-CNOs with HA.

Supplementary imaging has been carried out using field-emission scanning electron microscopy (FE-SEM) on p-CNOs (Fig. 3A). Statistical size-analysis of individual observed p-CNO nanoparticles in the FE-SEM micrograph indicates that p-CNOs have an approximate diameter of 6.5 ± 1.3 nm.

3.3.2. X-ray photoelectron (XPS)

X-ray photoelectron (XPS) studies of pristine and functionalised CNOs have been carried out to investigate their surface chemistry and verify successful covalent functionalisation of the carbon nanoparticles. These XPS analyses include survey studies, as well as high-resolution core level studies, which have been conducted to evaluate the functional groups in each material. XPS spectra have been visualised in (Fig. 3C) and (Figs. SI 4 to SI 7), and quantitative information regarding deconvoluted peak fitting, bonding environment contribution, elemental percentage and elemental ratios have been calculated and presented in (Tabs. SI 1 to SI 5).

The XPS spectra of p-CNOs (Fig. SI 4) conform with previous analyses of the material [13,40] and include a primary peak at 284.5 eV, which signifies the existence of sp^2 carbon atoms. Additionally, four minor peaks have been identified and associated with different bonding environments. Namely, at 285.1 eV we observe the presence of sp^3 carbon atoms; the peak at 286.5 eV suggests the existence of oxygen-bonded carbon, specifically in the forms of C—O and C═O; the peak appearing at 287.4 eV is indicative of COO groups; lastly, the peak at 290.9 eV is attributed to π-π* interactions.

The overall low contribution of oxygen in p-CNOs allows for verification of the successful surface oxidation, to form oxi-CNOs (Fig. SI 5). The significant increase of oxygen content indicates the introduction of oxygen containing groups to the p-CNO surface. The emergence of the O 1 *s* 532 eV peak is consistent with the introduction of C═O groups, including –COOH, as well as minor contribution from other possible oxygen-containing functional groups, such as lactones, ketones and pyrones. The presence of C—O/C═O and –COOH groups is also confirmed by the increase of the intensity of C 1 *s* components at 285.2 and 286.8 eV. Finally, the decrease in sp^2 character, and increase in sp^3 character further indicates covalent surface functionalisation (Tab. SI 2).

Similarly evidenced is the successful diamino-PEGylation of oxi-CNOs to form amino-PEG-CNOs (Fig. SI 6), and the subsequent covalent functionalisation with HA, to form HA-PEG-CNOs (Fig. 3C). The increase of N% and O% content indicates the introduction of surface amino-PEG groups. The decrease in C═O and increase in C—N character indicates the amidation of –COOH groups (i.e., due to amino-PEGylation) (Tab. SI 3). The increase in C—O character further indicates the introduction of the triether-containing PEG groups.

A contrasting feature in the spectra of HA-PEG-CNOs (Fig. 3C) is the presence of a minor sodium contribution, as seen in the Na 1 *s* peak at 1071 eV in the survey spectrum. HA forms a carboxylate anion in each glucuronate group at physiological pH. These charges are responsible for the excellent aqueous solubility of the biopolymer, and are typically balanced out by monoatomic cations [41]. Indeed, the form of hyaluronic acid utilised in our research is known as sodium hyaluronate, which is stabilised by binding the mobile Na^+ cations observed in the XPS spectra.

3.3.3. UV–Vis absorption and fluorescence spectroscopy

UV–Vis absorption spectroscopy studies have been carried out on all functionalised CNO materials in deionised water (Fig. SI 8), with the exception of p-CNOs on account of their intrinsic low aqueous solubility. The 0.1 % mass extinction coefficient, $\varepsilon^{n}_{0.1\%}$ $(mg/mL)^{-1}cm^{-1}$, was provided in each spectrum for reference; where *n* is the wavelength at which it was calculated, at concentrations 1, 2.5, 5, 10, 20, 50 and 100 μg/mL. For comparative clarity, only concentrations 50 and 100 μg/mL are depicted in (Fig. SI 8). Due to the many contributing factors to the light limiting effects of CNOs, there exists some variation in the $\varepsilon_{0.1\%}$ between the different functionalised CNOs, and even between repeat analyses of the same material (*data not shown*). A contributing factor to this variation is the stochastic nature of the sonication process by which the samples are dispersed for analysis.

Notwithstanding, the specific peak wavelengths stay highly consistent in batch-to-batch analyses; enabling a quantitative material-to-material comparison, wherein the differences in λ_{max} are small. All spectra of functionalised CNOs (Fig. SI 8) show a sharp absorption band around λ_{max} < 190–200 nm, and a broad absorption band around λ_{max} 250–280 nm. The former can be attributed to high-energy $\pi \rightarrow \pi^*$ transitions arising from the double bonds on the CNO surface. On the other hand, the latter band can be attributed to $n \rightarrow \pi^*$ transitions; these electronic transitions arise from the non-bonding O: or N: electrons, as could be found in the various introduced surface functional groups, such as the carboxyl.

In the spectra of oxi-CNOs, we observed these two bands at λ_{max} 197 ± 1 and 262 ± 2 nm. When oxi-CNOs were amino-PEGylated, the resulting amino-PEG-CNOs' spectra indicated a shift in the absorption bands to λ_{max} 191 ± 1 and 272 ± 2. This shift was consistent across three individual batches tested (±1 nm), and can be attributed to the change of electronic character of the material due to successive covalent functionalisation steps. Similarly, a more minor shift was also observed for HA-PEG-CNOs and fluo-HA-PEG-CNOs, with their $\pi \rightarrow \pi^*$ transitions now appearing at λ_{max} < 190. In the case of fluo-HA-PEG-CNOs, the UV–Vis absorption spectrum has more features, indicating the presence of fluo. Notably, the spectrum of HA and fluo-HA depicts a sharp band < 190 nm (Fig. SI 9), which arises from HA carboxyl $\pi \rightarrow \pi^*$ transitions [42]—the contribution of which is reflected by the hypsochromic shift observed in HA-PEG-CNOs and fluo-HA-PEG-CNOs.

N-acylated cytosine nucleosides typically absorb in the 210–300 nm range [43,44]. This similarity in the absorbance maxima with that of HA-PEG-CNOs is taken into consideration when observing the presence of C12GEM and C18GEM in the respective UV–Vis absorption spectra of C12GEM @ HA-PEG-CNOs and C18GEM @ HA-PEG-CNOs. It can be seen that the intensity of the HA-PEG-CNOs $n \rightarrow \pi^*$ transition increases when the prodrugs are introduced onto the nanocarrier. This additive contribution of the prodrugs to the peak intensity observed in the UV–Vis absorption spectra confirms successful drug-loading.

Fluorescence emission spectroscopy was carried out on fluo-HA and fluo-HA-PEG-CNOs (Fig. 3D) to verify the successful coupling of fluo-HA with amino-PEG-CNOs. Indeed, the fluorophore-tagged nanocarrier was fluorescent, with sufficient emission intensity for subsequent cellular uptake studies (Fig. 4B). It should be noted that, compared to fluo-HA,

the fluorescence intensity of fluo-HA-PEG-CNOs is affected by additional factors relating to the presence of CNOs; including quenching effects from the carbon nanoparticles, changes in the local environment around the fluorophore, and potential reabsorption effects [45]. The emission maxima is similarly affected by additional factors; including alterations in the fluorophore's local polarity and local pH environment, molecular interactions like π-π stacking with the carbon structure, and possible photoinduced electron transfer events. In fact, it can be observed that there is a 6 nm bathochromic shift in the emission maxima when fluo-HA (λ_{em} 518 nm) is coupled onto the carbon nanoparticles to make fluo-HA-PEG-CNOs (λ_{em} 524 nm). As fluorescein-type fluorophores are particularly pH sensitive [46], we can speculate that the minor bathochromic shift occurs probably due to the variety of basic and acidic sites present on carbon surfaces [47]. Notwithstanding, the fluorescent properties of fluo-HA-PEG-CNOs are excellent for cellular internalisation studies—the stokes-shift of fluo-HA in dH_2O was calculated to be 32 nm (Fig. 3D), highlighting the minimised crosstalk between excitation and emission that is crucial for clearer and more accurate cellular imaging [48], with the minor additional bathochromic shift observed in fluo-HA-PEG-CNOs further improving the matter.

3.3.4. Attenuated Total Reflectance Fourier-Transform Infrared Spectroscopy (ATR–FTIR)

Attenuated Total Reflectance Fourier-Transform Infrared Spectroscopy (ATR-FTIR) was carried out on CNOs at different stages of their functionalisation (Figs. SI 10 and SI 11), as these studies can serve as an affirmative indicator of successful surface modification. The ATR-FTIR spectra of carbon-based materials like CNOs are typically less distinct due to their high symmetry and the predominance of non-polar covalent C—C bonds. Consequently, their spectra generally appear featureless with a broad background, making the assignment of functional groups ambiguous. Therefore, in order to interpret such spectra, emphasis should be placed on the spectral changes following functionalisation rather than on the inherent spectra of the CNOs themselves. For instance, a contrast can be made between the ATR-FTIR spectra of p-CNOs, which are featureless, and the spectra of oxi-CNOs, where spectral features become apparent due to the introduction of surface bound oxygen-containing functional groups (Fig. SI 10). A similar contrast can be observed with amino-PEG-CNOs, the spectra of which has more features than that of oxi-CNOs given the progressively increased degree of functionalisation. This trend continues with HA-PEG-CNOs and fluo-HA-PEG-CNOs—it is especially evident when compared to the respective substituents utilised in the surface functionalisation of these CNO materials; namely diamino-PEG, HA and fluo-HA (Fig. SI 14).

Indeed, the ATR-FTIR spectral characteristics of CNOs differ significantly from those of small organic molecules, like GEM and its derived prodrugs (Fig. SI 12). In their spectra, distinct peaks associated with specific functional groups are evident. For instance, a prominent band at approximately 1650 cm^{-1} corresponds to the carbonyl stretch, a feature present in all three therapeutic molecules. Additionally, a sharp peak at around 1500 cm^{-1} is exclusive to the derived prodrugs, denoting the CH_2 bending from the aliphatic 4-(*N*)-acyl- sidechain. This shift in spectral features is supported by the disappearance of the two primary amine stretches, observed at 3120 and 3080 cm^{-1} in GEM's spectrum, as the side chain is integrated into GEM's primary amine via an amide bond. Coinciding with the introduction of the aliphatic sidechain, two bands at 2920 and 2850 cm^{-1} emerge, corresponding to the alkane sp^3 C—H stretching. By contrasting the intensity ratio of these bands with that of the carbonyl, a direct relationship between their intensity and the length of the aliphatic sidechain is observable; this intensity relationship has been visualised in (Fig. SI 12).

3.3.5. Dynamic light scattering (DLS) and zeta potential (ZP)

Dynamic Light Scattering (DLS) and Zeta Potential (ZP) studies were performed on all functionalised CNOs at 5, 10, and 20 μg/mL concentrations in deionised water, and the data was reported in (Tab. SI 6). p-CNOs were not included in these tests due to their poor dispersion in aqueous solvents, a characteristic stemming from their highly hydrophobic sp^2 hybridised carbon lattice and the inclination for non-covalent carbon–carbon interactions like π-π stacking [49,50,51].

Notably, the dispersion of such carbon-based nanoparticles can be improved through various surface functionalisation techniques, like the non-covalent loading of a HA-phospholipid conjugate [52,53]. In our nanocarrier's development, surface oxidation of p-CNOs proved extremely effective—oxi-CNOs formed particles with an average hydrodynamic diameter of < 180 nm at all tested concentrations. Furthermore, the ZP results were favourable, all values being under −40 mV. As expected, diamino-PEGylation of oxi-CNOs led to a slight reduction in their dispersibility due to partial utilisation of the surface-bound carboxylic acid moieties for amide bond formation with the linkers' primary amine. This especially evident in the ZP values of amino-PEG-CNOs, which are approx. −20 mV at all concentrations. However, the dispersibility decrease of amino-PEG-CNOs was not substantial as the material retained a good hydrodynamic diameter at all concentrations—the optimal results were observed at a concentration of 5 μg/mL, presenting a hydrodynamic diameter of 193 ± 22 nm and a ZP of −20 ± 1 mV. Further coupling of HA resulted in a larger hydrodynamic diameter, and a much improved ZP, with HA-PEG-CNOs having a hydrodynamic diameter of 248 ± 19 nm and a ZP of −39 ± 4 mV at 5 μg/mL. On the other hand, coupling of fluo-HA to amino-PEG-CNOs resulted in a reduced hydrodynamic diameter and a moderately increased ZP; 173 ± 11 nm and a ZP of −33 ± 1 mV at 5 μg/mL. The overall optimal hydrodynamic diameters were achieved for all materials are conducive to efficient cellular internalisation, and the good zeta potential results are an indicator of stability. In addition, these results indicate successful surface functionalisation, which can be derived from the distinct differences in the hydrodynamic diameter and ZP values observed for each material.

3.3.6. CNO-DDS drug-loading and release

Drug loading efficiencies were determined by HPLC—to assess drug-loading efficiency, the supernatant and the washing solutions were collected after the loading reaction. Subsequently, any residual drug were quantified by HPLC. The amount of drug loaded was calculated based on its initial and residual concentration. We demonstrated that a prodrug to CNO ratio of 1:7 w/w incubated overnight at room temperature allowed the highest drug-loading value in all the CNOs samples. Moreover, we observed that the loading efficiency of amino-PEG-CNOs was marginally higher (65 % for C12GEM; 80 % for C18GEM) compared to that of HA-PEG-CNOs (55 % for C12GEM; 70 % for C18GEM). From these data, we can confer two key observations: *a)* that the presence of HA on the CNO surface influences the drug-loading capacity; and *b)* that the physicochemical features of the prodrugs influence their loading.

In regards to *a)*, the impact of HA on loading—we can observe the influence of HA on prodrug loading efficiency given that for both C12GEM and C18GEM, loading efficiency is ~ 10 % higher on amino-PEG-CNOs than on HA-PEG-CNOs. The mechanisms underlying this difference are likely multifaceted, encompassing factors such as diffusion, competition with the solvent, steric hindrance, and various weak interactions prevalent in the supramolecular chemistry of CNOs, including dispersion forces, van der Waals forces, hydrogen bonding, and hydrophobic interactions [29,50]. For instance, the molecular flexibility of the aliphatic sidechain can contribute to the disposition of the prodrug onto the CNO surface. Moreover, the longer sidechain of C18GEM has a higher reach than that of C12GEM, enabling increased accessibility to the CNO surface—this may be of particular benefit in the case of HA-PEG-CNOs, where surface accessibility is more limited owing to the presence of surface-bound HA.

Regarding *b)*, the impact of prodrugs properties on loading—we observed that, compared to C12GEM, the loading efficiency of C18GEM was ~ 15 % higher on both amino-PEG-CNOs and HA-PEG-CNOs. In addition to the abovementioned factors, an interplay between the

lipophilic character of the drug and its size could also contribute to this difference in loading efficiency [28,29]. Indeed, the loading efficiency of the prodrugs is reflective of their lipophilicity, with the more lipophilic C18GEM (logP 7.91) exhibiting higher loading efficiency than C12GEM (logP 4.74). This observation suggests that the prodrugs favour loading through hydrophobic interactions between the aliphatic 4-(*N*)-acyl-sidechains and the CNO surface. At the same time, the hydrophilic dFdC core of the prodrug remains exposed to the hydrophilic HA chains and solvent.

In vitro C12GEM and C18GEM release experiments from drug-loaded HA-PEG-CNOs were investigated in PBS buffer at 37 °C. The release profile of drug-loaded amino-PEG-CNOs was also evaluated and a similar profile was observed (data not shown). The samples showed a slow release with a trend inverse to that found in the drug-loading experiments: C18GEM showed the highest loading and lowest release. After 72 h, approx. 15 % of C12GEM and only around 5 % of the more lipophilic C18GEM was released from HA-PEG-CNOs (Fig. SI 15).

It is possible that the steric hindrance of the HA coating contributes to the overall low prodrug release, with the amino-PEG coating possibly playing a more minor role–we have previously reported a similar case with HA-coated carbon nanotubes [11]. A longer sidechain also has a larger surface area available for non-covalent interaction with the CNO surface—therefore, it can be expected that C18GEM will bind more strongly onto the nanocarrier. Indeed, this is reflected in the release profile of the prodrug, with C18GEM exhibiting lower release compared to C12GEM, suggesting a relatively higher interaction between the prodrug and CNOs. Finally, the observation that the prodrugs' release profile was inversely proportional to their drug-loading efficiency suggests that adjusting the length of the 4-(*N*)-acyl- sidechain is critical in fine-tuning both the loading and release kinetics of the prodrug. Indeed, if the sidechain is too short, the prodrug may be too hydrophilic to non-covalently interact with the nanocarrier surface, leading to suboptimal loading [29]; similarly, suboptimal release may result if the sidechain is too long.

3.4. CNO-DDS — Biological evaluation

3.4.1. Biocompatibility studies

To verify that HA-PEG-CNOs are biocompatible and did not exert any cytotoxicity per se, we next measured the dose and time-dependent viability in the selected PDAC cell lines treated with HA-PEG-CNOs (Fig. 4A). Although there was a progressive decrease in cell viability at concentration > 10 μg/mL, and after 48 or 72 h incubation, in all the experimental conditions cell viability remained higher than 70 %, indicating a good biocompatibility of CNOs. The same profile was shown by fluo-HA-PEG-CNOs (Fig. SI 2A), indicating that the addition of the fluorophore did not alter the biocompatibility of CNOs.

A minor reduction in cell viability after 72 h incubation at the highest tested concentration is observed, but these concentrations are unlikely to be reached in an *in vivo* scenario. To further verify their biocompatibility, the viability of HA-PEG-CNOs was evaluated also in HPDE cells (Fig. SI 2B). The results of this further evaluation demonstrate a comparable level of biocompatibility to PDAC evaluations at all time points and tested concentrations. The findings suggest that the HA-PEG-CNO nanocarrier demonstrates a comparable level of biocompatibility in both the non-transformed HPDE cells and the PDAC cells.

Overall, the biocompatibility results are good and suggest that the potential for toxicity in a practical application is low. The present study is a valuable proof-of-concept of a new delivery system carrying GEM-derives, against highly chemoresistant PDAC cell lines.

3.4.2. CD44-target specificity and cellular uptake

Next, we assessed whether HA-conjugated CNOs were specifically taken up via CD44. To this aim, we compared the intracellular fluorescence of CD44-negative Capan-1 cells, and CD44-positive PANC-1 and MIA PaCa-2 cells (Fig. 4B), treated with fluo-HA-PEG-CNOs. As expected, the intracellular fluorescence increased in dose- and time-dependent way in PANC-1 and MIA PaCa-2 cells, suggesting a possible interaction with CD44, an event that may trigger the endocytosis of HA-conjugated CNOs/CD44 complex. The progressive increase of the intracellular fluorescence from 1 h to 24 h post-incubation is indeed typical of nanoconjugates internalised by a receptor-triggered endocytosis process [54]. Our hypothesis was confirmed by the absence of any increase in the intracellular fluorescence in CD44-negative Capan-1 cells, and by competition assays, showing a complete abrogation of intracellular fluorescence in PANC-1 and MIA PaCa-2 cells incubated with an excess of HA or with a CD44 blocking antibody.

3.4.3. Prodrug-loaded CNO-DDS cytotoxic efficacy

Finally, we compared the cytotoxic efficacy of C18GEM @ HA-PEG-CNOs with free GEM and the C18GEM prodrug (Fig. 5), as well as the cytotoxic efficacy of C12GEM @ HA-PEG-CNOs with free GEM and the C12GEM prodrug (Fig. 6).

In the case of C18GEM analyses, we detected a superior efficacy of C18GEM (prodrug alone) and C18GEM @ HA-PEG-CNOs in both GEM-resistant cell lines, PANC-1 and Capan-1. Moreover, in CD44-positive PANC-1 cells, C18GEM @ HA-PEG-CNOs were also more cytotoxic than C18GEM alone, while no differences were detected in CD44-negative Capan-1 cells. In line with the results observed with C18GEM (prodrug only), we did not detect a superior efficacy of C18GEM @ HA-PEG-CNOs compared to free GEM in chemosensitive MIA PaCa-2 cells.

These results can be explained by crossing the drug sensitivity/resistance profile and the expression of CD44. Indeed, the highest efficacy of C18GEM @ HA-PEG-CNOs was achieved in $CD44^{+}$ GEM-resistant PANC-1, which represents the most aggressive cell lines among those analysed. In this model, the cytotoxicity followed this rank order: C18GEM @ HA-PEG-CNOs > C18GEM > GEM. This phenotype can be explained at least by two mechanisms: the higher intracellular delivery of GEM granted by the endocytosis via the CD44 receptor and the possibility of overcoming drug efflux when GEM is conjugated to C18-PEG. Consistently, this was the only cell line where C18GEM @ HA-PEG-CNOs were significantly more effective than C18GEM, but they were characterised by a complete abrogation of the efficacy by HA or CD44 blocking antibody.

In Capan-1 cells, which are CD44-negative and GEM-resistant, both C18GEM (prodrug alone) and C18GEM @ HA-PEG-CNOs had higher efficacy than the parental GEM. This suggests a CD44-independent route wherein a higher intracellular drug delivery is enabled by the highly lipophilic profile of C18GEM. However, compared to C18GEM alone, we did not detect any additional benefit from C18GEM @ HA-PEG-CNOs. This is expected due to the absence of CD44 receptor. Consistently, the cytotoxicity of C18GEM @ HA-PEG-CNOs was not affected by co-incubation with HA or anti-CD44 antibody, likely because the uptake of C18GEM @ HA-PEG-CNOs follows a CD44-independent route.

We did not observe particular benefits from prodrugs or their formulation in GEM-sensitive MIA PaCa–2 cells, where GEM alone exerted the maximal cytotoxic efficacy. In any case, also in this model, the intracellular delivery of C18GEM, loaded in HA-PEG-CNOs, is mediated by the CD44 receptor, since it was abrogated by an excess of HA or blocking antibody.

Similar results were observed in the case of C12GEM analyses (Fig. 6). In contrast to parental GEM, C12GEM (prodrug alone) demonstrated a superior efficacy in both GEM-resistant PANC-1 and Capan-1 cell lines, with the composition C12GEM @ HA-PEG-CNOs showing more potency. Notably, the most aggressive cell line, CD44+ GEM-resistant PANC-1, demonstrated higher sensitivity to C12GEM @ HA-PEG-CNOs than C12GEM at 10 μM (prodrug concentration). This improvement is attributed to enhanced intracellular delivery via the CD44 receptor, as compounded by the observation that no difference in cytotoxicity was observed in Capan-1 cells, which are CD44-negative. A further key observation is that both GEM-resistant cell lines (Capan-1 and PANC-1) demonstrated a higher sensitivity to C12GEM (prodrug

alone). The observed improvement in the performance of C12GEM against GEM-resistant cells mirrors that of C18GEM. This emphasizes the effectiveness of our lipophilic GEM-derivatives in treating these complex cell lines. Lastly, in line with the results observed for C18GEM, GEM-sensitive MIA PaCa–2 cells reveal no added advantages from the C12GEM prodrug or its CNO-based nanoformulations.

4. Conclusions

In this study, we have presented a progressive step in the emerging field of employing carbon nanoparticles as nanocarriers for targeted drug delivery systems (DDSs). Specifically, we developed a novel carbon nano-onion (CNO)-based drug-delivery system. We tailored this nanocarrier to target cancer cells that express the hyaluronic acid receptor CD44, offering a strategic approach to enhance treatment efficacy and reduce adverse side effects of the chemotherapeutic drug. Our findings reveal not only the effective targeting and biocompatibility of this CNO-based system but also its amplified effectiveness when combined with gemcitabine-derived prodrugs, showcasing its potential in overcoming drug resistance in pancreatic ductal adenocarcinoma (PDAC) cells.

Our innovative system leveraged the CNO as its core scaffold, complemented with hyaluronic acid (HA)—the guiding component—covalently bound to the CNO surface through a PEG bridge. This DDS enabled non-covalent loading of lipophilic gemcitabine-derived prodrugs, namely 4-(*N*)-lauroyl-gemcitabine (C12GEM) and 4-(*N*)-stearoyl-gemcitabine (C18GEM) were selected for loading given their superior cytotoxicity we observed in PDAC cells. The vesicle design also allowed for adaptability; we utilised fluoresceineamine, isomer I (fluo)-labelled HA (fluo-HA) when fluorescence was of interest, broadening the scope for emission studies with this nanocarrier.

In evaluating biocompatibility, our DDS demonstrated a very good biocompatibility profile when incubated with various PDAC cell types, including Capan-1, PANC-1, and MIA PaCa-2, as well as in HPDE cells. This supports the versatility and potential safety of our nanocarrier for biological applications. Fluorescence-based cellular internalisation assessments, as enabled by fluo-HA, indicated that the DDS was specifically taken up by CD44-positive cells, further supporting the targeting efficiency of this nanocarrier.

Our research determined that C18GEM exhibits a higher loading efficiency than C12GEM, attributed to its superior lipophilicity. We also observed that amino-PEG-CNOs demonstrated a slightly better loading efficiency than HA-PEG-CNOs, suggesting that the presence of HA on the CNOs surface affects the drug-loading capacity. An inverse correlation was identified between drug-loading and release, with C18GEM showing the highest drug-loading but the lowest release. This indicates a robust interaction between the prodrug and the CNOs. Furthermore, both C12GEM and C18GEM demonstrated slow release from HA-PEG-CNOs, indicating the potential for controlled drug delivery.

We found that C18GEM @ HA-PEG-CNOs displayed superior cytotoxic efficacy compared to free GEM and C18GEM alone in GEM-resistant cell lines, PANC-1 and Capan-1; with no additional benefit was observed in GEM-sensitive MIA PaCa-2 cells. GEM resistance and CD44 status are two key parameters to determine the efficacy of C18GEM @ HA-PEG-CNOs. In perspective, they can be translated to other tumour types where gemcitabine is used and CD44 is expressed–such as non-small cell lung cancer, mesotheliomas, or recurrent ovarian cancer–to enlarge the treatment applications for this innovative nanoformulation.

Overall, in this study we present a valuable proof-of-concept for the use of CNOs as a nanocarrier for the targeted delivery of GEM-derived prodrugs. We highlight the capacity of our CNO-based DDS to improve treatment outcomes in CD44+ GEM-resistant PDAC cells, demonstrating the potential of CNOs as effective nanocarriers for targeted anti-cancer drug delivery. In a broader context, this research underscores the potential of carbon nanoparticle frameworks in enhancing targeted DDSs, and it represents a progressive step towards future work in translational applications of carbon nanoparticles in oncology.

CRediT authorship contribution statement

Michał Bartkowski: Data curation, Formal analysis, Investigation, Methodology, Software, Validation, Visualization, Writing – original draft. **Valeria Bincoletto:** Investigation. **Iris Chiara Salaroglio:** Investigation, Validation. **Giacomo Ceccone:** Data curation, Formal analysis, Investigation, Validation, Writing – review & editing. **Raul Arenal:** Investigation. **Sara Nervo:** Investigation. **Barbara Rolando:** Investigation, Validation. **Chiara Riganti:** Data curation, Investigation, Methodology, Supervision, Validation, Writing – review & editing. **Silvia Arpicco:** Conceptualization, Methodology, Project administration, Supervision, Writing – review & editing. **Silvia Giordani:** Conceptualization, Methodology, Project administration, Supervision, Writing – original draft, Funding acquisition.

Declaration of competing interest

The authors declare that they have no known competing financial interests or personal relationships that could have appeared to influence the work reported in this paper.

Data availability

No data was used for the research described in the article.

Acknowledgements

Financial assistance in the form of a Government of Ireland Postgraduate Scholarship (GOIPG) from the Irish Research Council (IRC) to M.B. is gratefully acknowledged (No. GOIPG/2019/1820). The FE-SEM, DLS & ZP, fluorescence emission and UV-Vis absorption spectroscopy were carried out at the Nano Research Facility (NRF) in Dublin City University (DCU) which was funded under the Programme for Research in Third Level Institutions (PRTLI) Cycle 5. The PRTLI is co-funded through the European Regional Development Fund (ERDF), part of the European Union Structural Funds Programme 2011-2015. Instrumental access to ATR-FTIR spectroscopy was provided by the School of Chemical Sciences (SCS), DCU. M.B. would like to acknowledge Adalberto Camisasca for their guidance and fruitful discussions. R.A. acknowledges funding from the Spanish MCIN (project grant PID2019-104739GB-100/AEI/10.13039/501100011033), from the Government of Aragon (project DGA E13-23R) and from the European Union H2020 program "ESTEEM3" (823717). Finally, we gratefully acknowledge the funding support from MUR (Italian Ministry of University and Research - PRIN 2022ZBZFX3) to S.A. and CR; and AIRC (Italian Association for Cancer Research; IG21408) to C.R.

Appendix A. Supplementary data

Supplementary materials: Flow cytometry data for quantification of cell lines' CD44-expression (Fig. SI 1); additional PDAC and HPDE cell viability studies (Fig. SI 2); HRTEM micrographs of pristine and functionalised CNOs (Fig. SI 3); XPS spectra of pristine and functionalised CNOs (Figs. SI 4 to SI 7) and respective tabulated XPS data (Tabs. SI 1 to SI 5); UV-Vis absorption spectra (Figs. SI 8 and SI 9); ATR-FTIR spectra (Figs. SI 10 to SI 14); DLS & ZP data (Tab. SI 6); and prodrug release profiles (Fig. SI 15). Supplementary data to this article can be found online at https://doi.org/10.1016/j.jcis.2023.12.166.

References

[1] Y. Barenholz, Doxil®–the First FDA-approved Nano-Drug: Lessons Learned, J. Control. Release 160 (2012) 117–134, https://doi.org/10.1016/j.jconrel.2012.03.020.

[2] D. Peer, J.M. Karp, S. Hong, O.C. Farokhzad, R. Margalit, R. Langer, Nanocarriers as an Emerging Platform for Cancer Therapy, Nat. Nanotechnol. 2 (2007) 751–760, https://doi.org/10.1038/nnano.2007.387.

[3] M.J. Mitchell, M.M. Billingsley, R.M. Haley, M.E. Wechsler, N.A. Peppas, R. Langer, Engineering Precision Nanoparticles for Drug Delivery, Nat. Rev. Drug Discov. 20 (2021) 101–124, https://doi.org/10.1038/s41573-020-0 090-8.

[4] D. Guimarães, A. Cavaco-Paulo, E. Nogueira, Design of Liposomes as Drug Delivery System for Therapeutic Applications, Int. J. Pharm. 601 (2021) 120571, https://doi.org/10.1016/j.ijpharm.2021.120571.

[5] A. Kumari, S.K. Yadav, S.C. Yadav, Biodegradable Polymeric Nanoparticles Based Drug Delivery Systems, Colloids Surf. B Biointerfaces 75 (2010) 1–18, https://doi.org/10.1016/j.colsurfb.2009.09.001.

[6] L.I. Atanase, Micellar Drug Delivery Systems Based on Natural Biopolymers, Polymers 13 (477) (2021), 10.3390/polym13030477.

[7] A. Kumar, X. Zhang, X.-J. Liang, Gold Nanoparticles: Emerging Paradigm for Targeted Drug Delivery System, Biotechnol. Adv. 31 (2013) 593–606, https://doi.org/10.1016/j.biotechadv.2012.10.002.

[8] T. Vangijzegem, D. Stanicki, S. Laurent, Magnetic Iron Oxide Nanoparticles for Drug Delivery: Applications and Characteristics, Expert Opin. Drug Deliv. 16 (2019) 69–78, https://doi.org/10.1080/17425247.2019.1554647.

[9] Y. Sun, L. Zheng, Y. Yang, X. Qian, T. Fu, X. Li, Z. Yang, H. Yan, C. Cui, W. Tan, Metal-Organic Framework Nanocarriers for Drug Delivery in Biomedical Applications, Nano-Micro Letters 12 (2020) 103, https://doi.org/10.1007/s40820-020-00423-3.

[10] F. Arcudi, L. Đorđević, Supramolecular Chemistry of Carbon-Based Dots Offers Widespread Opportunities, Small 19 (2023) 2300906, https://doi.org/10.1002/smll.202300906.

[11] S. Arpicco, M. Bartkowski, A. Barge, D. Zonari, L. Serpe, P. Milla, F. Dosio, B. Stella, S. Giordani, Effects of the Molecular Weight of Hyaluronic Acid in a Carbon Nanotube Drug Delivery Conjugate, Front. Chem. 8 (2020) 578008, https://doi.org/10.3389/fchem.2020.578008.

[12] J. Liu, L. Cui, D. Losic, Graphene and Graphene Oxide as New Nanocarriers for Drug Delivery Applications, Acta Biomater. 9 (2013) 9243–9257, https://doi.org/10.1016/j.actbio.2013.08.016.

[13] S. Lettieri, A. Camisasca, M. d'Amora, A. Diaspro, T. Uchida, Y. Nakajima, K. Yanagisawa, T. Maekawa, S. Giordani, Far-Red Fluorescent Carbon Nano-Onions as a Biocompatible Platform for Cellular Imaging, RSC Adv. 7 (2017) 45676–45681, https://doi.org/10.1039/C7RA09442F.

[14] H. Wang, Y. Liang, Y. Yin, J. Zhang, W. Su, A.M. White, J.X. Bin Jiang, Y. Zhang, S. Stewart, X. Lu, X. He, *Carbon Nano-Onion-Mediated Dual Targeting of P-selectin and P-glycoprotein to Overcome Cancer Drug Resistance*, Nature Communications 12 (2021) 312, https://doi.org/10.1038/s41467-020-20588-0.

[15] M. Bartkowski, S. Giordani, Carbon Nano-Onions as Potential Nanocarriers for Drug Delivery, Dalton Trans. 50 (2021) 2300–2309, https://doi.org/10.1039/D0DT04093B.

[16] R.C. Gupta, R. Lall, A. Srivastava, A. Sinha, Hyaluronic Acid: Molecular Mechanisms and Therapeutic Trajectory, Frontiers in Veterinary Science 6 (2019) 192, https://doi.org/10.3389/fvets.2019.00192.

[17] R.K. Sironen, M. Tammi, R. Tammi, P.K. Auvinen, M. Anttila, V.-M. Kosma, Hyaluronan in Human Malignancies, Exp. Cell Res. 317 (2011) 383, https://doi.org/10.1016/j.yexcr.2010.11.017.

[18] F. Dosio, S. Arpicco, B. Stella, E. Fattal, Hyaluronic Acid for Anticancer Drug and Nucleic Acid Delivery, Adv. Drug Deliv. Rev. 97 (2016) 204–236, https://doi.org/10.1016/j.addr.2015.11.011.

[19] R. Stern, A.A. Asari, K.N. Sugahara, Hyaluronan Fragments: An Information-Rich System, Eur. J. Cell Biol. 85 (2006) 699, https://doi.org/10.1016/j.ejcb.2006.05.009.

[20] D. Jiang, J. Liang, P.W. Noble, Hyaluronan in Tissue Injury and Repair, Annu. Rev. Cell Dev. Biol. 23 (2007) 435, https://doi.org/10.1146/annurev.cellbio.23.090506.123337.

[21] D. Naor, S. Nedvetzki, I. Golan, L. Melnik, Y. Faitelson, CD44 in Cancer, Crit. Rev. Clin. Lab. Sci. 39 (2002) 527, https://doi.org/10.1080/10408360290795574.

[22] X.-P. Li, X.-W. Zhang, L.-Z. Zheng, W.-J. Guo, Expression of CD44 in Pancreatic Cancer and Its Significance, Int. J. Clin. Exp. Path. 8 (2015) 6724–6731.

[23] C. Chen, S. Zhao, A. Karnad, J.W. Freeman, The Biology and Role of CD44 in Cancer Progression: Therapeutic Implications, J. Hematol. Oncol. 11 (2018) 64, https://doi.org/10.1186/s13045-018-0605-5.

[24] M. Amrutkar, I.P. Gladhaug, Pancreatic Cancer Chemoresistance to Gemcitabine, Cancers 9 (2017) 157, https://doi.org/10.3390/cancers9110157.

[25] P. Bhoopathi, P. Mannangatti, S. K. Das, P. B. Fisher, L. Emdad, *Chemoresistance in Pancreatic Ductal Adenocarcinoma: Overcoming Resistance to Therapy*, *Adv. Cancer Res. 159* (**2023**) 285–341, 10.101 6/bs.acr.2023.02.010.

[26] E. Dalla Pozza, C. Lerda, C. Costanzo, M. Donadelli, I. Dando, E. Zoratti, M. T. Scupoli, S. Beghelli, A. Scarpa, E. Fattal, S. Arpicco, M. Palmieri, *Targeting* Gem*citabine Containing Liposomes to CD44 Expressing Pancreatic Adenocarcinoma Cells Causes an Increase in the Antitumoral Activity*, *Biochim. Biophys. Acta (BBA) – Biomembr. 1828* (**2013**) 1396–1404, 10.1016/j.bbamem.2013.01.020.

[27] S. Arpicco, C. Lerda, E. Dalla Pozza, C. Costanzo, N. Tsapis, B. Stella, M. Donadelli, I. Dando, E. Fattal, L. Cattel, M. Palmieri, Hyaluronic Acid-Coated Liposomes for Active Targeting of Gemcitabine, Eur. J. Pharm. Biopharm. 85 (2013) 373–380, https://doi.org/10.1016/j.ejpb.2013.06.003.

[28] B. Stella, S. Arpicco, F. Rocco, V. Marsaud, J.-M. Renoir, L. Cattel, P. Couvreur, Encapsulation of Gemcitabine Lipophilic Derivatives into Polycyanoacrylate Nanospheres and Nanocapsules, Int. J. Pharm. 344 (2007) 71–77, https://doi.org/10.1016/j.ijpharm.2007.06.006.

[29] A. Malfanti, I. Miletto, E. Bottinelli, D. Zonari, G. Blandino, G. Berlier, S. Arpicco, Delivery of Gemcitabine Prodrugs Employing Mesoporous Silica Nanoparticles, Molecules 21 (2016) 522, https://doi.org/10.3390/molecules21040522.

[30] M.L. Immordino, P. Brusa, F. Rocco, S. Arpicco, M. Ceruti, L. Cattel, Preparation, Characterization, Cytotoxicity and Pharmacokinetics of Liposomes Containing Lipophilic Gemcitabine Prodrugs, J. Control. Release 100 (2004) 331–346, https://doi.org/10.1016/j.jconrel.2004.09.001.

[31] M. dela Fuente, B. Seijo, M.J. Alonso, *Novel Hyaluronic Acid-Chitosan Nanoparticles for Ocular Gene Therapy*, Investigative Opthalmol. Visual Sci. 49 (2008) 2016–2024, https://doi.org/10.1167/iovs.07-1077.

[32] A.N. De Belder, K. Wik, Preparation and Properties of Fluorescein-Labelled Hyaluronate, Carbohydr. Res. 44 (1975) 251–257, https://doi.org/10.1016/S0008-6215(00)84168-3.

[33] S. Lettieri, M. d'Amora, A. Camisasca, A. Diaspro, S. Giordani, Carbon Nano-Onions as Fluorescent on/off Modulated Nanoprobes for Diagnostics, Beilstein J. Nanotechnol. 8 (2017) 1878–1888, https://doi.org/10.3762/bjnano.8.188.

[34] M. d'Amora, V. Maffeis, R. Brescia, D. Barnes, E. Scanlan, S. Giordani, Carbon Nano-Onions as Non-Cytotoxic Carriers for Cellular Uptake of Glycopeptides and Proteins, Nanomaterials 9 (2019) 1069, https://doi.org/10.3390/nano908 1069.

[35] C.A. Schneider, W.S. Rasband, K.W. Eliceiri, NIH Image to ImageJ: 25 Years of Image Analysis, Nat. Methods 9 (2012) 671–675, https://doi.org/10.1038/nmeth.2089.

[36] F. Masetto, K. Chegaev, E. Gazzano, N. Mullappilly, B. Rolando, S. Arpicco, R. Fruttero, C. Riganti, M. Donadelli, MRP5 Nitration by NO-releasing Gemcitabine Encapsulated in Liposomes Confers Sensitivity in Chemoresistant Pancreatic Adenocarcinoma Cells, Biochim. Biophys. Acta (BBA) – Mol. Cell Res. 1867 (2020) 118824, https://doi.org/10.1016/j.bbamcr.2020.118824.

[37] A.M. Bergman, H.M. Pinedo, G.J. Peters, Determinants of Resistance to 2′,2′-Difluorodeoxycytidine (Gemcitabine), Drug Resist. Updat. 5 (2002) 19–33, https://doi.org/10.1016/S1368-7646(02)00002-X.

[38] J. Bartelmess, S. Giordani, Carbon Nano-Onions (Multi-Layer Fullerenes): Chemistry and Applications, Beilstein J. Nanotechnol. 5 (2014) 1980–1998, https://doi.org/10.3762/bjnano.5.207.

[39] M.E. Plonska-Brzezinska, Carbon Nano-Onions: A Review of Recent Progress in Synthesis and Applications, ChemNanoMat 5 (2019) 568–580, https://doi.org/10.1002/cnma.201800583.

[40] M. d'Amora, A. Camisasca, S. Lettieri, S. Giordani, Toxicity Assessment of Carbon Nanomaterials in Zebrafish during Development, Nanomaterials 7 (2017) 414, https://doi.org/10.3390/nano7120414.

[41] L. C. Becker, W. F. Bergfeld, D. V. Belsito, C. D. Klaassen, J. G. Marks, R. C. Shank, T. J. Slaga, P. W. Snyder, Cosmetic Ingredient Review Expert Panel, Washington, Dc, F. A. Andersen, *Final Report of the Safety Assessment of Hyaluronic Acid, Potassium Hyaluronate, and Sodium Hyaluronate*, *Int. J. Toxicol. 28* (**2009**) 5–67, 10.1177/1091581809337738.

[42] H. Chen, J. Qin, Y. Hu, Efficient Degradation of High-Molecular-Weight Hyaluronic Acid by a Combination of Ultrasound, Hydrogen Peroxide, and Copper Ion, Molecules (basel Switzerland) 24 (617) (2019), https://doi.org/10.3390/molecules24030617.

[43] G. Pasut, F. Canal, L. DallaVia, S. Arpicco, F.M. Veronese, O. Schiavon, Antitumoral Activity of PEG–Gemcitabine Prodrugs Targeted by Folic Acid, J. Control. Release 127 (2008) 239–248, https://doi.org/10.1016/j.jconrel.2008.02.002.

[44] O. Schiavon, G. Pasut, S. Moro, P. Orsolini, A. Guiotto, F. Veronese, PEG–Ara-C Conjugates for Controlled Release, Eur. J. Med. Chem. 39 (2004) 123–133, https://doi.org/10.1016/j.ejmech.2003.10.005.

[45] In *Principles of Fluorescence Spectroscopy*, (Ed.: J.R. Lakowicz), Springer US, Boston, MA, **2006**, pp. 27–61, 10.1007/978-0-387-46312-4_2.

[46] N.O. Mchedlov-Petrossyan, T.A. Cheipesh, A.D. Roshal, S.V. Shekhovtsov, E. G. Moskaeva, I.V. Omelchenko, Aminofluoresceins Versus Fluorescein: Peculiarity of Fluorescence, Chem. A Eur. J. 123 (2019) 8860–8870, https://doi.org/10.1021/acs.jpca.9b05812.

[47] M. Montes-Morán, D. Suárez, J. Menéndez, E. Fuente, On the Nature of Basic Sites on Carbon Surfaces: An Overview, Carbon 42 (2004) 1219–1225, https://doi.org/10.1016/j.carbon.2004.01.023.

[48] T. Zimmermann, J. Rietdorf, R. Pepperkok, Spectral Imaging and Its Applications in Live Cell Microscopy, FEBS Lett. 546 (2003) 87–92, https://doi.org/10.1016/S0014-5793(03)00521-0.

[49] J.C. Zuaznabar-Gardona, A. Fragoso, Determination of the Hansen Solubility Parameters of Carbon Nano-Onions and Prediction of Their Dispersibility in Organic Solvents, J. Mol. Liq. 294 (2019) 111646, https://doi.org/10.1016/j.molliq.2019.111646.

[50] M. Bartkowski, S. Giordani, Supramolecular Chemistry of Carbon Nano-Onions, Nanoscale 12 (2020) 9352–9358, https://doi.org/10.1039/D0NR01713B.

[51] J. Bartelmess, M. Frasconi, P.B. Balakrishnan, A. Signorelli, L. Echegoyen, T. Pellegrino, S. Giordani, Non-Covalent Functionalization of Carbon Nano-Onions with Pyrene–BODIPY Dyads for Biological Imaging, RSC Adv. 5 (2015) 50253–50258, https://doi.org/10.1039/C5RA07683H.

[52] H. Mohan, V. Bincoletto, S. Arpicco, S. Giordani, Supramolecular Functionalisation of B/N Co-Doped Carbon Nano-Onions for Novel Nanocarrier Systems, Materials 15 (2022) 5987, https://doi.org/10.3390/ma15175987.
[53] M. d'Amora, A. Camisasca, A. Boarino, S. Arpicco, S. Giordani, Supramolecular Functionalization of Carbon Nano-Onions with Hyaluronic Acid-Phospholipid Conjugates for Selective Targeting of Cancer Cells, Colloids Surf. B Biointerfaces 188 (2020) 110779, https://doi.org/10.1016/j.colsurfb.2020.110779.
[54] M.E. Cano, D. Lesur, V. Bincoletto, E. Gazzano, B. Stella, C. Riganti, S. Arpicco, J. Kovensky, Synthesis of Defined Oligohyaluronates-Decorated Liposomes and Interaction with Lung Cancer Cells, Carbohydr. Polym. 248 (2020), https://doi.org/10.1016/j.carbpol.2020.116798.

Supplementary Information

Michał Bartkowski [a], Valeria Bincoletto [b], Iris Chiara Salaroglio [c], Giacomo Ceccone [d], Raul Arenal [e, f, g], Sara Nervo [b], Barbara Rolando [b], Chiara Riganti [c, h], Silvia Arpicco [b], Silvia Giordani [a, *]

* Corresponding Author.
Email Address: silvia.giordani@dcu.ie (S. Giordani)

a. *School of Chemical Sciences, Dublin City University, Glasnevin, Dublin 9, Ireland*
b. *Department of Drug Science and Technology, University of Torino, Via P. Giuria 9, Torino, Italy*
c. *Department of Oncology, University of Torino, Via Nizza 44, Torino, Italy*
d. *European Commission, Joint Research Centre, Ispra, Italy*
e. *Instituto de Nanociencia y Materiales de Aragon (INMA), CSIC-U. de Zaragoza, 50009 Zaragoza, Spain*
f. *Laboratorio de Microscopias Avanzadas (LMA), Universidad de Zaragoza, 50018 Zaragoza, Spain*
g. *ARAID Foundation, 50018 Zaragoza, Spain*
h. *Molecular Biotechnology Center "Guido Tarone", University of Torino, Italy*

1. Biological Studies

1.1. Quantification of CD44-expression

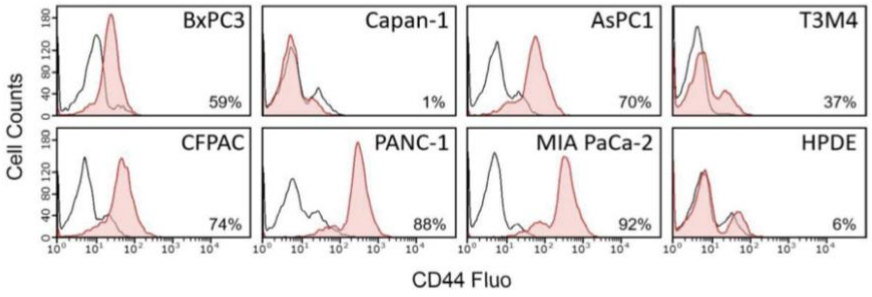

Fig. SI 1. Expression of cell-surface CD44 receptor. Flow cytometry results of CD44 receptor expression in different cell lines (% positive cells), where black is the anti-isotype control, and red is anti-CD44. PANC-1 and MIA PaCa-2 have high CD44 expression (88 and 92%), whereas Capan-1 has negligible CD44 expression (1%). Each plot is representative of 3 independent experiments.

1.2. Cell Viability

A. Cellular viability of fluo-HA-PEG-CNOs in PDAC cells

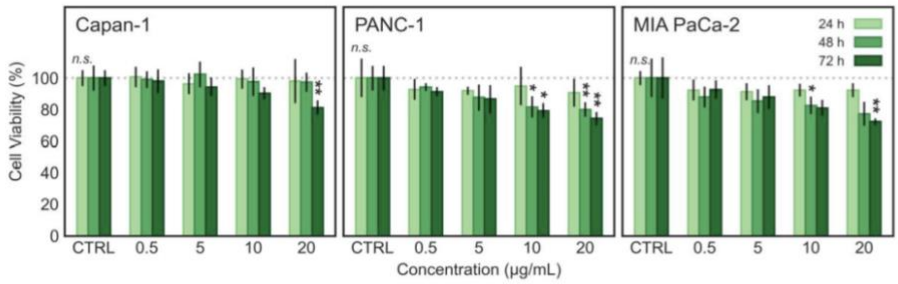

B. Cellular viability of HA-PEG-CNOs in HPDE cells

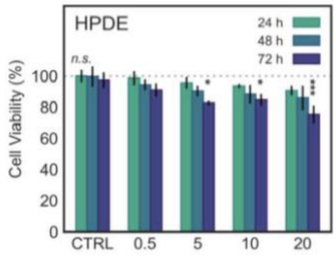

Fig. SI 2. | Cellular viability studies. A. Cellular viability of Capan-1 (CD44-negative control), PANC-1 and MIA PaCa-2 cells incubated with increasing concentrations of fluo-HA-PEG-CNOs (0.5, 5, 10 and 20 µg/mL) after 24, 48 and 72 h; and **B.** of HPDE cells incubated with HA-PEG-CNOs under the same conditions. Error bars represent the standard deviation of triplicate ($n = 3$) experiments. Statistical significance vs. respective control (CTRL) is represented as $*p < 0.05$, $**p < 0.01$, $***p < 0.001$; where *n.s.* = no significance.

2. Physicochemical Characterisation

2.1. High-resolution Transmission Electron Microscopy (HRTEM)

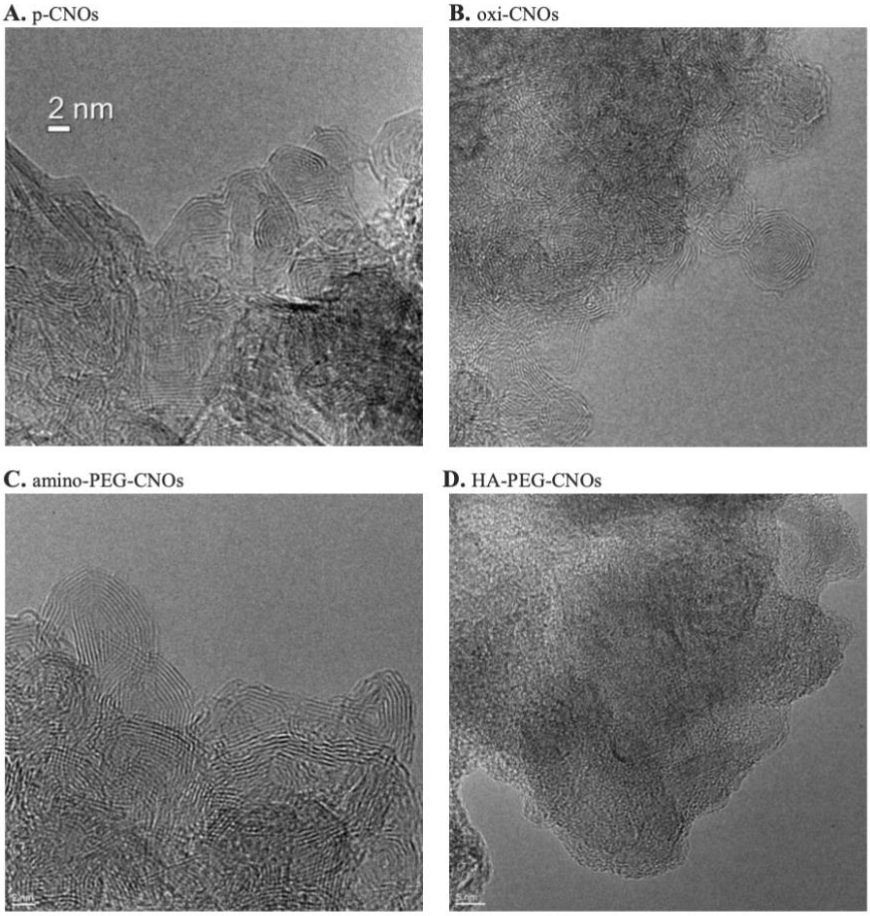

Fig. SI 3. | HRTEM studies. HRTEM micrographs of **A.** p-CNOs (*scale bar = 2 nm*); **B.** oxi-CNOs (*scale bar = 5 nm*); **C.** amino-PEG-CNOs (*scale bar = 2 nm*); and **D.** HA-PEG-CNOs (*scale bar = 5 nm*)

2.2. *X-ray Photoelectron Spectroscopy (XPS)*

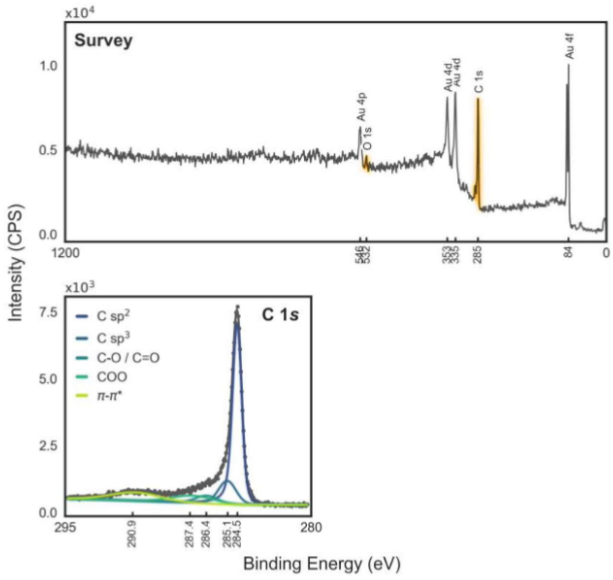

Fig. SI 4. | XPS spectra. XPS survey and high-resolution core level (C 1*s* and O 1*s*) spectra of p-CNOs on a Au substrate, including fitted peak deconvolution curves.

Tab. SI 1. | XPS data. Summary of XPS data of p-CNOs comprising: C 1*s* and O 1*s* contributions; elemental percentage (E%); and elemental ratio (E:R).

C 1*s*	**C sp²**	**C sp³**	**C=O**	**COO**	**π-π***
	284.5 eV (56.9%)	285.1 eV (13.5%)	286.3 eV (6.0%)	287.4 eV (10.2%)	290.9 eV (13.4%)
O 1*s*	**O=C**				
	532.8 eV (100%)				
E%	**C%**	**O%**			
	96.1%	3.9%			
E:R	**C/O**				
	24.6				

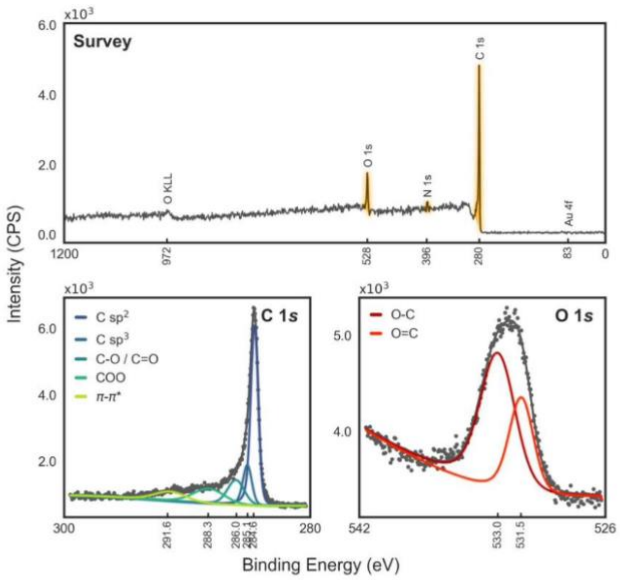

Fig. SI 5. | XPS spectra. XPS survey and high-resolution core level (C 1*s* and O 1*s*) spectra of oxi-CNOs on a Au substrate, including fitted peak deconvolution curves.

Tab. SI 2. | XPS data. Summary of XPS data of oxi-CNOs comprising: C 1*s* and O 1*s* contributions; elemental percentage (E%); and elemental ratio (E:R).

C 1*s*	**C sp²**	**C sp³**	**C-O / C=O**	**COO**	**π-π***
	284.5 eV (46.9%)	285.1 eV (12.4%)	286.0 eV (14.5%)	288.3 eV (16.0%)	291.6 eV (10.2%)
O 1*s*	**O=C**	**O-C**			
	531.5 eV (40.9%)	533.0 eV (59.1%)			
E%	**C%**	**O%**			
	91.2%	8.8%			
E:R	**C/O**				
	10.4				

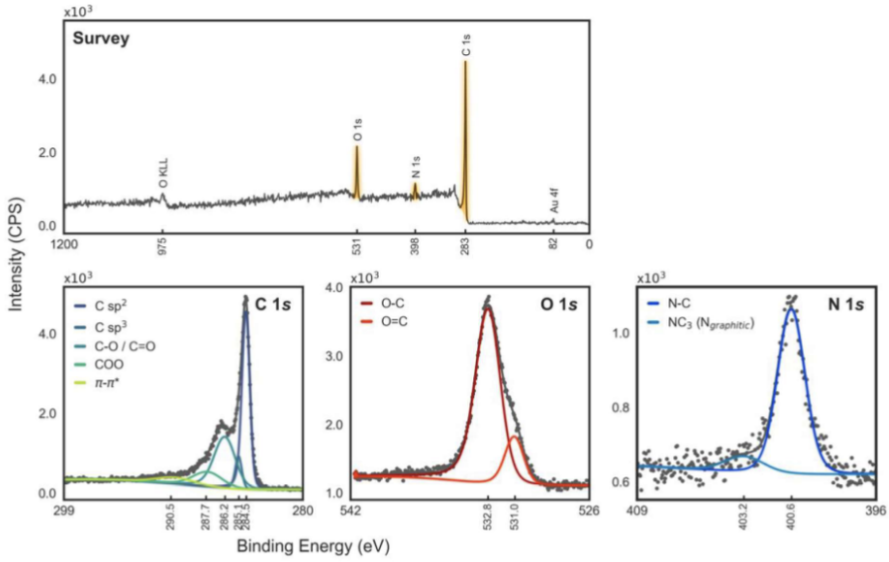

Fig. SI 6. | XPS spectra. XPS survey and high-resolution core level (C 1*s*, O 1*s* and N 1*s*) spectra of amino-PEG-CNOs on a Au substrate, including fitted peak deconvolution curves.

Tab. SI 3. | XPS data. Summary of XPS data of amino-PEG-CNOs comprising: C 1*s*, O 1*s* and N 1*s* contributions; elemental percentage (E%); and elemental ratios (E:R).

C 1*s*	**C sp²**	**C sp³**	**C-O / C=O / C-N**	**COO / CON**	**π-π***
	284.5 eV (41.0%)	285.1 eV (6.5%)	286.2 eV (32.4%)	287.7 eV (13.0%)	290.5 eV (7.1%)
O 1*s*	**O=C**	**O-C**			
	531.0 eV (17.6%)	532.8 eV (82.4%)			
N 1*s*	**N-C**	**NC_3**			
	400.1 eV (85.1%)	402.9 eV (14.9%)			
E%	**C%**	**O%**	**N%**		
	84.5%	11.6%	3.9%		
E:R	**C/O**	**C/N**	**O/N**		
	7.3	21.7	3.0		

Tab. SI 4. | XPS data. Summary of XPS data of HA-PEG-CNOs comprising: C 1*s*, O 1*s* and N 1*s* contributions; elemental percentage (E%); and elemental ratios (E:R). The corresponding XPS spectra can be found in (Fig. 3C).

C 1*s*	**C sp²**	**C sp³**	**C-O**	**COO**	**π-π***
	283.6 eV (34.7%)	284.2 eV (7.2%)	285.2 eV (26.0%)	286.8 eV (21.4%)	290.1 eV (10.7%)
O 1*s*	**O=C**	**O-C**			
	530.2 eV (6.8%)	532.3 eV (93.2%)			
N 1*s*	**N-Si**	**N-C**			
	397.5 eV (38.7%)	399.98 eV (61.3%)			
E%	**C%**	**O%**	**N%**	**Na%**	
	79.3%	15.2%	5.1%	0.4%	
E:R	**C/O**	**C/N**	**O/N**		
	5.2	15.5	3.0		

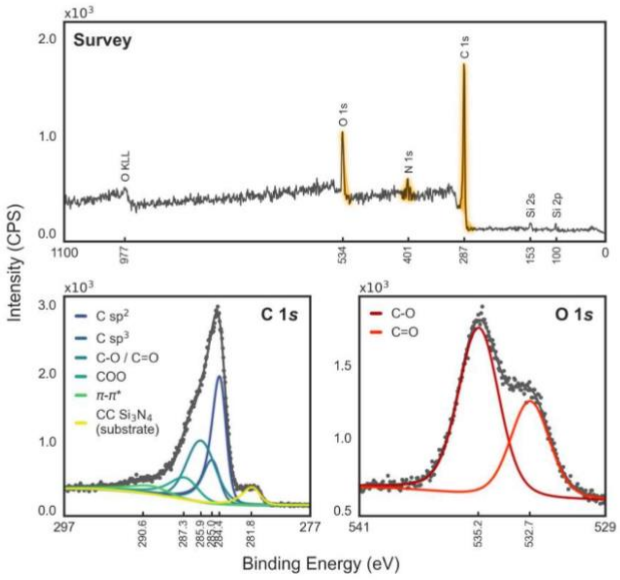

Fig. SI 7. | XPS spectra. XPS survey and high-resolution core level (C 1*s*, O 1*s*) spectra of fluo-HA-PEG-CNOs on a Si_3N_4 substrate, including fitted peak deconvolution curves.

Tab. SI 5. | XPS data. Summary of XPS data of fluo-HA-PEG-CNOs comprising: C 1*s*, O 1*s* and N 1*s* contributions; elemental percentage (E%); and elemental ratios (E:R).

C 1*s*	**C sp^2**	**C sp^3**	**C-O**	**COO**	**π-π^***	**CC-Si_3N_4**
	284.3 eV (34.61%)	284.9 eV (13.81%)	285.9 eV (28.04%)	287.1 eV (11.94%)	289.8 eV (6.0%)	281.6 eV (5.6%)
O 1*s*	**O=C**	**O-C**				
	532.7 eV (33.55%)	535.2 eV (66.45%)				
N 1*s*	**N-C**					
	402.4 eV (56.90%)					
E%	**C%**	**O%**	**N%**			
	82.5%	12.2%	5.3%			
E:R	**C/O**	**C/N**	**O/N**			
	6.8	15.6	2.3			

2.3. *UV-Vis Absorption and Fluorescence Emission Spectroscopy*

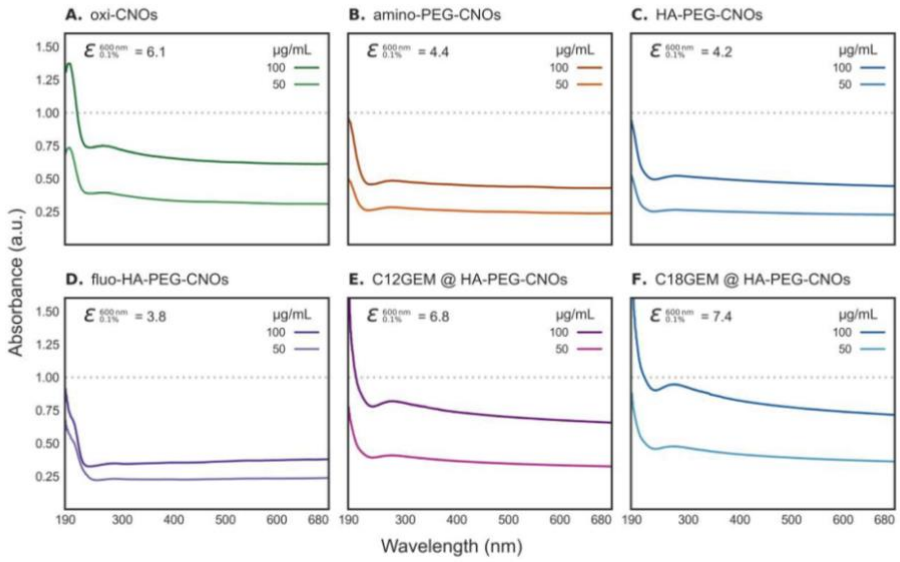

Fig. SI 8. | UV-Vis absorption studies. UV-Vis absorption spectra of all functionalised CNO materials in dH_2O at concentrations 50 and 100 µg/mL. The mass extinction coefficient $\varepsilon_{0.1\%}$ values have been provided as measured at 600 nm.

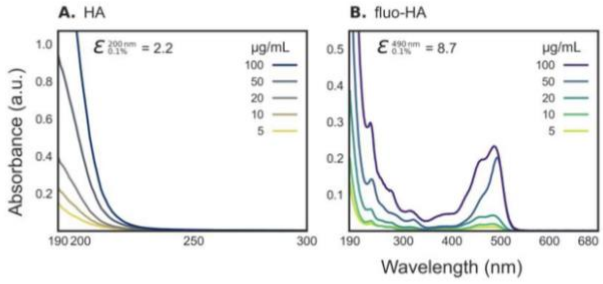

Fig. SI 9. | UV-Vis absorption studies. UV-Vis absorption spectra of **A.** HA; and **B.** fluo-HA; obtained in dH_2O at concentrations 5, 10, 20, 50 and 100 µg/mL. The mass extinction coefficient $\varepsilon_{0.1\%}$ values have been provided as measured at the wavelength specified.

2.4. *Attenuated Total Reflection Fourier-Transform Infrared Spectroscopy (ATRFTIR)*

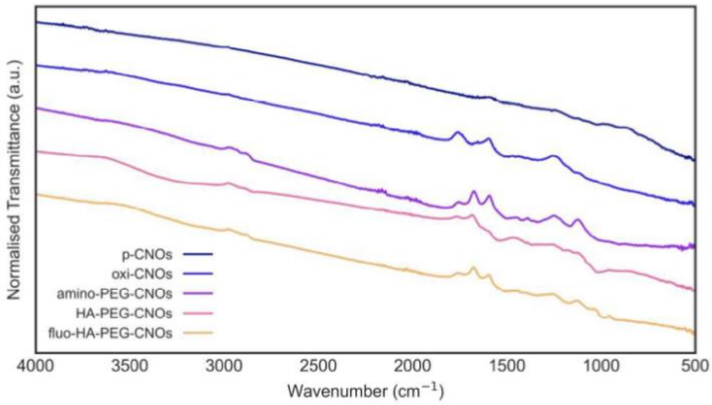

Fig. SI 10. | ATR-FTIR studies. ATR-FTIR spectra of p-CNOs, oxi-CNOs, amino-PEG-CNOs, HA-PEG-CNOs and fluo-HA-PEG-CNOs.

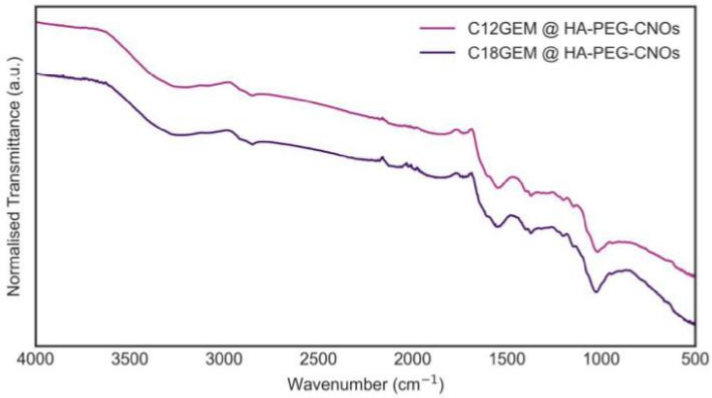

Fig. SI 11. | ATR-FTIR studies. ATR-FTIR spectra of C12GEM @ HA-PEG-CNOs and C18GEM @ HA-PEG-CNOs.

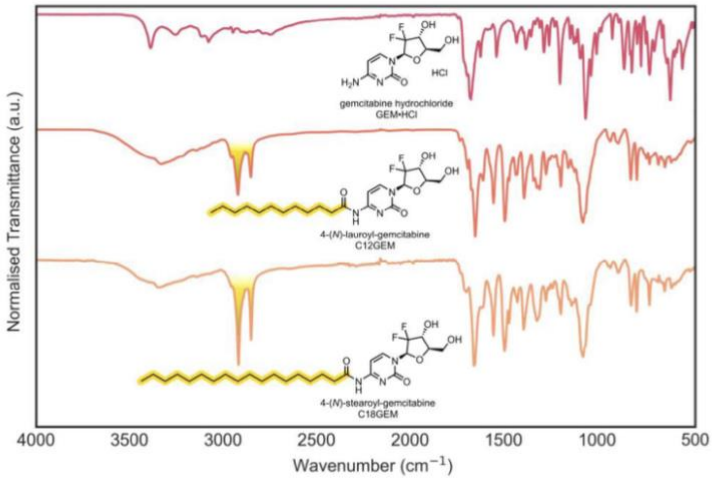

Fig. SI 12. | ATR-FTIR studies. ATR-FTIR spectra of GEM·HCl, C12GEM, and C18GEM (*highlighted yellow:* the effect of the lauroyl and stearoyl saturated aliphatic chains).

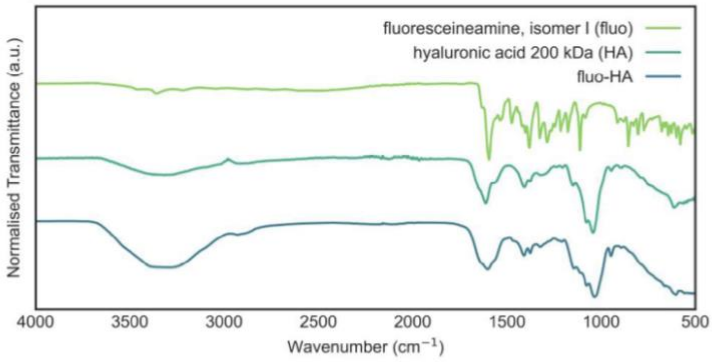

Fig. SI 13. | ATR-FTIR studies. ATR-FTIR spectra of fluo, fluo-HA and HA.

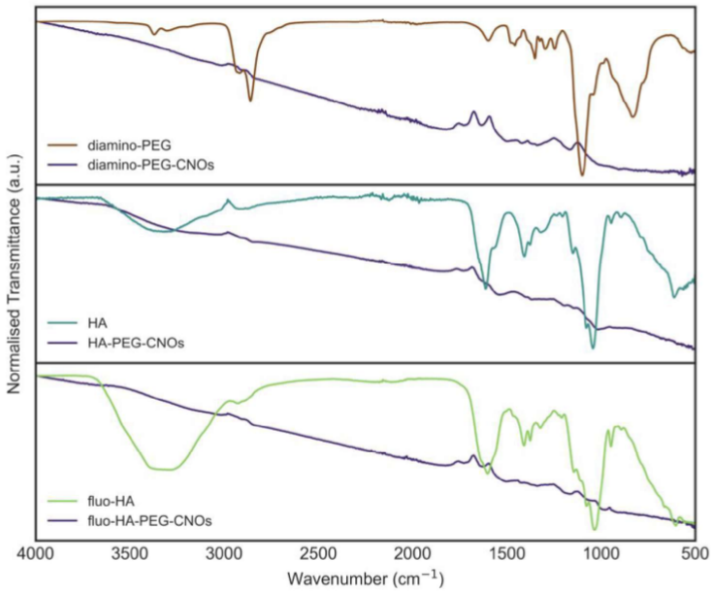

Fig. SI 14. | ATR-FTIR studies. Comparison between ATR-FTIR spectra (normalised) of diamino-PEG vs amino-PEG-CNOs; HA vs HA-PEG-CNOs; and fluo-HA vs fluo-HA-PEG-CNOs.

2.5. *Dynamic Light Scattering (DLS) and Zeta Potential (ZP)*

Tab. SI 6. | DLS and ZP data. DLS results of select nanocarriers' particle hydrodynamic diameter (Size) and zeta potential (ζ) in dH_2O at concentrations of 5, 10 and 20 μg/mL.

	Size (nm)	Size (nm)	Size (nm)	ζ (mV)	ζ (mV)	ζ (mV)
	5 μg/mL	*10 μg/mL*	*20 μg/mL*	*5 μg/mL*	*10 μg/mL*	*20 μg/mL*
oxi-CNOs	177 ± 3	164 ± 5	175 ± 3	-45 ± 2	-42 ± 1	-42 ± 1
amino-PEG-CNOs	193 ± 22	206 ± 15	229 ± 17	-20 ± 1	-19 ± 2	-16 ± 1
HA-PEG-CNOs	248 ± 19	258 ± 11	260 ± 13	-39 ± 4	-36 ± 2	-35 ± 1
fluo-HA-PEG-CNOs	173 ± 11	171 ± 5	180 ± 11	-33 ± 1	-26 ± 1	-26 ± 2

2.6. *Prodrug Release Profile*

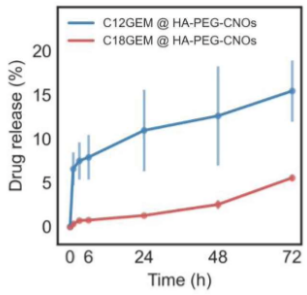

Fig. SI 15. | Drug-release studies. *In vitro* release profiles of C12GEM @ HA-PEG-CNOs and C18GEM @ HA-PEG-CNOs in PBS buffer at pH 7.4 and 37 °C measured over 72 h. Error bars represent the standard deviation of triplicate ($n = 3$) experiments.

3. Statistical Analyses

All results are presented as mean ± standard deviation (SD), where the number of experiments carried out is $n => 3$. For the interpretation of the results, a one-way analysis of variance (ANOVA) was conducted followed by a post-hoc Tukey's test to identify the groups that showed significant differences from each other. A p-value of less than 0.05 ($p < 0.05$) was considered statistically significant.

Wherein spectral data was presented with the term '*normalised*' specified in the y-axis, the data were normalised to the same range using (Eq. 1.1) for comparative purposes. No other spectral corrections were applied, unless otherwise specified.

Wherein FE-SEM data analysis was conducted, the statistical analysis was carried out to assess the p-CNOs diameter; wherein the data reported has been obtained by measuring the area of $n = 99$ observed nanoparticles, and calculating the equivalent circle diameter. A test for outliers was carried out. The final p-CNO diameter values of mean (μ), sample standard deviation (σ) and the variance (σ^2) were calculated to be: 6.56, 1.28 and 1.65 nm, respectively. A raincloud plot with a fitted boxplot depicting particle size-distribution, median and quartiles was plotted with python [55, 56], and visualised in (Fig. 3A).

Wherein cytotoxic evaluation of prodrugs was conducted, both alone and DDS-loaded, significant differences with respect to the control were reported as $^{*}p < 0.05$, $^{**}p < 0.01$ and $^{***}p < 0.001$. Statistical significance versus GEM at the same concentration were reported as $^{\circ}p < 0.05$, $^{\circ\circ}p < 0.01$ and $^{\circ\circ\circ}p < 0.001$. Statistical significance versus API @ amino-PEG-CNOs were reported as $^{\#}p < 0.05$ $^{\#\#}p < 0.01$ and $^{\#\#\#}p < 0.001$; where API is either C12GEM or C18GEM. Finally, statistical significance versus API @ HA-PEG-CNOs were reported as $^{\S}p < 0.05$, $^{\S\S}p < 0.01$ and $^{\S\S\S}p < 0.001$; where API is either C12GEM or C18GEM. Where relevant, the term *n.s.* is used to denote that no statistical significance was observed.

Smart hyaluronated micelles to enhance a gemcitabine prodrug efficacy

Ilaria Andreana, Valeria Bincoletto, Caterina Ricci, Iris Chiara Salaroglio, Maela Manzoli, Beatrice Zurletti, Jessica Milone, Barbara Rolando, Elena Del Favero, Chiara Riganti, Pietro Matricardi, Barbara Stella, Silvia Arpicco

---

Published in *Journal of Drug Delivery Science and Technology* 104 (2025) 106518

Micellar nanocarriers have garnered significant attention for their biocompatibility and capacity to solubilize hydrophobic drugs. HA mixed micelles represent a promising platform, as HA selectively binds CD44 receptors, which are commonly overexpressed on the surface of pancreatic cancer cells. This active targeting strategy has been shown to enhance cellular internalization and therapeutic efficacy, while minimizing systemic toxicity and off-target accumulation.

Main Aim

The study aimed to design and evaluate a smart, HA-functionalized micellar system for the delivery of a lipophilic gemcitabine prodrug (GEM-C18), with the goal of enhancing its antitumor activity and stability while promoting selective uptake by CD44-overexpressing cancer cells.

Specific Objectives

- To formulate stable mixed micelles using PEG-DSPE and HA-DPPE conjugate, incorporating GEM-C18.
- To assess the physicochemical characteristics and stability of the HA-GEM-C18 micelles.
- To evaluate *in vitro* uptake, cytotoxicity, and selectivity in overexpressing CD44 cancer cell lines.

Highlights

- Successfully formulated DSPE-PEG/HA micelles (composed of 1% molar ratio of HA, relative to the total amount of PEG-DSPE) with high encapsulation efficiency and good colloidal stability.
- Demonstrated enhanced cellular uptake of loaded decorated micelles in CD44 positive pancreatic cancer cells compared to non-targeted micelles or free drug.
- Loaded decorated micelles showed strong cytotoxicity *in vitro*.
- The HA-functionalized nanocarrier proved to be an effective strategy to boost the efficacy and selectivity of a GEM-based treatment.

Journal of Drug Delivery Science and Technology 104 (2025) 106518

Contents lists available at ScienceDirect

Journal of Drug Delivery Science and Technology

journal homepage: www.elsevier.com/locate/jddst

Smart hyaluronated micelles to enhance a gemcitabine prodrug efficacy

Ilaria Andreana [a], Valeria Bincoletto [a], Caterina Ricci [b], Iris Chiara Salaroglio [c], Maela Manzoli [a], Beatrice Zurletti [a], Jessica Milone [a], Barbara Rolando [a], Elena Del Favero [b], Chiara Riganti [c], Pietro Matricardi [d], Barbara Stella [a], Silvia Arpicco [a,*]

[a] Department of Drug Science and Technology, University of Turin, Via Pietro Giuria 9, 10125, Turin, Italy
[b] Department of Medical Biotechnology and Translational Medicine, University of Milan, Via Fratelli Cervi 93, 20054, Milan, Italy
[c] Department of Oncology, Interdepartmental Center of Molecular Biotechnology "Guido Tarone", University of Turin, Via Nizza 44, 10126, Turin, Italy
[d] Departments of Drug Chemistry and Technologies, Sapienza University of Rome, Piazzale Aldo Moro 5, 00185, Rome, Italy

ARTICLE INFO

Keywords:
Hyaluronic acid
4-(N)-Stearoyl gemcitabine
Micelles
CD44 receptor
Targeted drug delivery

ABSTRACT

Self-assembling drug delivery systems have drawn attention over recent decades thanks to their versatility and easy preparation processes. Of the various nanocarriers available, micelles are able to self-assemble from an amphiphilic molecule in an aqueous solution, making them simple to prepare. In this work, 1,2-distearoyl-*sn*-glycero-3-phosphoethanolamine-N-[methoxy(polyethylene glycol)-2000] (PEG-DSPE) was utilized to prepare lipid-based micelles for the encapsulation of a gemcitabine prodrug, GemC18, with the aim of improving its anticancer activity. Furthermore, an active targeting strategy was achieved by preparing Gem-C18-loaded PEG-DSPE micelles in the presence of a hyaluronic acid (4800 or 14,800 Da) (HA)-phospholipid conjugate (HA-DPPE) to provide actively targeted mixed micelles. This study presents the characterization of the mixed micelles, from basic characteristics (size, PDI, and zeta potential) to complex molecular structure (FESEM, X-ray diffraction, SAXS), and demonstrates that the presence of the HA-conjugate does not alter the physicochemical properties of the PEG-DSPE micelles. The mixed micelles display a size of below 100 nm, a negative zeta potential of −30 mV, and a high encapsulation efficiency (above 90 %). Finally, their preferential uptake, and consequently their cytotoxicity on cancer cell lines that overexpress the HA-specific receptor (CD44), has been assessed and confirmed using competition assays.

1. Introduction

Many chemotherapeutic agents exhibit various types of systemic toxicity and side effects that are caused by their poor accumulation in tumor tissues. Nanotechnologies have therefore been developed to increase tumor accumulation and reduce the systemic adverse effects of drug distribution in normal tissues [1–3]. Drug delivery systems of various nature (*e.g.* liposomes, polymer, and inorganic nanoparticles) have undergone extensive studies in order to improve their ability to encapsulate and deliver active molecules, including small molecules, genetic material, and imaging agents [4,5]. Micelles are one of the huge number of well-characterized nanocarriers, and are beginning to be considered one of the most attractive strategies [6]. Micelles are colloidal particles, ranging from 5 to 100 nm, formed *via* the self-assembly of amphiphilic molecules in aqueous solution, distinguishing them as a simple drug delivery system. The phenomenon of micelle formation starts when the concentration of the amphiphilic molecule exceeds a precise threshold of concentration, defined as the critical micelle concentration [7,8]. Micelles usually display smaller sizes than other drug delivery systems, and have been extensively investigated for the delivery of poorly soluble molecules [9–11], which can be incorporated into the hydrophobic cores of these structures after dispersion in an aqueous medium [12]. Amphiphilic copolymers can spontaneously form core-shell micelles made of a hydrophilic shell and a hydrophobic core, into which a hydrophobic drug can be easily incorporated [13,14]. Moreover, interest in lipid-based micelles has increased

* Corresponding author. Via Pietro Giuria 9, 10125, Torino, Italy.
E-mail addresses: ilaria.andreana@unito.it (I. Andreana), valeria.bincoletto@unito.it (V. Bincoletto), caterina.ricci@unimi.it (C. Ricci), irischiara.salaroglio@unito.it (I.C. Salaroglio), maela.manzoli@unito.it (M. Manzoli), beatrice.zurletti@unito.it (B. Zurletti), jessica.milone@edu.unito.it (J. Milone), barbara.rolando@unito.it (B. Rolando), elena.delfavero@unimi.it (E. Del Favero), chiara.riganti@unito.it (C. Riganti), pietro.matricardi@uniroma1.it (P. Matricardi), barbara.stella@unito.it (B. Stella), silvia.arpicco@unito.it (S. Arpicco).

https://doi.org/10.1016/j.jddst.2024.106518
Received 28 August 2024; Received in revised form 21 November 2024; Accepted 10 December 2024
Available online 10 December 2024

in recent years thanks to their biodegradability and biocompatibility. For example, a potent water-insoluble tyrosine kinase inhibitor showed enhanced water solubility and cellular uptake, compared to the free molecule, *via* incorporation into poly(ethylene glycol) (PEG)-lipid-based micelles [15]. The ability of PEG–phosphatidylethanolamine (PE) conjugates to form micelles in an aqueous environment was observed as early as 1994. The use of a lipid moiety as the hydrophobic block improves micelles stability thanks to the strong hydrophobic interactions between the alkyl chains of the phospholipids [16]. Moreover, the presence of PEG on micelle surfaces increases their circulation time *in vivo* by preventing their recognition by opsonins, and thus reducing their clearance. While PEG is the most commonly used hydrophilic block, because of its "stealth" ability, the composition of the hydrophobic block can be tailored to improve the encapsulation of lipophilic drugs. In recent times, the amphiphilic polymer 1,2-distearoyl-*sn*-glycero-3-phosphoethanolamine-N-[methoxy(polyethylene glycol)-2000] (PEG-DSPE) has often been used in nanomedicine to prepare nanocarriers because of its ability to form micellar structures in water. For example, PEG-DSPE, with a terminal amino group, has been covalently combined with a fullerene structure and self-assembled into micelles to deliver doxorubicin, thus enhancing the drug's *in vivo* efficacy and safety [17]. As is well known, the presence of the PEG shell prolongs the circulation time of drug delivery systems *in vivo* [18,19]. In addition, micelles can accumulate at tumor sites as their nanoscale structures can exploit the enhanced permeability and retention (EPR) effect [20–22].

However, the aspecific accumulation of drug delivery systems has underlined the urgent need for targeting strategies. Indeed, specific molecules on the nanocarrier surface can promote accumulation into organs or tissues and consequently improve the therapeutic effects [23].

Polysaccharides are considered to be amongst the most important materials when designing novel actively targeted nanosystems. Hyaluronic acid (HA) is a natural polysaccharide composed of alternating units of D-glucuronic acid and N-acetyl-D-glucosamine, linked *via* β-1,3- and β-1,4-glycosidic bonds. HA is a promising component, from a pharmaceutical standpoint, because it is biocompatible, biodegradable, nontoxic and non-immunogenic. It has also been used as a targeting moiety as it can bind the CD44 receptor, which is overexpressed on many tumor cells [24]. Moreover, HA contains several chemical groups to which other components can be conjugated. Thanks to all these features, HA has been widely employed in the development of drug delivery systems, in recent years, having been used, as such or as a ligand, in different types of nanosystems, to prepare nanoplatforms for actively targeted drugs, genes and diagnostic agents [25].

The anticancer drug gemcitabine, a cytidine analogue, is the first-line treatment for pancreatic adenocarcinoma. However, its clinical outcomes suffer from rapid metabolism that leads to drug administration in very high doses and the onset of acquired drug resistance [26]. A great deal of effort has therefore been made to overcome these limitations, with the identification of new derivatives with improved effects; one of these derivatives, the lipophilic prodrug 4-(N)-stearoyl gemcitabine (GemC18), has shown improved pharmacokinetics and superior antitumor efficacy [27]. Thanks to its suitable features, GemC18 has been incorporated in nanosystems of diverse nature to improve its activity, with these systems including liposomes [27], microparticles [28], and nano-onions [29]. GemC18 has also been exploited for incorporation into different types of micelles, like acid-sensitive [30], polymeric [31], and lipid-based micelles [32].

In this work, a very low amount of HA-phospholipid conjugate (HA-DPPE), at two different HA molecular weights (4800 or 14,800 Da) was added, during the preparation of PEG-DSPE micelles loaded with GemC18 to set up an active targeting strategy. The mixed micelles self-assembled, exposing HA on their surfaces, making it available for interaction with the CD44 receptor. The micelles were characterized, from basic characteristics to more complex methods including cellular uptake and cytotoxic activity towards pancreatic cancer cells with low (Capan-1) and high (Panc-1) CD44-receptor expression.

2. Materials and methods

2.1. Materials and general procedures

Sodium hyaluronate (HA) (4800 and 14,800 Da) was purchased from Lifecore Biomedical (Chaska, Minnesota, USA). 1,2-distearoyl-*sn*-glycero-3-phosphoethanolamine-N-[methoxy(polyethylene glycol)-2000] (ammonium salt) (PEG-DSPE), 1,2-dipalmitoyl-*sn*-glycero-3-phosphoethanolamine (DPPE), Nile Red, 0.22 μm nylon filters, pyrene and solvents (analytical grade) were obtained from Merck (Milan, Italy). Solvent evaporation was carried out on a rotating evaporator (Heidolph Laborota 400, Heidolph Instruments, Schwabach, Germany) equipped with a vacuum pump (Diaphragm Vacuum Pump DC-4). Spectra-Por® 12–14,000 molecular weight cut off dialysis membrane were obtained from Thermo Fisher Scientific (Monza, Italy).

Conjugates between DPPE and HA (HA_{4800}-DPPE and HA_{14800}-DPPE) were prepared using the method described in Arpicco et al. [33], with minor modifications. Briefly, HA (4800 or 14,8000 Da) was dissolved in a methanol/dimethyl sulfoxide mixture (1:1 v/v). An equimolar amount of DPPE was dissolved in a methanol/chloroform mixture (1:1 v/v) and added to the HA solution under stirring at 60 °C. The pH was adjusted to 4.5 using acetic acid and the suspension was stirred for 2 h at 60 °C. Sodium triacetoxyborohydride, dissolved in the methanol/chloroform mixture, was then added dropwise. The reaction was allowed to proceed for 96 h at 60 °C under continuous stirring. The organic solvents were removed under reduced pressure and then the mixture was dialyzed against water. The final product was purified by chromatography and lyophilized; ^{1}H NMR analysis confirmed the formation of the conjugate. The gemcitabine lipophilic prodrug (GemC18) was synthesized according to Immordino et al. [27].

2.2. Critical micelle concentration measurement

Critical micelle concentration (CMC) was measured by fluorescence spectroscopy using pyrene as a fluorescent dye [34]. Briefly, a stock solution of 2.00×10^{-5} M of pyrene was prepared in acetone; 50 μL aliquots of the solution were added to a series of glass tubes and acetone was completely evaporated by rotary evaporation under reduced pressure. Different amounts of PEG-DSPE, HA_{4800}-DPPE, HA_{14800}-DPPE, PEG-DSPE/HA_{4800}-DPPE or PEG-DSPE/HA_{14800}-DPPE ranging from 1.00×10^{-8} to 1.27×10^{-3} M were separately added to each tube to obtain a final pyrene concentration of 2.00×10^{-6} M. Each sample was incubated at 60 °C for 20 min and equilibrated overnight at room temperature. After filtration through a 0.22 μm nylon syringe filter, the fluorescent spectra of each sample were analyzed using a spectrofluorometer EnSight HH3400 (PerkinElmer, Inc., Waltham, Massachusetts, USA) equipped with a data recorder Kaleido 1.2 at the excitation wavelength of 339 nm, and the emission spectra were monitored from 360 to 450 nm. Excitation slit widths were set at 373, 384 and 390 nm. Results are expressed as the correlation between the log[phospholipid] and intensity ratio of either I_{373}/I_{384} or I_{390}.

2.3. Micelle preparation

PEG micelles (PEG-M) were prepared *via* the hydration and sonication of a PEG-DSPE film. Briefly, 2 mg of PEG-DSPE were dissolved in chloroform and evaporated using a rotary evaporator; the resulting thin film was dried under vacuum overnight. The film was hydrated with 3 mL of MilliQ® water at 60 °C and incubated for 10 min. The suspension was then cooled and sonicated in an ice bath with a probe sonicator VCX400 (Sonics & Materials Inc., Milan, Italy) for 10 min with pulses of 3 s on and 3 s off.

Mixed micelles (PEG-M/HA_{4800} or PEG-M/HA_{14800}) were prepared by adding a 1 % molar ratio of HA_{4800}-DPPE or HA_{14800}-DPPE to the

aqueous solution during the hydration of the PEG-DSPE film.

GemC18-loaded micelles were prepared by adding 500 μL of GemC18 solution (1 mg/mL in methanol) to the chloroform solution of PEG-DSPE (2 mg/200 μL); the solvents were evaporated under reduced pressure to obtain a homogeneous thin drug-lipid film. To prepare GemC18-PEG-M/HA-DPPE$_{4800}$ or GemC18-PEG-M/HA-DPPE$_{14800}$, the conjugates were dissolved in MilliQ® water (1 mg/mL) and the film was hydrated with 3 mL of MilliQ® water containing 60 μL of HA$_{4800}$-DPPE or 110 μL of HA$_{14800}$-DPPE aqueous solution. The resulting micelle suspension was purified *via* filtration through a 0.22 μm nylon syringe filter.

Fluorescently labelled micelles were prepared as well by adding 40 μL of a Nile Red solution (200 μg/mL) in dichloromethane/acetone during thin lipid film preparation.

Drug-loaded HA-DPPE micelles were prepared in a similar manner using a solution of HA$_{4800}$-DPPE or HA$_{14800}$-DPPE (0.7 mg/mL) in MilliQ® water to hydrate the GemC18 film.

2.4. Physicochemical characterization of micelles

The mean particle hydrodynamic diameter and polydispersity index (PDI) of the different micelle samples were determined at 25 °C *via* quasi-elastic light scattering (QELS) using a nanosizer (Zetasizer Pro, Malvern Inst., Malvern, UK). The selected angle was 173° and the measurements were performed on undiluted sample at pH 6.5. Each measurement was performed in triplicate. The particle surface charge of the preparations was investigated *via* zeta potential measurement at 25 °C using the Smoluchowski equation and the Zetasizer Pro directly on the pure samples. Each value is the average of three measurements.

The encapsulation efficiency (EE) and drug loading (DL) of GemC18-loaded micelles were determined by HPLC; samples were diluted 1:10 with acetonitrile to extract the incorporated drug. HPLC analysis was performed on a HP 1200 chromatograph system (Agilent Technologies, Palo Alto, California, USA) equipped with an injector (Rheodyne, Cotati, California, USA), a quaternary pump (model G1311A), a membrane degasser (model G1322A), a multiple wavelength UV detector (MWD, model G1365D) and a fluorescence detector (FL, model G1321A) integrated into the HP1200 system. Data were processed using a HP ChemStation system (Agilent Technologies). The analytical column was a AQUASIL C18 (200 × 4.6 mm, 5 μm; Thermo); the mobile phase consisted of acetonitrile/water/TFA, 90/9.9/0.1 (v/v/v), at a flow-rate of 1 mL/min. The injection volume was 20 μL (Rheodyne, Cotati, California, USA). The column effluent was monitored at 250 nm and 292 nm referenced against 800 nm wavelength.

GemC18 EE and DL were calculated as follows:

$$EE(\%) = \frac{A}{B} \times 100$$

where A is the amount of incorporated drug after micelle purification and B is the initial added amount of GemC18.

$$DL(\%) = \frac{C}{D} \times 100$$

where C is the weight of incorporated drug after micelle purification and D is the total micelle weight.

2.5. In vitro release study

To evaluate *in vitro* GemC18 release, 3 mL of each sample (GemC18-PEG-M, GemC18-PEG-M/HA$_{4800}$ and GemC18-PEG-M/HA$_{14800}$) were placed into a dialysis bag immersed in 300 mL of PBS 1 mM (pH 7.4) at 37 °C, and aliquots (100 μL) were withdrawn at predetermined time intervals (0, 0.5, 1, 3, 5, 24, 48 and 72 h). The amount of GemC18 content was determined by HPLC, as previously described.

2.6. Small angle X-ray scattering

SAXS experiments were performed at the European Synchrotron Radiation Facility (ESRF), at ID02 beamline (DOI:10.15151/ESRF-ES-1351189712). 30 μL of each sample were loaded into capillaries (KI-beam, ENKI, Concesio, Italy) and measured at 25 ± 1°C. The 2D spectra reported the scattered radiation as a function of the angle θ. To avoid any radiation damage, 10 frames with a short exposure time (0.1 s) were acquired, compared, and averaged. After normalization, background subtraction, and angular regrouping the 1D SAXS intensity profiles were obtained and reported as a function of the momentum transfer $q=(4\pi/\lambda)\sin(\theta/2)$ where $\lambda = 1$ Å is the radiation wavelength. To investigate a wide q region, 0.008 Å$^{-1} \leq q \leq 0.5$ Å^{-1}, SAXS spectra relative to different q ranges, modifying the sample-detector distance (1 m and 10 m), were acquired, compared and connected. SAXS data were analyzed with GENFIT software [35] to derive micellar structural parameters, size, shape and internal arrangement.

2.7. Power X-ray diffraction

Powder X-Ray Diffraction (PXRD) patterns were collected by using a PW3050/60 X'Pert PRO MPD diffractometer (PANalytical) working in Bragg–Brentano geometry, equipped with a high-powered ceramic tube PW3373/10 LFF with a Cu anode as a source (Cu Kα radiation λ = 1.5406) with a Ni filter to attenuate Kβ. Scattered photons were collected by a real time multiple strip (RTMS) X'celerator detector. Data were acquired in the $3° \leq 2\theta \leq 60°$ angular range, with 0.02° 2θ steps. The as received samples in the form of powders were examined using a spinning sample holder to minimize preferred orientations.

For the analyses, two drops of each sample were deposited onto aluminum stubs coated with a conducting adhesive and then left to dry in the air at room temperature. The dried samples underwent Cr metallization (ca. 5 nm) by employing an Emitech K575X sputter coater (Quorumtech, Laughton, 226 East Sussex, UK) to avoid charging effects and inserted into the instrument chamber using a motorized procedure.

2.8. Field Emission Scanning Electron Microscopy

Field Emission Scanning Electron Microscopy (FESEM) analyses were performed by a Tescan S9000G FESEM 3010 microscope (Tescan Orsay Holding a.s., Brno- Kohoutovice, Czech Republic) working at 30 kV, equipped with a high brightness Schottky emitter and fitted with Energy Dispersive X-ray Spectroscopy (EDS) analysis by an Ultim Max Silicon Drift Detector (SDD, Oxford, UK). For the analysis, two drops of the prepared sample were deposited onto an aluminum stub coated with a conducting adhesive and subsequently left to dry in the air at room temperature. The dried sample was submitted to Cr metallization (ca. 5 nm) using an Emitech K575X sputter coater (Quorumtech, Laughton, East Sussex, UK) to avoid charging effects and then inserted into the chamber by a motorized procedure. Histogram of the particle size distribution built for the PEG-M/HA$_{14800}$ sample was obtained by considering a representative number of particles and the mean particle diameter (d_m) was calculated by applying the following equation:

$d_m = \Sigma d_i n_i / \Sigma n_i$, being n_i the number of particles with diameter d_i.

2.9. Cell lines culture and characterization

Human pancreatic adenocarcinoma cells Capan-1 and PANC-1 were purchased from ATCC (Manassas, Virginia, USA) and maintained in their respective medium (DMEM for Capan-1, RPMI-16140 for PANC-1, by Invitrogen Life Technology, Milan, Italy), containing 1 % v/v penicillin-streptomycin and 10 % fetal bovine serum (Merck). The surface amount of CD44, the receptor for HA, was evaluated by flow

cytometry as previously described [36], using a Guava Millipore flow cytometer equipped with EasyCite software (Millipore, Bedford, Massachusetts, USA). Capan-1 and PANC-1 cells were classified as CD44-low and high expressing cells [29].

2.10. Micelle uptake

1×10^5 cells were seeded into a 96-well black plate in 200 μL medium, and incubated for 1, 3, 6, and 24 h with Nile Red-loaded micelles without HA (NR-PEG-M) or with HA (NR-PEG-M/HA_{4800} or NR-PEG-M/HA_{14800}), at final dilutions of 1:2, 1:5 and 1:10. When indicated, a saturating amount of blocking anti-CD44 antibody (#ab157107; Abcam, Cambridge, UK; diluted 1/100) or HA (100 μM) was added to the cells incubated with micelles diluted 1:2. After two washing with PBS, cells were detached with trypsin/EDTA, collected in 300 μL PBS and sonicated. A 50 μL aliquot was used to measure the cellular proteins (BCA kit); the remaining samples were transferred into a dark-wall 96 well plate and the intracellular fluorescence, corresponding to the amount of uptake of Nile Red, was read at λ excitation 559 nm and λ emission 635 nm, using a Synergy HT Microplate Reader. The results were expressed as fluorescence units (FU)/mg cellular proteins. In each experimental set, the autofluorescence – *i.e.* the fluorescence of untreated cells – was 0.26 ± 0.6 nmol/mg for Capan-1 cells and 0.28 ± 0.6 nmol/mg for PANC-1 cells and was subtracted from the fluorescence of any other experimental conditions.

2.11. Cell viability

1×10^4 cells were seeded into a 96-well white plate and incubated for 24, 48 and 72 h with the fresh medium, medium containing free gemcitabine (Gem), free GemC18 or GemC18-loaded micelles (with or without HA), containing a concentration of GemC18 corresponding to 100 nM, 1 μM, 10 μM. When indicated, the cells treated with 10 μM GemC18-loaded micelles containing HA_{4800}-DPPE or HA_{14800}-DPPE were co-incubated for 72 h with blocking anti-CD44 antibody diluted 1/100 or HA (100 μM). Cell viability was measured by a chemiluminescent-based commercial kit (ATPlite Luminescence Assay System, PerkinElmer, Waltham, MA), using a Synergy HT Microplate Reader, setting the luminescence units detected in untreated cells as 100 %. The luminescence units of each condition were expressed as percentage versus untreated cells.

2.12. Statistical analysis

Data in the text and figures are provided as means ± SD. The results were analyzed by a one-way analysis of variance (ANOVA) and Tukey's test. $p < 0.05$ was considered significant.

3. Results and discussion

3.1. Preparation and characterization of micelles

HA is widely used as a platform for the specific delivery of anticancer drugs because of its ability to recognize the specific CD44 receptor, which is overexpressed on the surface of several tumors [37]. Moreover, HA is biocompatible, biodegradable, nontoxic and non-immunogenic. We previously synthesized HA-phospholipid conjugates that were used for the preparation of decorated liposomes actively targeted towards CD44-overexpressing cancer cells [33,38]. Furthermore, we demonstrated the potential cryoprotective effect that the HA-DPPE conjugate has on liposomes and poly(lactic-*co*-glycolic acid) (PLGA) nanoparticles; the addition of the conjugate during the formulation of lipid or polymer-based nanosystems led to the physicochemical properties of the redispersed sample being retained after lyophilization [39].

In this work, we initially proposed the use of HA-DPPE conjugates prepared using HA at two different molecular weights (4800 and 14,800 Da) for the preparation of micelles.

We decided to investigate the ability of the micelles as a vehicle for the specific delivery of GemC18 towards pancreatic cancer cells, overexpressing the specific HA CD44 receptor. In previous works, we demonstrated that GemC18, a lipophilic prodrug of Gem that is currently the gold standard treatment for pancreatic cancer, displays significant anticancer activity [27,29].

Here, GemC18-loaded HA-DPPE formulations showed an encapsulation efficiency of around 60 % and fast drug release; 60 % of GemC18 was released after 1 h in PBS at 37 °C. To improve GemC18 loading and stability, we decided to use PEG-DSPE as the main component for micelle preparation because of its well-known ability to form micelles in aqueous media [16]. A similar approach has previously been exploited to form self-assembled mixed micelles that incorporated GemC18 and promoted slow drug release and preferential drug accumulation in the tumor *via* the EPR effect [32]. Moreover, to improve the targeting ability of the GemC18-loaded micelles towards pancreatic cancer cells overexpressing the CD44 receptor, we initially decided to test HA-DPPE at different amounts ranging from 1 % to 20 % of PEG-DSPE. The 1 % molar ratio of HA-DPPE (4800 or 14,800 Da) was then chosen to obtain mixed micelles (Fig. 1) with suitable physico-chemical characteristics.

To the best of our knowledge, for the first time the use of a very low amount of HA-lipid conjugate has been proposed for the preparation of actively targeted micelles.

CMC is a key parameter as, it not only indicates the solubilization efficiency of micelles, but also demonstrates their stability. To determine the CMC of micelles, the pyrene method was chosen for its versatility and easy applicability. The CMC of PEG-M and the mixed micelles was measured by fluorimetry in the presence of pyrene, as a hydrophobic fluorescence probe, which organizes in a hydrophobic environment, changing its spectrum. The CMC values of PEG-M, PEG-M/HA_{4800} and PEG-M/HA_{14800} were 1×10^{-5} M indicating that the presence of the targeting agent did not affect the systems' ability to self-assemble. This range is similar to that calculated for other PEG-phospholipid conjugates [16,40], and is reported to be at least 100-fold lower than conventional detergents [41]. This low CMC value guarantees the retention of the micelles' physicochemical properties, and thus their integrity, even upon strong dilution.

Micelles were prepared *via* thin PEG-DSPE film hydration followed by sonication; a simple and versatile approach for self-assembling nanocarriers compared to other drug delivery systems that require a numerous procedure steps. Moreover, minimal amounts of organic solvents were used during their preparation unlike other nanosystems that were prepared through complex chemical reactions [42,43].

The derivatization of Gem with a stearoyl chain promotes hydrophobic interactions and the stable incorporation of GemC18 into the hydrophobic core of PEG-M and PEG-M/HA.

DPPE anchors to the PEG-DSPE lipid matrix during micelle formation, forming an outer HA shell without affecting the ability of the micelles to self-assemble. Unloaded micelles showed an average diameter below 50 nm, specifically ranging from 42 nm to 34 nm in the presence of HA-DPPE, and a negative zeta potential of approximately −25 mV. We found that the mean particle size of the loaded micelles was below 90 nm regardless of the presence of the HA conjugate, with PDI ranging from 0.272 to 0.315 (Table 1). The mean size was 82 nm for GemC18-PEG-M, 71 nm for GemC18-PEG-M/HA_{4800} and 68 nm for GemC18-PEG-M/HA_{14800}. Indeed, the low amount of HA-DPPE conjugate added during the preparation of actively targeted mixed micelles does not have dramatic impact on the physicochemical characteristics of the micelles. The zeta potential values were around −30 mV for all the loaded nanosystems. Moving to drug encapsulation, the presence of the HA-conjugate still guarantees high encapsulation efficiencies: 90 % and 96 % for PEG-M/HA_{4800} and PEG-M/HA_{14800}, respectively (Table 1). For all the formulations, the drug loading was about 18 %.

The ability of the micelles to retain GemC18 for an extended period of time is an important prerequisite for their use as drug delivery

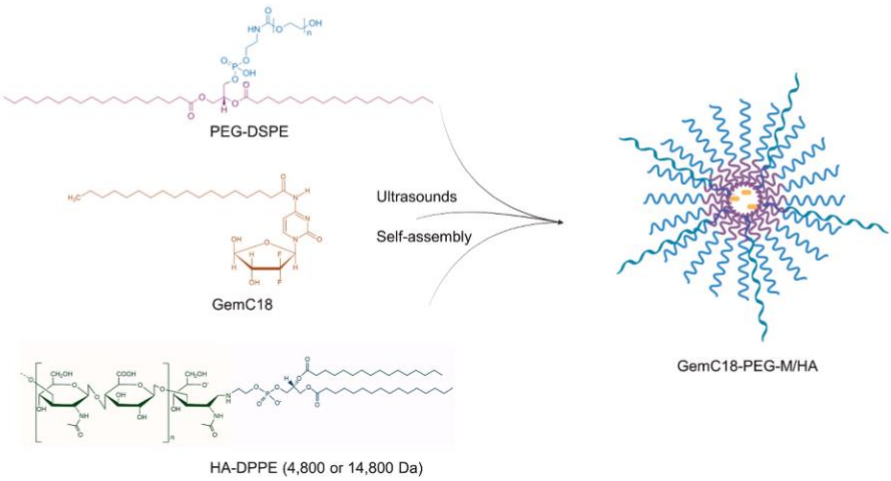

Fig. 1. Preparation process of GemC18-PEG-M/HA (created with BioRender.com).

Table 1
Physicochemical characteristics of GemC18-loaded micelles ($n = 3$).

GemC18-loaded micelles	mean diameter (nm) ± S.D.	PDI	zeta potential (mV) ± S.D.	E.E. (%)
PEG-M	82 ± 10	0.315	−29 ± 4	87 ± 10
PEG-M/HA_{4800}	71 ± 8	0.279	−31 ± 6	90 ± 4
PEG-M/HA_{14800}	68 ± 10	0.272	−27 ± 8	96 ± 3

systems. Thus, drug release was evaluated in PBS at 37 °C using a dialysis membrane. The lipophilic prodrug of Gem was retained inside the micellar matrix for an extended period of time: after an initial release of about 20 % of the loaded drug in the first hours (probably a burst effect due to the portion of GemC18 on the outer part of the micelles), PEG-M, PEG-M/HA_{4800} and PEG-M/HA_{14800} slowly released the drug and they still contained 60 % of their GemC18 after 72 h, demonstrating that GemC18 is strongly associated to the PEG-DSPE matrix.

We observed that the presence of the HA-conjugate did not affect the GemC18 release profile (Fig. S1), which was similar to that of the undecorated micelles, as has already been demonstrated for liposomal formulations [38].

The size, shape and the detailed internal structures of PEG-M/HA_{14800}, GemC18-PEG-M and GemC18-PEG-M/HA_{14800} were investigated using small angle x-ray scattering (SAXS), which is suitable for observing the arrangement of complex particles at the nanoscale [44,45]. The scattering curves I(q) for the different samples are reported in Fig. 2. In aqueous solutions, the scattering profiles of the polymer-phospholipid complexes show the typical features of nano-sized globular particles. Differences between unloaded and GemC18-loaded profiles are visible mainly in the low q region, corresponding to longer distances within the particle. A number of different models have been considered to extract detailed information about the size, shape, and internal core-shell structure of the systems.

The intensity profile of the unloaded PEG-M/HA_{14800} (1:0.4 mol) has been fitted to a core multi-shell sphere model with GENFIT software [35]. This form factor is suitable for the modelling of spherical micelles with a hydrophobic core surrounded by an extended hydrophilic shell. The fitting parameters are reported in Table 2. PEG-M/HA_{14800} shows an overall radius of 76 Å, with a hydrophobic central core of about 21 Å, compatible with the length of the C18 and C16 phospholipid saturated hydrocarbon tails. The micellar aggregation number, namely the number of PEG-HA molecules into the micellar structure, $Nagg = 4\pi R_{core}^3 / 3\, V_{HC}$ can be evaluated, being R_{core} the radius of the hydrophobic core and V_{HC} the volume of the hydrocarbon moiety (1016 $Å^3$ for DSPE and 960.2 $Å^3$ for DPPE). The aggregation number N_{agg} is about 40 and the interfacial area per headgroup is about 120 $Å^2$. The hydrophobic core is surrounded by a hydrophilic extended layer that can be modelled by two concentric shells, characterized by scattering length densities (Sld) higher than both the core and the solvent. The internal shell has a thickness $t_1 = 23$ Å and a Sld 9.44 10^{-6} $Å^{-2}$, while the external shell has a thickness $t_2 = 32$ Å and a Sld 9.42 10^{-6} $Å^{-2}$. The Sld decrease, observed as the distance from the core surface increases, indicates a high level of hydration of the shell, as expected for PEG and HA chains. The size of the micelle is about 154 Å, smaller than the mean hydrodynamic diameter measured by DLS, about 340 Å (PDI 1). The discrepancy may be partially due to the presence of few large aggregates in the suspension, that both could shift the average size and increase the polydispersity of the system. Moreover, the HA chains (MW 14,800 Da) have length longer than 150 Å, protruding from the micellar surface. These long hairs do not affect the SAXS profile up to long distances, due to their very low density on the surface of micelles. Rather, they may slow down the collective diffusion of micelles observed by DLS, corresponding to a calculated larger hydrodynamic size.

When GemC18 is loaded, the SAXS profile modifies compared to unloaded system, however showing an identical profile in the absence or presence of HA, as reported in Fig. 2. The scattered intensity, at constant concentration, increases compared to the unloaded micelles, suggesting the self-aggregation of the components in larger particles. Notably, in the low-q region, the intensity profiles assume a decay behaviour $I(q) \div q^{-1}$, characteristic of elongated rather than spherical particles. In the high-q region, the oscillations of the different intensity curves show similar features in all systems, indicating a core-shell internal arrangement also in the presence of GemC18. The overall structure can be modelled to a three-shell prolate ellipsoidal particle (Fig. 2C and D), with fitting parameters reported in Table 2. The hydrophobic core of the micelles shows a slight asymmetric equatorial section (a = 22 Å, b = 48 Å) and an extremely longer polar axis (c = 353 Å). The rod-like core is surrounded by a hydrophilic extended layer that can be modelled by two

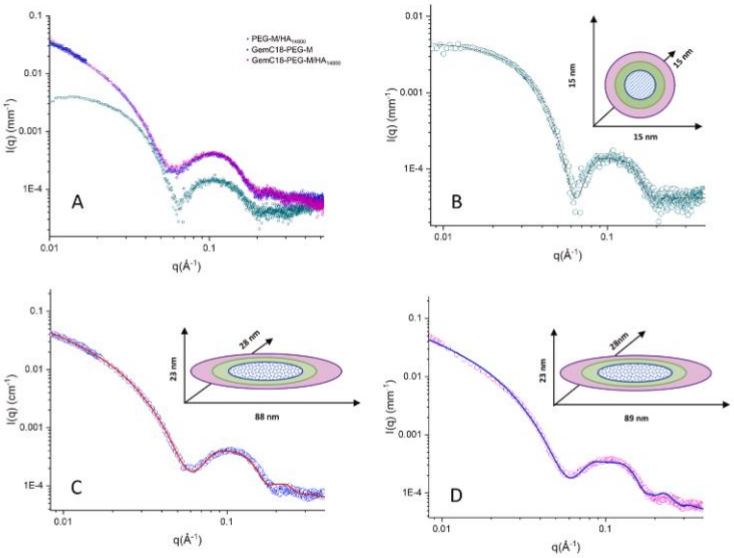

Fig. 2. SAXS intensity profiles for PEG-M/HA_{14800} (green), GemC18-PEG-M (blue) and GemC18-PEG-M/HA_{14800} (magenta). A) comparison of the different systems, B) PEG-M/HA_{14800} (green) with the best fit (solid black line) and a schematic representation of the fitting model (core-multishell sphere), C) GemC18-PEG-M (blue) with the best fit (solid red line) and a schematic representation of the fitting model (core-multishell prolate triaxial ellipsoid), GemC18-PEG-M/HA_{14800} (magenta) with the best fit (solid blue line) and a schematic representation of the fitting model (core-multishell prolate triaxial ellipsoid). Structural parameters are reported in Table 2. (For interpretation of the references to colour in this figure legend, the reader is referred to the Web version of this article.)

Table 2
Structural parameters of micelles as derived from SAXS data. Sld scattering length density, R_{core} hydrophobic core radius, a/b/c ellipsoid semiaxes, t_1 thickness of the internal hydrophilic shell, t_2 thickness of the external hydrophilic shell.

PEG-M/HA_{14800}								
Sld core (10^{-6} Å^{-2})	R core (Å)	Sld 1 (10^{-6} Å^{-2})	t_1 (Å)	Sld 2 (10^{-6} Å^{-2})	t_2 (Å)	Sld solvent (10^{-6} Å^{-2})		
9.36	22	9.44	23	9.42	32	9.41		
GemC18-PEG-M								
Sld core (10^{-6} Å^{-2})	a (Å)	b (Å)	c (Å)	Sld 1 (10^{-6} Å^{-2})	t_1 (Å)	Sld 2 (10^{-6} Å^{-2})	t_2 (Å)	Sld solvent (10^{-6} Å^{-2})
9.12	22	48	351	10.55	12	9.42	80	9.41
GemC18-PEG-M/HA_{14800}								
Sld core (10^{-6} Å^{-2})	a (Å)	b (Å)	c (Å)	Sld 1 (10^{-6} Å^{-2})	t_1 (Å)	Sld 2 (10^{-6} Å^{-2})	t_2 (Å)	Sld solvent (10^{-6} Å^{-2})
9.30	22	48	353	9.99	13	9.42	78	9.41

concentric shells, the internal one characterized by a thickness $t_1 = 13$ Å and Sld 9.99 10^{-6} Å^{-2}, and the external one by a thickness $t_2 = 75$ Å and a Sld 9.416 10^{-6} Å^{-2}. The presence of GemC18 (1:1 M ratio) changes the packing parameter of monomers within the aggregate, triggering a sphere-to-elongated transition in the overall shape of micelles. Assuming a hydrophobic volume about 500 Å^3 GemC18, it is possible to roughly estimate the aggregation number $N_{agg} = 1600$ and the mean area per molecule at the hydrophobic/hydrophilic interface A = 60 Å^2. The structural changes, both in size and shape of loaded micelles, reflect also on the hydrodynamics of the rod-like particles (axial ratio about 10), resulting in the high hydrodynamic size measured by DLS.

PXRD and FESEM were employed to investigate the crystallinity of the obtained micelles and their morphology upon dehydration. The comparison among the PXRD patterns of PEG-M/HA_{14800} (green line), GemC18-PEG-M (blue line) and GemC18-PEG-M/HA_{14800} (magenta line) is shown in Fig. 3A. The quite intense and broad signal at 2Theta=4.9° could be due to the presence of micelle. Nevertheless, the micellar organization did not affect the crystallinity of the components. Indeed, the peaks at 2Theta 15.0°, 19.1°, 21.9°, 23.2° and 26.8° are related to crystalline PEG (JCPDS file number 00-049-2095). Characteristic diffraction peaks of the PEG phase at 2Theta=19.2° and 23.2° were assigned either to the (115) and (016) [46] or (120) and (032) lattice planes [47]. The peak at 2Theta 28.4° is not typical of PEG, but it was observed in all samples: it can be reasonably due to PEG modified by the conjugation with DSPE.

It is worth noting that the peaks at 2Theta 26.7°, 31.6° and 45.3° related to the (0 0 13), (−1 1 8) and (2 0 23) crystal planes of stearic acid in the monoclinic phase (JCPDS file number 00-003-0252) were observed only in the PXRD pattern of GemC18-PEG-M (blue line) and that these signals were depleted in the presence of HA-DPPE (magenta line), which possibly indicates that the presence of HA could modify the GemC18 crystallinity.

FESEM observations pointed out the presence of elongated structures with size of about 5 μm in length and <1 μm width for both GemC18-PEG-M (Fig. 3B and Fig. S2) and GemC18-PEG-M/HA_{14800} (Fig. 3C). These structures appeared embedded in a residual matrix resulting from water evaporation. However, the morphology drastically changed in the case of PEG-M/HA_{14800}, since spherical particles with size roughly ranging between 0.5 and 1 μm were detected (Fig. 3D and detail in Fig. 3E). These features indicate that the presence of GemC18 strongly influenced the morphology of the micelles as previously observed by SAXS, in contrast to other lipid-based nanosystems [48]. It can be proposed that, during the evaporation of the sample drop, both elongated

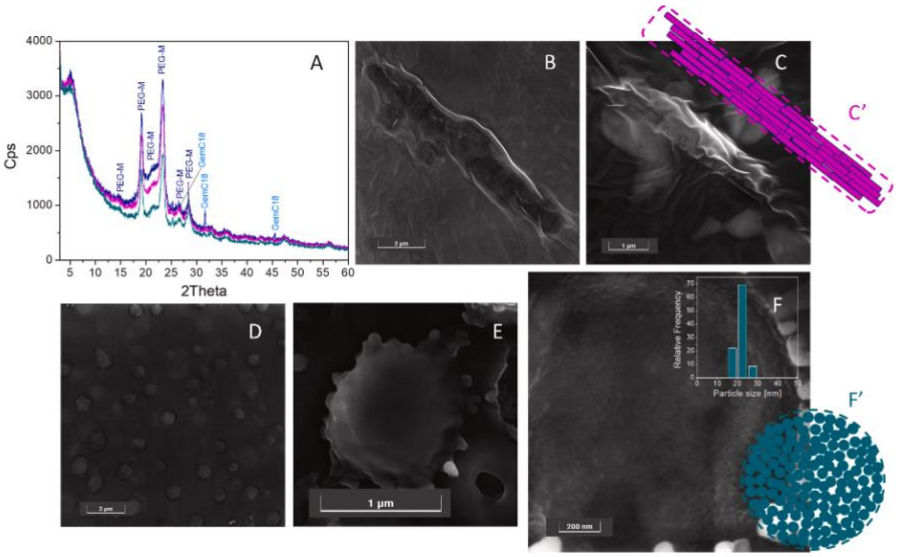

Fig. 3. A) PXRD patterns of PEG-M/HA_{14800} (green line), GemC18-PEG-M (blue line) and GemC18-PEG-M/HA_{14800} (magenta line). FESEM in-beam SE representative images of B) GemC18-PEG-M, C) GemC18-PEG-M/HA_{14800}, D), PEG-M/HA_{14800}, E) spherical superstructure of the same sample and F) spherical micelles inside the superstructure. Images collected in Ultra High-resolution mode at 5 keV, B), E) and F), and at 15 keV, C) and D). Instrumental magnification: 30000 × , 50000 × , 24000 × , 80000 × and 210000 × , respectively. Inset in F): particle size distribution of spherical micelles. Schematic representations of the elongated C') and spherical F') micelles organization. (For interpretation of the references to colour in this figure legend, the reader is referred to the Web version of this article.)

and spherical micelles self-assembled into much larger superstructures, *i.e.* supramolecular micelles which kept the single micelle original morphology, according to the occurrence of a sort of memory effect [49], as schematically depicted in Fig. 3C' and Fig. 3F'. Our hypothesis is further valorized by the observation of spherical small particles inside a spherical superstructure upon degradation under the electron beam, as shown in Fig. 3F. The average size of these small particles is d_m=21 ± 3 nm (around 210 Å), that is intermediate between the values obtained by SAXS (154 Å) and DLS (340 Å). The spherical superstructures as well as the elongated ones appeared decorated by particles of residual salts crystallized during evaporation (Fig. S3A and Fig. S4). However, looking at the EDS elemental maps shown in Fig. S3B, the spatial distributions of Na (cyan) and Cl (yellow) were not matching, conversely the map of Na overlapped the map of O (green), putting in evidence an enrichment of these elements at the surface of the spherical superstructures. Indeed, the signal related to C (red) is lower in correspondence of these particles, likely indicating the presence of this element in their internal part. This feature can be taken as an evidence that the polar heads of micelles of PEG-M/HA_{14800} are exposed in the external part and that they are able to coordinate the Na^+ ions dispersed in the solution during evaporation.

3.2. Biological validation assay

The uptake results indicate that, in Capan-1 cells, which have low levels of CD44, there were no significant differences in the uptake of fluorescently-labelled micelles, whether undecorated (NR-PEG-M) or decorated with HA_{4800}-DPPE or HA_{14800}-DPPE (NR-PEG-M/HA_{4800} or NR-PEG-M/HA_{14800}) (Fig. 4A). Similarly, in high-CD44 expressing PANC-1 cells, neither PEG-M, PEG-M/HA_{4800} or PEG-M/HA_{14800} showed any differences in uptake at the lowest dilution at any time. PEG-M/HA_{4800} and PEG-M/HA_{14800}, diluted 1:5, demonstrated time-dependent intracellular uptake which was greater with micelles diluted 1:2. Both PEG-M/HA_{4800} and PEG-M/HA_{14800} produced a significantly higher intracellular fluorescence compared to autofluorescent cells (Fig. 4B), indicating the efficient delivery of micelles cargo at these concentrations. The uptake of PEG-M/HA_{4800} or PEG-M/HA_{14800} was dependent on CD44-mediated endocytosis, as demonstrated by the reduction of the intracellular uptake of Nile Red loaded in these particles, but not in undecorated PEG-M, at the highest concentration (1:2 dilution) when CD44 highly expressing PANC-1 cells where co-incubated with a saturating amount of a CD44-neutralizing antibody or with HA, the CD44 substrate (Fig. 4C). This assay indicated that the uptake of the mixed micelles decorated with HA occurs *via* a receptor-mediated endocytosis, while the uptake of the undecorated mixed micelles occurs *via* passive diffusion.

Hence, the 1 % of HA-DPPE added during micelle formation may allow HA to expose on the surface of lipid matrix at an optimal density to bind CD44 receptor and promote GemC18 uptake to tumor site.

We next compared the cytotoxic effects of the different GemC18 prodrug-containing micelles *versus* free Gem, the first line treatment for pancreatic cancer. A time-dependent increase in cell death was observed for free Gem, GemC18, and GemC18-loaded micelles, either undecorated (GemC18-PEG-M) or decorated with HA_{4800}-DPPE or HA_{14800}-DPPE (GemC18-PEG-M/HA_{4800} or GemC18-PEG-M/HA_{14800}) at all time-points in Capan-1 cells. Free Gem had an IC_{50} > 10 µM at all time points and significantly reduced viability after 72 h. For free GemC18 the IC_{50} was below 1 µM at 48 h and 100 nM at 72 h. A significant reduction in cell viability was observed after 24 h of incubation at 10 µM, as well as after 48 h of incubation at 1 µM, for GemC18 and GemC18-loaded micelles. However, the encapsulation within micelles did not offer further advantage: indeed, the IC_{50} of GemC18-PEG-M, GemC18-PEG-M/HA_{4800} and GemC18-PEG-M/HA_{14800} was higher than that of free GemC18. At 48 h it remained >10 µM for all three formulations. At 72 h, GemC18-PEG-M and GemC18-PEG-M/HA_{4800} displayed an IC_{50} of 10 µM, while IC_{50} of GemC18-PEG-M/HA_{14800} was 100 nM (Fig. 5A). In these cells, GemC18 was the most effective drug, compared to both free Gem and GemC18-loaded micelles. It is likely that the free drug enters more promptly than micelles inducing stronger cell

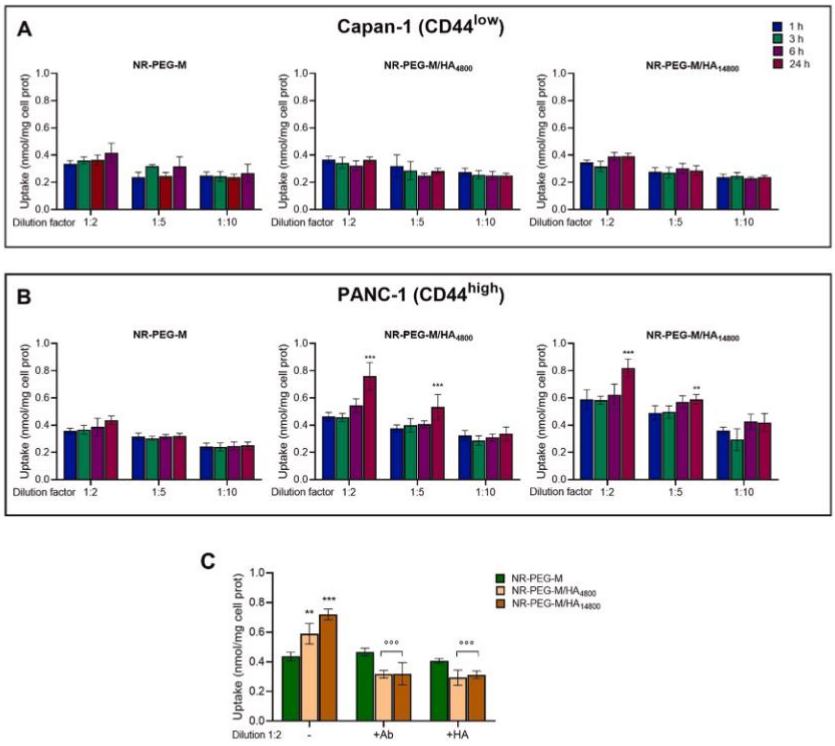

Fig. 4. (A–B) Cellular uptake by Capan-1 and PANC-1 cells of micelles, diluted 1:2, 1:5 and 1:10, labelled with Nile Red (NR), undecorated (NR-PEG-M) or decorated with PEG/HA_{4800} (NR-PEG-M/HA_{4800}) or PEG/HA_{14800} (NR-PEG-M/HA_{4800}), after 1, 3, 6 or 24 h. The autofluorescence of untreated cells was subtracted from each value. Data are presented as means ± SD (n = 3). **p < 0.01, ***p < 0.001: *vs* untreated cells. (C) PANC-1 cells were treated with micelles diluted 1:2 for 24 h, in the presence of anti-CD44 antibody diluted 1/100 (Ab) and HA (100 μM). Data are presented as means ± SD (n = 3). **p < 0.01, ***p < 0.001: *vs* untreated cells; p < 0.001: HA/Ab-treated NR-PEG-M/HA_{4800} or NR-PEG-M/HA_{14800} *vs* NR-PEG-M/HA_{4800} or NR-PEG-M/HA_{14800}. (For interpretation of the references to colour in this figure legend, the reader is referred to the Web version of this article.)

killing in this cell line. Moreover, the very low expression of CD44 implies that GemC18-PEG-M/HA_{4800} and GemC18-PEG-M/HA_{14800} offer no advantages compared to free GemC18.

In high-CD44 expressing PANC-1 cells, free Gem decreased cell viability less than in Capan-1, confirming the higher resistance of Gem of the former cells. The toxicity exerted by GemC18 and GemC18-PEG-M was like Gem; cell viability of free GemC18-treated cells at 48 and 72 h reflected increased resistance to Gem treatment: indeed, the IC_{50} of GemC18 was 10 μM and 100 nm at 48 and 72 h, respectively, while the IC_{50} of Gem was >10 μM at both time points. GemC18-PEG-M/HA_{4800} and GemC18-PEG-M/HA_{14800} were observed to be more cytotoxic relative to GemC18-PEG-M, inducing a significant reduction in cell viability in the micromolar range after 24 h, and, in the nanomolar range, after 48 and 72 h. The IC_{50} of GemC18-PEG-M was >10 μM at both 48 and 72 h; for GemC18-PEG-M/HA_{4800} it was 10 μM (48 h) and 1 μM (72 h), for GemC18-PEG-M/HA_{14800} it was 10 μM (48 h) and 100 nM (72 h), in line with the toxicity profile of GemC18 (Fig. 5B). Both GemC18-PEG-M/HA_{4800} and GemC18-PEG-M/HA_{14800} were more potent than Gem at 10 μM at all three time-points, and also at lower concentrations at 48 and 72 h. The GemC18-PEG-M/HA_{14800} formulation was more potent than GemC18-PEG-M/HA_{4800}, and was also significantly more cytotoxic than GemC18-PEG-M at the highest concentration (10 μM) at 24 h and when starting from 100 nM after 48 and 72 h. The cytotoxicity of HA-decorated micelles was dependent on their internalization *via* CD44. Indeed, when PANC-1 cells were incubated with GemC18-PEG-M/HA_{4800} and GemC18-PEG-M/HA_{14800} at the highest concentration and for the longest time with saturating amount of HA or the neutralizing anti-CD44 antibody, no cytotoxic effect was abrogated (Fig. 5C). Although both GemC18-PEG-M/HA_{4800} and GemC18-PEG-M/HA_{14800} were internalized by CD44-mediated endocytosis, the different HA-chain lengths may determine different interactions with the receptor, since the PEG-M/HA_{14800} were more internalized than the PEG-M/HA_{4800}, as suggested by the uptake assays (Fig. 4B). GemC18-PEG-M/HA_{14800} deliver the prodrug in a more efficient way than GemC18-PEG-M/HA_{4800}, resulting the more cytotoxic formulation (Fig. 5B). This behavior confirms previous observations in which liposomes decorated with HA at two different molecular weights showed different affinities for the CD44 receptor, *in vitro* and *in vivo* as a function of the increase of the polymer molecular weight [33]. The GemC18-PEG-M/HA_{14800} are also more effective than free GemC18 at 100 nM, at all the time points, while no significant differences were detected at micromolar concentrations.

Furthermore, the IC_{50} values for blank micelles exceeded 10 μM, indicating no reduction in cell viability at concentrations up to this threshold.

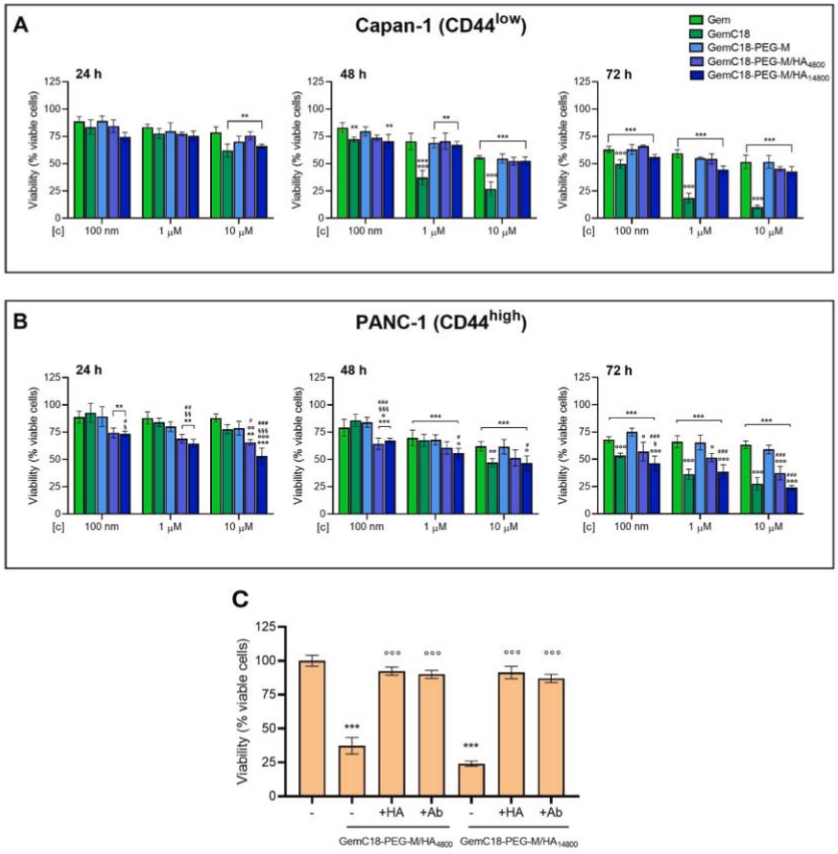

Fig. 5. (A–B) Cell viability of Capan-1 and PANC-1 cells was measured by a chemiluminescent-based commercial kit. Cells were incubated with gemcitabine (Gem), GemC18, or micelles carrying GemC18, undecorated (GemC18-PEG-M), or decorated with HA_{4800}-DPPE or HA_{14800}-DPPE (GemC18-PEG-M/HA_{4800} or GemC18-PEG-M/HA_{14800}), containing different concentrations (100 nM, 1 μM, 10 μM) of GemC18, for 24, 48 or 72 h. Cell viability of untreated cells was 100 % for all experimental conditions. Data are presented as means ± SD (n = 3). $^{**}p < 0.01$, $^{***}p < 0.001$: *vs* untreated cells; $^{\circ}p < 0.05$, $^{\circ}p < 0.01$, $p < 0.001$: GemC18-PEG-M/HA_{4800} and GemC18-PEG-M/HA_{14800} *vs* Gem; §p < 0.05, §§§p < 0.001; GemC18-PEG-M/HA_{4800} or GemC18-PEG-M/HA_{14800} *vs* GemC18; #p < 0.05, ##p < 0.01, ###p < 0.001; GemC18-PEG-M/HA_{4800} or GemC18-PEG-M/HA_{14800} *vs* GemC18-PEG-M. (C) PANC-1 cells were grown for 72 h in fresh medium (−) or in the presence of GemC18-PEG-M/HA_{4800} or GemC18-PEG-M/HA_{14800} containing 10 μM GemC18, in the absence (−) or presence of HA (100 μM) or anti-CD44 antibody diluted 1/100 (Ab), then cell viability was measured. Data are presented as means ± SD (n = 3). $^{***}p < 0.001$: *vs* untreated cells; $p < 0.001$: HA/Ab-treated GemC18-PEG-M/HA_{4800} or GemC18-PEG-M/HA_{14800} *vs* GemC18-PEG-M/HA_{4800} or GemC18-PEG-M/HA_{14800}.

4. Conclusions

This work has demonstrated that the presence of a very low amount (1 % molar ratio) of HA-DPPE conjugate (4800 or 14,800 Da) in the PEG-DSPE micelles confers appreciable targeting ability and improves drug delivery efficiency. The Gem prodrug GemC18 was efficiently encapsulated into the micellar core, modifying the nanoparticle shape; the micelles were identified as being elongated once the amphiphilic prodrug was incorporated. *In vitro* tests on cancer cells then showed that the HA-decorated micelles display enhanced intracellular internalization and cytotoxicity towards target cells that overexpress the HA-specific receptor CD44, compared to undecorated analogs. This targeting strategy promotes enhanced binding and uptake of the HA-decorated micelles through CD44-mediated endocytosis, resulting in increased intracellular drug accumulation, specifically in resistant cells. This approach leverages both the overexpression of CD44 on cancer cells and the natural endocytic pathways to directly address drug resistance challenges. Further applications of this nanosystems could involve the co-encapsulation of multiple anticancer drugs to overcome specific resistance mechanisms. In a translational perspective, it is interesting to know that the effects of HA-decorated micelles are more pronounced in Gem-resistant cancer cells, producing a significant cytotoxic effect where Gem was ineffective. Hence, the system can set the basis of an alternative strategy to conventional Gem in pancreatic adenocarcinomas, particularly in those with high expression of CD44.

The next steps will concern the incorporation of both lipophilic and amphiphilic drugs into the PEG/HA mixed micelles to widen the number of possible applications and evaluate the influence of the drug's chemical characteristics on the shape and efficacy of the mixed micelles. This approach could then pave the way for the setup of an easily prepared platform for the targeted delivery of anticancer drugs with improved intracellular delivery.

CRediT authorship contribution statement

Ilaria Andreana: Writing – review & editing, Writing – original draft, Validation, Methodology, Investigation, Formal analysis, Data curation, Conceptualization. **Valeria Bincoletto:** Writing – review & editing, Methodology, Investigation, Data curation. **Caterina Ricci:** Writing – review & editing, Methodology, Investigation, Data curation. **Iris Chiara Salaroglio:** Writing – review & editing, Methodology, Investigation, Data curation. **Maela Manzoli:** Writing – review & editing, Supervision, Methodology, Investigation, Data curation, Conceptualization. **Beatrice Zurletti:** Writing – review & editing, Methodology, Investigation, Data curation. **Jessica Milone:** Writing – review & editing, Methodology, Investigation, Data curation. **Barbara Rolando:** Writing – review & editing, Methodology, Investigation, Data curation. **Elena Del Favero:** Writing – review & editing, Supervision, Methodology, Investigation, Data curation, Conceptualization. **Chiara Riganti:** Writing – review & editing, Supervision, Methodology, Investigation, Data curation, Conceptualization. **Pietro Matricardi:** Writing – review & editing, Supervision, Conceptualization. **Barbara Stella:** Writing – review & editing, Supervision, Project administration, Funding acquisition, Conceptualization. **Silvia Arpicco:** Writing – review & editing, Writing – original draft, Supervision, Project administration, Funding acquisition, Conceptualization.

Data availability

All data generated or analyzed during this study are included in this published article. Additional data related to this paper may be requested from the authors.

Declaration of generative AI in scientific writing

Authors did not use generative AI and AI-assisted technologies in the writing process.

Declaration of competing interest

The authors declare that they have no known competing financial interests or personal relationships that could have appeared to influence the work reported in this paper.

Acknowledgments

The authors thank ESRF for financial support and beamtime (DOI: 10.15151/ESRF-ES-1351189712), ID02 staff for technical support and PSCM facility (Grenoble) for allowing on-site sample preparation. E.D.F. thanks BIOMETRA Dept. for partial support (PSR2021_DEL_FAVERO). This work benefited from the use of the SasView application. This research was funded by Italian Ministry for University and Research (MIUR) - University of Torino, "Fondi Ricerca Locale (ex-60 %) and PRIN 2022 (grant 2022ZBZFX3).

Appendix A. Supplementary data

Supplementary data to this article can be found online at https://doi.org/10.1016/j.jddst.2024.106518.

Data availability

Data will be made available on request.

References

[1] X. Liu, Y. Cheng, Y. Mu, Z. Zhang, D. Tian, Y. Liu, X. Hu, T. Wen, Diverse drug delivery systems for the enhancement of cancer immunotherapy: an overview, Front. Immunol. 15 (2024) 1328145, https://doi.org/10.3389/fimmu.2024.1328145.

[2] E.S. Ali, S.M. Sharker, M.T. Islam, I.N. Khan, S. Shaw, M.A. Rahman, S.J. Uddin, M. C. Shill, S. Rehman, N. Das, et al., Targeting cancer cells with nanotherapeutics and nanodiagnostics: current status and future perspectives, Semin. Cancer Biol. 69 (2021) 52–68, https://doi.org/10.1016/j.semcancer.2020.01.011.

[3] G. Wei, Y. Wang, G. Yang, Y. Wang, R. Ju, Recent progress in nanomedicine for enhanced cancer chemotherapy, Theranostics 11 (2021) 6370–6392, https://doi.org/10.7150/thno.57828.

[4] F. Rommasi, N. Esfandiari, Liposomal nanomedicine: applications for drug delivery in cancer therapy, Nanoscale Res. Lett. 16 (2021) 95, https://doi.org/10.1186/s11671-021-03553-8.

[5] Z. Edis, J. Wang, M.K. Waqas, M. Ijaz, M. Ijaz, Nanocarriers-mediated drug delivery systems for anticancer agents: an overview and perspectives, Int J Nanomedicine 16 (2021) 1313–1330, https://doi.org/10.2147/ijn.S289443.

[6] D. Hwang, J.D. Ramsey, A.V. Kabanov, Polymeric micelles for the delivery of poorly soluble drugs: from nanoformulation to clinical approval, Adv. Drug Deliv. Rev. 156 (2020) 80–118, https://doi.org/10.1016/j.addr.2020.09.009.

[7] Y. Yuan, W. Tan, Y. Mi, L. Wang, Z. Qi, Z. Guo, Effect of hydrophobic chain length in amphiphilic chitosan conjugates on intracellular drug delivery and smart drug release of redox-responsive micelle, Mar. Drugs 22 (2023), https://doi.org/10.3390/md22010018.

[8] A. Phungula, A.Y. Waddad, M.D. Fernandez Leyes, P. Di Gianvincenzo, B. Espuche, S. Zuffi, S.E. Moya, F. Albericio, B.G. de la Torre, Self-assembly of NrTP6 cell-penetrating lipo-peptide with variable number of lipid chains: impact of phosphate ions on lipid association, J. Colloid Interface Sci. 654 (2024) 124–133, https://doi.org/10.1016/j.jcis.2023.09.161.

[9] C. Wang, H. Zhao, Polymer brushes and surface nanostructures: molecular design, precise synthesis, and self-assembly, Langmuir (2024), https://doi.org/10.1021/acs.langmuir.3c02813.

[10] X. Wang, Y. Wang, T. Tang, G. Zhao, W. Dong, Q. Li, X. Liang, Curcumin-loaded RH60/F127 mixed micelles: characterization, biopharmaceutical characters and anti-inflammatory modulation of airway inflammation, Pharmaceutics 15 (2023), https://doi.org/10.3390/pharmaceutics15122710.

[11] M. Zhang, N. Ying, J. Chen, L. Wu, H. Liu, S. Luo, D. Zeng, Engineering a pH-responsive polymeric micelle co-loaded with paclitaxel and triptolide for breast cancer therapy, Cell Prolif. (2024) e13603, https://doi.org/10.1111/cpr.13603.

[12] J. Liu, Y. Zhang, C. Liu, Y. Jiang, Z. Wang, X. Li, Paclitaxel prodrug-encapsulated polypeptide micelles with redox/pH dual responsiveness for cancer chemotherapy, Int J Pharm 645 (2023) 123398, https://doi.org/10.1016/j.ijpharm.2023.123398.

[13] C. Xu, Y. Ding, J. Ni, L. Yin, J. Zhou, J. Yao, Tumor-targeted docetaxel-loaded hyaluronic acid-quercetin polymeric micelles with p-gp inhibitory property for hepatic cancer therapy, RSC advances 6 (2016) 27542–27556, https://doi.org/10.1039/C6RA00460A.

[14] M. Huo, H. Wang, Y. Zhang, H. Cai, P. Zhang, L. Li, J. Zhou, T. Yin, Co-delivery of silybin and paclitaxel by dextran-based nanoparticles for effective anti-tumor treatment through chemotherapy sensitization and microenvironment modulation, J Control Release 321 (2020) 198–210, https://doi.org/10.1016/j.jconrel.2020.02.017.

[15] Q. Yang, K.R. Moulder, M.S. Cohen, S. Cai, L.M. Forrest, Cabozantinib loaded DSPE-PEG(2000) micelles as delivery system: formulation, characterization and cytotoxicity evaluation, BAOJ Pharm Sci 1 (2015).

[16] A.N. Lukyanov, V.P. Torchilin, Micelles from lipid derivatives of water-soluble polymers as delivery systems for poorly soluble drugs, Adv. Drug Deliv. Rev. 56 (2004) 1273–1289, https://doi.org/10.1016/j.addr.2003.12.004.

[17] B. Xu, Z. Ding, Y. Hu, T. Zhang, S. Shi, G. Yu, X. Qi, Preparation and evaluation of the cytoprotective activity of micelles with DSPE-PEG-C60 as a carrier against doxorubicin-induced cytotoxicity, Front. Pharmacol. 13 (2022) 952800, https://doi.org/10.3389/fphar.2022.952800.

[18] P. Graván, J. Peña-Martín, J.L. de Andrés, M. Pedrosa, M. Villegas-Montoya, F. Galisteo-González, J.A. Marchal, P. Sánchez-Moreno, Exploring the impact of nanoparticle stealth coatings in cancer models: from PEGylation to cell membrane-coating nanotechnology, ACS Appl. Mater. Interfaces 16 (2024) 2058–2074, https://doi.org/10.1021/acsami.3c13948.

[19] E. Blanco, H. Shen, M. Ferrari, Principles of nanoparticle design for overcoming biological barriers to drug delivery, Nat. Biotechnol. 33 (2015) 941–951, https://doi.org/10.1038/nbt.3330.

[20] Y. Takakura, Y. Takahashi, Strategies for persistent retention of macromolecules and nanoparticles in the blood circulation, J Control Release 350 (2022) 486–493, https://doi.org/10.1016/j.jconrel.2022.05.063.

[21] Q. Guo, L. Zhang, M. He, X. Jiang, J. Tian, Q. Li, Z. Liu, L. Wang, H. Sun, Doxorubicin-loaded natural daptomycin micelles with enhanced targeting and anti-tumor effect in vivo, Eur. J. Med. Chem. 222 (2021) 113582, https://doi.org/10.1016/j.ejmech.2021.113582.

[22] Q. Du, F. Lv, J. Huang, X. Tang, Z. Zhao, J. Chen, A multiple environment-sensitive prodrug nanomicelle strategy based on chitosan graftomer for enhanced tumor therapy of gambogic acid, Carbohydr. Polym. 267 (2021) 118229, https://doi.org/10.1016/j.carbpol.2021.118229.

[23] Y. Zheng, Y. Oz, Y. Gu, N. Ahamad, K. Shariati, J. Chevalier, D. Kapur, N. Annabi, Rational design of polymeric micelles for targeted therapeutic delivery, Nano Today 55 (2024), https://doi.org/10.1016/j.nantod.2024.102147.

[24] R.K. Sironen, M. Tammi, R. Tammi, P.K. Auvinen, M. Anttila, V.M. Kosma, Hyaluronan in human malignancies, Exp. Cell Res. 317 (2011) 383–391, https://doi.org/10.1016/j.yexcr.2010.11.017.

[25] H.-J. Cho, Recent progresses in the development of hyaluronic acid-based nanosystems for tumor-targeted drug delivery and cancer imaging, Journal of pharmaceutical investigation 50 (2020) 115–129, https://doi.org/10.1007/s40005-019-00448-w.

[26] H.A. Burris 3rd, M.J. Moore, J. Andersen, M.R. Green, M.L. Rothenberg, M. R. Modiano, M.C. Cripps, R.K. Portenoy, A.M. Storniolo, P. Tarassoff, et al., Improvements in survival and clinical benefit with gemcitabine as first-line therapy for patients with advanced pancreas cancer: a randomized trial, J. Clin. Oncol. 41 (2023) 5482–5492, https://doi.org/10.1200/jco.22.02777.
[27] M.L. Immordino, P. Brusa, F. Rocco, S. Arpicco, M. Ceruti, L. Cattel, Preparation, characterization, cytotoxicity and pharmacokinetics of liposomes containing lipophilic gemcitabine prodrugs, J Control Release 100 (2004) 331–346, https://doi.org/10.1016/j.jconrel.2004.09.001.
[28] L. Neutsch, E.M. Wirth, S. Spijker, C. Pichl, H. Kählig, F. Gabor, M. Wirth, Synergistic targeting/prodrug strategies for intravesical drug delivery–lectin-modified PLGA microparticles enhance cytotoxicity of stearoyl gemcitabine by contact-dependent transfer, J Control Release 169 (2013) 62–72, https://doi.org/10.1016/j.jconrel.2013.04.004.
[29] M. Bartkowski, V. Bincoletto, I.C. Salaroglio, G. Ceccone, R. Arenal, S. Nervo, B. Rolando, C. Riganti, S. Arpicco, S. Giordani, Enhancing pancreatic ductal adenocarcinoma (PDAC) therapy with targeted carbon nano-onion (CNO)-mediated delivery of gemcitabine (GEM)-derived prodrugs, J. Colloid Interface Sci. 659 (2024) 339–354, https://doi.org/10.1016/j.jcis.2023.12.166.
[30] S. Zhu, P. Wonganan, D.S. Lansakara-P, H.L. O'Mary, Y. Li, Z. Cui, The effect of the acid-sensitivity of 4-(N)-stearoyl gemcitabine-loaded micelles on drug resistance caused by RRM1 overexpression, Biomaterials 34 (2013) 2327–2339, https://doi.org/10.1016/j.biomaterials.2012.11.053.
[31] Z. Daman, S. Ostad, M. Amini, K. Gilani, Preparation, optimization and in vitro characterization of stearoyl-gemcitabine polymeric micelles: a comparison with its self-assembled nanoparticles, Int J Pharm 468 (2014) 142–151, https://doi.org/10.1016/j.ijpharm.2014.04.021.
[32] Y. Wang, W. Fan, X. Dai, U. Katragadda, D. McKinley, Q. Teng, C. Tan, Enhanced tumor delivery of gemcitabine via PEG-DSPE/TPGS mixed micelles, Mol. Pharm. 11 (2014) 1140–1150, https://doi.org/10.1021/mp4005904.
[33] S. Arpicco, C. Lerda, E. Dalla Pozza, C. Costanzo, N. Tsapis, B. Stella, M. Donadelli, I. Dando, E. Fattal, L. Cattel, et al., Hyaluronic acid-coated liposomes for active targeting of gemcitabine, Eur. J. Pharm. Biopharm. 85 (2013) 373–380, https://doi.org/10.1016/j.ejpb.2013.06.003.
[34] Z. Song, R. Feng, M. Sun, C. Guo, Y. Gao, L. Li, G. Zhai, Curcumin-loaded PLGA-PEG-PLGA triblock copolymeric micelles: preparation, pharmacokinetics and distribution in vivo, J. Colloid Interface Sci. 354 (2011) 116–123, https://doi.org/10.1016/j.jcis.2010.10.024.
[35] F. Spinozzi, C. Ferrero, M.G. Ortore, A. De Maria Antolinos, P. Mariani, GENFIT: software for the analysis of small-angle X-ray and neutron scattering data of macromolecules in solution, J. Appl. Crystallogr. 47 (2014) 1132–1139, https://doi.org/10.1107/s1600576714005147.
[36] M.E. Cano, D. Lesur, V. Bincoletto, E. Gazzano, B. Stella, C. Riganti, S. Arpicco, J. Kovensky, Synthesis of defined oligohyaluronates-decorated liposomes and interaction with lung cancer cells, Carbohydr. Polym. 248 (2020) 116798, https://doi.org/10.1016/j.carbpol.2020.116798.
[37] H. Xu, M. Niu, X. Yuan, K. Wu, A. Liu, CD44 as a tumor biomarker and therapeutic target, Exp. Hematol. Oncol. 9 (2020) 36, https://doi.org/10.1186/s40164-020-00192-0.
[38] E. Gazzano, I. Buondonno, A. Marengo, B. Rolando, K. Chegaev, J. Kopecka, S. Saponara, M. Sorge, C.M. Hattinger, A. Gasco, et al., Hyaluronated liposomes containing H2S-releasing doxorubicin are effective against P-glycoprotein-positive/doxorubicin-resistant osteosarcoma cells and xenografts, Cancer Lett. 456 (2019) 29–39, https://doi.org/10.1016/j.canlet.2019.04.029.
[39] I. Andreana, V. Bincoletto, M. Manzoli, F. Rodà, V. Giarraputo, P. Milla, S. Arpicco, B. Stella, Freeze drying of polymer nanoparticles and liposomes exploiting different saccharide-based approaches, Materials 16 (2023), https://doi.org/10.3390/ma16031212.
[40] Z. Sezgin, N. Yüksel, T. Baykara, Preparation and characterization of polymeric micelles for solubilization of poorly soluble anticancer drugs, Eur. J. Pharm. Biopharm. 64 (2006) 261–268, https://doi.org/10.1016/j.ejpb.2006.06.003.
[41] M.J. Rosen, J.T. Kunjappu, Surfactants and Interfacial Phenomena, John Wiley & Sons, 2012.
[42] X. He, Z. Jiang, O.U. Akakuru, J. Li, A. Wu, Nanoscale covalent organic frameworks: from controlled synthesis to cancer therapy, Chem. Commun. 57 (2021) 12417–12435, https://doi.org/10.1039/d1cc04846e.
[43] C. Zhao, X. Tang, X. Chen, Z. Jiang, Multifaceted carbonized metal-organic frameworks synergize with immune checkpoint inhibitors for precision and augmented cuproptosis cancer therapy, ACS Nano 18 (2024) 17852–17868, https://doi.org/10.1021/acsnano.4c04022.
[44] E. Di Cola, L. Cantu, P. Brocca, V. Rondelli, G.C. Fadda, E. Canelli, P. Martelli, A. Clementino, F. Sonvico, R. Bettini, et al., Novel O/W nanoemulsions for nasal administration: structural hints in the selection of performing vehicles with enhanced mucopenetration, Colloids Surf. B Biointerfaces 183 (2019) 110439, https://doi.org/10.1016/j.colsurfb.2019.110439.
[45] C.I. Camara, L. Bertocchi, C. Ricci, R. Bassi, A. Bianchera, L. Cantu, R. Bettini, E. Del Favero, Hyaluronic acid-dexamethasone nanoparticles for local adjunct therapy of lung inflammation, Int. J. Mol. Sci. 22 (2021), https://doi.org/10.3390/ijms221910480.
[46] Y. Li, X. Li, F. Xiang, T. Huang, Y. Wang, J. Wu, Z. Zhou, Crystallization, rheological, and mechanical properties of PLLA/PEG blend with multiwalled carbon nanotubes, Polym. Adv. Technol. 22 (2011) 1959–1970, https://doi.org/10.1002/pat.1702.
[47] R. Li, Y. Wu, Z. Bai, J. Guo, X. Chen, Effect of molecular weight of polyethylene glycol on crystallization behaviors, thermal properties and tensile performance of polylactic acid stereocomplexes, RSC Adv. 10 (2020) 42120–42127, https://doi.org/10.1039/d0ra08699a.
[48] R. Bahramabadi, H. Hakimi, A. Saljooqi, M. Barani, D. Razmjoue, M. Zare-Bidaki, M. Mohamadi, The essential oil of rocket seeds maintains its antibacterial effects after encapsulation in nanoliposomes, J. Herb. Med. 47 (2024) 100924, https://doi.org/10.1016/j.hermed.2024.100924.
[49] D. Wang, G. Tong, R. Dong, Y. Zhou, J. Shen, X. Zhu, Self-assembly of supramolecularly engineered polymers and their biomedical applications, Chem. Commun. 50 (2014) 11994–12017, https://doi.org/10.1039/c4cc03155e.

Supplementary Material

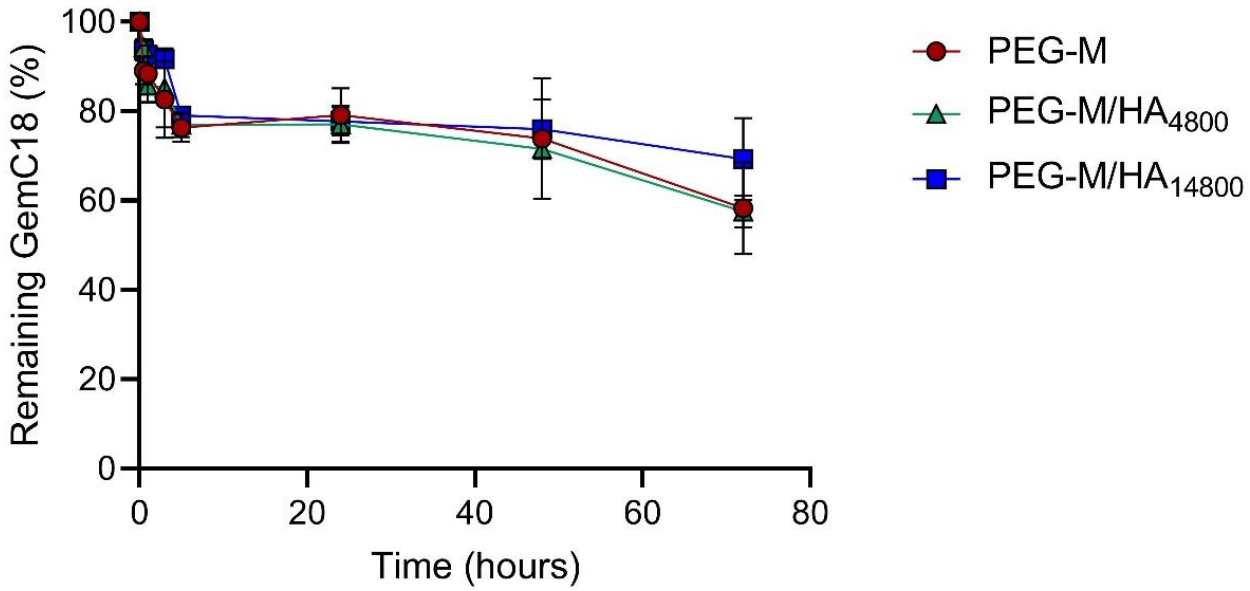

Fig. S1. GemC18 release from PEG-M, PEG-M/HA_{4800} and PEG-M/HA_{14800} as a function of time in PBS pH 7.4 at 37 °C.

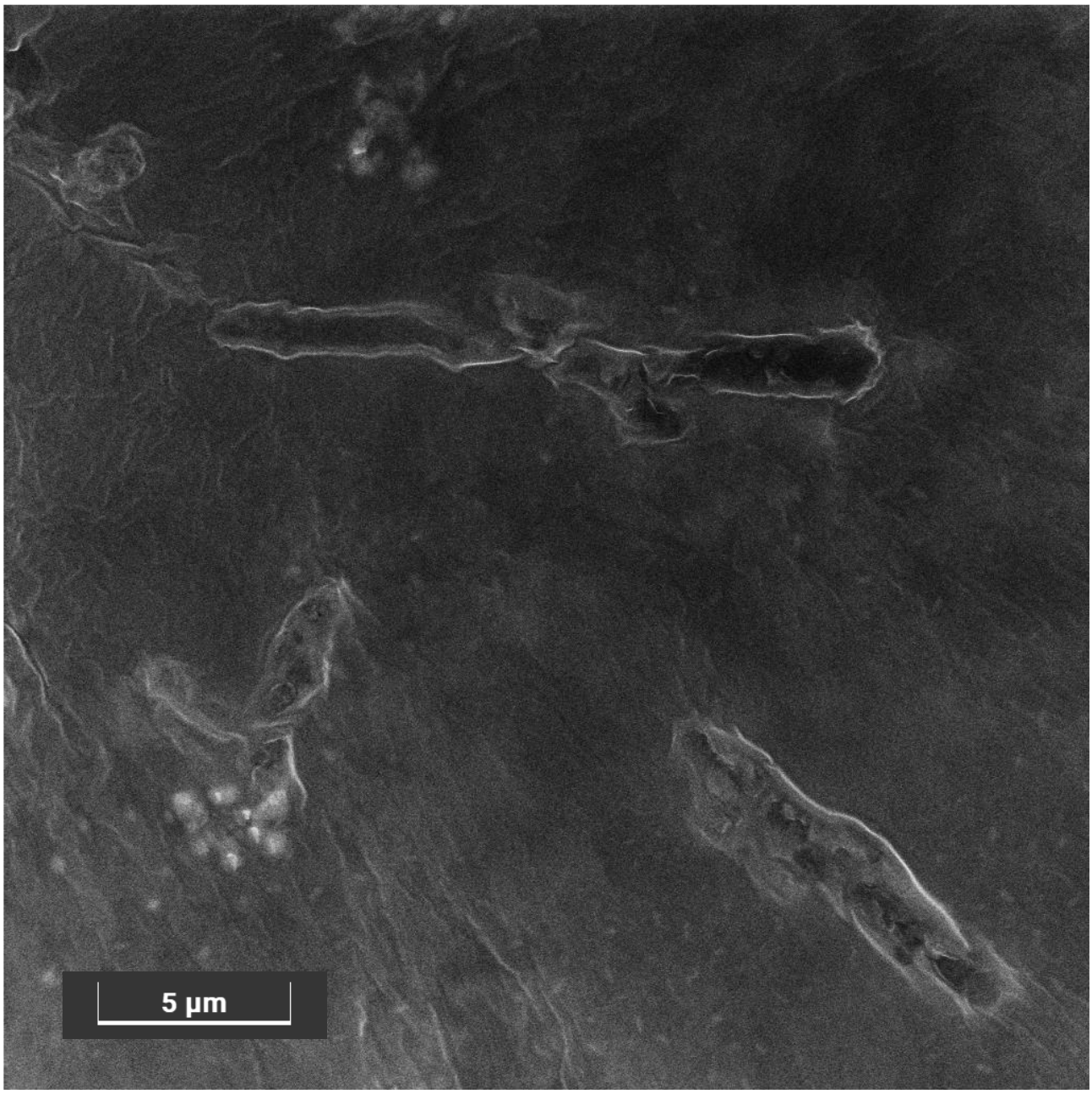

Fig. S2. FESEM representative image showing the presence of elongated structures as for the-GemC18-PEG-M sample collected with in-beam SE detector in Ultra High-resolution mode at 15 keV. Instrumental magnification: 10000×.

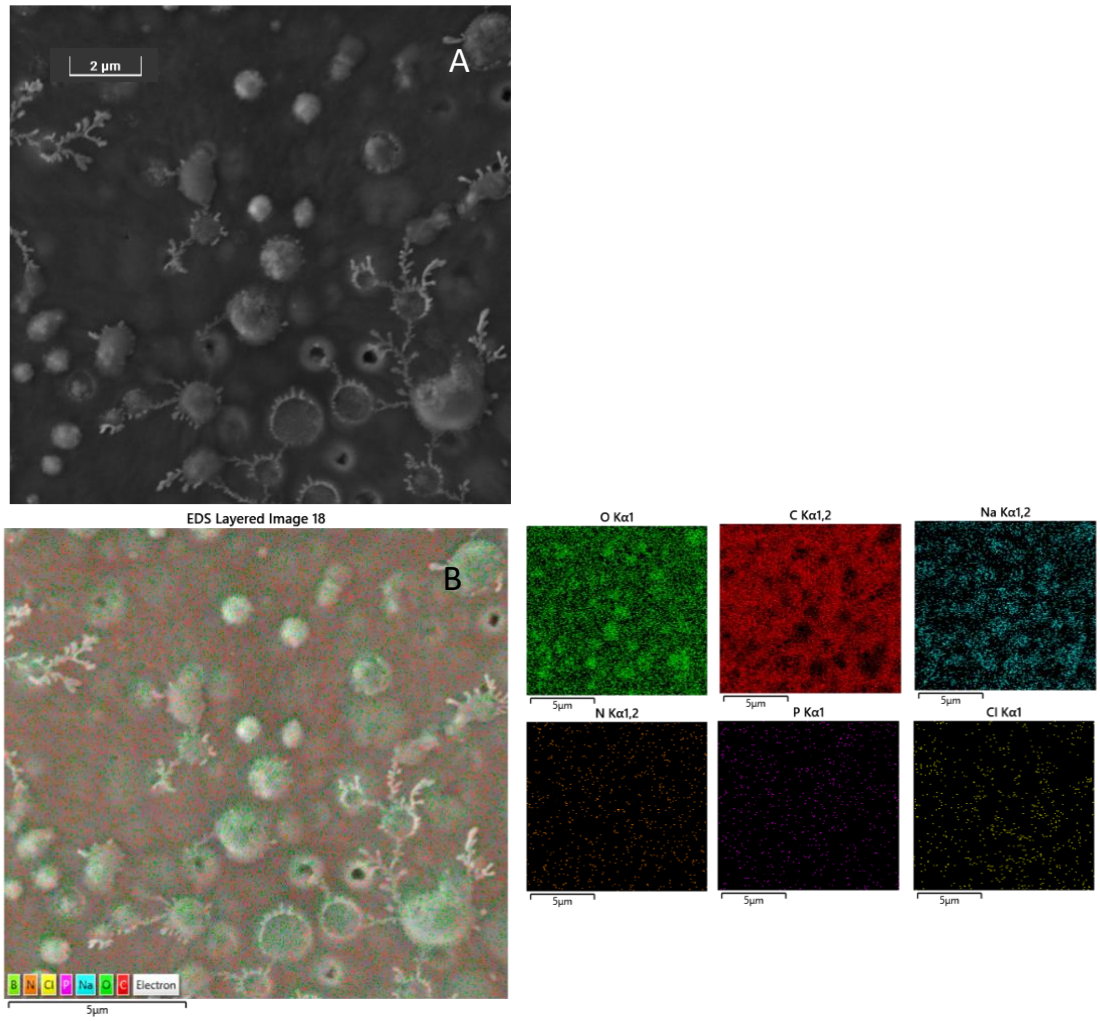

Fig. S3. A) FESEM representative image showing the presence of spherical structures decorated by residual crystal salts formed during evaporation of the PEG-M/HA$_{14800}$ solution collected with in-beam SE detector in Ultra High-resolution mode at 5 keV. Instrumental magnification: 22000×. B) EDS sum map of the region shown in A) and maps of the single elements.

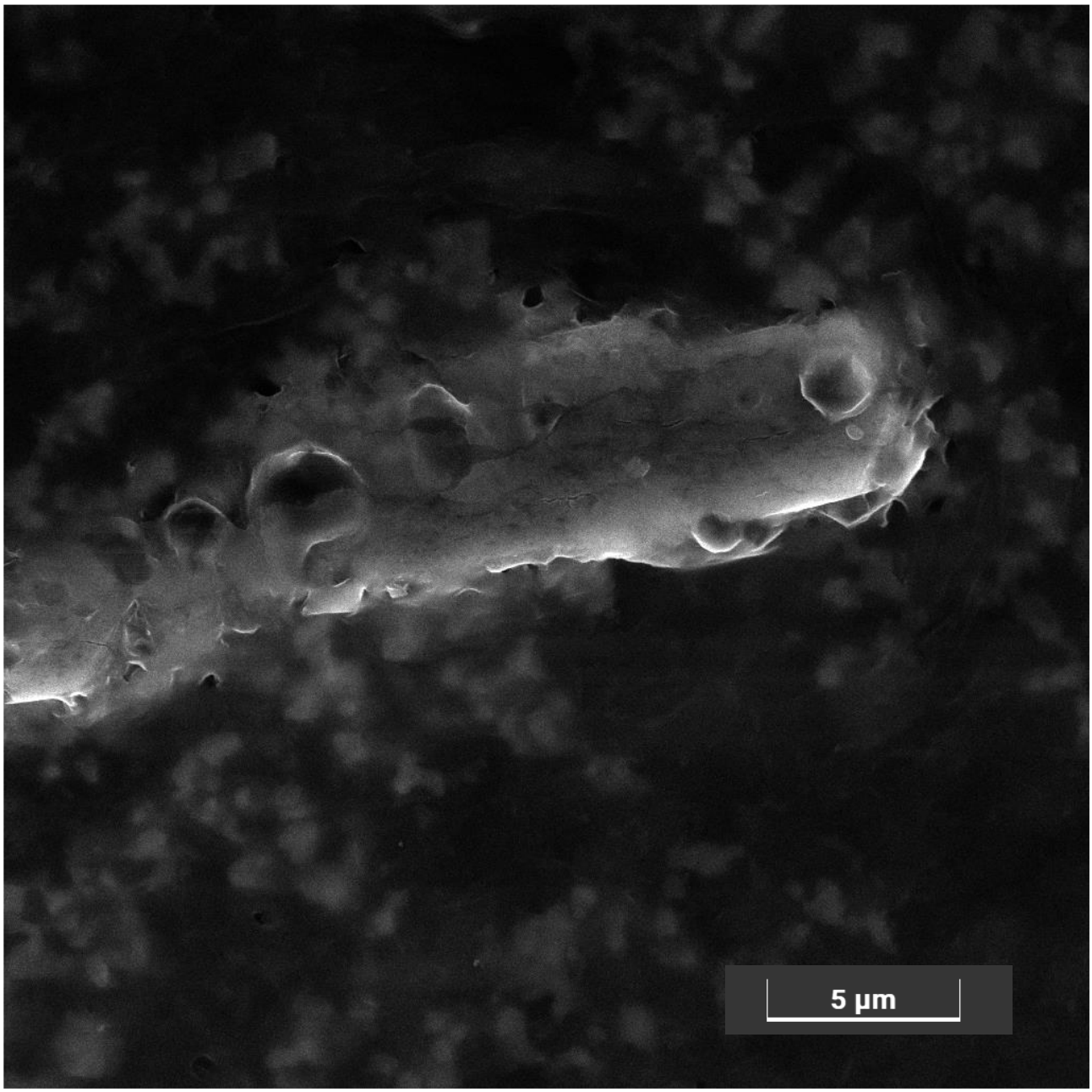

Fig. S4. FESEM representative image showing the presence of elongated superstructures decorated by residual crystal salts formed during evaporation of the GemC18-PEG-M/HA$_{14800}$ solution collected with in-beam SE detector in Ultra High-resolution mode at 15 keV. Instrumental magnification: 10000×.

Study of synergistic tumor toxicity in pancreatic cancer cells through liposomal drug combination therapy

Valeria Bincoletto, Ilaria Andreana, Barbara Stella, Tania Limongi, Federico Cesano, Barbara Rolando, Giorgia Urbinati, Silvia Arpicco

---

Submitted to *European Journal of Pharmaceutics and Biopharmaceutics*

Liposomes have emerged as a powerful strategy in cancer therapy due to their ability to enhance the pharmacokinetic profile, stability, and bioavailability of chemotherapeutic agents while reducing systemic toxicity. In the context of pancreatic cancer, where drug resistance and poor therapeutic efficacy pose significant clinical challenges, liposomes represent a promising platform to improve treatment outcomes by synergistic drug combinations.

Main Aim

The main aim of this study was to develop lipid-based delivery systems capable of improving GEM's therapeutic performance by combining it with DSF, a repurposed drug with anti-cancer potential, in a synergistic liposomal formulation.

Specific Objectives

- Design and prepare liposomes encapsulating GEM or its lipophilic prodrug, GEM-C18.
- Evaluation and comparison of *in vitro* toxicity of the free drugs and the liposomal formulations.
- Combining free drugs and liposomal formulations with DSF.
- Find a synergy among these drugs combinations.

Highlights of the Article

- The study demonstrated the successful preparation of stable liposomal systems encapsulating GEM or GEM-C18, which resulted in the controlled release of the drugs.
- Combining GEM or GEM-C18 free drugs with DSF enhances anticancer activity and may help overcome chemoresistance mechanisms in pancreatic cancer.
- Liposomal formulations may require extended exposure times in PANC-1 cells to achieve enhanced efficacy when administered in combination with DSF.

Study of synergistic tumor toxicity in pancreatic cancer cells through liposomal drug combination therapy

Valeria Bincoletto[a], Ilaria Andreana[a], Federico Cesano[b], Tania Limongi[a], Barbara Rolando[a], Barbara Stella[a], Giorgia Urbinati[c,d*], Silvia Arpicco[a*]

[a] Department of Drug Science and Technology, University of Turin, Via P. Giuria 9, 10125, Turin, Italy

[b] *Department of Chemistry and NIS Interdepartmental Centre, University of Turin & INSTM-UdR, Via P. Giuria 7, 10125, Turin, Italy*

[c] Université Paris Cité, CNRS, INSERM, UTCBS (https://utcbs.u-paris.fr/), 4 avenue de l'Observatoire, F-75006, Paris

[d] Université Paris-Saclay, UMR CNRS 9018, Institut Gustave Roussy, 94805 Villejuif, France

[*]Corresponding authors e-mail address: silvia.arpicco@unito.it; giorgia.urbinati@u-paris.fr

Abstract

Pancreatic cancer is a highly lethal malignancy, frequently diagnosed at an advanced stage due to its asymptomatic progression and the lack of effective screening methods. Gemcitabine has long been the standard chemotherapeutic agent for pancreatic cancer treatment, although its clinical efficacy is limited by rapid degradation and the occurrence of drug resistance. In this study, liposomal formulations were developed to deliver gemcitabine and its lipophilic prodrug 4-(*N*)-stearoyl-gemcitabine, and combined with disulfiram, a repurposed drug known to inhibit aldehyde dehydrogenase and P-glycoprotein-mediated drug efflux, thereby enhancing the cytotoxic effects of chemotherapy. The formulations were characterized in terms of size, polydispersity index, zeta potential, encapsulation efficiency, and drug release profile. 4-(*N*)-stearoyl-gemcitabine-loaded liposomes exhibited a more sustained release profile compared to gemcitabine-loaded liposomes. Moreover, the combination with disulfiram significantly augmented the *in vitro* efficacy of gemcitabine in resistant pancreatic ductal adenocarcinoma cell line (PANC-1), and the synergistic effect was observed through MTT assays and confirmed by the combination index analysis. These findings support the potential of combining lipophilic prodrugs in nanocarrier systems with repurposed agents as a promising strategy to improve therapeutic outcomes in pancreatic cancer.

Keywords

Pancreatic cancer; gemcitabine; disulfiram; liposomes; synergism.

1. Introduction

Pancreatic cancer (PC) is a particularly challenging and deadly form of cancer. Often described as a "silent" disease due to its asymptomatic onset and rapid progression, PC is

typically diagnosed at an advanced stage, contributing to its poor prognosis [1]. Its high metastatic potential and the late appearance of non-specific symptoms-such as jaundice, weight loss, abdominal pain, and digestive disturbances-further complicate early diagnosis [2]. The challenges associated with the early detection of PC are further exacerbated by the absence of reliable screening methods and the deep location of the pancreas, which makes it difficult to assess through routine imaging. Despite advancements in medical research, the survival rate for PC remains low [3]. Numerous chemotherapeutic agents have been explored for PC treatment, yet therapeutic progress has been hampered by the tumor intrinsic resistance mechanisms. Standard chemotherapeutics such as gemcitabine (GEM) and 5-fluorouracil (5-FU) are routinely used, although with limited clinical benefit [4]. In the clinical management of PC, combination chemotherapy regimens have demonstrated superior efficacy in comparison to monotherapy. Two common protocols are FOLFIRINOX (5-FU, leucovorin, irinotecan, and oxaliplatin) and nab-paclitaxel/GEM. FOLFIRINOX has improved survival, especially in patients with good performance status, but has more toxicity. Nab-paclitaxel/GEM is more tolerable but remains a standard first-line treatment for patients who may not tolerate intensive regimens. These combination treatments are the current mainstay of therapy for advanced PC [5]. Given the toxicity of the current treatment modalities, there is an imperative to explore alternative therapeutic interventions. Novel targeted therapies aim to block specific molecular pathways involved in cancer cell proliferation, although their success has been inconsistent. Moreover, recent advancements in nanoparticle-based drug delivery systems show promise in enhancing the effectiveness of existing treatments while reducing side effects. Ongoing research continues to explore new drug combinations and precision medicine approaches to improve outcomes for PC patients [6].

GEM has been a fundamental component in the therapeutic management of PC for an extended period. As a nucleoside analog, GEM functions by hindering DNA synthesis, thereby preventing cancer cells from replicating. While GEM has demonstrated some degree of efficacy in enhancing overall survival and ameliorating symptoms in patients with PC, its benefits are frequently minimal, and resistance to the drug can occur within few months. As a result, there is a need for ongoing research to identify ways to enhance the efficacy of GEM, including combination therapies and strategies to overcome resistance mechanisms, as synthesis of prodrugs or encapsulation in nanosystems [7-9]. As previously stated, nanomedicine has the potential to address the challenges posed by drug resistance and the efficacy of pharmaceuticals. The field of nanomedicine has attracted considerable interest in

the domain of cancer therapy, owing to its capacity to enhance various pharmacological parameters, including drug absorption, permeability, site-specific targeting, and controlled release. The utilization of nanosystems in this field has the potential to bypass biological barriers, prevent premature drug degradation, and improve cancer diagnosis and treatment [10-12]. In this context, we decided to encapsulate GEM in stealth liposomes and further exploit 4-(*N*)-stearoyl-gemcitabine (GEM-C18), a prodrug previously synthesized by our research group, to overcome the challenges encountered with GEM [13].

With the intent of unrevealing the synergy of new combination therapies, disulfiram (DSF) has garnered attention as a potential repurposed pharmaceutical agent for cancer therapy, including PC. The therapeutic effects of DSF are attributed to its capacity to inhibit the enzyme aldehyde dehydrogenase, which plays a crucial role in the detoxification of reactive aldehydes [14]. Researchers have demonstrated that DSF can augment the cytotoxic effects of chemotherapy drugs such as GEM by sensitizing PC cells to treatment through the inhibition of the P-glycoprotein efflux pump. Furthermore, DSF has been found to disrupt the capability of cancer stem cells to repair DNA damage, a critical process for sustaining tumor growth and resistance to therapy [15, 16]. Nevertheless, a more comprehensive study of DSF was deemed necessary.

In this study, we evaluated the antitumor efficacy of free DSF, its copper complex (DSF/Cu), GEM, and GEM-C18. To address limitations associated with the free forms of GEM and GEM-C18, both were encapsulated in liposomes and characterized for their physicochemical properties. We then tested the combination of these liposomal formulations with free DSF *in vitro*, aiming to enhance cytotoxic activity and overcome drug resistance in PANC-1 pancreatic cancer cells.

2. *Materials and Methods*

2.1 Materials

Fetal bovine serum (FBS) and dimethylthiazol-2-yl-2,5-diphenyltetrazolium bromide (MTT) were purchased from Merck (Saint-Quentin-Fallavier, France). Dulbecco's Modified Eagle Medium (DMEM) culture medium and TrypLE™ Express Enzyme were obtained from Thermo Fisher Scientific (Courtaboeuf, France). Gemcitabine (GEM) was purchased from Trylead Chemical (Tianjin, China). All other reagents were purchased from Merck (Milan. Italy) unless otherwise specified.

4-(*N*)-stearoyl-gemcitabine (GEM-18) was previously synthesized in our laboratory according to the method of Immordino *et al.* [13]. Disulfiram copper complex (DSF/Cu) was prepared according to the method described by Marengo *et al.* [17].

2.2 Liposomes preparation

Gemcitabine-loaded liposomes (LipoGEM) were prepared using the pH gradient method. Liposomes were obtained by mixing chloroform solutions of the lipids 1,2-distearoyl-*sn*-glycero-3-phosphocholine (DSPC)/cholesterol (CHOL)/1,2-distearoyl-*sn*-glycero-phosphoethanolamine-N-[amino(polyethylene glycol)-2000] (PEG-DSPE) in 65:30:5 molar ratio, respectively. The solution was evaporated on a rotary evaporator; the resulting thin film was dried under vacuum overnight and then hydrated with 900 µL of citrate buffer (100 mM, pH 4.5), vortexed, and bath sonicated for 60 min at 60 °C. The formulation was then sequentially extruded (Extruder, Lipex, Vancouver, Canada) under nitrogen onto 400 and 200 nm polycarbonate filters (Costar, Corning Incorporated, NY, USA) at 60 °C. In the following step, the external pH of the liposomal suspension was modified through a gel filtration conducted with a Sepharose® CL-4B column (Merck). This alteration in the external environment was achieved through the elution with [4-(2-hydroxyethyl) piperazine-1-ethanesulfonic acid] (HEPES) buffer (40 mM, pH 7.4). Thereafter, 100 µL of a solution of GEM hydrochloride (5 mg/ml in HEPES buffer) was added dropwise to liposomes suspension under moderate stirring and incubated at 70 °C for 90 min. Unencapsulated GEM was removed by gel filtration as reported above, and the liposomes were then stored at 4 °C. GEM-C18 encapsulating liposomes (LipoGEM-C18) were prepared according to the method described in Immordino *et al.* [13], with modifications. Briefly, LipoGEM-C18 were prepared by the thin lipid film-hydration method by mixing lipids DSPC/CHOL/PEG-DSPE (65:30:5 molar ratio) and 0.5 mg of GEM-C18 in a chloroform solution, which was then evaporated. The resulting film was hydrated with 900 µL of HEPES buffer (40 mM, pH 7.4) and then sequentially extruded as reported above. The resulting suspension was purified from unencapsulated GEM-C18 by gel filtration. Empty liposomes were also prepared for comparison.

2.3 Liposomes characterization

The mean particle hydrodynamic diameter and polydispersity index (PDI) of the liposomes were determined at 25 °C *via* quasi-elastic light scattering (QELS) using a nanosizer (Zetasizer Pro, Malvern Inst., Malvern, UK). The selected angle was 90° and the measurements were performed in triplicate samples diluted 1:10 with MilliQ® water. The

particle surface charge of the preparations was investigated *via* zeta potential measurement at 25 °C using the Smoluchowski equation and the Zetasizer Pro. Each value is the average of three measurements. Phospholipid phosphorous was assessed in each liposome preparation by phosphate assay after destruction with perchloric acid [18].

The amount of encapsulated drugs (GEM and GEM-C18) was determined by reverse phase-high performance liquid chromatography (RP-HPLC). HPLC analyses were performed on an HP 1200 chromatograph system (Agilent Technologies, Palo Alto, CA, USA) equipped with an injector (Rheodyne, Cotati, CA, USA), a quaternary pump (model G1311A), a membrane degasser (model G1322A), a multiple wavelength UV detector (MWD, model G1365D) and a fluorescence detector (FL, model G1321A) integrated into the HP1200 system. Data were processed using a HP ChemStation system (Agilent Technologies). The analytical column selected for LipoGEM and LipoGEM-C18 was an AQUASIL C18 (200 × 4.6 mm, 5 µm; Thermo). The injection volume was 20 µL (Rheodyne). LipoGEM-C18 was diluted 1:10 with acetonitrile to extract the incorporated drug, sonicated, vortexed, and filtered through 0.45 µm PTFE filters (Alltech, Nicholasville, KY, USA) and immediately analyzed by HPLC. The mobile phase consisted of acetonitrile (CH_3CN) 0.1% trifluoracetic acid (TFA, solvent A) and water 0.1% TFA (solvent B) at a flow rate of 1 mL/min with gradient conditions: 10% A until 4 min, from 10 to 90% A between 4 and 10 min, 90% A between 10 and 20 min, and from 90 to 10% A between 20 and 25 min. The column effluent was monitored at 250 nm and 292 nm wavelengths. LipoGEM was diluted 1:10 in a mixture of CH_3CN/water 0.1% TFA, 50/50 v/v to extract the incorporated drug, sonicated, vortexed, filtered through o.45 µm PTFE filters (Alltech) and immediately analyzed by HPLC. The mobile phase consisted of CH_3CN 0.1% TFA (solvent A) and water 0.1% TFA (solvent B), at flow rate of 0.5 mL/min with gradient conditions: from 10 to 40% A in 5 min, and 40% A between 5 and 10 min. The column effluent was monitored at 270 nm wavelength.

The entrapment efficiency (EE%) of the liposomes was calculated as the ratio between the drug-to-lipid molar ratio after purification and the drug-to-lipid molar ratio measured after extrusion.

The drug release was evaluated for all formulations by incubation at 37 °C in HEPES buffer. Aliquots of 100 uL were withdrawn after several time intervals (0, 1, 3, 5, 24, 48, and 72 h) and purified through chromatography on Sepharose CL-4B columns, eluting with HEPES buffer. Subsequently, an analysis of the drug and lipid content was conducted on the collected fractions. Liposomes were assessed also for their drug release in FBS (0, 1, 3, 5, 24, and 48 h), by diluting the sample in a 1:1 volume ratio (liposomes:FBS) after

purification. Subsequently, the procedure remains unchanged from that previously reported for incubation in HEPES buffer.

The physical stability of liposomes under storage conditions (4 °C) was assessed by measuring the diameter, zeta potential, and drug leakage at various interval times (0, 1, 2, 3, 4 weeks).

Differential scanning calorimetry (DSC) analysis was carried out on liposomal formulations using a Q200 DSC (TA Instruments, New Castle, DE). Approximately 15 mg of sample suspensions were introduced into a 40 uL aluminum pan and subsequently analyzed. DSC runs were conducted from 25 °C to 80 °C at a heating rate of 5 °C/min under a constant nitrogen flow (50 mL/min). The main transition temperature (Tm) was determined as the onset temperature (T_{onset}) of the highest peak.

2.4 Cell cultures

Human pancreatic cancer PANC-1 cells were kindly provided by Dr. Nazanine Modjtahedi's laboratory. Cells were maintained in DMEM high glucose, supplemented with 10% (v/v) FBS and 1% (v/v) penicillin-streptomycin. Cultures were incubated at 37 °C in a humidified atmosphere with 5% CO_2. Mycoplasma contamination was routinely monitored using a commercial detection kit.

2.5 MTT assay

MTT assays were conducted to assess the dose-response effect of the free drugs and their combinations. PANC-1 cells were seeded at 3×10^3 cells/well and treated the next day with the following treatments: GEM, GEM-C18, DSF or DSF/Cu in the free form. Empty liposomes, LipoGEM, LipoGEM-C18 and the combination of GEM and GEM-C18 free drugs or liposomal formulations with DSF were also evaluated. The concentrations of GEM and GEM-C18 free drugs and in liposomal formulations were spanning from 0.0025 to 10 µM, and from 0.01 to 10 µM for DSF and DSF/Cu free drugs. Following 72 h from the treatment, thiazolyl blue tetrazolium bromide (MTT) was prepared at a concentration of 5 mg/mL in 1x PBS and was utilized for this assay. MTT (5 mg/mL, 20 µL per well) was added directly to all the wells. The plates were then incubated at 37 °C for 2 h. Thereafter, the MTT and medium were removed, and 200 µl of dimethyl sulfoxide (DMSO) were added to each well and mixed gently for 15 min using a shaker. Finally, the plates were read on a multimode plate reader (Multiplate Reader Infinite Pro 200, Tecan) at 570 nm. Dose-response curves were obtained with Prism 9. Each assay was performed in quadruplicates and repeated three to four times. Results are expressed as mean ± standard deviation (SD). Non-parametric

statistical test Kruskal Wallis and multi-comparison test Dunn's were applied to identify significative differences.

2.6 Determination of Combination Index

To examine potential synergistic, additive or antagonist effects of GEM/GEM-C18 combined with DSF, all data obtained by the MTT test were analyzed using the CompuSyn software 1.0 by the Chou–Talalay method [19]. The Combination Index (CI) was then calculated using the following classic isobologram equation:

$$CI = \frac{D1}{(Dx)_1} + \frac{D2}{(Dx)_2}$$

where $(Dx)_1$ and $(Dx)_2$ are the individual doses of GEM/GEM-C18 and DSF required to inhibit a given level of viability (y), and D1 and D2 are the doses of GEM/GEM-C18 and DSF required to inhibit the same level of viability (x) in combination. The CI values facilitate the determination of whether the combination exerts an antagonistic effect (CI > 1) or a synergistic effect (CI < 1). The CI value of 1 represents additive effect.

3. Results and discussion

GEM is a first-line chemotherapeutic agent for PC; however, its clinical efficacy is limited by rapid systemic degradation and the emergence of resistance. To address these challenges, strategies such as nanoformulation, prodrug synthesis, and combination therapies have been investigated to enhance stability, improve tumor targeting, and overcome resistance mechanisms [20].

In this study, the cytotoxic activity of GEM, its lipophilic prodrug GEM-C18 (previously synthesized in our laboratory [13]), DSF, and the DSF/Cu complex was evaluated *in vitro* using PANC-1 pancreatic cancer cells. These strategies are based on the experience of our group on the delivery of compounds for the treatment of pancreatic cancer, as reported in different papers [17, 21-23]. As a first step, each compound was tested individually to determine its half-maximal inhibitory concentration (IC_{50}) and to identify suitable doses for subsequent combination experiments. Based on these results, selected combinations of GEM or GEM-C18 with DSF were investigated to assess potential synergistic effects.

Following this, GEM and GEM-C18 were encapsulated in liposomes, which were physico-chemically characterized. These liposomal formulations were then evaluated in combination with DSF on PANC-1 cells, using concentrations identified as most promising in previous studies [17, 24].

3.1 Preparation and characterization of liposomes

To enhance the efficacy of GEM in addressing PC and to overcome the resistance exhibited by the pancreatic cell line PANC-1, liposomes containing GEM or GEM-C18 were developed. A range of preparation methods and phospholipid mixtures were assessed to identify the most effective encapsulation strategy for GEM (Table 1). In total 7 formulations were investigated, changing lipids, lipid ratios and method of preparation. Formulation 3 was identified as the optimal solution, as it demonstrated the highest degree of reproducibility in terms of physico-chemical characteristics and EE%. This was achieved through the utilization of citrate buffer and an incubation period of 90 min at a temperature of 70 °C.

Table 1. Summary of liposomal formulations investigated for LipoGEM.

Formulation	**Lipids (molar ratio)**	**Method of preparation**	**Temperature of drug loading incubation (°C)**	**Incubation time (min)**
1	DSPC:CHOL:PEG-DSPE 75:20:5	Ethanol injection	50/75	60
2	DSPC:CHOL:PEG-DSPE 56.5:38.5:5	Ethanol injection	60	60
3	DSPC:CHOL:PEG-DSPE 65:30:5	pH gradient citrate/sulfate	60/70	30/60/90/120
4	DPPC:CHOL:PEG-DSPE 65:30:5	pH gradient citrate/sulfate	45	30/60
5	DSPC:CHOL:PEG-DSPE 75:20:5	pH gradient citrate/sulfate	60	30/60
6	DPPC:CHOL:PEG-DSPE 75:20:5	pH gradient citrate/sulfate	45	30/60
7	DSPC:CHOL:PEG-DSPE 65:30:5	Ethanol injection	75	60

In order to develop two analogous and straightforward formulations, the identical lipid composition was selected for both LipoGEM and LipoGEM-C18. The DSPC is the phospholipid chosen as the main component of these formulations because of its long,

saturated acyl chains and high phase transition temperature, which impart rigidity to liposome membranes. In fact, its phase transition is around 54 °C, which is higher than human body temperature (37 °C). This means that at physiological temperature, membranes made from DSPC remain in the gel state, characterized by an ordered and rigid arrangement of lipids [25]. In addition, CHOL was added in an important amount to achieve more stable liposomes with reduced drug release. Moreover, in literature is reported that the replacement of phosphatidylglycerol (PG) with PEG has been demonstrated to enhance the plasma half-life of the liposomes [26]. It has been found to prevent the liposomes from being recognized by the immune system, thereby reducing premature drug release [27, 28]. This is the rationale behind the decision to formulate liposomes with PEG, with the assumption that future pharmacokinetic studies could confirm the findings reported in the literature.

Given the hydrophilic nature of GEM, it was encapsulated within the aqueous core of liposomes using the pH gradient method. Under the acidic conditions established by the citrate buffer inside the core, the amino group of GEM becomes protonated. Upon protonation, GEM is expected to form an insoluble salt with citrate ions, which helps to retain the drug within the liposomal *core* by preventing its diffusion across the phospholipid bilayer. [29]. In the case of the LipoGEM prepared in our laboratory, achieving this ideal situation was more complicated. The explanation for this phenomenon lies in the substantial discrepancy between the volumes of the hydration medium and those that are entrapped within the aqueous cavity of the liposome [30, 31]. Conversely, GEM-C18, which is a more hydrophobic molecule, was encapsulated in the phospholipid bilayer. Contrary to the liposomes with GEM-C18 that had been previously prepared by Immordino *et al*. [13], the formulation under investigation is characterized by an increased amount of CHOL within the phospholipid bilayer in order to improve the stability of the formulation, as previously reported [32].

As a result, the EE% achieved for LipoGEM was around 20%, which is much lower than that of LipoGEM-C18 (around 95%). The underlying reason for this phenomenon is most likely attributable to the fact that GEM is a weak base, with a pKa of 3.6, which is probably not sufficient to allow high ionization at the pH of the buffer used, unlike, for example, liposomal doxorubicin. Consequently, the proportion of GEM that will not be protonated is likely to rapidly diffuse from the liposomes, resulting in low encapsulation efficiency [33]. The decision of our research group to employ the method for the preparation of liposomes was informed by our experience. Despite the relatively low EE%, the quantity of encapsulated GEM is adequate for the characterization and the further *in vitro* studies on cell

lines. The result obtained in this study is consistent with the findings reported in the literature; in studies employing a pH gradient for the preparation of liposomes, the EE% has been observed to be less than 20%, which is the value that is obtained with LipoGEM [13, 34, 35]. Numerous other studies have obtained EE% levels significantly higher than this (between 50 and 98%), yet these employed divergent methodologies from the pH gradient method. These methods encompass the use of ethanol injection [36], hydration of the lipid film [37], and a combination approach involving a pH gradient, followed by freezing and thawing or small volume injection [33, 38].

Conversely, the high lipophilicity of GEM-C18, due to the presence of the stearoyl moiety, facilitates its insertion into the phospholipid bilayer. This allows for the formation of hydrophobic interactions with the lipid chains, resulting in high encapsulation efficiency and improved formulation stability [39].

All the formulations were characterized in terms of size (< 170 nm), zeta potential (around -30 mV) and polydispersion index (PDI) (< 0.2), summarized in Table 2. Despite the different methods employed in the preparation of LipoGEM and LipoGEM-C18, the results showed that their sizes do not change significantly. This is presumably because GEM-C18 does not influence the size of the system; on the other hand, GEM is added after liposome formation and, being encapsulated in the aqueous core, again it does not change the size. Consequently, the mean size of loaded liposomes does not differ from the size of empty liposomes. Regarding the zeta potential, LipoGEM and empty liposomes exhibit a slightly lower negative charge than LipoGEM-C18. This observation suggests that GEM-C18 may interact with phospholipids in the bilayer, affecting the packing and orientation of molecules at the surface and thus modifying the zeta potential value [40].

Table 2. Characteristics of liposomal formulations (means ± SD, n=3).

	mean size (nm) ± SD	**PDI**	**zeta potential (mV) ± SD**	**EE* (%) ± SD**
Empty liposomes	157 ± 3	0.112	-26.8 ± 0.1	/
LipoGEM	165 ± 2	0.123	-27.8 ± 0.4	20 ± 5
LipoGEM-C18	163 ± 1	0.131	-31.0 ± 0.3	95 ± 1

* Entrapment efficiency (EE): ratio between drug/lipid molar ratio after purification and drug/lipid molar ratio after extrusion.

The drug release of all the formulations was evaluated in HEPES buffer (40 mM, pH 7.4) at 37 °C. Aliquots were withdrawn from each sample, purified from the released drug by gel

chromatography and the residual drug and lipid content were subjected to quantification. As reported in Figure 1A, the release of drugs from liposomes occurs in a gradual manner. The controlled release of drugs from liposomal systems is a key strategy for enhancing the therapeutic performance of anticancer agents that suffer from rapid deamination and a short plasma half-life [41]. The sustained release of drugs facilitated by liposomes enables the prolongation of systemic circulation and the guarantee of sustained exposure of tumor tissues to the active compound. This approach has been shown to enhance bioavailability and to minimize peak plasma concentrations, thereby reducing systemic toxicity [42]. Furthermore, a key objective of this study was to evaluate the combination of GEM and GEM-C18 with DSF *in vitro*. It was hypothesized in the research that DSF may be the first to interact with the tumor cell, acting against the cellular resistance mechanism by blocking P-glycoprotein (P-gp), a drug efflux pump [43]. This strategy may enhance the intracellular accumulation of GEM or GEM-C18 following their release from liposomes. In addition, PC cells often acquire chemoresistance by maintaining low intracellular levels of reactive oxygen species (ROS) through the upregulation of antioxidant defense mechanisms. Elevating ROS levels has been shown to restore GEM sensitivity, indicating that redox modulation could be a promising approach to overcome drug resistance. Literature studies have demonstrated that DSF can modulate ROS production, thereby promoting apoptosis and enhancing the antitumor activity of both GEM and GEM-C18 [44].

In our study, GEM showed a fast release from liposomes (50% of the drug was released after 3 h at 37 °C). The release profile of GEM-encapsulating liposomes was studied for a longer period (72 h) when compared to some other studies: for instance, Aparicio-Lopez *et al.* assessed the release of GEM from liposomes for a short period of time, *i.e.* 30 min; during this time, the GEM concentration remained almost stable within the liposomes, whereas LipoGEM has been observed to release approximately 20% of the administered drug within the first 30 min [45]. Conversely, Tang *et al.* evaluated the release of GEM from liposomes over a similar time period to that used in our study and obtained analogous profiles, but with a slightly slower release. Indeed, following a 48-hour period, GEM encapsulated in Tang's liposomes retained 40% of its initial value, whereas in our system, it decreased to 20% of the original GEM concentration. However, it is noteworthy that liposomes of the former were prepared using a different method than that employed in our study, and that they explored a different composition of lipids: in this work, Tang's group employed the small volume incubation method and microfluidic technique. Moreover, the lipid composition differs from our study in that it contains additional components such as DOPE (1,2-dioleoyl-

sn-glycero-3-phosphoethanolamine) and CHEMS (cholesteryl hemisuccinate) [46]. In combination with helper lipids such as DOPE, CHEMS contributes to the maintenance of the lamellar structure of the bilayer at neutral pH, thereby preventing premature drug leakage [47].

On the other hand, LipoGEM-C18 showed a slower drug release: after 72 h, only 20% of GEM-C18 was released. The modification of the phospholipid composition in LipoGEM-C18 proved to be advantageous in achieving liposomes that exhibited enhanced stability in comparison to those previously prepared by Immordino *et al*. As reported in the aforementioned study, after an incubation period of approximately 30 h in a buffer solution at a temperature of 37 °C, about 30% of GEM-C18 was released from the liposomes, whereas in our study 20% was released by LipoGEM-C18 after the same period. The observed enhanced stability can be attributed to the incorporation of PEG-DSPE in the formulation, in conjunction with the increased CHOL content, allowing GEM-C18 to interact more strongly with the phospholipid bilayer [13, 39].

To more accurately simulate the behavior of liposomes in a cellular environment, the drug release process was also evaluated in the presence of FBS at 37 °C (Figure 1B). The results demonstrated that GEM and GEM-C18 reached 38% and 66% of the initial concentrations after 3 h and 48 h, respectively, thus confirming the higher stability of LipoGEM-C18 compared to LipoGEM. In comparison with liposomes prepared by Immordino *et al.*, GEM-C18 was released more gradually by LipoGEM-C18. LipoGEM-C18 encapsulated 80% of the initial drug content after 20 h, while liposomes prepared by Immordino approximately maintained 60% of the initial GEM-C18 after the same amount of time. [13].

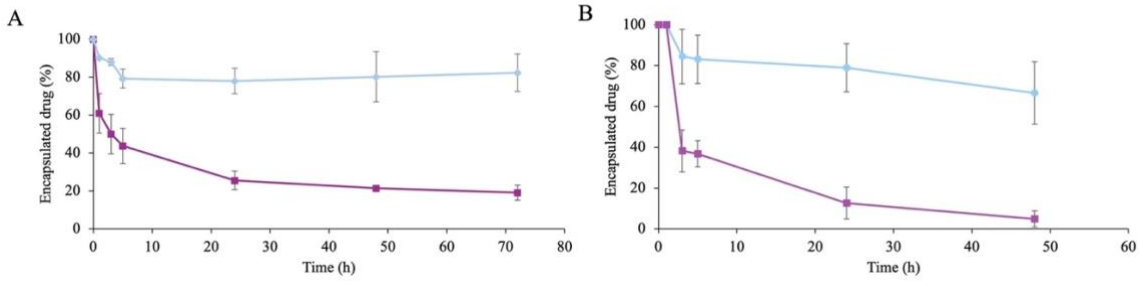

Figure 1. A) *In vitro* release profile of LipoGEM (purple) and LipoGEM-C18 (light blue) in HEPES buffer at 37 °C, at 0, 1, 3, 5, 24, 48, 72 h. Every point is presented as mean ± SD (n=3). B) *In vitro* release profile of LipoGEM (purple) and LipoGEM-C18 (light blue) in FBS at 37 °C, at 0, 1, 3, 5, 24, 48 h. Every point is presented as mean ± SD (n=2).

Furthermore, the stability of all formulations under storage conditions (HEPES buffer at 4 °C) was evaluated and the results showed that LipoGEM maintained their physico-chemical stability for a period of about 28 days, exhibiting minimal size change (< 10% for all formulations) and no aggregation or precipitation. Notably, LipoGEM-C18 exhibit minimal

fluctuations in size after one month, ensuring stability for a minimum of three weeks. Concurrently, the zeta potential remained unaltered for both the formulations for the duration of the study (Figure 2).

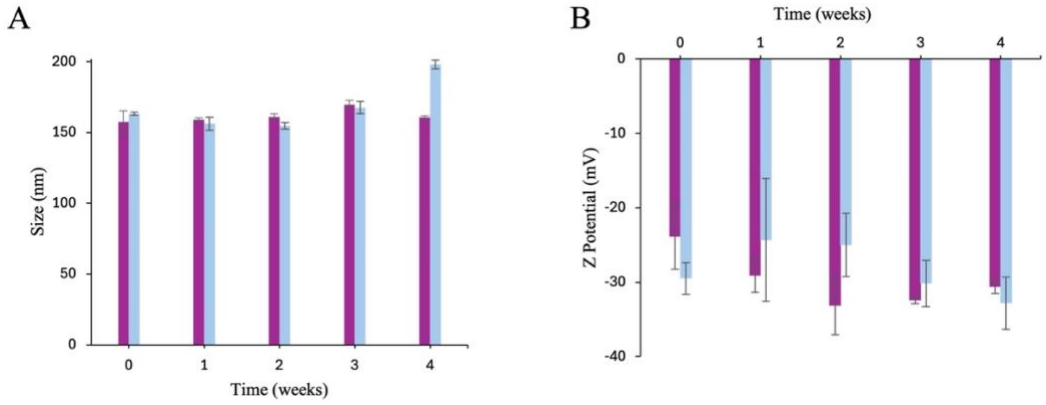

Figure 2. Stability in storage conditions -A) size, B) Z potential- of LipoGEM (purple) and LipoGEM-C18 (light blue) for 0, 1, 2, 3, 4 weeks. Every point is presented as mean ± SD (n=3).

To assess the interactions between GEM-C18 and the liposome membrane, a DSC analysis was conducted (Figure 3). Liposomes are typically analyzed in the absence of CHOL. This method enables the observation of the thermotropic phase transition of the phospholipid bilayer with enhanced clarity. CHOL has demonstrated to modulate the membrane fluidity and disrupt the cooperative behavior of phospholipid acyl chains, resulting in the broadening or complete suppression of the main phase transition peak. Therefore, the utilization of cholesterol-free systems enables a more precise assessment of thermal parameters [48].

The thermogram of pure DSPC presented the main transition, related to the passage from the ripple gel phase (Pβ) to the lamellar liquid–crystalline phase (Lα), at T_{onset} 54.5 °C. Upon incorporation of GEM-C18, the main transition was shifted to lower temperatures (T_{onset} 53.9 °C), and a substantial broadening of melting temperature peaks was observed. This finding indicates that GEM-C18 interacts with the phospholipid bilayer through hydrophobic interactions, thereby perturbing the phase transition behavior [39]. The subsequent addition of PEG-DSPE brought about a negligible lowering of the peak, T_{onset} 53.8 °C. In conclusion, these DSC results confirm that GEM-C18 prodrug intercalates into the DSPC bilayer and makes the lipid transition less coordinated, whereas PEG-DSPE only slightly changes the transition temperature.

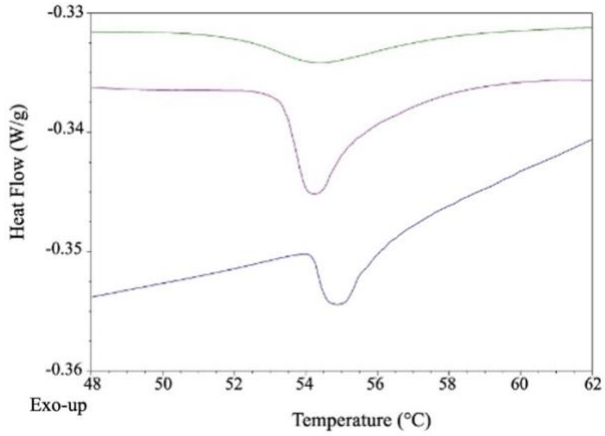

	T_{onset} (°C)
DSPC	54.5
DSPC/GEM-C18	53.9
DSPC/GEM-C18/PEG-DSPE	53.8

Figure 3. DSC thermograms of pure DSPC (blue line), DSPC/PEG-DSPE/GEM-C18 (purple line), and DSPC/PEG-DSPE (green line).

3.2 Cell viability tests by MTT assay

First, GEM, GEM-C18, DSF and DSF/Cu were tested on the GEM resistant pancreatic cancer cell line PANC-1 to determine the IC_{50} at 72 h (Table 3). The GEM and GEM-C18 concentrations were spanned from 0.0025 to 10 µM, DSF and DSF/Cu concentrations from 0.01 to 10 µM. A particularly noteworthy element of this study concerns the different responsiveness of the cells observed when GEM and its prodrug GEM-C18 were administered. Indeed, GEM attains a plateau of efficacy starting from 0.25 µM up to the highest tested concentration (10 µM), precluding the calculation of a specific IC_{50} at 72 h. This result was expected as PANC-1 cells are known to be resistant to GEM [49]. Interestingly, GEM-C18 exhibits a more pronounced and linear toxicity profile, enabling the calculation of the IC_{50}: 3.17 µM. This phenomenon can be attributed to the incorporation of a lipophilic chain, which may promote drug internalization and bypass the drug uptake limiting step often correlated with GEM-resistance. The cell line also responded differently to DSF and its complex DSF/Cu. The viability of the cells treated with DSF presented a biphasic profile. The decreased cell viability at lower concentrations was followed by a subsequent recovery phase at higher concentrations to further diminish at the highest concentration (10µM) (data not shown). In the existing literature, DSF has demonstrated a biphasic cytotoxic response, characterized by an initial reduction in cell viability, subsequently followed by an increase [50]. This observation suggests that the interaction between DSF and the cellular mechanisms that govern cellular survival and death is a complex phenomenon. The biphasic response may be attributed to the activation of cellular stress pathways. The unfolded protein response, for instance, can lead to autophagy, process which promotes cell survival under conditions of stress. This finding potentially explains the observed recovery in cell viability following the initial cytotoxic effect. By contrast, DSF/Cu

achieves considerably lower IC_{50} values than conventional DSF. However, its toxicity level is so high when administered as a single agent that combining it with GEM may result in low tolerability and unacceptable toxicity in clinical practice. Indeed, multi-drug regimens that are less toxic and more tolerable are needed for patients with fragile overall health. Consequently, it may not be the most optimal pharmaceutical agent for co-administration. The aim of this study is to identify combinations that are as or more effective than single agents, while reducing the concentration of each drug to keep low the toxicity profile. Therefore, we concentrated the studies on the combination of GEM and GEM-C18 with DSF, rather than pursuing with the DSF/Cu complex.

Table 3. IC_{50} of free GEM, GEM-C18, DSF and DSF/Cu on PANC-1 cell line at 72 h.

Drug	IC_{50} (μM)
GEM	>10
GEM-C18	3.17
DSF	5.11
DSF/Cu	0.12

Once the efficacy profiles of the free drugs on PANC-1 have been established, their effect in combination was investigated. The GEM and GEM-C-18 were combined with DSF, to identify possible additive or synergistic effects. For this, four concentrations of each drug were selected, which represented the range of cell viability impairment, spanning from 80 to 20%. In the case of GEM specifically, as the cell viability never fell below 50%, two of the four concentrations were selected from the beginning (0.025 μM) and the end (10 μM) of the viability plateau. Precisely, the concentrations chosen for DSF, GEM and GEM-C18 are 10, 5, 1, 0.1 μM; 10, 0.025, 0.015, 0.005 μM and 2.5, 0.5, 0.05, 0.005 μM, respectively. The combination of GEM and DSF decreased the cell viability more efficiently than the single agents and the most promising results were observed when GEM was combined with DSF at 1 and 0.1 μM (Figure 4A and Figure 4B respectively). The cell viability values were also analyzed with the Compusyn software, showing Combinatory Index (CI) lower than 1 which corresponds to synergetic behavior between all the combinations included in Figure 4 (Table S1). On the contrary, the combination of GEM with high doses of DSF (10 and 5 μM) did not reveal any synergy effect, as expected, because the DSF alone is already highly potent (Figure S1). The combinations which were detected statistically different when

compared to the single free drugs were the following: DSF 1 μM with GEM 0.025 or 0,015 μM or 10 μM and DSF 0.1 μM with GEM 0.015 μM. Therefore, we succeeded in identifying lower GEM and DSF concentrations while preserving the antitumor efficacy to mitigate potential adverse effects. The circles surrounding the statistical symbols in Figure 4 represent the synergetic and most relevant concentrations of GEM and DSF to be combined in terms of therapeutic significance.

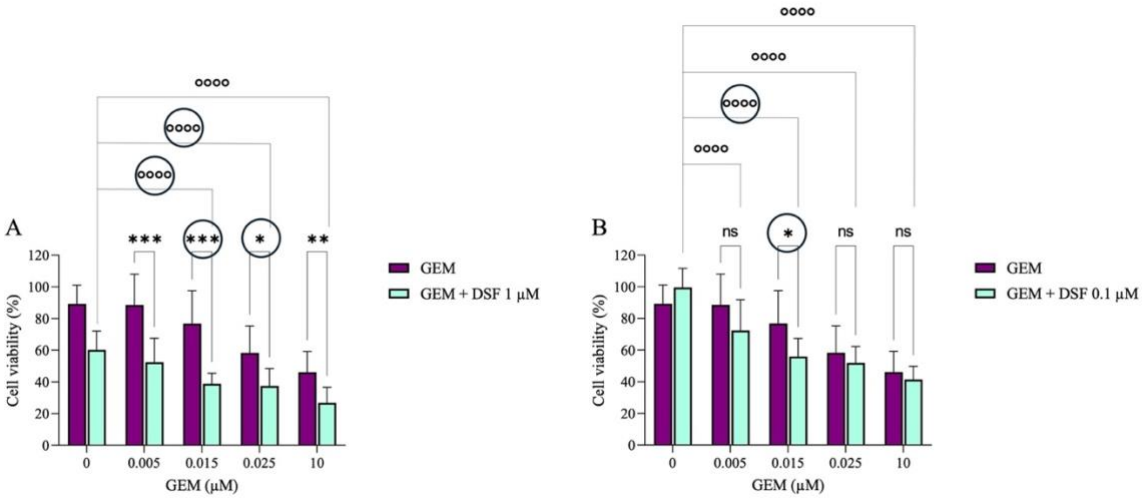

Figure 4. Cell viability on PANC-1 cells when treated with GEM combined with DSF at A) 1 μM or B) DSF 0.1 μM, after 72 h. Data are presented as means ± SD (n=3). *p <0.1; **p <0.05, ***p <0.01: *vs* GEM alone; °p <0.1; °°p <0.05, °°°p <0.01, °°°°p<0.001: *vs* DSF alone. O = the synergetic and most relevant concentrations of GEM and DSF to be combined for therapeutic purposes.

Regarding the combination of GEM-C18 with DSF, synergetic effects were observed when DSF was administered at both 1 and 0,1 μM (Figure 5). Even though, to obtain not only synergetic but also statistical different results, drugs must be combined with GEM-C18 at the concentrations of 2.5, 0.5 and 0.05 μM and DSF at a concentration of 1 μM. The combination of GEM-C18 with DSF 10 μM and 5 μM did not give significative results as shown in Figure S2.

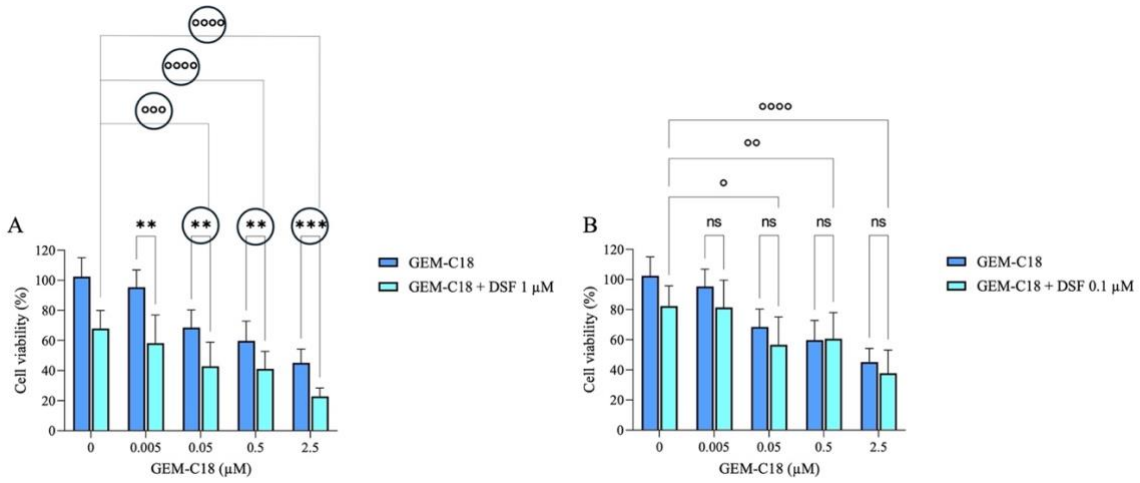

Figure 5. Cell viability on PANC-1 cells of GEM-C18 and DSF -A) DSF 1 μM, B) DSF 0.1 μM- in combination, after 72 h. Data are presented as means ± SD (n=3). *p <0.1; **p <0.05, ***p <0.01: vs GEM-C18 alone; °p <0.1; °°p <0.05, °°°p <0.01, °°°°p<0.001: vs DSF alone. O = the synergetic and most relevant concentrations of GEM and DSF to be combined for therapeutic purposes.

The drugs combinations that were previously identified as synergetic and statistically different from the single agents were then considered when GEM and GEM-C-18 were encapsulated in liposomes to study their efficacy on the same cell line.

The cell viability test on liposomes yielded results that are different with respect to the free drugs.

The lowest concentration of LipoGEM (0.015) when combined with DSF at 1μM is statistically different only from LipoGEM (Figures 6A). No statistical difference is observed toward free GEM and DSF, and there is no synergy. When increasing the dose of LipoGEM at 0.025μM combined with DSF 1μM, the statistical differences remain the same as those described above, but a slight synergism begins to appear. Finally, when LipoGEM is administered at 0.25 μM combined with DSF 1μM, this combination becomes statistically different with respect to both LipoGEM and the single free drugs. Furthermore, the CI assumes the remarkable value of 0.7.

Overall, the lowest concentrations of liposomal GEM combined with DSF are not synergistic and are only statistically different from lipoGEM. However, when increasing the doses of liposomal Gem combined with DSF, the results gradually become more statistically different not only from the encapsulated molecule but also toward the free drugs. Of the same manner, the combinatory index of synergy is also increasingly pronounced as the doses of LipoGEM increase (Table S1).

We hypothesize that this behavior is the result of slow release of the drug from its liposomal form as shown previously in Figure 1. In fact, although the administered doses are

equivalent, the GEM released from the liposomes is lower, resulting in reduced efficacy that yet should be prolonged over a longer period of time. The dose-response profiles when comparing free Gem and LipoGEM corroborate this hypothesis (Figure S3). As a matter of fact, the first concentration at which the efficacy of the encapsulated drug is equivalent to that of the free molecule (0.25 µM), yields statistically significant and synergistic results (Figure 6A).

When LipoGEMs are associated with a lower concentration of DSF (Figures 6B), the delayed release of GEM by the liposomes greatly influences the efficacy of the combination, and we can only mention a statistical difference given by the combination LipoGEM (0.25µM) + DSF 0.1µM toward DSF 0.1µM as single agent and a strong CI of 0.48.

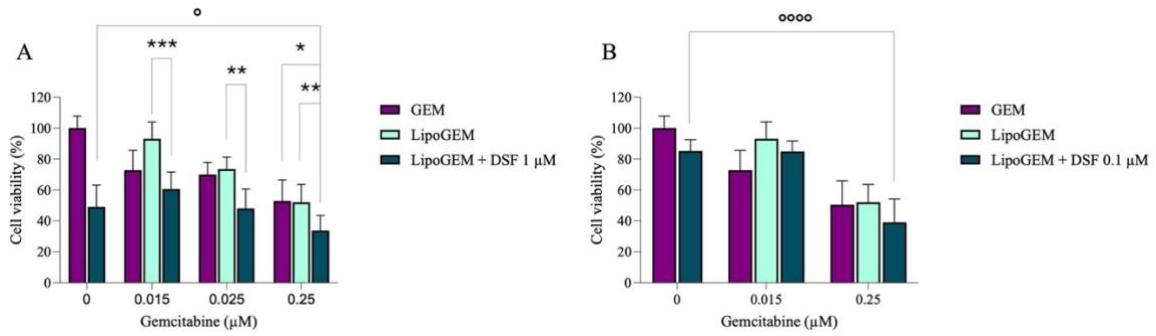

Figure 6. Cell viability on PANC-1 cells of LipoGEM and DSF 1 µM (A) and 0.1 µM (B) in combination, after 72 h. Data are presented as means ± SD (n=3). *p <0.1; **p <0.05, ***p <0.01, ****p <0.001: *vs* GEM or LipoGEM alone; °p <0.1; °°p <0.05, °°°p <0.01, °°°°p<0.001: *vs* DSF alone.

The effect of sustained release on the impairment of cellular viability is even more pronounced in combinations that include LipoGEM-18 because the release profile of the molecule is even slower for LipoGEM-C18 than for LipoGEM (Figure 1B). Figure 7 shows that the combination with the best CI and statistical difference toward LipoGEM-C18 and DSF as single agents is the combination of LipoGEM-C18 (2.5µM) with DSF at 1µM. The LipoGEM-C18 probably releases too little drug to achieve a statistically different effect compared to the free GEM. Although, an onset of synergy already occurs at the combination LipoGEM-C18 (0.5µM) with DSF at 1µM straightening the interest of combining liposomal GEM with DSF.

These findings could substantiate the hypothesis that liposomes, with their controlled and slow-release mechanism, necessitate a more protracted exposure period to attain an effect that is commensurate with or exceeds that of equivalent free drugs at equivalent concentrations. On the other hand, the sustained release of the drug, is particularly needed to preserve the integrity of the drug over time. In fact, it is imperative to acknowledge the inherent fragility of GEM, which is rapidly metabolized in more complex systems, such as

the organoids, bloodstream, and generally *in vivo*. In such contexts, the potential of liposomes to enhance GEM's protective properties is likely to be more pronounced, thereby underscoring their effectiveness.

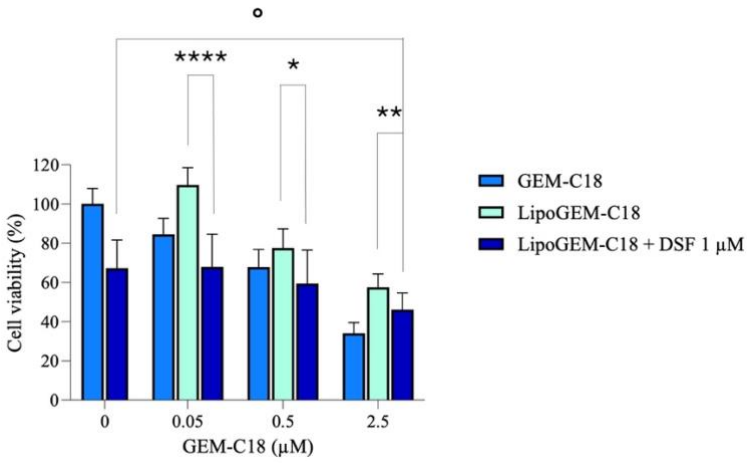

Figure 7. Cell viability on PANC-1 of LipoGEM-C18 and DSF in combination, after 72 h. Data are presented as means ± SD (n=3). *p <0.1; **p <0.05, ***p <0.01, ****p <0.001: *vs* LipoGEM-C18 alone; °p <0.1; °°p <0.05, °°°p <0.01, °°°°p<0.001: *vs* DSF alone.

4. Conclusions

The objective of this study was multifaceted: to assess the effectiveness of combining anti-cancer drugs, namely GEM and its prodrug GEM-C18, with DSF, a drug that has recently been repurposed as an anti-cancer agent; to prepare and characterize GEM and GEM-C18 encapsulation liposomes to increase drugs half-life and protect the drugs from biological environment degradation; to investigate the potential of encapsulating the drugs in liposomes to enhance their efficacy. The encapsulation of GEM and GEM-C18 in liposomes was generally successful, facilitating enhanced transport and protection of the drugs, thereby ensuring controlled release. A synergistic effect of combining GEM- or GEM-C18-free drugs with DSF was demonstrated, resulting in an increased cell viability impairment when compared to drugs administered alone in the GEM-resistant cell line PANC-1. Conversely, the efficacy of liposomes combined with DSF was more difficult to determine, only reaching significance at the highest tested concentrations. It is hypothesized that the controlled release of the GEM from liposomes results in a lower concentration of the active ingredient at 72 h compared to free drug. Liposomes will be tested over extended periods, and the effects on more complex models, such as spheroids and organoids, will be examined to ascertain the potential of the protection provided by the liposomes and the resulting therapeutic outcomes. Furthermore, the liposomes have the potential to be functionalized with an active targeting

agent in order to achieve enhanced internalization and, consequently, further improve the efficacy.

Aknowlegments

The research was supported by the Italian Ministry of University and Research - University of Turin “Fondi Ricerca Locale (ex-60%)”. B.V. is the recipient of a fellowship from the Italian Ministry of University and Research. The authors gratefully acknowledge Dr. Nazanine Modjtahedi (Unité Physiopathologie et Génétique du Neurone et du Muscle, UMR CNRS 5261, Inserm U1315, Université Claude Bernard Lyon 1, Lyon, France) for kindly providing the PANC-1 pancreatic cancer cell line and for her helpful suggestions and scientific inspiration, which guided our research.

Declaration of interests

Declarations of interest: none.

Authors contribution

Valeria Bincoletto: Roles/Writing - original draft; and Writing - review & editing, Data curation, Formal analysis, Investigation, Validation. **Ilaria Andreana:** Data curation, Writing - review & editing. **Federico Cesano:** Data curation, Investigation, Software, Writing - review & editing. **Tania Limongi:** Writing - review & editing. **Barbara Rolando:** Formal analysis, Methodology. **Barbara Stella:** Methodology, Writing - review & editing. **Giorgia Urbinati:** Roles/Writing - original draft; and Writing - review & editing, Conceptualization, Funding acquisition, Resources, Supervision, Data curation, Methodology, Investigation, Validation. **Silvia Arpicco:** Roles/Writing - original draft; and Writing - review & editing, Conceptualization, Methodology, Funding acquisition, Resources, Supervision, Project administration.

References

[1] P.D. Leiphrakpam, S. Chowdhury, M. Zhang, V. Bajaj, M. Dhir, C. Are, Trends in the global incidence of pancreatic cancer and a brief review of its histologic and molecular subtypes, J Gastrointest Cancer. 56 (2025) 71. https://10.1007/s12029-025-01183-2

[2] N. Silvestris, O. Brunetti, A. Bittoni, I. Cataldo, D. Corsi, S. Crippa, M. D’Onofrio, M. Fiore, E. Giommoni, M. Milella, R. Pezzilli, E. Vasile, M. Reni, Clinical practice guidelines for diagnosis, treatment and follow-up of exocrine pancreatic ductal adenocarcinoma: evidence evaluation and recommendations by the Italian Association of Medical Oncology (AIOM), Cancers. 12 (2020) 1681. https://10.3390/cancers12061681

[3] V. D'Ambra, C. Ingaldi, C. Ricci, L. Alberici, G. Capretti, E. Jovine, C.C. Zingaretti, R. Salvia, R. Casadei, Pancreatic cancer and long survivors: a survey of Italian society of oncological surgery (SICO), Updates Surg. 77 (2025) 57-64. https://10.1007/s13304-024-02039-3

[4] P. Fan, L. Liu, Y. Yin, Z. Zhao, Y. Zhang, P.S. Amponsah, X. Xiao, N. Bauer, A. Abukiwan, C.C. Nwaeburu, J. Gladkich, C. Gao, P. Schemmer, W. Gross, I. Herr, MicroRNA-101-3p reverses gemcitabine resistance by inhibition of ribonucleotide reductase M1 in pancreatic cancer, Cancer Lett. 373 (2016) 130-137. https://10.1016/j.canlet.2016.01.038

[5] I. Garajová, M. Peroni, F. Gelsomino, F. Leonardi, A simple overview of pancreatic cancer treatment for clinical oncologists, Curr Oncol. 30 (2023) 9587-9601. https://10.3390/curroncol30110694

[6] X. Zhao, G. Wu, X. Tao, D. Dong, J. Liu, Targeted mitochondrial therapy for pancreatic cancer, Transl Oncol. 54 (2025) 102340. https://10.1016/j.tranon.2025.102340

[7] L. Yan, W. Lu, W. Huang, A.B. Zoa, J. Zheng, M. Qin, J. Du, Q. Xiao, Z. Liu, Y. Tian, A meta-analysis and systematic review of randomized controlled trials in combination gemcitabine with erlotinib in the pancreatic cancer, Chin Clin Oncol. 13 (2024) 66. https://10.21037/cco-24-45

[8] J. Wang, J. Yang, A. Narang, J. He, C. Wolfgang, K. Li, L. Zheng, Consensus, debate, and prospective on pancreatic cancer treatments, J Hematol Oncol. 17 (2024) 92. https://10.1186/s13045-024-01613-x

[9] H. Momose, S. Kudo, T. Yoshida, N. Hasui, R. Matsuki, M. Kogure, Y. Sakamoto, Trends in the treatment of advanced pancreatic cancer, Biosci Trends. 18 (2024) 224-232. https://10.5582/bst.2024.01156

[10] Y. Liu, Y. Zhang, H. Li, T.Y. Hu, Recent advances in the bench-to-bedside translation of cancer nanomedicines, Acta Pharm Sin B. 15 (2025) 97-122. https://10.1016/j.apsb.2024.12.007

[11] M. Espona-Fiedler, C. Patthey, S. Lindblad, I. Sarró, D. Öhlund, Overcoming therapy resistance in pancreatic cancer: New insights and future directions, Biochem Pharmacol. 229 (2024) 116492. https://10.1016/j.bcp.2024.116492

[12] F. Susa, S. Arpicco, C.F. Pirri, T. Limongi, An Overview on the physiopathology of the blood-brain barrier and the lipid-based nanocarriers for central nervous system delivery, Pharmaceutics. 16 (2024). https://10.3390/pharmaceutics16070849

[13] M.L. Immordino, P. Brusa, F. Rocco, S. Arpicco, M. Ceruti, L. Cattel, Preparation, characterization, cytotoxicity and pharmacokinetics of liposomes containing lipophilic gemcitabine prodrugs, J Control Release. 100 (2004) 331-346. https://10.1016/j.jconrel.2004.09.001

[14] M. Zeng, B. Wu, W. Wei, Z. Jiang, P. Li, Y. Quan, X. Hu, Disulfiram: A novel repurposed drug for cancer therapy, Chin Med J (Engl). 137 (2024) 1389-1398. https://10.1097/cm9.0000000000002909

[15] S.K. Kim, H. Kim, D.H. Lee, T.S. Kim, T. Kim, C. Chung, G.Y. Koh, H. Kim, D.S. Lim, Reversing the intractable nature of pancreatic cancer by selectively targeting ALDH-high, therapy-resistant cancer cells, PLoS One. 8 (2013) e78130. https://10.1371/journal.pone.0078130

[16] E. Dalla Pozza, M. Donadelli, C. Costanzo, T. Zaniboni, I. Dando, M. Franchini, S. Arpicco, A. Scarpa, M. Palmieri, Gemcitabine response in pancreatic adenocarcinoma cells is synergistically enhanced by dithiocarbamate derivatives, Free Radic Biol Med. 50 (2011) 926-933. https://10.1016/j.freeradbiomed.2011.01.001

[17] A. Marengo, S. Forciniti, I. Dando, E. Dalla Pozza, B. Stella, N. Tsapis, N. Yagoubi, G. Fanelli, E. Fattal, C. Heeschen, M. Palmieri, S. Arpicco, Pancreatic cancer stem cell proliferation is strongly inhibited by diethyldithiocarbamate-copper complex loaded into hyaluronic acid decorated liposomes, Biochim Biophys Acta Gen Subj. 1863 (2019) 61-72. https://10.1016/j.bbagen.2018.09.018

[18] G.R. Bartlett, Phosphorus assay in column chromatography, J Biol Chem. 234 (1959) 466-468.

[19] T.C. Chou, Drug combination studies and their synergy quantification using the Chou-Talalay method, Cancer Res. 70 (2010) 440-446. https://10.1158/0008-5472.Can-09-1947

[20] L. Guerassimoff, M. Ferrere, S. Van Herck, S. Dehissi, V. Nicolas, B.G. De Geest, J. Nicolas, Thermosensitive polymer prodrug nanoparticles prepared by an all-aqueous nanoprecipitation process and application to combination therapy, J Control Release. 369 (2024) 376-393. https://10.1016/j.jconrel.2024.03.049

[21] E. Dalla Pozza, C. Lerda, C. Costanzo, M. Donadelli, I. Dando, E. Zoratti, M.T. Scupoli, S. Beghelli, A. Scarpa, E. Fattal, S. Arpicco, M. Palmieri, Targeting gemcitabine containing liposomes to CD44 expressing pancreatic adenocarcinoma cells causes an increase in the antitumoral activity, Biochim Biophys Acta. 1828 (2013) 1396-1404. https://10.1016/j.bbamem.2013.01.020

[22] F. Masetto, K. Chegaev, E. Gazzano, N. Mullappilly, B. Rolando, S. Arpicco, R. Fruttero, C. Riganti, M. Donadelli, MRP5 nitration by NO-releasing gemcitabine encapsulated in liposomes confers sensitivity in chemoresistant pancreatic adenocarcinoma cells, Biochim Biophys Acta Mol Cell Res. 1867 (2020) 118824. https://10.1016/j.bbamcr.2020.118824

[23] M. Bartkowski, V. Bincoletto, I.C. Salaroglio, G. Ceccone, R. Arenal, S. Nervo, B. Rolando, C. Riganti, S. Arpicco, S. Giordani, Enhancing pancreatic ductal adenocarcinoma (PDAC) therapy with targeted carbon nano-onion (CNO)-mediated delivery of gemcitabine (GEM)-derived prodrugs, J Colloid Interface Sci. 659 (2024) 339-354. https://10.1016/j.jcis.2023.12.166

[24] M. Wehbe, M. Anantha, I. Backstrom, A. Leung, K. Chen, A. Malhotra, K. Edwards, M.B. Bally, Nanoscale reaction vessels designed for synthesis of copper-drug complexes suitable for preclinical development, PLoS One. 11 (2016) e0153416. https://10.1371/journal.pone.0153416

[25] S. Mielke, R. Sorkin, J. Klein, Effect of cholesterol on the mechanical stability of gel-phase phospholipid bilayers studied by AFM force spectroscopy, Eur Phys J E Soft Matter. 46 (2023) 77. https://10.1140/epje/s10189-023-00338-y

[26] A. Sarode, Y. Fan, A.E. Byrnes, M. Hammel, G.L. Hura, Y. Fu, P. Kou, C. Hu, F.I. Hinz, J. Roberts, S.G. Koenig, K. Nagapudi, C.C. Hoogenraad, T. Chen, D. Leung, C.W. Yen, Predictive high-throughput screening of PEGylated lipids in oligonucleotide-loaded lipid nanoparticles for neuronal gene silencing, Nanoscale Adv. 4 (2022) 2107-2123. https://10.1039/d1na00712b

[27] J. Lee, A.L. De La Torre, F.L. Rawlinson, D.B. Ness, L.D. Lewis, W.F. Hickey, C.C.Y. Chang, T.Y. Chang, Characterization of stealth liposome-based nanoparticles encapsulating the ACAT1/SOAT1 Inhibitor F26: efficacy and toxicity studies in vitro and in wild-type mice, Int J Mol Sci. 25 (2024). https://10.3390/ijms25179151

[28] M. Martínez-Negro, D. Russo, S. Prévost, J. Teixeira, S. Morsbach, K. Landfester, Poly(ethylene glycol)-based surfactant reduces the conformational change of adsorbed proteins on nanoparticles, Biomacromolecules. 23 (2022) 4282-4288. https://10.1021/acs.biomac.2c00744

[29] H. Meng, Y. Zhao, J. Dong, M. Xue, Y.S. Lin, Z. Ji, W.X. Mai, H. Zhang, C.H. Chang, C.J. Brinker, J.I. Zink, A.E. Nel, Two-wave nanotherapy to target the stroma and optimize gemcitabine delivery to a human pancreatic cancer model in mice, ACS Nano. 7 (2013) 10048-10065. https://10.1021/nn404083m

[30] T. Yamamoto, M. Yokoyama, P. Opanasopit, A. Hayama, K. Kawano, Y. Maitani, What are determining factors for stable drug incorporation into polymeric micelle carriers? Consideration on physical and chemical characters of the micelle inner core, J Control Release. 123 (2007) 11-18. https://10.1016/j.jconrel.2007.07.008

[31] J.O. Eloy, M. Claro de Souza, R. Petrilli, J.P.A. Barcellos, R.J. Lee, J.M. Marchetti, Liposomes as carriers of hydrophilic small molecule drugs: strategies to enhance encapsulation and delivery, Colloids and Surfaces B: Biointerfaces. 123 (2014) 345-363. https://https://doi.org/10.1016/j.colsurfb.2014.09.029

[32] P. Siani, E. Donadoni, L. Ferraro, F. Re, C. Di Valentin, Molecular dynamics simulations of doxorubicin in sphingomyelin-based lipid membranes, Biochim Biophys Acta Biomembr. 1864 (2022) 183763. https://10.1016/j.bbamem.2021.183763

[33] H. Tamam, J. Park, H.H. Gadalla, A.R. Masters, J.A. Abdel-Aleem, S.I. Abdelrahman, A.A. Abdelrahman, L.T. Lyle, Y. Yeo, Development of liposomal gemcitabine with high drug loading capacity, Mol Pharm. 16 (2019) 2858-2871. https://10.1021/acs.molpharmaceut.8b01284

[34] Z. Zheng, M. Li, J. Yang, X. Zhou, Y. Chen, E.K. Silli, J. Tang, S. Gong, Y. Yuan, Y. Zong, J. Kong, P. Chen, L. Yu, S. Luo, Y. Wang, C. Tan, Growth inhibition of pancreatic cancer by targeted delivery of gemcitabine via fucoidan-coated pH-sensitive liposomes, Int J Biol Macromol. 277 (2024) 134517. https://10.1016/j.ijbiomac.2024.134517

[35] H. Xu, J. Paxton, J. Lim, Y. Li, W. Zhang, L. Duxfield, Z. Wu, Development of high-content gemcitabine PEGylated liposomes and their cytotoxicity on drug-resistant pancreatic tumour cells, Pharm Res. 31 (2014) 2583-2592. https://10.1007/s11095-014-1353-z

[36] T. Higuchi, T. Yokobori, R. Takahashi, T. Naito, H. Kitahara, T. Matsumoto, C. Kakinuma, S. Hagiwara, H. Kuwano, K. Shirabe, T. Asao, FF-10832 enables long survival via effective gemcitabine accumulation in a lethal murine peritoneal dissemination model, Cancer Sci. 110 (2019) 2933-2940. https://10.1111/cas.14123

[37] E.K. Silli, Z. Zheng, X. Zhou, M. Li, J. Tang, R. Guo, C. Tan, Y. Wang, Design optimization of Fucoidan-coating Cationic Liposomes for enhance Gemcitabine delivery, Invest New Drugs. (2024). https://10.1007/s10637-024-01455-x

[38] M. Celano, M.G. Calvagno, S. Bulotta, D. Paolino, F. Arturi, D. Rotiroti, S. Filetti, M. Fresta, D. Russo, Cytotoxic effects of Gemcitabine-loaded liposomes in human anaplastic thyroid carcinoma cells, BMC Cancer. 4 (2004) 63. https://10.1186/1471-2407-4-63

[39] F. Castelli, M.G. Sarpietro, F. Rocco, M. Ceruti, L. Cattel, Interaction of lipophilic gemcitabine prodrugs with biomembrane models studied by Langmuir-Blodgett technique, J Colloid Interface Sci. 313 (2007) 363-368. https://10.1016/j.jcis.2007.04.018
[40] M.C. Smith, R.M. Crist, J.D. Clogston, S.E. McNeil, Zeta potential: a case study of cationic, anionic, and neutral liposomes, Anal Bioanal Chem. 409 (2017) 5779-5787. https://10.1007/s00216-017-0527-z
[41] E. Mini, S. Nobili, B. Caciagli, I. Landini, T. Mazzei, Cellular pharmacology of gemcitabine, Ann Oncol. 17 Suppl 5 (2006) v7-12. https://10.1093/annonc/mdj941
[42] T.M. Allen, P.R. Cullis, Liposomal drug delivery systems: from concept to clinical applications, Adv Drug Deliv Rev. 65 (2013) 36-48. https://10.1016/j.addr.2012.09.037
[43] D.W. Miller, M. Fontain, C. Kolar, T. Lawson, The expression of multidrug resistance-associated protein (MRP) in pancreatic adenocarcinoma cell lines, Cancer Lett. 107 (1996) 301-306. https://10.1016/0304-3835(96)04384-4
[44] A. Nasrollahzadeh, M. Momeny, H. Fasehee, M. Yaghmaie, D. Bashash, S. Hassani, S.A. Mousavi, S.H. Ghaffari, Anti-proliferative activity of disulfiram through regulation of the AKT-FOXO axis: A proteomic study of molecular targets, Biochim Biophys Acta Mol Cell Res. 1868 (2021) 119087. https://10.1016/j.bbamcr.2021.119087
[45] C.B. Aparicio-Lopez, S. Timmerman, G. Lorino, T. Rogers, M. Pyle, T.B. Shrestha, M.T. Basel, Thermosensitive liposomes for gemcitabine delivery to pancreatic ductal adenocarcinoma, Cancers (Basel). 16 (2024). https://10.3390/cancers16173048
[46] M. Tang, S.B. Yarragudi, P. Pan, K. Yang, M. Kanamala, Z. Wu, Effect of size and pH-sensitivity of liposomes on cellular uptake pathways and pharmacokinetics of encapsulated gemcitabine, J Liposome Res. 35 (2025) 44-54. https://10.1080/08982104.2024.2389969
[47] J. Huang, W. Song, L. Meng, Y. Shen, R. Zhou, Role of polyplex charge density in lipopolyplexes, Nanoscale. 14 (2022) 7174-7180. https://10.1039/d1nr07897f
[48] H. Kitayama, Y. Takechi, N. Tamai, H. Matsuki, C. Yomota, H. Saito, Thermotropic phase behavior of hydrogenated soybean phosphatidylcholine-cholesterol binary liposome membrane, Chem Pharm Bull (Tokyo). 62 (2014) 58-63. https://10.1248/cpb.c13-00587
[49] M. Amrutkar, K. Berg, A. Balto, M.G. Skilbrei, A.V. Finstadsveen, M. Aasrum, I.P. Gladhaug, C.S. Verbeke, Pancreatic stellate cell-induced gemcitabine resistance in pancreatic cancer is associated with LDHA- and MCT4-mediated enhanced glycolysis, Cancer Cell Int. 23 (2023) 9. https://10.1186/s12935-023-02852-7
[50] X. Zhang, P. Hu, S.Y. Ding, T. Sun, L. Liu, S. Han, A.B. DeLeo, A. Sadagopan, W. Guo, X. Wang, Induction of autophagy-dependent apoptosis in cancer cells through activation of

ER stress: an uncovered anti-cancer mechanism by anti-alcoholism drug disulfiram, Am J Cancer Res. 9 (2019) 1266-1281.

Supporting Information

Table S1. Combination Index (CI) of GEM and GEM-C18 free or liposomal formulations, combined with DSF 1 and 0.1 μM.

	Dose DSF (μM)	Dose GEM (μM)	Dose GEM-C18 (μM)	CI
Free drugs	1	10	/	0.10969
	1	0.025	/	0.07858
	1	0.015	/	0.08478
	1	0.005	/	0.13956
	0.1	10	/	0.85688
	0.1	0.025	/	0.02749
	0.1	0.015	/	0.03224
	0.1	0.005	/	0.13659
	1	/	2.5	0.27409
	1	/	0.5	0,47503
	1	/	0.05	0.28596
	1	/	0.005	0.72908
	0.1	/	2.5	0.99235
	0.1	/	0.5	1.43333
	0.1	/	0.05	0.16261
	0.1	/	0.005	0.59844
LipoGEM and LipoGEM-C18	1	0.025		0.97222
	1	0.015	/	1.90656
	1	0.25	/	0.72219
	0.1	0.015	/	1.64534
	0.1	0.25	/	0.47890
	1	/	2.5	0.47697
	1	/	0.5	0.61250
	1	/	0.05	1.04733

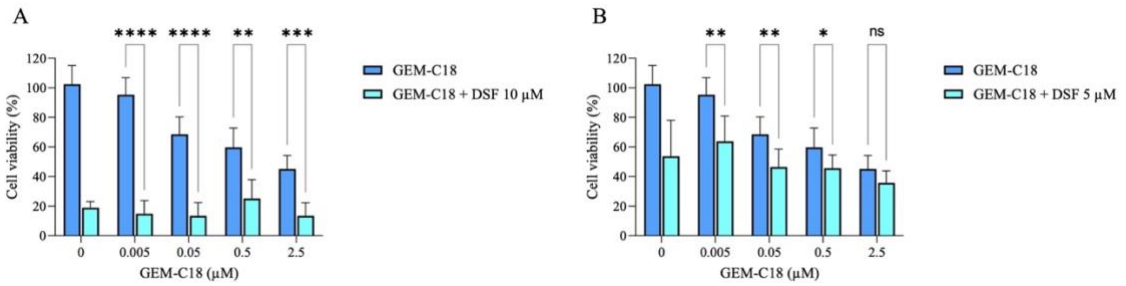

Figure S1. Cell viability on PANC-1 cells of GEM and DSF (A- DSF 10 µM, B- DSF 5 µM) in combination, after 72 h. Data are presented as means ± SD (n=3). *p<0.1, **p <0.05, ***p <0.01 *vs* GEM alone; °p<0.1 vs DSF alone.

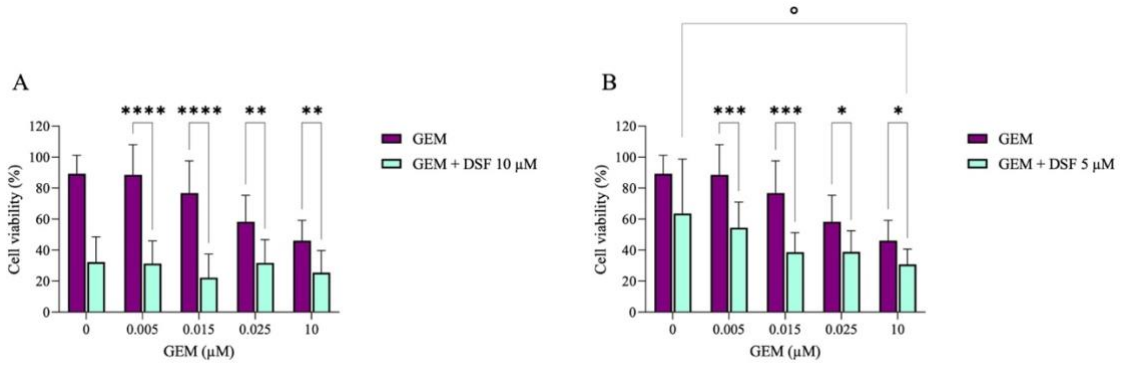

Figure S2. Cell viability on PANC-1 cells of GEM-C18 and DSF (A- DSF 10 µM, B- DSF 5 µM) in combination, after 72 h. Data are presented as means ± SD (n=3). *p<0.01, **p <0.05, ***p <0.01 *vs* GEM-C18 alone.

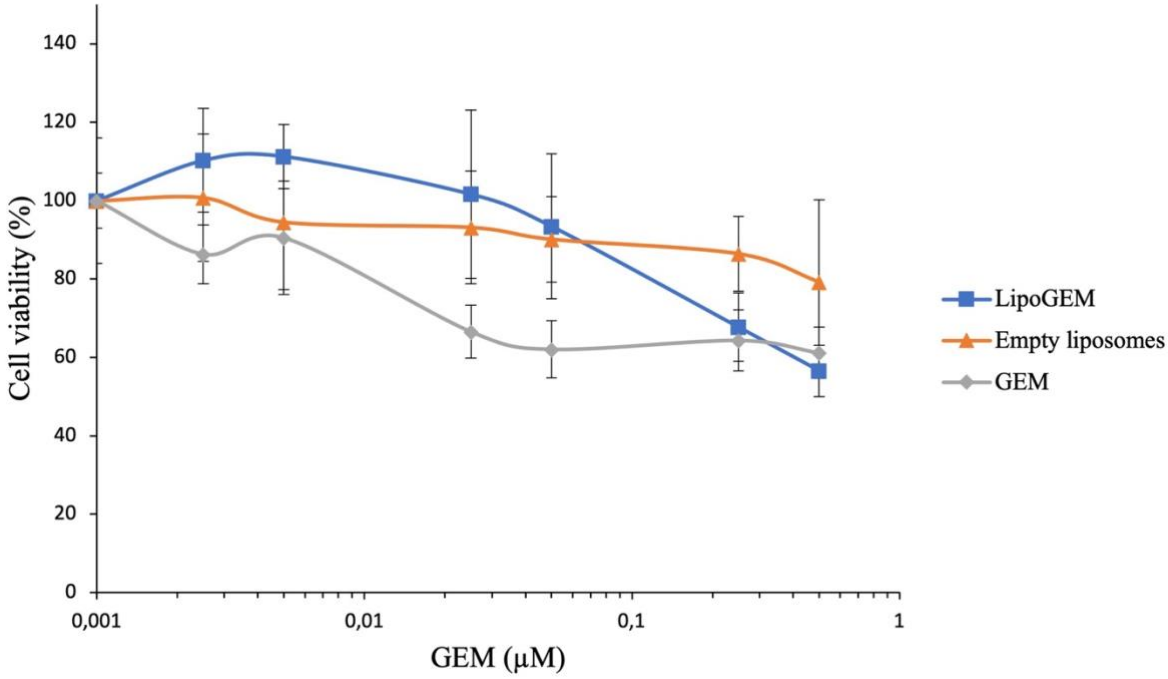

Figure S3. Cell viability on PANC-1 cells of LipoGEM, Empty liposomes and GEM, after 72 h. Data are presented as means ± SD (n=3).

Discussion

This PhD project was carried out at the Department of Drug Science and Technology of the University of Turin. Part of the project was performed during a research period abroad at the Laboratoire METSY, UMR 9018 CNRS, at the Gustave Roussy Cancer Hospital in Villejuif (France).

The present discussion will encompass the experimental work carried out in this doctoral thesis.

Nanomedicine is a multidisciplinary field in which nanotechnology is applied to several different areas. Exploiting nanoscale materials and devices, nanomedicine aims to improve the efficiency and precision of medical interventions. This approach offers significant advantages, including targeted drug delivery, improved bioavailability and minimized side effects [1, 2]. Nanomedicine also holds promise in areas such as cancer therapy [3, 4], tissue regeneration [5] and diagnostic imaging [6]. However, despite its potential, there are challenges related to the safety, ethical concerns and regulatory aspects of nanomaterials [7]. Understanding both the benefits and limitations of nanomedicine is essential for its successful integration into clinical practice, paving the way for more personalized and effective medical treatments.

This research aimed to improve the efficacy of old drugs in pancreatic cancer by the application of nanomedicine. In particular, the encapsulation of these drugs in different drug delivery systems aimed to improve their stability and thus their pharmacokinetic and pharmacodynamic properties. In addition, our main objective was to try to overcome the well-established resistance that pancreatic cancer cells develop [8].

There are many different types of drug delivery systems, each with their own characteristics, but all of which can be used for the same purpose. In this context, three different types of nanosystems were explored: i) carbon nano-onions (CNOs), which, due to their inorganic nature and multilayer structure, are able to offer controlled drug release [9]; ii) micelles, because of their reduced size and consequent ability to better penetrate cellular barriers [10]; iii) liposomes, because of their biocompatibility and biodegradability, as well as their stability and ability to encapsulate both hydrophilic and hydrophobic drugs [11]. It has been possible to study these nanosystems in depth thanks to the skills and experience of our laboratory and the collaborators we have worked with.

These nanosystems are designed to encapsulate gemcitabine (GEM), the gold standard drug for the treatment of pancreatic cancer. However, monotherapy with free GEM has been abandoned in recent years due to its poor therapeutic efficacy and the tendency of cells to develop drug resistance. For these reasons, both GEM and its lipophilic prodrugs 4-(*N*)-

lauroyl-gemcitabine (GEM-C12) and 4-(*N*)-stearoyl-gemcitabine (GEM-C18), which have previously been synthesized in our laboratory [12, 13], have been encapsulated within these different nanosystems. The employment of the prodrugs is intended to improve GEM stability and increase its lipophilicity, thus facilitating their encapsulation in nanosystems [14]. Concurrently, following a comprehensive review of the extant literature, a review article was submitted to *Critical Reviews in Oncology/Hematology*. This investigation involved the administration of these compounds in combination with another drug, disulfiram (DSF). DSF has a long history as an anti-alcoholic drug, but several works has identified new mechanisms of action that enable its repurposing as an anti-cancer molecule, particularly in combination with other drugs [15, 16].

Furthermore, hyaluronic acid (HA) was selected for the functionalization of the surface of CNOs and micelles, with the objective of achieving active targeting and thereby enhancing the efficacy of the delivered drugs. The rationale for the selection of HA as the targeting agent is derived from its non-toxicity and signaling role in dynamic cellular processes. Indeed, HA-receptor (CD44) interactions play an instructive role in cancer, mediating various signaling pathways [17, 18]. In pathological conditions, CD44 is overexpressed on the surface of cancer cells, promoting cancer cell adhesion to extracellular matrix components and facilitating their migration [19]. Consequently, the expression of CD44 in cancer cells represents a significant therapeutic target for the development of targeted cancer therapies, including HA-based drug delivery systems.

In this context, it was decided that the project would start based on our research group's previous experience with carbon nanotubes (CNTs). Their high surface area, coupled with their compatibility for functionalization, enables the formation of covalent and non-covalent interactions with other molecules. In a previous work, CNTs were derivatized through non-covalent interactions with conjugates synthesized in our laboratory. These conjugates were obtained reacting HA of different molecular weight with a phospholipid (1,2-dimyristoyl-*sn*-glycero-3-phosphoethanolamine, DMPE). In these conjugates (named HA-DMPE) the DMPE amino group is randomly linked to the carboxylic residues of HA. The condensation reaction between HA and DMPE resulted in the formation of an amidic bond between the carboxylic groups of HA and the amino group of DMPE [20]. A series of varying molecular weights of HA were evaluated to ascertain the most effective option for achieving optimal dispersibility and active targeting of the CNTs. The data showed that HA-DMPE conjugate prepared using 200 kDa HA exhibited the best activity among all the conjugates [21].

Based on this experience, CNOs were investigated as drug delivery system due to the

existence of numerous parallels between these two nanosystems: both are sp2-hybridised carbon compounds with a high surface area that can potentially be modified with different functional groups. The decision to switch to CNOs was based on the evidence that CNTs are potentially more toxic and less biocompatible; additionally, the surface functionalization of CNOs, which include the capacity for easy binding with active targeting agents, is comparatively more straightforward [22]. Moreover, CNOs are systems that have recently emerged as a promising platform for the delivery of anti-cancer drugs, due to their unique properties [23, 24]. In this work CNOs were covalently functionalized with HA. This method differs significantly from the hydrophobic functionalization technique employed in the derivatization of CNTs. The CNOs were synthesized and functionalized with HA 200 kDa, by Professor Silvia Giordani of the University of Dublin. HA was clinked to the surface of the CNOs through the use of a PEG linker to obtain HA-PEG-CNOs [25]. Furthermore, fluo-HA-PEG-CNOs were synthesized using a fluorescent labelled HA previously prepared in our laboratory and were further tested in the *in vitro* biological test [26]. Preliminary experiments were conducted to investigate the process of GEM loading on carbon nanotubes (CNTs). This research was undertaken due to the previous research work that had provided a substantial understanding of these systems. It was observed that the process of loading GEM onto these carbon nanosystems was particularly challenging, likely due to its high hydrophilicity. Consequently, GEM-C12 and GEM-C18 were loaded onto CNOs; these GEM-prodrugs demonstrated a higher loading efficiency in various nanoparticle systems, including liposomes, lipid nano capsules, and mesoporous silica nanoparticles, compared to the parent drug. Furthermore, both GEM-C12 and GEM-C18 have demonstrated favorable activity both *in vitro* and *in vivo* [13, 27, 28].

In this work, following a substantial body of research, it was determined that the 1:7 (prodrug:CNOs) ratio demonstrated optimal balance between the constituent elements, thereby ensuring optimal drug loading and stability. Thus, the two GEM prodrugs were loaded on PEG-CNOs and HA-PEG-CNOs and we observed an increase of the size in HA-PEG-CNOs due to the presence of HA on the surface. Furthermore, HA-PEG-CNOs exhibit a significantly more negative Z potential value in comparison to PEG-CNOs, as a consequence of the contribution of the negatively charged HA carboxylic groups. With regard to the encapsulation efficiency (EE%), both formulations exhibited higher values when GEM-C18 was employed. This phenomenon is presumably attributable to the correlation between the lipophilic character of the drug and its size. In essence, the observed prodrug loading efficiency appears to exhibit a direct proportional relationship with prodrug

lipophilicity [27]. In this regard, the more lipophilic GEM-C18 (logP 7.91) exhibited higher loading efficiency compared to its less lipophilic counterpart GEM-C12 (logP 4.74). Furthermore, the hydrophobic nature of the interaction between the prodrug and CNOs results in a reversible bond. This enables the nanosystem to release the drug in a gradual and progressive manner over time. *In vitro* GEM-C12 and GEM-C18 release experiments from drug-loaded CNOs were investigated in a PBS buffer at 37 °C. After 72 hours, approximately 15% of C12GEM and only around 5% of the more lipophilic GEM-C18 was released from HA-PEG-CNOs. It can be hypothesized that the steric hindrance of the HA coating, in conjunction with the length of the sidechain of the GEM-prodrug, contributed to the overall drug release. Furthermore, the reduced release of GEM-C18 suggests a comparatively stronger interaction between the prodrug and the surface of the CNOs [27].

Thus, a biological characterization of CNOs has been conducted. Initially, the unloaded CNOs were tested for their biocompatibility, which was confirmed in the concentrations tested on pancreatic cancer cells (PANC-1, MIA PaCa-2, Capan-1). In addition, fluo-HA-PEG-CNOs were employed for the evaluation of their internalization in pancreatic cancer cells that exhibit elevated levels of CD44 (PANC-1 and MIA PaCa-2), obtaining increased internalization in dose- and time-dependent way.

Finally, GEM-prodrug loaded HA-PEG-CNOs displayed higher cytotoxicity compared to free GEM and prodrugs alone in GEM-resistant cell lines (PANC-1 and Capan-1). The IC_{50} values for HA-PEG-CNOs loaded with C12 and C18 was between 10 nM and 100 nM on both cell lines. In contrast, IC_{50} was found to be 10 μM for GEM and 100 nM for the prodrugs.

In conclusion, CNOs represent a promising and innovative platform for drug delivery applications. However, current literature on CNO-based drug delivery systems remains limited, especially when compared to the extensive research conducted on other carbon nanomaterials. For example, unloaded CNTs functionalized with PEG have been proposed to increase apoptosis on pancreatic cancer cells using phototherapy [29]. Moreover, Yin *et al.* investigated a multifunctional graphene oxide (GO)-based nanocarrier system for the targeted treatment of pancreatic cancer. This group developed PEG- and folic acid-functionalized GO nanosheets capable of co-delivering two siRNAs targeting HDAC1 and K-Ras genes, which are critical for pancreatic tumor growth. The system was also designed to enable near-infrared (NIR) photothermal therapy [30]. Furthermore, our study proffers substantiated proof-of-concept for the utilization of CNOs as a novel nanocarrier for targeted delivery of GEM-derived prodrugs and other drugs with activity on pancreatic cancer,

thereby extending their potential through targeted modulation of the overexpressed CD44 receptor. For instance, given their affinity for lipophilic drugs, it might be possible to study the loading of CNOs with paclitaxel or docetaxel, which are used to treat pancreatic cancer [31, 32]. The loading of hydrophilic drugs is possible through derivatization of the CNOs, thereby forming bonds with functional groups present on the surface of the nanosystem (e.g. monoclonal antibodies such as erlotinib) [33]

The subsequent stage of the research was to concentrate on a different nanosystem, namely mixed micelles, due to their hybrid composition. The formulation strategy for mixed micelles preparation was based on two components. Firstly, 1,2-distearoyl-*sn*-glycero-3-phosphoethanolamine-poly(ethylene glycol) (DSPE-PEG) was chosen as the main component of the nanosystem, as it is widely used for micelle preparation. The rationale behind the selection of DSPE-PEG is threefold: i) its capacity to establish robust hydrophobic interactions between phospholipid chains [34]; ii) its presence on the surface of the micelles prevents the opsonins recognition, thus increasing their half-life; iii) the phospholipids chains allows encapsulation of lipophilic drugs [35]. The second component of the mixed micelles was HA, proposed with the aim to actively target pancreatic cancer cells, overexpressing the CD44 receptor. HA was incorporated in the form of a HA-1,2-dipalmitoyl-*sn*-glycero-3-phosphorylethanolamine (DPPE) conjugate (HA-DPPE), which had been previously synthesized in our laboratory. Briefly, HA-DPPE conjugates were obtained by covalently linking the aldehyde group of HA to the amino group of DPPE *via* a stable secondary amine bond formed by reductive amination [13]. In this case, conjugates composed of HA of two different low molecular weights (around 5 and 15 kDa) were employed, in a very low amount (1% molar ratio of the total content of PEG-DSPE).

This formulation approach yielded mixed micelles that expose HA on their surface, thereby facilitating interaction with the receptor. The general strategy was to encapsulate GEM-C18: it is hypothesized that the increased lipophilicity of the compound may facilitate the achievement of better hydrophobic interactions than GEM-C12, resulting in a more stable formulation with improved drug loading and sustained drug release.

In this study, micelles without HA (GEM-C18-PEG-M) and with HA (GEM-C18-PEG-M/HA) were prepared by a straightforward method, involving the hydration of a PEG-DSPE and GEM-C18 thin film with an aqueous solution (which contains the HA-DPPE conjugate in case of PEG-M/HA). Unloaded micelles were prepared for comparison (PEG-M, PEG-M/HA). Micelles are self-assembling systems, and as a result their formation occurs after the film has been hydrated and vortexed. However, to obtain small, uniformly sized systems,

the sonication method was exploited. This approach is notably more suitable than other approach, which require much more complex preparation methods. For example, Zhao *et al.* prepared metal–organic frameworks (MOFs) composed of HKUST-1. MOFs were synthesized by heating a 3:1 mixture of HKUST-1 and selenium powder under argon flow in a muffle furnace at 700°C for 1 hour. It was crucial to direct the flow of argon through the selenium prior to reaching the MOF, to facilitate the reaction in the vapor phase. After cooling, the powder was washed with nitric acid and subjected to centrifugation, after which it was dried under vacuum at 60°C for a period of 12 hours [36]. In our research, the micelles obtained are below 100 nm in size, with a Z potential of approximately -30 mV. During the process of micelle formation, DPPE inserts itself into the matrix formed by PEG-DSPE and HA is exposed on the surface. Notwithstanding this fact, the micelles retain the ability to self-assemble and the presence of the conjugate does not exert a significant effect on the size and encapsulation efficiency of GEM-C18. This is likely attributable to the low amount of HA-DPPE conjugated added.

The loading efficiency was around 90% for both HA molecular weights. This finding is further supported by another study on mixed micelles composed of PEG-DSPE and tocopheryl polyethylene glycol 1000 succinate (TPGS), which were also used to encapsulate GEM-C18. In these systems, TPGS contributed to the formation of a stabilizing outer layer around the PEG-based matrix, enhancing the retention of GEM-C18 within the micelles. Notably, a high EE% of 95% was achieved, comparable to that observed in our formulation [37]. GEM-C18 demonstrated prolonged retention within the micellar matrix, with an initial release of approximately 20% during the first hours, likely attributable to a burst effect resulting from a proportion of GEM-C18 residing on the exterior of the micelles. Then, GEM-C18-PEG-M, GEM-C18-PEG-M/HA4800 and GEM-C18-PEG-M/HA14800 exhibited a more sustained release profile, with a 60% remaining content after 72 hours, thereby underscoring the strong binding affinity of GEM-C18 to the PEG-DSPE matrix. Moreover, all formulations, both decorated and undecorated, show a similar release profile, demonstrating that the presence of HA does not affect drug release. These data have already been demonstrated by our group in previous studies on other nanosystems [38]. To achieve a more detailed characterization of the systems under investigation, small angle X-ray scattering (SAXS) was employed, a method which is well-suited to the observation of the arrangement of complex particles at the nanoscale. The size, shape and the detailed internal structures of PEG-M/HA14800, GEM-C18-PEG-M and GEM-C18-PEG-M/HA14800 were investigated. The parameters found for unloaded micelles were found to be suitable for the

modelling of spherical micelles with a hydrophobic core surrounded by an extended hydrophilic shell. However, in the presence of GEM-C18, the overall structure can be modelled as a three-shell prolate ellipsoidal particle. The presence of GEM-C18 has been demonstrated to induce a transition from a spherical to an elongated micelle shape, concomitant with alterations in the packing parameter of monomers within the aggregate. These results were corroborated by FESEM analysis, which revealed that the presence of GEM-C18 exerted a pronounced influence on the morphology of the micelles, an observation that had previously been observed by SAXS, in contrast to other lipid-based nanosystems. For instance, Bahramabadi *et al.* prepared liposomes containing the essential oil of Eruca sativa and analyzed them to ascertain whether the presence of the essential oil altered the morphological characteristics of the liposomes. In this instance, no significant disparities were observed: both formulations exhibited a spherical morphology, with no discernible structural alterations between them [39]. Subsequently, the micelles were assessed *in vitro* to evaluate their uptake and cytotoxicity in the same pancreatic cancer cells that had been selected for CNOs. A fluorescent molecule was incorporated into the micellar matrix to evaluate cellular uptake. A significant increase in uptake was observed in cells overexpressing the CD44 receptor for PEG-M/HA, with particularly evidence in micelles formulated with HA of higher molecular weight, indicating that the increase of repeating units improves the interactions with the receptor, as previously reported [13, 21]. The uptake of PEG-M/HA occurs *via* a receptor-mediated endocytosis, while the uptake of the PEG-M occurs *via* passive diffusion. During cellular uptake studies, CD44-overexpressing cells were incubated with PEG-M/HA micelles in the presence of either a saturating concentration of a CD44-neutralizing antibody or free HA. A significant reduction in micelles internalization was observed under both conditions, indicating that the uptake of PEG-M/HA is mediated by CD44 receptor–dependent endocytosis. In contrast, the uptake of non-decorated micelles remained unaffected, suggesting that their internalization occurs predominantly through passive diffusion mechanisms. It is also noteworthy that, despite the low HA content (1%) in the micellar formulation, HA is effectively exposed on the micelle surface. This is evidenced by the enhanced cellular uptake observed in CD44-overexpressing cells, confirming the accessibility and functional presentation of HA for receptor-mediated interactions. In accordance with the extant literature, these findings have been corroborated by numerous other studies, which have demonstrated that, across disparate nanosystems, hyaluronic acid enables the particles to be internalized in the same manner. For example, Wu *et al.* prepared gadolinium oxide nanoparticles using HA as the active targeting agent:

the uptake studies showed that HA functionalized gadolinium oxide nanoparticles enter cancer cells via receptor-mediated endocytosis through CD44 receptors. This targeting leads to enhanced cellular uptake, low cytotoxicity and improved biocompatibility. In contrast, non-targeting nanoparticles are associated with non-specific uptake mechanisms such as passive diffusion or non-selective endocytosis [40]. Subsequently, the cytotoxicity of GEM-C18-loaded micelles was assessed, with particular attention to the targeting efficiency of HA-decorated formulations. An increase in cytotoxic activity was observed with higher HA molecular weight, indicating enhanced CD44-mediated targeting and cellular uptake. Confirming our findings, Wang *et al.* discussed how the length of hyaluronic acid (HA) chains can influence the cytotoxicity of drug-loaded micellar systems in pancreatic cancer cells. Specifically, they showed that longer HA chains enhance cellular uptake *via* CD44 receptor-mediated endocytosis, leading to increased drug delivery and greater cytotoxic effects. This behavior is in contrast to shorter HA chains or systems without HA, which are less efficiently taken up and therefore have less anti-cancer activity [37].

Consequently, it can be concluded that even a system less rigid than that of CNOs is able of efficiently delivering GEM-C18 to pancreatic cancer cells; furthermore, the addition of HA in a small percentage resulted in active targeting and thus increased toxicity.

The studies carried out on micelles prompted the investigation of another nanosystem, liposomes. Indeed, the development of micelles empowered a comparison to be made between the effect of free GEM and the encapsulated GEM-C18, as micelles are systems capable of carrying lipophilic drugs. The employment of liposomes in this study enabled the encapsulation of GEM, thereby facilitating a more precise comparison between this drug and its prodrug GEM-C18. The structural characteristics of liposomes allow them to encapsulate both lipophilic drugs in the phospholipid bilayer and hydrophilic drugs in the aqueous core. Among several studies extent in literature, Arya *et al*. encapsulated lycorine hydrochloride - a hydrophilic alkaloid - in the aqueous core of the liposomes. This is consistent with the general behavior of hydrophilic drugs, which are typically entrapped in the inner aqueous compartment of liposomes during formulation. In contrast, gefitinib, which is a lipophilic molecule, was most likely localized within the lipid bilayer of the liposomes [41, 42].

In our study, two distinct formulations have been developed: one containing GEM and the other containing GEM-C18. The objective of this work was to identify a methodology for enhancing the efficacy of GEM and to overcome the resistance exhibited by pancreatic cancer cells. To this end, two strategies were employed: firstly, the encapsulation of GEM or its prodrug GEM-C18 in liposomes, to protect the drugs from degradation and prolong its

half-life. Concurrently, it was decided to enhance the efficacy of GEM and its derivatives through their co-administration with DSF, a drug that had previously been utilized in the treatment of alcoholism. This repositioning of DSF as an anti-cancer agent is a development driven by a deeper understanding of its mechanism of action [43]. Notably, its ability to block efflux pumps (e.g. Pgp) that contribute to tumor cell resistance, in addition to its capacity to augment ROS production, has emerged as a valuable tool in the field of cancer research [44, 45]. For example, a study of pegylated liposomes co-encapsulating DSF and doxorubicin (DOXO) in a 1:3 ratio and able to release the drugs in a controlled manner was carried out in our laboratory; we observed that DSF was first released and blocked P-glycoprotein, allowing DOXO to exert its anti-tumor effect on breast cancer cells [15].

On this basis, liposomal formulations were developed for the encapsulation of GEM (LipoGEM) and its lipophilic prodrug, GEM-C18 (LipoGEM-C18), separately using the same phospholipidic mixture. GEM was encapsulated within the aqueous core of liposomes thanks to its hydrophilic properties, while the lipophilic GEM-C18 was encapsulated in the phospholipid bilayer. Despite the differences in terms of encapsulated compound and preparation method, the obtained liposomes have similar physico-chemical characteristics in terms of size (approximately 160 nm) and zeta potential (approximately -30 mV). Liposomes were designed to be relatively rigid, with the phospholipid DSPC being utilized due to its relatively high phase transition temperature and lipophilic chain devoid of unsaturation. A high percentage of cholesterol (CHOL, 30%) was added to ensure the retention of GEM within the liposome core and without compromising the loading of GEM-C18 into the phospholipid bilayer. This was important to investigate because it has been reported that the loading of certain drugs can be influenced by the presence of CHOL in the bilayer, due to competition between them [46]. In this case, the percentage of CHOL selected does not impact the quantity of encapsulated GEM-C18, thereby enabling an EE% of over 90%. Regarding the encapsulation of GEM in liposomes, the process proved more complex. Based on the expertise of our laboratory, we decided to use the *pH gradient* method after applying different preparation methods. The attainment of this gradient was facilitated by the exploitation of the acidic pH of the citrate buffer (pH 4.5), which remained within the aqueous core, and the physiological pH of the HEPES buffer, which was maintained outside the liposomes (pH 7.4). Theoretically, in an acidic environment, the ionizable group of GEM protonates, forming salts with citrate and remaining trapped in the aqueous core [47]. Despite this, the amount of GEM encapsulated in liposomes was found to be around 20%, which was enough to reach a concentration useful for the further *in vitro* tests. Consequently,

the EE% obtained did not hinder the research. Notably, other research groups employing the same encapsulation strategy reported entrapment efficiencies comparable to or lower than those obtained in this work. For example, Immordino *et al.* were unable to achieve encapsulation of GEM [12]. In another study, Xu and his team developed liposomal formulations comparable to those investigated in the present study. They used a pH gradient in the presence of a sulfate buffer. Nonetheless, the encapsulation efficiency that resulted was limited to 12%, thereby further underscoring the difficulties in achieving a high GEM loading under these conditions [48].

In addition, the drug release profile of the two formulations was evaluated in HEPES buffer pH 7.4 (to mimic a physiological medium) and in FBS (the objective was to create a model that will simulate the environment that the system would find once it is delivered into the cells). LipoGEM-C18 showed better drug retention (after 72 h only 20% of drug released in HEPES buffer and 40% in FBS). We demonstrated that the modification of the phospholipid composition improved the stability LipoGEM-C18 in comparison to the work of Immordino *et al*. [12] in which approximately 30% of GEM-C18 was released from the liposomes after 30 h in a buffer solution at 37°C, whereas 20% of GEM-C18 was released from LipoGEM-C18 after the same period in our study. The same behavior was observed for the release profile in serum. On the other hand, LipoGEM showed a more rapid release, reaching 50% and 62% of drug released after 3h in HEPES buffer and FBS, respectively. In the literature, some groups have achieved improvements in drug release, reaching 60% of the drug released after 72 hours in buffer solution (versus our 80%), with a similar phospholipid formulation (DPPC:CHOL:PEG) but combining the pH gradient method with a second method (*e.g*. the small volume injection) to increase the amount of GEM encapsulated in the liposome [49].

In contrast, both formulations demonstrated stability for a period of at least three weeks when stored at 4°C. LipoGEM-C18 was also analyzed using the DSC technique to further confirm the presence of GEM-C18 in the phospholipid bilayer. Since the transition temperatures were lower in the presence of GEM-C18, it was suggested that all the components present in the formulation were interacting, leading to a decrease in the crystallinity of the drug and an increase in its amorphous behavior [50].

Then, *in* vitro biological studies were assessed on the liposomal formulations. The experiments were conducted in collaboration with Dr. Giorgia Urbinati and Dr. Nazanine Modjtahedi, at the Gustave Roussy Hospital in Villejuif (France) during an international research period. Initially, the focus was on the study of the cytotoxic effect of free drugs, with the objective being to determine their IC_{50}. In addition, as previously reported, DSF is

a repurposed pharmaceutical agent used to treat various types of cancer, including pancreatic cancer. Consequently, the in vitro studies conducted in this research aim to ascertain the optimal concentrations required to achieve a synergistic effect between GEM or GEM-C18 (both free and liposomal) and DSF or its prodrug, DSF/Cu. In relation to the assays conducted on the free drugs, a noteworthy observation was made concerning GEM. It was observed that the drug attained a toxicity plateau from 0.25 μM to 10 μM, at which point 60% of cell viability was maintained. Consequently, the calculation of a specific IC50 at the tested concentrations at 72 h was precluded. This is in accordance with data found in the literature, thus confirming the low sensitivity of PANC-1 cells to the drug. For example, Fryer et al. manage to find an IC_{50} at 48 h but at much higher concentrations than we evaluated in our research, *i.e.*, approx. 100 mM. Conversely, GEM-C18 exhibited a more pronounced cytotoxicity curve, and an IC50 of 3.17 μM could be determined. Finally, the cellular toxicity of DSF and its prodrug DSF/Cu was evaluated to ascertain whether its use would benefit the combination with GEM and GEM-C18. However, the results showed a very high toxicity of DSF/Cu, which would probably be too high if administered in combination with additional drugs. The decision to discard DSF/Cu was also influenced by the potential for this toxicity to result in an incidence of adverse effects [51]. In order to test liposomes in combination with free DSF, it was first necessary to test free drugs in combination with each other. This approach enabled the identification of concentrations that would facilitate a synergistic effect between the two pharmaceutical agents (DSF and GEM, DSF and GEM-C18). The Combination Index must fall under the threshold of 1 in order to be considered a synergy [52].

The concentrations that were found to be synergic were exploited for the purpose of testing liposomes in combination with DSF. However, the outcomes were found to be less promising than anticipated. Indeed, the combination of liposomes with DSF did not demonstrate a significantly higher level of effectiveness than the combination of free drugs. However, a marginal enhancement in the level of cell death was observed in combinations involving DSF at a concentration of 0.1 μM and GEM. However, the only combination of interest for GEM-C18 is that with GEM-C18 at a higher concentration. It can be hypothesized that the controlled release of the drug by liposomes might require further investigation, as the times at which the tests were conducted may not have been sufficiently prolonged. Consequently, subsequent studies will involve the variation of both the time of drug administration and the duration of the assays to assess cellular toxicity.

Overall, this research project concluded that the encapsulation of GEM and its prodrug

GEM-C18 in nanosystems of a different nature results in increased toxicity compared to free drugs. Combining them with DSF also seems to be a good strategy for overcoming the resistance of pancreatic cancer cells to drugs, although this latter study should be investigated further to find the right parameters for meaningful results.

References

[1] A. Kumar, *et al.*, "Clinical applications of targeted nanomaterials",, *Pharmaceutics,* vol. 17, no. 3, Mar 17 2025, doi: 10.3390/pharmaceutics17030379.

[2] B. Wang, *et al.*,"The potential of nano-formulated natural drugs in melanoma treatment: a review of pharmacological efficacy and mechanistic insights", *Int J Nanomedicine,* vol. 20, pp. 3527-3539, 2025, doi: 10.2147/ijn.S505394.

[3] W. Xu, *et al.*, "Dual-mode treatment of hepatocellular carcinoma using rgd cyclopeptide-modified liposomes loaded with Ce6/DOX", *Int J Nanomedicine,* vol. 20, pp. 3845-3860, 2025, doi: 10.2147/ijn.S509387.

[4] C. Yoo, *et al.*, "Liposomal irinotecan for previously treated patients with biliary tract cancer: A pooled analysis of NIFTY and NALIRICC trials", *J Hepatol,* Mar 25 2025, doi: 10.1016/j.jhep.2025.03.013.

[5] S. Sánchez-Salcedo, *et al.*, "Nanodevices based on mesoporous glass nanoparticles enhanced with zinc and curcumin to fight infection and regenerate bone", *Acta Biomater,* vol. 166, pp. 655-669, Aug 2023, doi: 10.1016/j.actbio.2023.04.046.

[6] G. M. Saladino, *et al.*, "Multimodal imaging approach to track theranostic nanoparticle accumulation in glioblastoma with magnetic resonance imaging and intravital microscopy", *Nanoscale,* Mar 26 2025, doi: 10.1039/d5nr00447k.

[7] M. E. Neganova, *et al.*,"Benefits and limitations of nanomedicine treatment of brain cancers and age-dependent neurodegenerative disorders", *Semin Cancer Biol,* vol. 86, no. Pt 2, pp. 805-833, Nov 2022, doi: 10.1016/j.semcancer.2022.06.011.

[8] Y. Binenbaum, *et al.*, "Gemcitabine resistance in pancreatic ductal adenocarcinoma", *Drug Resist Updat,* vol. 23, pp. 55-68, Nov 2015, doi: 10.1016/j.drup.2015.10.002.

[9] O. Kearns, *et al.*, "Hyaluronic Acid-Conjugated Carbon Nanomaterials for Enhanced Tumour Targeting Ability", *Molecules,* vol. 27, no. 1, Dec 22 2021, doi: 10.3390/molecules27010048.

[10] C. Li, *et al.*, "Intelligent micelles for on-demand drug delivery targeting extracellular matrix of pancreatic cancer", *J Control Release,* vol. 373, pp. 879-889, Sep 2024, doi: 10.1016/j.jconrel.2024.07.058.

[11] F. Raza *et al.*, "Liposome-based diagnostic and therapeutic applications for pancreatic cancer", *Acta Biomater,* vol. 157, pp. 1-23, Feb 2023, doi: 10.1016/j.actbio.2022.12.013.

[12] M. L. Immordino, *et al.*, "Preparation, characterization, cytotoxicity and pharmacokinetics of liposomes containing lipophilic gemcitabine prodrugs", *J*

Control Release, vol. 100, no. 3, pp. 331-46, Dec 10 2004, doi: 10.1016/j.jconrel.2004.09.001.

[13] S. Arpicco, *et al.*, "Hyaluronic acid-coated liposomes for active targeting of gemcitabine", *Eur J Pharm Biopharm,* vol. 85, no. 3 Pt A, pp. 373-80, Nov 2013, doi: 10.1016/j.ejpb.2013.06.003.

[14] Y. Seo, *et al.*, "Recent progress of lipid nanoparticles-based lipophilic drug delivery: focus on surface modifications", *Pharmaceutics,* vol. 15, no. 3, Feb 26 2023, doi: 10.3390/pharmaceutics15030772.

[15] F. Rolle, *et al.*, "Coencapsulation of disulfiram and doxorubicin in liposomes strongly reverses multidrug resistance in breast cancer cells", *Int J Pharm,* vol. 580, p. 119191, Apr 30 2020, doi: 10.1016/j.ijpharm.2020.119191.

[16] L. Xu, *et al.*, "Disulfiram: a food and drug administration-approved multifunctional role in synergistically drug delivery systems for tumor treatment", *Int J Pharm,* vol. 626, p. 122130, Oct 15 2022, doi: 10.1016/j.ijpharm.2022.122130.

[17] R. K. Sironen, *et al.*, "Hyaluronan in human malignancies", *Exp Cell Res,* vol. 317, no. 4, pp. 383-91, Feb 15 2011, doi: 10.1016/j.yexcr.2010.11.017.

[18] F. Dosio, *et al.*, "Hyaluronic acid for anticancer drug and nucleic acid delivery", *Adv Drug Deliv Rev,* vol. 97, pp. 204-36, Feb 1 2016, doi: 10.1016/j.addr.2015.11.011.

[19] S. Banella, *et al.*, "In Vitro assessment of cisplatin/hyaluronan complex for loco-regional chemotherapy", *Int J Mol Sci,* vol. 24, no. 21, Oct 29 2023, doi: 10.3390/ijms242115725.

[20] C. Surace, *et al.*, "Lipoplexes targeting the CD44 hyaluronic acid receptor for efficient transfection of breast cancer cells", *Mol Pharm,* vol. 6, no. 4, pp. 1062-73, Jul-Aug 2009, doi: 10.1021/mp800215d.

[21] S. Arpicco, *et al.*, "Effects of the molecular weight of hyaluronic acid in a carbon nanotube drug delivery conjugate", *Front Chem,* vol. 8, p. 578008, 2020, doi: 10.3389/fchem.2020.578008.

[22] J. Ahlawat, *et al.*, "Application of carbon nano onions in the biomedical field: recent advances and challenges", *Biomater Sci,* vol. 9, no. 3, pp. 626-644, Feb 9 2021, doi: 10.1039/d0bm01476a.

[23] J. Bartelmess, *et al.*, "Modulation of Efficient Diiodo-BODIPY in vitro Phototoxicity to Cancer Cells by Carbon Nano-Onions", *Front Chem,* vol. 8, p. 573211, 2020, doi: 10.3389/fchem.2020.573211.

[24] H. Mohan, *et al.*, "Supramolecular functionalisation of B/N co-doped carbon nano-onions for novel nanocarrier systems", *Materials (Basel),* vol. 15, no. 17, Aug 30 2022, doi: 10.3390/ma15175987.

[25] M. Bartkowski, *et al.*, "Supramolecular chemistry of carbon nano-onions", *Nanoscale,* vol. 12, no. 17, pp. 9352-9358, May 7 2020, doi: 10.1039/d0nr01713b.

[26] A. N. de Belder, *et al.*, "Preparation and properties of fluorescein-labelled hyaluronate", *Carbohydr Res,* vol. 44, no. 2, pp. 251-7, Nov 1975, doi: 10.1016/s0008-6215(00)84168-3.

[27] A. Malfanti, *et al.*, "Delivery of Gemcitabine prodrugs employing mesoporous silica nanoparticles", *Molecules,* vol. 21, no. 4, p. 522, Apr 21 2016, doi: 10.3390/molecules21040522.

[28] L. Pinton, *et al.*, "Targeting of immunosuppressive myeloid cells from glioblastoma patients by modulation of size and surface charge of lipid nanocapsules", *J Nanobiotechnology,* vol. 18, no. 1, p. 31, Feb 17 2020, doi: 10.1186/s12951-020-00589-3.

[29] T. Mocan, *et al.*, "Photothermal treatment of human pancreatic cancer using pegylated multi-walled carbon nanotubes induces apoptosis by triggering mitochondrial membrane depolarization mechanism", *J Cancer,* vol. 5, no. 8, pp. 679-88, 2014, doi: 10.7150/jca.9481.

[30] F. Yin, *et al.*, "SiRNA delivery with PEGylated graphene oxide nanosheets for combined photothermal and genetherapy for pancreatic cancer", *Theranostics,* vol. 7, no. 5, pp. 1133-1148, 2017, doi: 10.7150/thno.17841.

[31] A. M. Shabana, *et al.*, "Thermosensitive and biodegradable hydrogel encapsulating targeted nanoparticles for the sustained co-delivery of gemcitabine and paclitaxel to pancreatic cancer cells", *International Journal of Pharmaceutics,* vol. 593, p. 120139, 2021/01/25/ 2021, doi: 10.1016/j.ijpharm.2020.120139.

[32] N. A. D. Guchelaar, *et al.*, "Intraperitoneal chemotherapy for unresectable peritoneal surface malignancies", *Drugs,* vol. 83, no. 2, pp. 159-180, Feb 2023, doi: 10.1007/s40265-022-01828-7.

[33] B. Mangla, *et al.*, "Multifaceted role of erlotinib in various cancer: nanotechnology intervention, patent landscape, and advancements in clinical trials", *Med Oncol,* vol. 41, no. 7, p. 173, Jun 12 2024, doi: 10.1007/s12032-024-02414-5.

[34] A. N. Lukyanov, *et al.*, "Micelles from lipid derivatives of water-soluble polymers as delivery systems for poorly soluble drugs", *Adv Drug Deliv Rev,* vol. 56, no. 9, pp. 1273-89, May 7 2004, doi: 10.1016/j.addr.2003.12.004.

[35] B. Xu, *et al.*, "Preparation and Evaluation of the cytoprotective activity of micelles with DSPE-PEG-C60 as a carrier against doxorubicin-induced cytotoxicity", *Front Pharmacol,* vol. 13, p. 952800, 2022, doi: 10.3389/fphar.2022.952800.

[36] C. Zhao, *et al.*, "Multifaceted carbonized metal-organic frameworks synergize with immune checkpoint inhibitors for precision and augmented cuproptosis cancer therapy", *ACS Nano,* vol. 18, no. 27, pp. 17852-17868, Jul 9 2024, doi: 10.1021/acsnano.4c04022.

[37] Y. Wang, *et al.*, "Enhanced tumor delivery of gemcitabine via PEG-DSPE/TPGS mixed micelles", *Mol Pharm,* vol. 11, no. 4, pp. 1140-50, Apr 7 2014, doi: 10.1021/mp4005904.

[38] E. Gazzano, *et al.*, "Hyaluronated liposomes containing H2S-releasing doxorubicin are effective against P-glycoprotein-positive/doxorubicin-resistant osteosarcoma cells and xenografts", *Cancer Lett,* vol. 456, pp. 29-39, Aug 1 2019, doi: 10.1016/j.canlet.2019.04.029.

[39] J. Hemmati, *et al.*, "Surface modified niosomal quercetin with cationic lipid: an appropriate drug delivery system against Pseudomonas aeruginosa Infections", *Sci Rep,* vol. 14, no. 1, p. 13362, Jun 11 2024, doi: 10.1038/s41598-024-64416-7.

[40] C. Wu, *et al.*, "Hyaluronic acid-functionalized gadolinium oxide nanoparticles for magnetic resonance imaging-guided radiotherapy of tumors", *Nanoscale Research Letters,* vol. 15, no. 1, p. 94, Apr 2020, doi: 10.1186/s11671-020-03318-9.

[41] D. K. Arya, *et al.*, "Dual-ligand functionalized liposomes with iRGD/trastuzumab co-loaded with gefitinib and lycorine for enhanced metastatic breast cancer therapy", *J Liposome Res,* pp. 1-15, Feb 2 2025, doi: 10.1080/08982104.2025.2457453.

[42] Y. Mu, *et al.*, "Lactoferrin-functionalized PEGylation liposomes loaded with norcantharidin acid for targeted therapy of hepatocellular carcinoma", *Int J Pharm,* vol. 671, p. 125245, Feb 25 2025, doi: 10.1016/j.ijpharm.2025.125245.

[43] Y. Feng, *et al.*, "Disulfiram-Loaded PLGA nanoparticles modified with a phenyl borate chitosan conjugate enhance hepatic carcinoma treatment", *Int J Pharm,* vol. 671, p. 125293, Feb 25 2025, doi: 10.1016/j.ijpharm.2025.125293.

[44] K. L. Swetha, *et al.*, "Overcoming drug resistance with a docetaxel and disulfiram loaded pH-sensitive nanoparticle", *J Control Release,* vol. 356, pp. 93-114, Apr 2023, doi: 10.1016/j.jconrel.2023.02.023.

[45] M. Yuan, *et al.*, "Disulfiram/copper triggers cGAS-STING innate immunity pathway via ROS-induced DNA damage that potentiates antitumor response to PD-1 checkpoint blockade", *Int J Biol Sci,* vol. 21, no. 4, pp. 1730-1748, 2025, doi: 10.7150/ijbs.105575.

[46] A. Karewicz, *et al.*, "Interaction of curcumin with lipid monolayers and liposomal bilayers", *Colloids Surf B Biointerfaces,* vol. 88, no. 1, pp. 231-9, Nov 1 2011, doi: 10.1016/j.colsurfb.2011.06.037.

[47] J. Gubernator, "Active methods of drug loading into liposomes: recent strategies for stable drug entrapment and increased in vivo activity", *Expert Opin Drug Deliv,* vol. 8, no. 5, pp. 565-80, May 2011, doi: 10.1517/17425247.2011.566552.

[48] H. Xu, *et al.*, "Development of high-content gemcitabine PEGylated liposomes and their cytotoxicity on drug-resistant pancreatic tumour cells", *Pharm Res,* vol. 31, no. 10, pp. 2583-92, Oct 2014, doi: 10.1007/s11095-014-1353-z.

[49] H. Tamam, *et al.*, "Development of Liposomal Gemcitabine with High Drug Loading Capacity", *Molecular Pharmaceutics,* vol. 16, no. 7, pp. 2858-2871, 2019/07/01 2019, doi: 10.1021/acs.molpharmaceut.8b01284.

[50] S. Paliwal, *et al.*, "Flurbiprofen-loaded ethanolic liposome particles for biomedical applications", *J Microbiol Methods,* vol. 161, pp. 18-27, Jun 2019, doi: 10.1016/j.mimet.2019.04.001.

[51] P. E. Tawari, *et al.*, "The cytotoxic mechanisms of disulfiram and copper(ii) in cancer cells", *Toxicol Res (Camb),* vol. 4, no. 6, pp. 1439-1442, Nov 19 2015, doi: 10.1039/c5tx00210a.

[52] T. C. Chou, "Drug combination studies and their synergy quantification using the Chou-Talalay method", *Cancer Res,* vol. 70, no. 2, pp. 440-6, Jan 15 2010, doi: 10.1158/0008-5472.Can-09-1947.

Conclusions and perspectives

This research work explored several nanocarrier systems for the delivery of GEM and its lipophilic prodrugs, 4-(*N*)-lauroyl-gemcitabine (GEM-C12) and 4-(*N*)-stearoyl-gemcitabine (GEM-C18). overcoming drug resistance and improving therapeutic outcomes in pancreatic cancer. The overarching objective was to develop and characterize innovative delivery strategies to enhance GEM stability, optimize its tumor targeting, and boost its efficacy in chemoresistant cellular models.

The first part of the study focused on carbon nano-onions (CNOs) functionalized with HA *via* a covalent linkage, using PEG as a spacer. This surface modification conferred active targeting capability toward CD44-overexpressing pancreatic cancer cell lines, resulting in improved cellular uptake and enhanced cytotoxicity. Drug loading onto CNOs was achieved through hydrophobic interactions, enabling controlled and sustained release. This system not only demonstrated the potential of HA-mediated targeting but also showed versatility as a delivery platform for other lipophilic prodrugs. CNOs offer multiple promising avenues for future research. The covalent HA binding ensured long-term stability and functionalization flexibility, paving the way for future applications involving other anticancer agents that benefit from CD44-targeted delivery. The efficacy of HA-mediated targeting indicates the possibility for dual-drug co-delivery to achieve synergistic effects while enhancing tumor-specific accumulation. The CNOs surface could also be adapted for dual-targeting strategies, for instance by combining HA with other ligands like EGFR or mesothelin to better address tumor heterogeneity. Furthermore, the incorporation of stimuli-responsive linkers (e.g., redox- or pH-sensitive moieties) could facilitate a selective release in the tumor microenvironment. The validation of CNOs efficacy *in vivo* on pancreatic tumor models will be essential to confirm therapeutic impact and biodistribution.

The second nanocarrier investigated was based on mixed micelles composed of the commercially available PEG-DSPE and a HA-DPPE conjugate previously prepared in our laboratory. These micelles offered two significant advantages: a straightforward preparation process and, for the first time to our knowledge, the demonstration that even a low amount (1%) of HA-DPPE conjugate was sufficient to achieve a targeting effect. HA-DPPE was incorporated during the hydration step, allowing HA chains (of either 4800 or 14,800 Da) to be displayed on the micelle surface. GEM-C18 was encapsulated through hydrophobic interactions, and drug loading led to a shape transformation from spherical to elongated morphology, as confirmed by FESEM, SAXS, and X-ray diffraction analysis. The resulting micelles exhibited high encapsulation efficiency (>90%) and sustained drug release. *In vitro* tests revealed significantly enhanced cytotoxicity and uptake, particularly with high

molecular weight HA, confirming the role of HA-CD44 interactions. HA-DPPE/PEG-DSPE mixed micelles exhibit considerable promise for additional development. Systematic studies should optimize HA density, molecular weight, and PEG/HA ratios to balance stealth and targeting properties. Consequently, a detailed evaluation of the shape and morphology of these systems is fundamental. Beyond GEM-C18, this platform could be investigated to encapsulate other lipophilic drugs or gene-drug combinations, thereby expanding its versatility. Subsequent investigation is required to substantiate the findings in more intricate *in vitro* and *in vivo* models. This will facilitate a more comprehensive evaluation of micelle stability, biodistribution, and efficacy under clinically relevant conditions. Additionally, its easy hydration-based production process renders it suitable for large-scale manufacturing and regulatory translation, provided that long-term stability studies substantiate shelf-life and consistency.

The final part of this research deals with liposomal formulations for the delivery of GEM and GEM-C18. Two distinct approaches were employed due to the different physico-chemical characteristics of the two compounds: the more hydrophilic GEM was encapsulated in the aqueous core of liposomes (LipoGEM) while the lipophilicity of GEM-C18 allowed its encapsulation into the lipid bilayer (LipoGEM-C18). Both liposomal formulations exhibited favorable physico-chemical properties, with high stability (up to three weeks) and encapsulation efficiencies of 20% and 95%, respectively. LipoGEM showed rapid drug release, probably due to its high hydrophilicity, while LipoGEM-C18 showed sustained drug release over 72 and 48 h in HEPES buffer (pH 7.4) and in FBS respectively. Importantly, the presence of the drugs did not alter liposome size or morphology. *In vitro* assays on PANC-1 cells demonstrated higher cytotoxicity for liposomes contained GEM-C18 compared to those with GEM. Furthermore, the combination of GEM and GEM-C18 free drugs with DSF, an emerging repurposed anticancer agent, showed synergistic effects. However, the liposomal combinations with DSF did not show significant improvement over the free drug combinations, possibly due to suboptimal timing or release kinetics. These liposomal platforms developed demonstrate considerable promise for additional refinement. Future directions in this field include the integration of active targeting moieties, such as HA, peptides, antibodies, or aptamers, to improve selective uptake by pancreatic cancer cells and overcome biological barriers such as the dense stromal matrix. These actively targeted liposomes have the potential to enhance accumulation in pancreatic cancer cells, thereby increasing therapeutic efficacy *in vivo*. Furthermore, dual-drug co-encapsulation strategies may be pursued to deliver both GEM

and DSF within the same liposomal carrier, enabling synchronized intracellular delivery. This approach has the potential to better address the suboptimal synergy observed when combining separately delivered liposomes with DSF. Another key priority will be to extend the evaluation of LipoGEM and LipoGEM-C18 to 3D pancreatic spheroids and organoids, as well as orthotopic and patient-derived xenograft models. These sophisticated models will facilitate a more precise evaluation of liposomal penetration, retention, and therapeutic efficacy in environments that closely resemble the *in vivo* tumor microenvironment.
To further support and contextualize this research, a review article was authored and submitted to WIREs Nanomedicine and Nanobiotechnology, summarizing recent advancements in dual-drug and liposomal delivery strategies for pancreatic cancer. This comprehensive review provided a valuable foundation for identifying emerging trends and designing the present study.

Overall, this thesis has significantly contributed to the design, development, and preliminary evaluation of nanocarrier-based strategies for pancreatic cancer therapy. The multidisciplinary approach facilitated a significant advancement in our technological knowledge, thereby profoundly enhancing our comprehension of nanosystems that have potential applications in the domain of drug delivery. Moreover, this work has enabled a more profound immersion in biological research, leading to the identification of novel opportunities in this field.